Biofabrication of articular cartilage: Development of an efficient *in vivo* repair technique using autologous stem cells

Dr Sam L. Francis

MBBS, MTrauma

ORCID: 0000-0001-7070-7712

Submitted in total fulfilment of the requirements for the degree of

Doctor of Philosophy

August 2020

The University of Melbourne, Faculty of Medicine, Dentistry, and Health Science

Department of Surgery, St. Vincent's Hospital Melbourne, Australia

THESIS SUMMARY

Articular cartilage defects represent a major clinical challenge due to the lack of long-term management options available for young patients who present with a symptomatic and functional burden.

Microfracture is the traditional standard treatment of care and has no long-term benefit demonstrated beyond 2 years, with patients reporting symptom relapse and functional compromise. Other techniques used to treat chondral defects include Autologous Chondrocyte Implantation and Matrix-induced Autologous Chondrocyte Implantation, both of which are not superior in comparison to the cheap and easily performed microfracture technique.

Cartilage tissue engineering approaches using stem cells and bioscaffolds have become of significant research focus; additionally, the emergence of bioprinting technology has opened up the ability to efficiently and accurately deliver engineered tissue constructs. Biological tissue can be generated by printing cells and scaffolds together in a 'bioink' composition rather than using prefabricated scaffold constructs; this approach is coined 'Biofabrication', which is a rapidly growing field.

Biofabrication approaches show promise in treating chondral defects; however, we are no closer today to a human clinical trial. Several hurdles currently prevent the progression of such research; a significant barrier is the use of long periods of laboratory-based cell culture and expansion. This increased culture duration leads to concerns with the use of animal serum-based media, sterility, senescence, loss of differentiation potential, and tumorigenic transformation. To overcome these issues, human tissue harvest, cell isolation and reimplantation should be performed efficiently, thereby reducing the exposure to the risks mentioned above. Furthermore, by establishing a specific timeframe in which a biofabrication procedure can be achieved, surgical planning and patient preparation can be structured and adequately performed.

This thesis aimed to develop an efficient biofabrication procedure for cartilage repair using an autologous cell population, which could produce neocartilage in clinically relevant defects. The chapters in this work present several critical developments concerning the overall aim.

First, the most chondrogenic cell source from those tested within the knee joint was identified to be the human Adipose-Derived Stem Cell (hADSC). A rapid 85-minute hADSCs isolation protocol from the Infrapatellar Fat Pad (IFP) was then developed by optimising the time-consuming aspects of the standard IFP-derived hADSCs isolation protocol (>27 hours) and shown to be comparable.

Secondly, the minimum chondrogenic requirements of rapidly isolated hADSCs before reimplantation were established. It was determined that 5 days is the earliest time point during cellular expansion in which hADSCs could be driven into chondrogenesis. Therefore, the minimum biofabrication turnaround time is roughly 1-week (5 days and 85 minutes to be precise). Next, 5.0 million hADSCs/mL of a biocompatible hydrogel was shown to be the minimum concentration required to produce *in vitro* neocartilage. Finally, the maximum defect volume treatable in a 1-week turnaround was shown to be 380 µL (mm^3) or 760 µL (mm^3) using one or two IFPs respectively, representing clinically significant defect volumes.

The next section of this thesis aimed to establish a biofabrication model that could be adapted for surgical use and be implemented in an animal model. In this chapter, a safe, efficient and user-friendly procedure was designed and validated *in vitro*. First a representative cell source was selected and validated. Next, suitable hydrogel compositions and gelation times were identified, and finally, a safe intraoperative crosslinking set-up was developed.

The final element of this work was a proof of concept study, where the newly devised biofabrication approach was performed on a rabbit model to evaluate chondral repair. This procedure was successfully implemented, and the associated degree of cartilage repair was superior compared to the microfracture (clinical standard) and empty control groups.

In conclusion, an efficient 1-week biofabrication approach was established for chondral repair, and this approach was shown to treat clinically significant defect volumes. The newly developed procedure has been validated for short term repair *in vivo* and is superior to the existing standard treatment. The next step is to provide mid-long-term efficacy of therapy *in vivo* using a large animal model, which if successful, paves the way to human translation. This work presents promise in the future management of chondral defects in young patients with a low-risk strategy that could one day treat/halt the progression to early-onset osteoarthritis.

DECLARATION OF AUTHENTICITY

This declaration is to certify that:

(i) This thesis comprises only my original work towards my PhD except where indicated in the Preface

(ii) Due acknowledgement has been made in the text to all other material used

(iii) This thesis is less than 100,000 words in length, exclusive of tables, bibliographies and appendices



Dr Sam L. Francis

August 2020

PREFACE

This project was supported by the Australian Research Council Industrial Transformation Training Centre (ARC-ITTC) in Additive Biomanufacturing, the AVANT doctor in training (DIT) grant, the St Vincent's Hospital Melbourne Research Endowment Fund (REF 90178) grant and the Biomed tech horizons program through MTP Connect.

The publication status of each chapter is detailed below:

Chapter	Publication status
1: Literature review	Elements of this chapter have been published as a literature review; this has been adapted for the thesis and is not used in its published form. The original paper was published in Stem Cells International and is attached as appendix 1.
2: Knowledge gaps, Hypotheses and Research aims	N/A
3: Materials, Protocols and Methods	N/A
4: Chondrogenic potential of cell sources within the knee joint and optimisation of the cell isolation protocol	Elements of this chapter have been published as a literature review; this has been adapted for the thesis and is not used in its published form. The original paper was published in Frontiers in surgery and is attached as appendix 2. A research article has been prepared for publication; this will be submitted after a provisional patent application has been assessed (under review).
5: Minimum chondrogenic requirements of IFP-derived hADSCs prior to reimplantation	A research article has been prepared for publication along with aspects of the data obtained in chapter 7. This manuscript will be submitted after a provisional patent application has been reviewed (in progress).
6: Establishing a biofabrication procedure for *in vivo* chondral repair	This work in this chapter represents a design/validation embodiment. No publication has been prepared at this stage.
7: Cartilage biofabrication using the minimum chondrogenic hADSCs concentration – a pilot *in vivo* rabbit model	A research article has been prepared for publication along with the data obtained in chapter 5; this will be submitted after a provisional patent application has been assessed (under review).

The co-author contributions for each paper are listed below:

Publication	Author contribution
Francis SL, Di Bella, C, Wallace GG, & Choong PFM. Cartilage Tissue Engineering using Stem Cells and Bioprinting Technology – Barriers to Clinical Translation. Frontiers in Surgery, 2018; 5:70. DOI:10.3389/fsurg.2018.00070	SLF reviewed the literature, wrote the manuscript and prepared the figures. CDB, GGW and PFMC edited and approved the manuscript.
Francis SL, Duchi S, Onofrillo C, Di Bella C, & Choong PFM. Adipose Derived Mesenchymal Stem Cells in the Use of Cartilage Tissue Engineering: The Need for a Rapid Isolation Procedure. Stem Cells International, 2018, 8947548. DOI:10.1155/2018/8947548	SLF reviewed the literature, wrote the manuscript and prepared the figures. SD and CO provided intellectual input and edited the manuscript. CDB and PFMC edited and approved the manuscript.
Francis SL, Duchi S, Onofrillo C, Di Bella C, & Choong PFM. Rapid isolation of stem cells to treat critical size cartilage defects in an efficient surgical biofabrication procedure. Manuscript for submission.	SLF designed, performed the experiments, wrote the manuscript and prepared the figures. SD and CO provided intellectual input, technical support and edited the manuscript. CDB and PFMC edited and approved the manuscript.
Francis SL, Duchi S, Onofrillo C, Di Bella C, & Choong PFM. The minimum required stem cell concentration for cartilage biofabrication – An i*n vitro* and *in vivo* study. Manuscript for submission.	SLF designed, performed the experiments, wrote the manuscript and prepared the figures. SD and CO provided intellectual input, technical support and edited the manuscript. CDB and PFMC edited and approved the manuscript.

No other work towards this thesis has been submitted for additional qualifications. No work towards this thesis was carried out before enrolment in the degree. No third-party editorial assistance was provided in the preparation of this thesis.

ACKNOWLEDGEMENTS

I would like to thank all those who have helped me directly and indirectly during the undertaking of this project, without whom this work would not have been feasible.

I would like to express my gratitude to my supervisors Professor Peter Choong, Associate Professor Claudia Di Bella and Professor Gordon Wallace, for their guidance, mentorship and expert insights throughout this PhD project. This voyage of scientific endeavour, innovation and determination has been generously nurtured through their efforts and support.

I would like to thank my laboratory mentors and dear friends, Dr Serena Duchi and Dr Carmine Onofrillo, who have extensively trained me in a vast range of scientific skills and have guided me throughout my candidature. I am very appreciative for all your time, support and assistance provided throughout this project.

I would like to thank all the other researchers in the broader Biofab3D laboratory for their assistance in select aspects of this project, including Dr Cathal O'Connell and Ms Cheryl Augustine. I would also like to extend my thanks to Anna Defterios and Amanda Rixon at the Experimental Medical and Surgical Unit of St Vincent's Hospital for their expertise and technical assistance with the animal experiments. I am also grateful to all the surgeons within the department of orthopaedics (St Vincent's Hospital Melbourne) who assisted and participated in the harvesting of tissue. I would like to thank Maria Pia Cumani from the Rizzoli Orthopaedic Institute at the Department University of Bologna for her assistance with graphical design.

To my fellow students at Biofab3D, thank you for your support and company throughout my candidature, it has been a delightful time and a pleasure working with you, and I wish you all the very best in your future endeavours.

Finally, I would like to thank my partner Rachel and my family for their unconditional support and love throughout this time.

TABLE OF CONTENTS

THESIS SUMMARY **2**

DECLARATION OF AUTHENTICITY **4**

PREFACE **5**

ACKNOWLEDGEMENTS **7**

TABLE OF CONTENTS **8**

LIST OF TABLES, FIGURES AND ABBREVIATIONS **11**

PUBLICATIONS ARISING AND PREPARED FROM THIS WORK **15**

CONFERENCE PRESENTATIONS ARISING FROM THIS WORK **16**

PRIZES AND NOMINATIONS ARISING FROM THIS WORK **17**

SCHOLARSHIPS AND GRANTS RECEIVED FOR THIS WORK **17**

GRANTS RECEIVED FOR THIS WORK **17**

PATENT APPLICATIONS ARISING FROM/RELATED TO THIS WORK **17**

CHAPTER 1: INTRODUCTION AND LITERATURE REVIEW **18**

1.1 INTRODUCTION 19
1.2 ARTICULAR CARTILAGE 20
1.2.1 GENERAL *20*
1.2.2 DEVELOPMENT *20*
1.2.3 COMPOSITION *23*
1.2.4 STRUCTURE- ARTICULAR CARTILAGE ZONES *24*
1.2.5 BIOMECHANICAL PROPERTIES *25*
1.2.6 AGEING PROCESS *27*
1.2.7 POST TRAUMATIC ARHTRITIS *28*
1.3 CURRENT TREATMENT STRATEGIES 29
1.3.1 NON-SURGICAL OPTIONS *29*
1.3.2 SURGICAL OPTIONS *32*
1.4 EMERGING TREATMENT - CARTILAGE TISSUE ENGINEERING 34
1.4.1 CELLS *35*
1.4.2 SCAFFOLDS *38*
1.4.3 CHEMICAL STIMULATION: SIGNALLING MOLECULES *41*
1.4.4 MECHANICAL/PHYSICAL AND ENVIRONMENTAL STIMULATION *42*
1.5 GENERATION AND DELIVERY OF THE TISSUE CONSTRUCT 43
1.5.1 GAPS AND DOWNFALLS IN CARTILAGE TISSUE ENGINEERING *43*
1.5.2 THE CONCEPT OF BIOFABRICATION *44*
1.5.3 3D BIOPRINTING *45*
1.5.4 SUITABLE CONSTRUCT DELIVERY METHODS FOR CARTILAGE TISSUE REPAIR *48*
1.6 CURRENT MODELS USED FOR *IN VIVO* CARTILAGE REPAIR 50
1.6.1 LARGE ANIMAL MODELS *50*
1.6.2 SMALL ANIMAL MODELS *51*
1.6.3 ECTOPIC MODELS *52*

CHAPTER 2: KNOWLEDGE GAPS, HYPOTHESES AND RESEARCH AIMS **53**

2.1 CHONDROGENIC POTENTIAL OF CELL SOURCES WITHIN THE KNEE JOINT AND OPTIMISATION OF THE CELL ISOLATION PROTOCOL 54
2.2 MINIMUM CHONDROGENIC REQUIREMENTS OF IFP-DERIVED HADSCS PRIOR TO REIMPLANTATION 57
2.3 ESTABLISHING A BIOFABRICATION PROCEDURE FOR IN VIVO CHONDRAL REPAIR 60
2.4 CARTILAGE BIOFABRICATION USING THE MINIMUM CHONDROGENIC HADSCS CONCENTRATION – A PILOT *IN VIVO* RABBIT MODEL 64

CHAPTER 3: MATERIALS, PROTOCOLS AND METHODS **66**

3.1 CELL HARVEST AND ISOLATION 67

3.1.1 HUMAN TISSUE HARVESTING - ETHICAL APPROVAL *67*
3.1.2 STANDARD IFP-DERIVED MESENCHYMAL STEM CELL ISOLATION PROTOCOL *67*
3.1.3 MATURE ARTICULAR CHONDROCYTE ISOLATION PROTOCOL *68*
3.1.4 ARTICULAR PROGENITOR CELL ISOLATION PROTOCOL *69*
3.1.5 CHEMICAL DIGESTION TIMEFRAMES *69*
3.1.6 MATRIGEL-COATED TCPS WELLS FOR HADSCS ADHERENCE *70*
3.1.7 THE RAPID IFP-DERIVED MSCS (HADSCS) ISOLATION PROTOCOL *70*
3.2 *IN VITRO* CELL CULTURE 71
3.2.1 CHONDROGENIC DIFFERENTIATION – PELLET CULTURE (HUMAN CELLS) *71*
3.2.2 CHONDROGENIC DIFFERENTIATION – 3D BIOSCAFFOLDS (HUMAN CELLS) *71*
3.2.3 CHONDROGENIC DIFFERENTIATION – PELLET CULTURE (RABBIT CELLS) *71*
3.2.4 OSTEOGENIC DIFFERENTIATION – MONOLAYER 2D CULTURE (HUMAN CELLS) *71*
3.2.5 ADIPOGENIC DIFFERENTIATION – MONOLAYER 2D CULTURE (HUMAN CELLS) *72*
3.3 PHENOTYPICAL *ANALYSIS* 72
3.3.1 HAEMATOXYLIN, FAST GREEN AND SAFRANIN 0 STAINING *72*
3.3.2 IMMUNOSTAINING – PELLET CULTURE *72*
3.3.3 IMMUNOSTAINING AND COLLAGEN 2 INTENSITY– 3D BIOSCAFFOLDS *73*
3.3.4 IMMUNOPHENOTYPING – FLOW CYTOMETRY *74*
3.4 MOLECULAR ANALYSIS 74
3.4.1 RNA EXTRACTION AND REVERSE TRANSCRIPTION *74*
3.4.2 CHONDROGENIC GENE EXPRESSION (QPCR) *74*
3.4.3 OSTEOGENIC GENE EXPRESSION (QPCR) *75*
3.4.4 ADIPOGENIC GENE EXPRESSION (QPCR) *76*
3.4.5 CHONDROGENIC ASSESSMENT - GAG/DNA QUANTIFICATION (HUMAN AND RABBIT CELLS) *76*
3.5 *IN VITRO* BIOFABRICATION - 3D BIOSCAFFOLDS 77
3.5.1 BIOINK FORMULATIONS *77*
3.5.2 GENERATION OF BIOSCAFFOLD MOULDS *77*
3.5.3 BIOFABRICATION PROCEDURE - GENERATION OF 3D BIOSCAFFOLDS *77*
3.6 DESIGN OF *IN VIVO* BIOFABRICATION PROCEDURE 79
3.6.1 BIOINK FORMULATIONS *79*
3.6.2 MECHANICAL TESTING OF HYDROGELS– COMPRESSION TESTING *79*
3.6.3 HYDROGEL GELATION TIME – FILAMENT FORMATION TEST *80*
3.6.4 SELECTION AND FIXATION OF THE LIGHT SOURCE (CROSSLINKING) AND DISTANCE *81*
3.7 *IN VIVO* BIOFABRICATION - RABBIT MODEL OF CARTILAGE REPAIR 82
3.7.1 ANIMAL ETHICS STATEMENT *82*
3.7.2 SURGICAL MODEL OF CHONDRAL REPAIR *82*
3.7.3 MACROSCOPIC EVALUATION *85*
3.7.4 BIOMECHANICAL EVALUATION - ATOMIC FORCE MEASUREMENT *86*
3.7.5 MICROSCOPIC EVALUATION- HISTOLOGY AND SCORING *87*
3.7.6 MICROSCOPIC EVALUATION- IMMUNOSTAINING *89*
3.8 THEOREMS 89
3.8.1 CELLULAR ADHERENCE *89*
3.8.2 GROWTH KINETICS - DOUBLING TIME *89*
3.8.3 THE MAXIMUM DEFECT VOLUME REPAIRABLE *90*
3.9 STATISTICAL ANALYSIS 90
CHAPTER 4: CHONDROGENIC POTENTIAL OF CELL SOURCES WITHIN THE KNEE JOINT AND OPTIMISATION OF THE CELL ISOLATION PROTOCOL **91**
4.1 INTRODUCTION 92
4.2 RESULTS 92
CHONDROGENC POTENTIAL OF DIFFERENT CELL TYPES WITHIN THE KNEE JOINT *92*
4.2.1 PHENOTYPICAL PROFILES OF THE THREE CELL TYPES TESTED *93*
4.2.2 CHONDROGENIC DIFFERENTIATION CAPACITY OF THE THREE CELL TYPES TESTED *93*
OPTIMISATION OF THE CURRENT IFP-DERIVED hADSCs ISOLATION PROTOCOL *95*
4.2.3 REDUCTION IN CHEMICAL DIGESTION DURATION *95*
4.2.4 REDUCTION IN SELECTIVE TCPS ADHERENCE DURATION *96*
THE NEWLY GENERATED RAPID IFP-DERIVED hADSCs PROTOCOL *97*

VALIDATION OF THE RAPID ISOLATION PROTOCOL ... *97*
4.2.5 CELL RETRIEVAL EFFICIENCY ... *98*
4.2.6 IMMUNOPHENOTYPIC CHARACTERISATION ... *99*
4.2.7 TRILINEAGE DIFFERENTIATION OF RAPIDLY ISOLATED HADSCS ... *100*
4.3 DISCUSSION ... 105
4.4 CONCLUSION ... 107
CHAPTER 5: MINIMUM CHONDROGENIC REQUIREMENTS OF IFP-DERIVED HADSCS PRIOR TO REIMPLANTATION ... **108**
5.1 INTRODUCTION ... 109
5.2 RESULTS ... 109
THE EARLIEST POINT WHEN IFP-DERIVED hADSCs CELLS BECOME CHONDROGENEIC ... *109*
5.2.1 THE EARLIEST POINT DURING EXPANSION WHEN CELLS FORM 3D PELLETS ... *109*
5.2.2 CHONDROGENIC ASSESSMENT OF 5 AND 7 DAY EXPANDED CELLS ... *110*
THE MINIMUM hADSCs CONCENTRATION REQUIRED TO PRODUCE NEOCARTILAGE FORMATION IN A HYDROGEL ... *112*
5.2.3 IMMUNOFLOURESCENCE IMAGING AND COLLAGEN 2 STAINING INTENSITY ... *112*
5.2.4 GAG/DNA QUANTIFICATION AND GENE EXPRESSION (QPCR) ... *115*
THE MAXIMUM DEFECT VOLUME REPAIRABLE USING A RAPIDLY ISOLATED HADSCS POPULATION WHICH IS EXPANDED FOR 5 DAYS ... *117*
5.3 DISCUSSION ... 118
5.4 CONCLUSION ... 120
CHAPTER 6: ESTABLISHING A BIOFABRICATION PROCEDURE FOR *IN VIVO* CHONDRAL REPAIR ... **121**
6.1 INTRODUCTION ... 122
6.2 RESULTS ... 123
6.2.1 CHONDROGENIC VALIDATION OF A COMMERCIAL RABBIT MSCs LINE ... *123*
6.2.2 MECHANICAL ASSESSMENT OF A SOFT AND HARD GELATIN-BASED HYDROGEL ... *124*
6.2.3 ASSESSMENT OF THE GELATION TIME OF CHOSEN HYDROGELS ... *124*
6.2.4 DESIGN OF A SAFE INTRAOPERATIVE CROSSLINKING METHOD ... *126*
FINAL SET-UP OF THE IN VIVO BIOFABRICATION REPAIR PROCEDURE ... *127*
6.3 DISCUSSION ... 128
6.4 CONCLUSION ... 129
CHAPTER 7: CARTILAGE BIOFABRICATION USING THE MINIMUM CHONDROGENIC HADSCS CONCENTRATION – A PILOT *IN VIVO* RABBIT MODEL ... **130**
7.1 INTRODUCTION ... 131
7.2 RESULTS ... 131
CARTILAGE REPAIR USING A NOVEL BIOFABRICATION PROCEDURE IN VIVO ... *131*
7.2.1 POSTOPERATIVE OUTCOMES ... *131*
7.2.2 MACROSCOPIC ASSESSMENT ... *132*
7.2.3 BIOMECHANICAL ASSESSMENT – ATOMIC FORCE MICROSCOPY ... *135*
7.2.4 MICROSCOPIC ASSESSMENT ... *136*
7.3 DISCUSSION ... 140
7.4 CONCLUSION ... 142
CHAPTER 8: DISCUSSION, FUTURE DIRECTIONS AND CONCLUSIONS ... **143**
CHAPTER 9: REFERENCES ... **152**
CHAPTER 10: APPENDICES ... **175**
APPENDIX 1: CARTILAGE TISSUE ENGINEERING USING STEM CELS AND BIOPRINTING TECHNOLOGY - BARRIERS TO CLINICAL TRANSLATION ... 176
APPENDIX 2: ADIPOSE-DERIVED MESENCHYMAL STEM CELLS IN THE USE OF CARTILAGE TISSUE ENGINEERING: THE NEED FOR A RAPID ISOLATION PROCEDURE ... 188
APPENDIX 3: FLOW CYTOMETRY FROM THREE DIFFERENT CELL TYPES ... 197
APPENDIX 4: FLOW CYTOMETRY FROM THREE DIFFERENT PATIENT LINES ... 198
APPENDIX 5: EFFECT OF DIFFERENT SOURCES OF COATED TCPS ON CELLULAR ATTACHMENT ... 199

LIST OF TABLES, FIGURES AND ABBREVIATIONS

TABLES

Table 1.1	Major components of the articular cartilage extracellular matrix
Table 1.2	Operative treatment indications for chondral repair based on lesion size
Table 1.3	Comparison of cell sources used in cartilage tissue engineering
Table 1.4	Advantages and disadvantages of different 3D bioprinting methods
Table 1.5	Comparison of 3D bioprinting methods
Table 1.6	Common large animal models used in cartilage research
Table 1.7	Common small animal models used in cartilage research
Table 3.1	Probes used to assess chondrogenesis using RT- qPCR with the TAQMAN system
Table 3.2	Probes used to assess osteogenesis using for RT- qPCR with the TAQMAN system
Table 3.3	Probes used to assess adipogenesis using RT- qPCR with the SYBR green system
Table 3.4	Distribution of rabbits and treatment groups
Table 3.5	Macroscopic scoring system of cartilage repair
Table 3.6	Microscopic scoring system of cartilage repair
Table 4.1	Flow cytometry results summary of key markers tested in hADSCs, chondrocytes and hAPCs
Table 4.2	Patient demographics of the three different patient lines tested
Table 4.3	Summary of flow cytometry results of markers tested in both isolation groups
Table 5.1	Details of cell population groups tested, including sample size, number of cells, doubling time and ability to form 3D pellets
Table 5.2	Defect volumes repairable using rapidly isolated hADSCs expanded for 5 days with the minimum required neocartilage forming concentration
Table 6.1	Assessment of the gelation time required for hydrogel printability (String test) using the room temperature of 23°C
Table 6.2	Assessment of the gelation time required for hydrogel printability (String test) using a cooled temperature of 4°C
Table A1	Flow cytometry results summary of key markers tested for with the hADSCs phenotype

FIGURES

Figure 1.1	Limb development: phases and regions involved
Figure 1.2	Mechanism of chondrogenic regulation
Figure 1.3	Endochondral ossification pathway
Figure 1.4	Hyaline cartilage morphology and structure
Figure 1.5	Viscoelastic behaviour of articular cartilage
Figure 1.6	Current surgical cartilage regeneration techniques
Figure 1.7	General components of cartilage tissue engineering
Figure 1.8	Different cell types used in cartilage tissue engineering based on potency
Figure 1.9	Ontogeny of the infrapatellar fat pad (IFP)
Figure 1.10	Different types of scaffold biomaterials used in cartilage tissue engineering
Figure 1.11	Mesenchymal stem cell expansion and chondrogenic differentiation pathway
Figure 1.12	Bioreactor system designs
Figure 1.13	Biofabrication in tissue engineering (TE) and regenerative medicine (RM)
Figure 1.14	Concept of cartilage biofabrication
Figure 1.15	Different types of bioprinting mechanisms used in tissue engineering
Figure 1.16	The 'Axcelda®pen' handheld extrusion-based 3D bioprinter
Figure 1.17	Intra-operative photograph of the Axcelda®pen used in a sheep model
Figure 2.1	Sagittal magnetic resonance imaging scan of the knee joint showing the relationship of the IFP to the articular cartilage
Figure 2.2	Human adipose-derived mesenchymal stem cell (hADSCs) isolation protocol from Infrapatellar fat tissue
Figure 2.3	Set-up of an *in situ* biofabrication repair procedure for in vivo chondral defect repair
Figure 3.1	Design and preparation of scaffold template and moulds
Figure 3.2	Graphical representation of the biofabrication procedure
Figure 3.3	The filament formation test – assessment of hydrogel printability
Figure 3.4	The distance required to crosslink the entire defect repair surface area safely
Figure 3.5	Graphical representation of treatments groups used in the rabbit model of cartilage repair
Figure 3.6	Graphical representation of how the maximal repairable chondral defect volume is calculated
Figure 4.1	Chondrogenic assessment of hADSCs, chondrocytes and hAPCs
Figure 4.2	Effect of different durations of chemical digestion on cell yield and viability

Figure 4.3	Cellular adherence on non-coated versus Matrigel-coated TCPS based on duration
Figure 4.4	Graphical representation of the experimental design and timeframes of both rapid and control isolation groups
Figure 4.5	Comparison of rapid and control isolation groups with respect to yield, viability, and adherence
Figure 4.6	Chondrogenic assessment of rapidly isolated hADSCs
Figure 4.7	Osteogenic assessment of rapidly isolated hADSCs
Figure 4.8	Adipogenic assessment of rapidly isolated hADSCs
Figure 5.1	The growth kinetics of IFP-derived hADSCs during expansion prior to passaging
Figure 5.2	Chondrogenic assessment of 5- and 7-day expanded cell populations in pellet culture over 3 weeks using Safranin 0 and Immunostaining
Figure 5.3	Confocal microscopy images of whole scaffold sections for the three different cell concentrations
Figure 5.4	Neocartilage assessment of bioscaffolds generated using three different cell concentrations
Figure 5.5	Collagen 2 (Col 2) staining intensity of bioscaffolds
Figure 5.6	Chondrogenic assessment of GelMA/HA bioscaffolds generated using three different cell concentrations
Figure 6.1	GAG/DNA ratio over 3-weeks of chondrogenic stimulation using a commercial (cyagen) rabbit MSCs line
Figure 6.2	Compression testing of acellular GelMA scaffolds the day after printing
Figure 6.3	Ultraviolet light source adapter set- up at a fixed distance of 1cm
Figure 6.4	Summary of final biofabrication procedure
Figure 7.1	Cartilage morphology and macroscopic scoring
Figure 7.2	Atomic Force Microscopy (AFM) mechanical testing of cartilage repair
Figure 7.3	Histology, immunostaining and microscopic scoring of cartilage repair
Figure A1	Flow cytometry profiles from three different cell types
Figure A2	Flow cytometry profiles of hADSCs from three different patient lines tested
Figure A3	Effect of different Tissue culture polystyrene (TCPS) coatings on cellular attachment

ABBREVIATIONS

2D:	Two dimensional
3D:	Three dimensional
ACI:	Autologous chondrocyte implantation
ADSCs:	Adipose-derived mesenchymal stem cells
APCs:	Articular progenitor cells
BMP:	Bone morphogenetic protein
BMSCs:	Bone marrow-derived stem cells
CD:	Cluster differentiation
COL:	Collagen
CS:	Corticosteroid
CZ:	Calcified zone
DNA:	Deoxyribonucleic acid
DZ:	Deep zone
ECM:	Extracellular matrix
EMSU:	Experimental medical and surgical unit
ESCs:	Embryonic stem cells
GAG:	Glycosaminoglycan
GelMA:	Gelatin-Methacryloyl/Methacrylate
HA:	Hyaluronic acid
hADSCs:	Human adipose-derived mesenchymal stem cells
IA:	Intra-articular
IFP:	Infrapatellar fat pad
IGF:	Insulin-like growth factor
IPSCs:	Induced pluripotent stem cells
LAP:	Lithium phenyl-2,4,6-trimethylbenzoylphosphinate
LCST:	Lower critical solution temperature
MA:	Methacryloyl/Methacrylate
MACI:	Matrix-induced autologous chondrocyte implantation
MF:	Microfracture
MMP:	Metal metalloproteinase
MZ:	Middle zone
MSCs:	Mesenchymal stem cells
PG:	Proteoglycan
PRP:	Platelet-rich plasma
RM:	Regenerative medicine
SEM:	Standard error margin
SLA:	Stereolithography
SZ:	Superficial zone
TCPS:	Tissue culture polystyrene
TE:	Tissue engineering
TGF:	Transforming growth factor
UV:	Ultraviolet
VDR:	Vitamin D receptor
VEGF:	Vascular endothelial growth factor

PUBLICATIONS ARISING AND PREPARED FROM THIS WORK

Publications/Manuscripts directly related to this thesis:

Francis SL*, Di Bella C, Wallace GG, & Choong PFM. Cartilage Tissue Engineering using Stem Cells and Bioprinting Technology – Barriers to Clinical Translation. Frontiers in Surgery, 2018; 5:70. DOI: 10.3389/fsurg.2018.00070.

Francis SL*, Duchi S, Onofrillo C, Di Bella C, & Choong PFM. Adipose-Derived Mesenchymal Stem Cells in the Use of Cartilage Tissue Engineering: The Need for a Rapid Isolation Procedure. Stem Cells International, 2018; 8947548. DOI: 10.1155/2018/8947548.

Francis SL*, Duchi S, Onofrillo C, Di Bella C, & Choong PFM. Rapid isolation of stem cells to treat critical size cartilage defects in an efficient surgical biofabrication procedure. Manuscript for submission post-patent review.

Francis SL*, Duchi S, Onofrillo C, Di Bella C, & Choong PFM. The minimum required stem cell concentration for cartilage biofabrication – An i*n vitro* and *in vivo* study. Manuscript for submission post-patent review.

Publications/Manuscripts not directly related to this thesis:

Francis SL*, Yao A, & Choong PFM. Culture Time Needed to Scale up Infrapatellar Fat Pad Derived Stem Cells for Cartilage Regeneration: A Systematic Review. Bioengineering, 2020, 7:3. DOI: 10.3390/bioengineering7030069.

Onofrillo C, Duchi S, **Francis SL***, O'Connell C, Caballero Aguilar L, Doyle S, Yue Z, Wallace GG, Choong PFM & Di Bella C. FLASH: Fluorescently LAbelled Sensitive Hydrogel to monitor bioscaffolds degradation during neocartilage generation. Biomaterials, 2021, 264:120383. DOI: 10.1016/j.biomaterials.2020.120383

CONFERENCE PRESENTATIONS ARISING FROM THIS WORK

Selected presentations during candidature:

Francis SL*, Duchi S, Onofrillo C, Di Bella C, & Choong PFM. The minimum chondrogenic stem cell concentration required in a bioscaffold to produce neocartilage- An *in vitro* and *in vivo* rabbit study. Royal Australasian College of Surgeons Annual scientific meeting, Melbourne, May 2020. *(Oral Presentation-International)*

Francis SL*, Duchi S, Onofrillo C, Di Bella C, & Choong PFM. Development of a single-stage repair procedure for clinically significant chondral defects using stem cells and biofabrication. Surgical Research Society of Australasia Conference, Royal Australasian College of surgeons Melbourne, November 2019. *(Oral Presentation-International)*

Francis SL*, Duchi S, Onofrillo C, Di Bella C, & Choong PFM. Treatment of Clinically Significant Cartilage Defects in One Surgical Biofabrication Procedure. Tissue Engineering and Regenerative Medicine International Society– Asia Pacific Chapter and Australasian Society for Biomaterials and Tissue Engineering (TERMIS-AP + ABMC7) Congress, October 2019. *(Oral Presentation-International)*

Francis SL*, Duchi S, Onofrillo C, Di Bella C, & Choong PFM. Rapid isolation of mesenchymal stem cells to treat clinically significant cartilage defects in one surgical biofabrication procedure. Australian and New Zealand Orthopaedic Research Society Annual Conference, Canberra, October 2019. *(Oral Presentation-International)*

Francis SL*, Duchi S, Onofrillo C, Di Bella C, & Choong PFM. Cartilage Repair Using Stem Cell Technology: Barriers to Clinical Translation. Australasian Society for Biomaterials and Tissue Engineering, Fremantle, April 2017. *(Oral Presentation-International)*

Francis SL*, Di Bella C, Wallace GG, & Choong PFM. Cartilage Repair Using Stem Cell Technology: Barriers to Clinical Translation. Australasian Society for Biomaterials and Tissue Engineering, Fremantle, April 2017. *(Poster Presentation- International)*

PRIZES AND NOMINATIONS ARISING FROM THIS WORK

- Peter Ryan Prize for Surgical Research, St Vincent's Hospital, Melbourne, 2019
- Best Oral Presentation on the day, Aikenhead Centre for Medical Discovery Research Week, Melbourne, 2019
- Runner up, Young Investigator Award, Section of Academic Surgery, Royal Australasian College of Surgeons 2019
- Orthopaedic Innovation Prize Finalist, Australian and New Zealand Orthopaedic Research Society Annual Conference, Canberra 2019
- Biocurate Best Translational Project Prize and ExoPharm Best Regenerative Project Prize finalist, Biomed link conference, The University of Melbourne, Melbourne 2019

SCHOLARSHIPS AND GRANTS RECEIVED FOR THIS WORK

- Australian research council industry training centre (ITTC) in additive biomanufacturing PhD scholarship (2017-19)
- Jane Ariadne McLauren and Barclay Thomson Arthritis scholarship, The University of Melbourne (2017-19)
- Viola Edith Bequest scholarship, The University of Melbourne (2018-19)

GRANTS RECEIVED FOR THIS WORK

- AVANT doctor in training (DIT) grant (2019/20), $12,500
- St. Vincent's Hospital Melbourne, The Margaret Young bequest for arthritis-related research - Research endowment fund (2019/20), $19,400
- Eastern Hill travel grant, University of Melbourne, 2019, $1,000

PATENT APPLICATIONS ARISING FROM/RELATED TO THIS WORK

- Axcelda Uni – Provisional application submitted. "Methods for cell isolation, priming and therapy using a universal polymer" - UoM Ref: [UMT2019-096]; FPA ref: M53068757]. **Privileged and confidential*
- Axcelda Qik – Provisional application being prepared for submission: "Methods for single-stage therapy using autologous stem cells ". **Privileged and confidential*

CHAPTER 1: INTRODUCTION AND LITERATURE REVIEW

1.1 INTRODUCTION

Articular hyaline tissue is a specialised form of cartilage, allowing for shock absorption and the transmission of large amounts of force, ultimately contributing to skeletal movement and function (1). Although this tissue is strong and resilient, once injured, there is no intrinsic ability to self-repair or regenerate (2). Therefore, articular cartilage (chondral) defects/injuries are a major clinical challenge in the field of musculoskeletal medicine.

Non-surgical management options such as pharmacological agents can be dispensed orally or delivered as an intra-articular injection. Oral medications can provide symptomatic control; however, they have no evidence for cartilage repair or regeneration (3). Intra-articular stem cell injections are associated with an early improvement in symptomatic benefit up to 2 years (4); however, there is no evidence supporting long-term clinical outcome or cartilage regeneration (5).

Regarding isolated chondral repair, several surgical options are available, including Microfracture (MF), Autologous Chondrocyte Implantation (ACI) and Matrix-induced Autologous Chondrocyte Implantation (MACI) (6). MF repair is an arthroscopic technique where the subchondral bone is fractured to allow blood from the bone marrow to enter, clot and stimulate cartilage repair (7). It is the current standard of care for isolated chondral defects and provides up to 2 years of symptomatic and functional benefit (8). Clinical trials performed using ACI and MACI aimed to provide a more extended therapeutic benefit; to date, they have not demonstrated superiority over the cheaper and easily performed MF procedure (9, 10). Therefore, MF has remained the go to treatment option, albeit a poor one.

Emerging research over the past few decades has focussed on tissue-engineering (TE), a technique in which tissue is created and maintained *in vitro* using cells, bioscaffolds, chemical and physical stimulation (11, 12). Advances in bioprinting technology over the past decade have expanded the field of TE. The definition of bioprinting is “the process of patterning biomaterials in an organisational manner’’ (13). More recently, the concept of biofabrication has emerged, which could be described as the combination of TE and bioprinting techniques (14). Biofabrication technology enables the creation or delivery of tissue constructs in a precise and controlled fashion (14). These developments in the research field are promising; however, we are still no closer to translating these techniques into human clinical trials.

1.2 ARTICULAR CARTILAGE

1.2.1 GENERAL

Articular hyaline cartilage is a specialised form of connective tissue found in the freely moveable joints (diarthrodial/synovial joints) of mammals. It provides a structural and biological barrier between two bony surfaces leading to a smooth, uniform range of motion (1). Articular cartilage has unique biomechanical properties stemming from its structure and composition (15). The lubricated surface provides a low friction environment allowing for shock absorption and efficient articular motion. The extracellular matrix (ECM) and high-water content provide resistance to forceful and repetitive compressive and shear forces (1).

1.2.2 DEVELOPMENT

During embryogenesis (Figure 1.1), limb cartilage is specifically formed (initiation) via the lateral plate mesoderm (16). Then during limb growth and development, the lateral plate mesoderm, apical and lateral ectoderm layer contribute to the outgrowth and patterning of the limbs (16). Forelimb development (upper limb in humans) occurs ahead of the hind limb (lower limb humans).

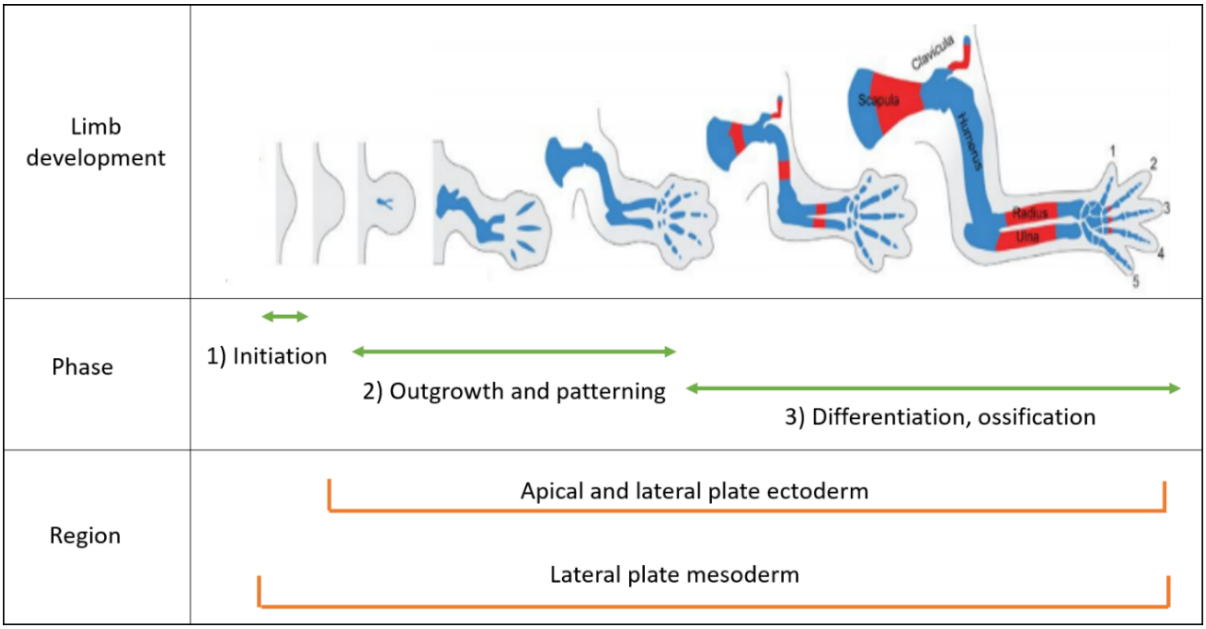


Figure 1.1. Limb development: phases and regions involved. Modified and used with permission from Lippincott Williams & Wilkins/Wolters Kluwer Health (Langman's Medical Embryology 12th edition) under the Creative Commons Attribution 4.0 International License (17).

The formation of cartilage (chondrogenesis) is a dynamic cellular process, where mesenchymal progenitor cells are recruited, then migrate and condense (18). This is followed by differentiation into the various types of cartilage tissue (hyaline, elastic and fibrous). The surrounding tissue and epithelium influence the differentiation of mesenchymal progenitor cells into chondrocytes (18). Chondrogenesis is tightly regulated by cellular interaction with the extracellular matrix (ECM), growth factors and environmental factors that can activate or suppress cellular signalling pathways and gene transcription, (Figure 1.2) (18).

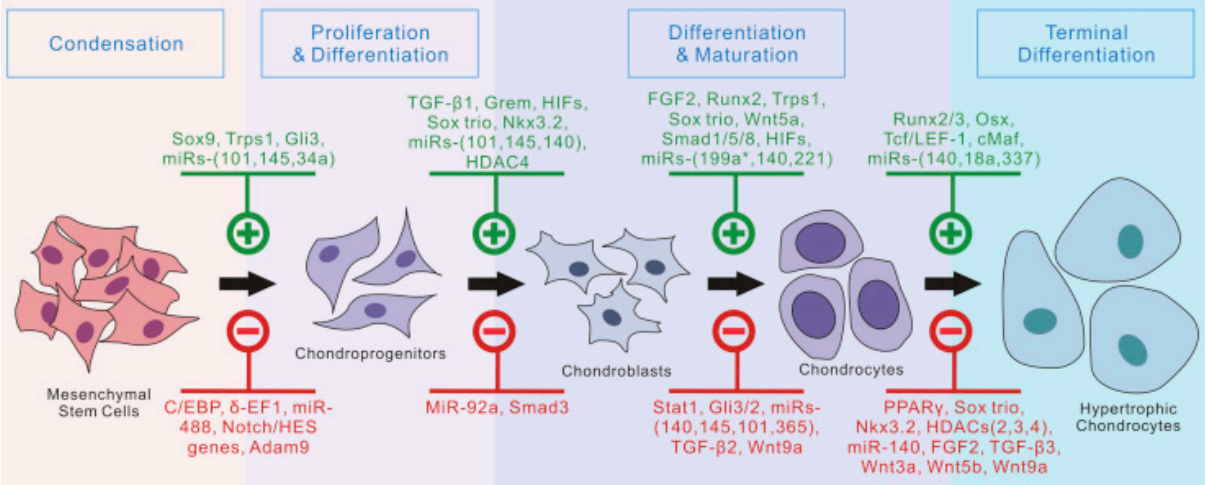


Figure 1.2. Mechanism of chondrogenic regulation. Signalling molecules, transcription factors, microRNAs and other regulators are listed. Positive regulators are shown in green, while the inhibitory regulators are shown in red. Used with permission from Genes and Diseases under the Creative Commons Attribution 4.0 International License (19).

Cartilage is a precursor to endochondral ossification, a process where bone gradually replaces cartilage in a systematic manner (Figure 1.3) during development (20). In adulthood, cartilage is evident on the articular surfaces and within the growth plates of bone, which permits growth during childhood (20). From mature skeletal age onwards, hyaline cartilage is apparent only at the lubricated articular surface of limb joints. This tissue is specialised to enable the reduction in friction at the moveable joint surface and serves as a shock-absorber to the underlying bone (21). Like other connective tissues, cartilage contains few cells and has a large amount of ECM, mostly in the form of collagens and proteoglycans (15). However, unlike other connective tissues, it lacks a blood supply and neural innervation, resulting in the lack of or reduction in the ability to repair and regenerate (2).

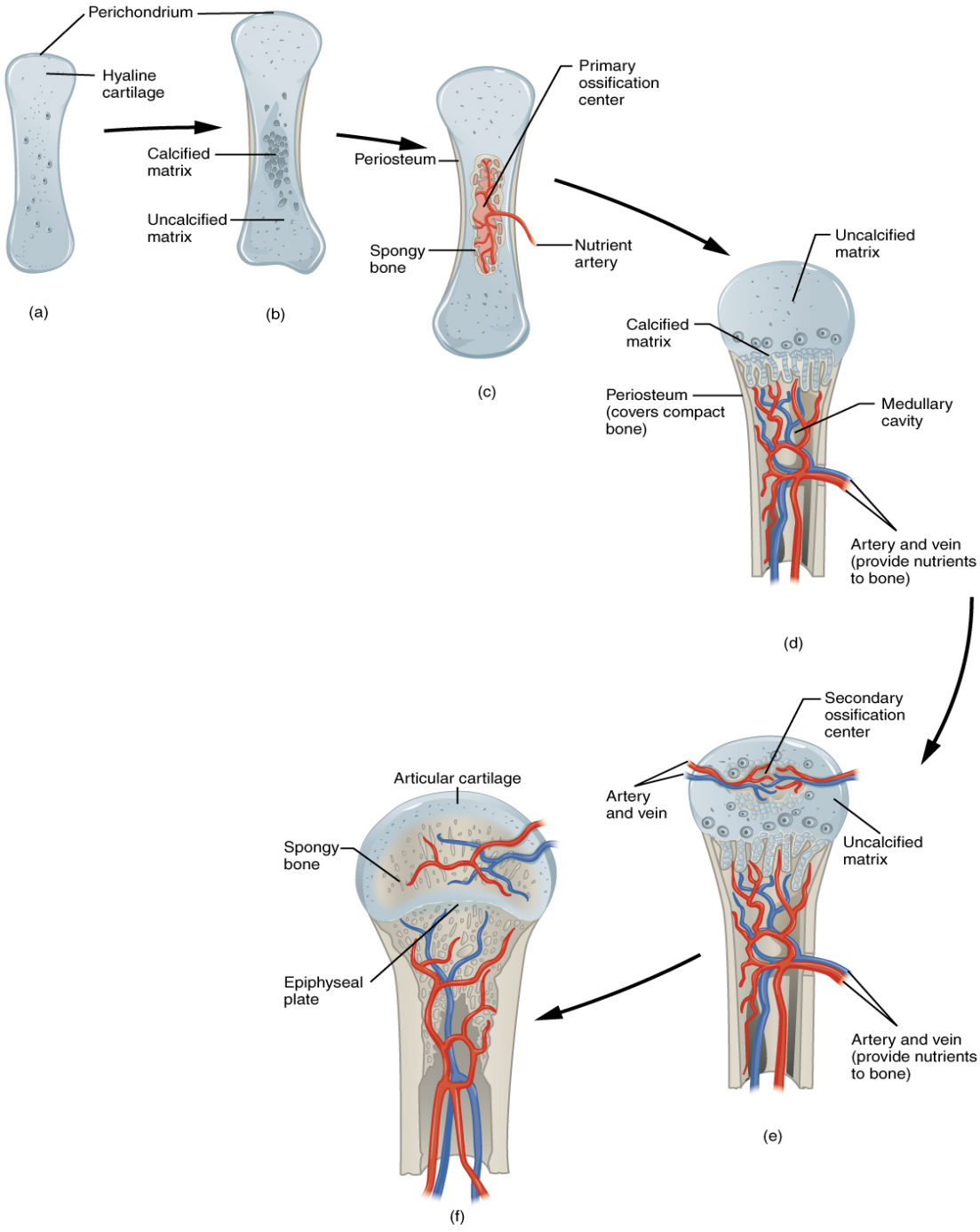


Figure 1.3. Endochondral ossification pathway. (a) Mesenchymal cells differentiate into chondrocytes. (b) The cartilage model of the future bony skeleton and the perichondrium form. (c) Capillaries penetrate cartilage. Perichondrium transforms into periosteum. Periosteal collar develops. Primary ossification centre develops. (d) Cartilage and chondrocytes continue to grow at ends of the bone. (e) Secondary ossification centres develop. (f) Cartilage remains at epiphyseal (growth) plate and the joint surface as articular cartilage. Used with permission from Anatomy and Physiology (OpenStax book) under the Creative Commons Attribution 4.0 International License.

1.2.3 COMPOSITION

Articular cartilage is composed of a dense ECM with only one cell type, the chondrocyte. The ECM (Table 1.1) is primarily composed of water, collagen type II, proteoglycans (15) and small amounts of glycoproteins and non-collagenous structural proteins.

Component	Wet Weight %	Dry Weight %	Function
Collagen	Type 2 – 10-20 Other types <2	50-75	Tensile resistance
Proteoglycans	5-10	20-30	Compressive and flow-dependent resistance
Chondrocytes	<5-10	<5-10	ECM regulation
Water and electrolytes (E.g. Sodium and Potassium)	60-80	-	Nutrition exchange with synovium and lubrication
Glycoproteins and other non-collagenous proteins	<1%	<1%	Organisation/structural maintenance of ECM

Table 1.1. Major components of the articular cartilage extracellular matrix. The total volume percentage of each element varies with the solid (dry) and fluid (wet) phase transformations that occur.

Collagen is the main component of the ECM, and in articular cartilage type II collagen predominates with other types being type I, IX, X and XI (22). Collagen molecules form fibres, which are crosslinked to create a fibrillar network that entraps other ECM components. The collagen network provides cartilage with its tensile strength (22). Hyaluronic acid (HA) is a large, non-sulphated glycosaminoglycan (GAG) molecule that facilitates the aggregation of proteoglycan (PG) monomers such as aggrecan (23). Aggrecan collects small, negatively charged, sulphated GAG (sGAG) molecules such as keratin sulphate and chondroitin sulphate. The net negative charge of the tissue generated by a large number of sGAG units attracts positively charged cations such as Na^+ (sodium) and K^+ (potassium,) which leads to an influx of water into the tissue in a non-loaded state (24). This effect provides articular cartilage with compressive strength and the initial ability to shock-absorb.

1.2.4 STRUCTURE- ARTICULAR CARTILAGE ZONES

Variations in structure and composition are seen in the different depth 'zones' of articular cartilage (Figure 1.4), enabling it to resist complex loads and forces encountered during daily activity (1).

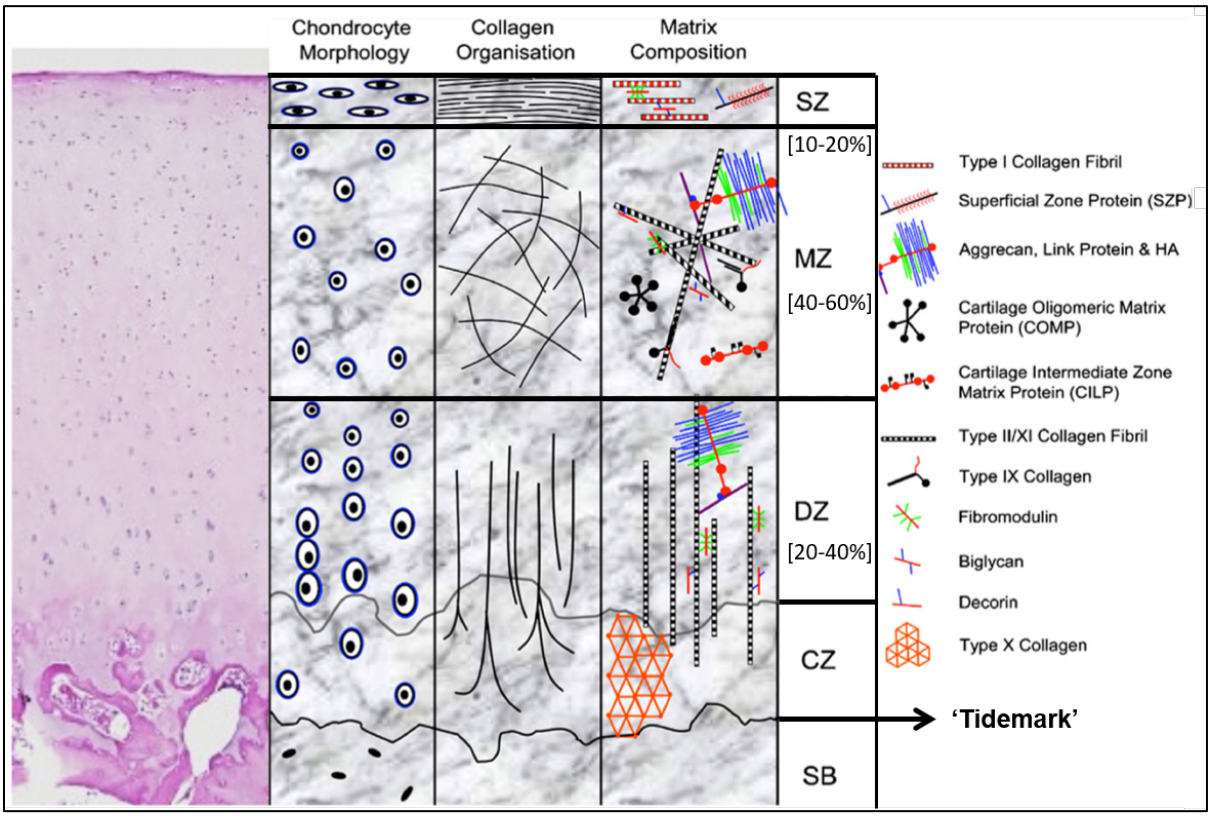


Figure 1.4. Hyaline cartilage morphology and structure. Superficial Zone (SZ). Middle Zone (MZ), Deep Zone (DZ), Calcified Zone (CZ) and Subchondral Bone (SB). Modified and used with permission from Frontiers in Surgery under the Creative Commons Attribution 4.0 International License (25).

The Superficial Zone (SZ), which is the outermost zone directly in contact with synovial fluid, contains dense collagen fibrils orientated parallel to the articular surface, with a relatively high density of ellipsoid-shaped chondrocytes (26). The SZ accounts for 10%–20% of cartilage depth and is essential for distributing loads over a larger surface area, thus protecting cells against impact loading, shear and tensile forces (1).

The Middle or "Transitional" Zone (MZ), contains collagen fibrils orientated obliquely, contributing to the resistance of shear loading encountered at the cartilage surface (26). Accounting for 40%–60% of the cartilage depth, the MZ is a transitional region between the

SZ and Deep Zone (DZ), and in comparison to the SZ, the MZ has a higher PG content and a lower density of spherically shaped chondrocytes (1).

The DZ or ''Radial zone'' is heavily abundant with collagen fibrils which are orientated perpendicular to the articulating surface and accounts for 30-40% of cartilage depth (1). The DZ has a higher PG content compared to the MZ and the lowest density of chondrocytes. These chondrocytes are vertically aligned (26). The DZ provides the highest resistance to compressive forces (1). The Calcified Zone (CZ) anchors cartilage to the underlying subchondral bone and is separated from the DZ by a demarcated calcified line, the "Tidemark" (27).

1.2.5 BIOMECHANICAL PROPERTIES

Hyaline cartilage is a smooth connective tissue with a lubricated weight-bearing surface, allowing for even distribution of mechanical load to the subchondral bone. Its specialised biomechanics relies heavily upon the structural and biochemical organisation, where water, proteoglycans and collagen interact to provide compression, tension and shear properties (28, 29).

During compression, hyaline cartilage functions as a biphasic medium, consisting of 2 phases: a fluid phase and a solid phase (28). Water is the primary component of the liquid phase, while the porous and permeable ECM characterises the solid phase. The relationship between PG aggregates and the interstitial fluid provides compressive resistance through negative electrostatic repulsion (30). Contact forces to the articular surface during joint loading (compression) causes an immediate increase in the interstitial fluid pressure, leading to fluid flow out of the ECM, this reverses with the removal of the compressive load (30). The low permeability of articular cartilage prevents fluid from being rapidly squeezed out of the matrix (28, 31). The bones of the joint confine the cartilage under the contact surface, creating a boundary designed to restrict mechanical deformation.

Another important, specialised function of articular cartilage is viscoelasticity, viscoelastic materials display both viscous and elastic material properties, and exhibits time-dependent behaviour when subjected to a constant load or deformation (Figure 1.5) (32). When constant compressive stress is applied to the tissue, its deformation increases with time, and it deforms

or creeps until an equilibrium value is reached (33). Similarly, when the cartilage is deformed and held at a constant strain, the stress will rise to a peak, which will be followed by a slow stress-relaxation process until an equilibrium value is reached (33). These properties allow cartilage to counteract large amounts of load, leading to reduced stress acting on the solid matrix during times of high demand joint activity.

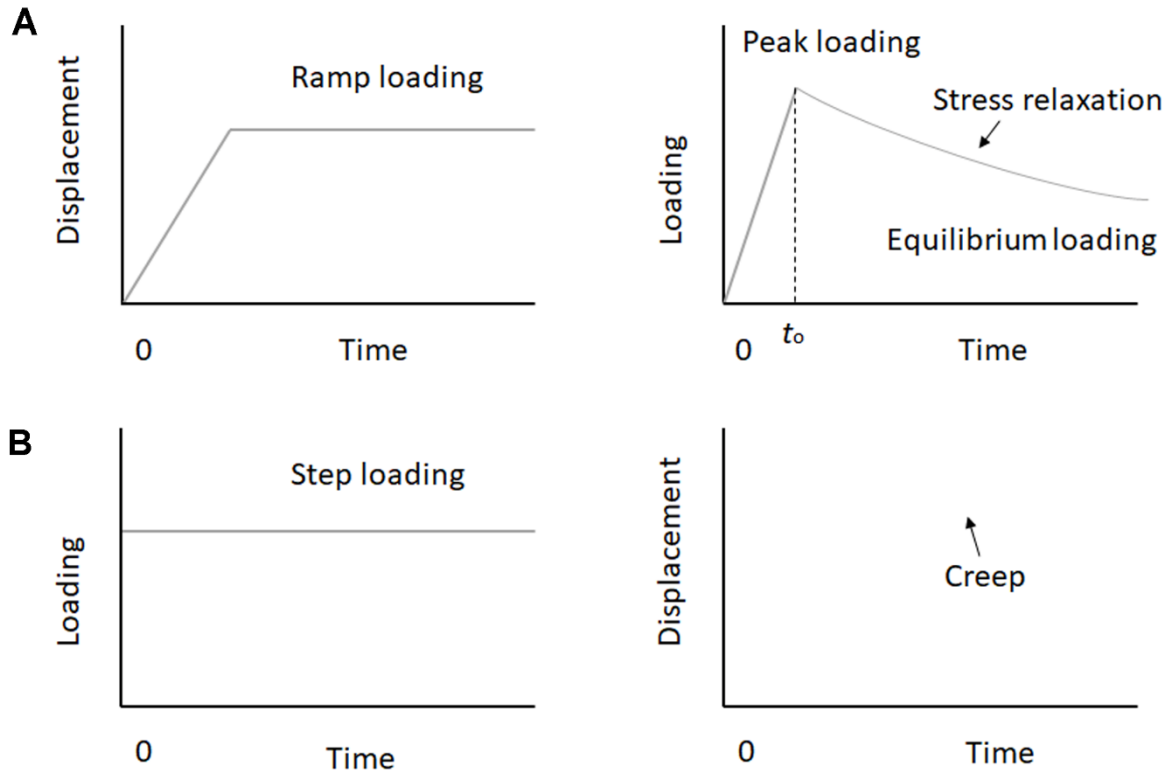


Figure 1.5. Viscoelastic behaviour of articular cartilage. (A) In a stress-relaxation test, displacement is continuously applied until a desired level of compression is reached. This displacement results in a rise in force, followed by a period of stress relaxation until an equilibrium force value is reached. (B) In a creep test, a step force is suddenly applied (stepwise) onto cartilage, resulting in a transient increase in deformation (i.e., creep). Modified and used with permission from Medicine and Science in Sports and Exercise under the Creative Commons Attribution 4.0 International License (34).

Tensile strength is provided by the sliding of cartilage units against each other which leads to stretching of the elastic collagen fibrils in the superficial tissue zone (32). Shear associated deformation is evident during normal joint articulation, and the shear strain reduces

proportional to the depth of cartilage tissue, this is due to the structural variation from a tangential to arch-like collagen fibre orientation leading to a larger shear-modulus in deeper zones compared to the superficial zone (35).

The friction coefficient of health articular cartilage is described as 5.0×10^{-3} - 2.5×10^{-2}, which is lower than that of any synthetic material (24, 36). Low friction between articular surfaces can be contributed by elasto-hydrodynamic lubrication squeeze film lubrication (synovial fluid), boundary lubrication, and fluid pressurization (37-42). Under load, the interstitial fluid of cartilage de-pressurizes over time and the compressive and frictional forces are increasingly supported by the solid components of the cartilage matrix (e.g., the collagen network), and boundary lubrication becomes the dominant mechanism of lubrication (43, 44). Deficient or defective lubrication is likely to play a key role in the development of osteoarthritis (45, 46); however, surprisingly few studies have investigated the consequences of tribology (lubrication, friction and wear) on the cartilage disease and tissue engineering, which could be due to the lack of suitable model systems (45-47).

1.2.6 AGEING PROCESS

Age-related changes in hyaline cartilage affect both the cells and the ECM. A change in either will aggravate the other since an altered ECM leads to increased mechanical stress on cells, while cell loss/dysfunction leads to the deficient regulation of the ECM (48).

With increasing age, the zonal distribution of chondrocytes changes; however, the total number of chondrocytes generally remains unchanged. Chondrocyte numbers reduce significantly in the superficial zone, whereas there is an increase in the number of cells in the deeper layers where proliferation leads to ‘cell clusters/cloning’ (49). This abnormal chondrocyte activation, however, does not contribute significantly to repair. With age, the matrix- water content reduces, leading to an increase in the compressive stiffness (50); furthermore, the size of PG aggregates within the ECM decreases, ultimately affecting the pore size distribution and solute permeability. Age-related changes to hyaline tissue composition and structure can lead to micro-tears which can propagate over time into significant and symptomatic defects compromising joint function.

1.2.7 POST TRAUMATIC ARHTRITIS

Post-traumatic arthritis (PTA), results from either direct chondral damage secondary to trauma such as motor vehicle accidents or sporting injury, or from repetitive microtrauma such as occupational injuries (51). Between 20-50% of PTA patients are reported to develop osteoarthritis (OA), with PTA accounting for roughly 10-15% of osteoarthritis cases (52, 53). Generally, symptoms of PTA (swelling and pain) resolve spontaneously, the persistence of symptoms beyond 6 months is considered chronic and can lead to early onset PTA-related osteoarthritis (PTOA) (51). Common causes leading to PTOA include intra-articular fractures and meniscal, ligamentous and chondral injuries (54). Given the earlier onset of symptoms and the level of disability to young working patients, PTA is a key focus of research with the aim of preventing/decelerating, the need for joint replacement. Furthermore, compared to OA, PTA can be identified early and acted upon prior to the development of a significant change in the arthritic environment (51).

Although many agents have been tested in preclinical studies, there are no approved therapies targeting acute PTA; therefore, chronic PTA can't be prevented. The primary goals of PTA treatment are symptomatic relief leading to a reduction in pain and loss of function. These treatments include anti-inflammatory agents (non-steroidal anti-inflammatory drugs or intra-articular injections of cortisone), low impact exercise (e.g. swimming) and lifestyle modification such as adequate weight control (51). However, not all patients benefit from non-operative conservative management, and chronic arthritis can develop for which surgery is the next option.

An increased understanding of the molecular, mechanobiological and cellular events involved in the pathogenesis of chronic PTA may open interesting perspectives concerning new therapeutic opportunities and thereby offer patients safer and more effective drugs (55). Many molecules have been explored as potential targets for treatment in preclinical studies which will be detailed in the next section: Current treatment strategies.

Irrespective of the nature of the injury, cartilage is unable to self-repair (2) due to its avascular and aneural nature (2, 24). This limited capacity to intrinsically heal is a significant challenge in the field of orthopaedics. Overtime with no treatment, fibrocartilage is formed at the defect site; this is a stiff form of cartilage that is functionally different from hyaline cartilage (56).

Precise repair of tissue is required to preserve articular cartilage function, which is highly dependent on its oriented architecture (23). The unique and complex structure of articular cartilage makes it challenging to adequately repair damage (57).

Notably, the knee is the most commonly injured joint with respect to chondral injuries and the development of PTOA (58, 59), approximately 60% of diagnostic knee arthroscopies report significant defects (60). The knee is the largest joint in the body, and there is a substantial transmission of force through it with daily activity and in traumatic injury patterns (61). Therefore, research is mostly focussed on chondral defect repair techniques using the knee joint as a model of articular cartilage.

1.3 CURRENT TREATMENT STRATEGIES

1.3.1 NON-SURGICAL OPTIONS

Physical activity and pharmacological therapies

The main aims of non-surgical treatments are to improve function and reduce pain. Physical activity and exercise are non-invasive, non-pharmacological strategies that can assist with symptom burden and overall health (62, 63). Notably, no pharmacological agent has been able to promote cartilage regeneration effectively.

Analgesic pharmacologic agents assist with pain control for patients with symptomatic chondral lesions, and adequate analgesia can improve daily functional activity; however, each agent has its own safety profile, and the long-term use of analgesics can be systemically detrimental (64). Supplements such as glucosamine and chondroitin sulphate (CS) can help control pain and slow cartilage degradation (65). Glucosamine and CS serve as building blocks for glycosaminoglycan (GAG) and hyaluronic acid (HA) synthesis and are thought to facilitate and theoretically promote cartilage repair (25). The analgesic effects of these drugs have been shown to be comparable to other oral analgesics; however, there are no high-quality prospective studies to support this (66).

Intra-Articular Pharmacological Therapies

Pharmacological agents can be directly administered into the knee joint in an injectable form; these include Orthobiologics, Corticosteroids (CS), Hyaluronic acid (HA) and Platelet Rich Plasma (PRP).

Orthobiologic strategies investigated to treat OA include biological inhibitors, chemo/cytokine and growth factors. Injection of ECM-degrading enzyme inhibitors, such as matrix metalloproteinases (MMPs) (67), and pro-inflammatory factors, such as interleukin- 1 (IL-1) (68) and tumour necrosis factor alpha (TNF-α) (69) could inhibit pathological signalling pathways. Endogenous stem/progenitor cell recruitment using chemo- or cytokine-attractants, such as TGF-β (70), or growth factors, such as bone morphogenetic proteins (BMPs), insulin-like growth factor-1 (IGF-1), and fibroblast growth factor (FGF-2) could stimulate cartilage and bone regeneration and potentially treat OA (71, 72).

Despite the successful use of all these agents in reducing the progression of chronic PTA in animal models, only one small randomised pilot clinical trial has been performed (73). In this study, IL-1Ra injected intra-articularly within 30 days of ACL injury, reduced pain and improved function at 2 weeks compared to placebo (73). Although this strategy has proved to be efficacious in the early postinjury phase, the results obtained must be confirmed in larger and longer-term studies to demonstrate prevention of chronic PTA.

Intra-articular (IA) CS injections are indicated in the management of acute joint pain or inflammation associated with known cartilage injury in patients who have failed or exhausted the use of oral analgesic therapies (74). Symptomatic relief is reported to last up to six weeks; however, there are well documented idiosyncratic responses and a paucity of clinical studies that support their efficacy (75). Cartilage degradation and arthropathy have been reported to occur with repeated IA-CS injections; thus, no more than three injections are recommended per year in any one joint and should be used judiciously (76, 77).

HA is a large, naturally occurring, viscoelastic GAG that is present in both the articular cartilage and synovial fluid (78). Physiologically, HA aids in the absorption and distribution of forces during high-impact activities while acting as a viscous lubricant during slow movements (79). Supplementation with IA-HA aims to provide and maintain intra-articular lubrication leading to an increase in the viscoelastic properties of the synovium, this is known as 'viscosupplementation'(80). The development of higher molecular weight IA-HA formulations > 500 kDa (kilodaltons) have been shown to provide up to 6 months of pain relief (81, 82). However, there is no evidence to support a persistent increase in HA content after the rise from the initial injection (83). A high incidence of side effects have been reported including

pain at the injection site (1-33%), local joint pain and swelling (<1-30%) and local skin reactions (3-21%) (84). Furthermore, there is a distinct lack of prospective outcome studies that have analysed the effectiveness of HA injections in cartilage repair. Therefore, considering the cost, risk profile and complexity of the intervention, this option is recommended against (85).

PRP is a plasma-based suspension rich in platelets; it can be autologously derived and is prepared by using centrifuged blood (86). Platelets are rich in cytokines and growth factors which can help stimulate cellular growth, proliferation, vascularisation, regeneration and collagen synthesis (86). PRP can be used in leukocyte-poor and leukocyte-rich form, based on the collection and separation method. The leukocyte-poor formulation has been shown to better in several studies (87, 88), which could be due to the significant inflammatory effects associated with leukocytes (87, 88). Overall with respect to clinical data, IA-PRP injection is a new technique, which has been poorly studied; there is no consensus on the preparation technique, platelet concentration, number and frequency of doses to be used (85, 89).

Intra-Articular Stem Cell Therapies

Mesenchymal stem cells (MSCs), can be sourced autologously from different tissues and are associated with immunomodulatory functions that can assist with anti-inflammatory effects and in promoting new cartilage-like cells *in vitro* (90) and *in vivo* (4). The efficacy of IA-MSCs injections has been tested in several small randomised controlled studies (91); however, these are small studies and are at serious risk of bias. A recent meta-analysis demonstrated that IA-MSCs have limited evidence in pain relief and functional improvement associated with osteoarthritis of the knee (5). Furthermore, current evidence didn't support the use of IA-MSCs for improving cartilage repair in knee osteoarthritis (5). Given the use of human cells in this IA approach, there is a strong recommendation against this therapy, until replication of high quality, large randomised controlled trials are performed and reported (85, 92)

1.3.2 SURGICAL OPTIONS

Acute high-grade chondral injuries in younger patients and the failure of symptomatic control with non-operative modalities are indications for surgical repair (93, 94). The goal is to debride/remove flaps/loose tissue and allow for healing with the proximation of blood or with cell-based repair (Figure 1.6) (61). Surgical chondral repair options include Microfracture (MF), Autologous Chondrocyte Implantation (ACI) and Matrix-induced Autologous Chondrocyte Implantation (MACI) (6, 21, 95, 96) which are indicated based on patient factors and defect sizes (Table 1.2).

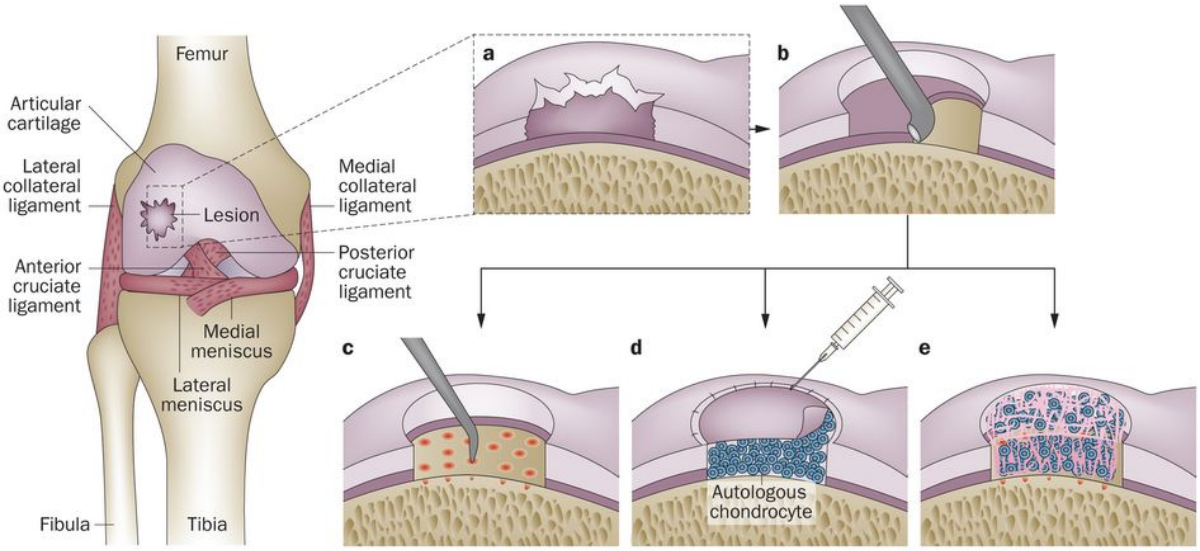


Figure 1.6. Current surgical cartilage regeneration techniques. (A) A full-thickness chondral lesion. (B) Initial debridement of the lesion to allow for healthy and stable margins. (C) MF: Channels are created using a 45° awl to penetrate the subchondral bone, allowing MSCs to migrate from the marrow to the cartilage defect. (D) ACI: The debrided lesion is filled with autologous chondrocytes and covered with a periosteal flap membrane. (E) MACI: The autologous chondrocyte population is expanded in vitro and then seeded onto an absorbable 3D matrix prior to implantation. The scaffold is then secured with fibrin glue. Used with permission from Nature reviews, Rheumatology, under the Creative Commons Attribution 4.0 International License.

Lesion Size (Total surface area, cm^2)	Treatment options
< 1.0	Debridement, Microfracture
1.0 -2.0	Microfracture, ACI, MACI
2.0-3.0	ACI, MACI
>3.0	ACI or allograft

Table 1.2. Operative treatment indications for chondral repair based on lesion size. ACI, autologous chondrocyte implantation; MACI, matrix-assisted autologous chondrocyte implantation.

Microfracture is an arthroscopic technique, where the subchondral bone is fractured to allow blood from the bone marrow to proximate, clot and stimulate cartilage repair (Figure 1.6C) (7). ACI is a two-step procedure in which chondrocytes isolated from non-weight-bearing portions of joints, are expanded *in vitro* and then reimplanted into an area of cartilage damage with a periosteal flap (Figure 1.6D), (61). MACI is a progression of the ACI technique, in which cultured chondrocytes are expanded *in vitro* then embedded within a matrix/scaffold and delivered as a cell-scaffold construct which is attached using fibrin glue without the need for suturing/anchorage of the implant (Figure 1.6E) (97).

Knutsen et al (2007), demonstrated no difference in clinical, histological and radiographic results five years post-surgery in patients who underwent microfracture versus ACI treatment (9). A randomised control trial comparing ACI to MACI in 91 patients with chondral knee defects showed no significant improvement in the overall international cartilage repair scores (97). Therefore, it is evident that there is no superiority of the newer, more expensive and technically demanding ACI and MACI techniques compared to the affordable and efficiently performed microfracture technique. Thus, why microfracture remains the go to standard surgical treatment option for chondral defects in the knee today (9).

Microfracture associated studies show better functional and symptomatic outcome in younger patients with small isolated lesions $< 2\ cm^2$ in total surface area (61). Longer-term studies, however, show a significant reduction in clinical outcome at 36-month follow-up (98). Therefore, this technique can only be provided to a small subset of patients and lacks a

reliable long-term result. Reasons for poor long-term outcomes include fibrocartilage production, patient age, functional level, location and defect size (98-100).

Techniques such as osteochondral grafting and transplantation are not discussed, as they are indicated for osteochondral repair, which is outside the scope of this thesis (focus on isolated chondral repair).

1.4 EMERGING TREATMENT - CARTILAGE TISSUE ENGINEERING

Poor long-term results from the previously mentioned treatment modalities led to the emergence of research focussed on cartilage tissue engineering (TE). Langer and Vacanti (1993), first described TE as 'an interdisciplinary field which applies the principles of engineering and life sciences toward the development of biological substitutes that restore, maintain, or improve tissue function' (11).

Cartilage TE involves using either a mature cell source or a progenitor source which can be expanded before being embedded within a 3D scaffold. Subsequently, the engineered construct is exposed to growth factors and molecules which enables for differentiation into specific tissue. The overall aim is to develop bio-mimetic tissue resembling hyaline cartilage. Initially, TE was based on three domains: cells, scaffolds and growth factors/cytokines. Engineered components resembling hyaline cartilage had a significant reduction in mechanical properties when compared to native cartilage (101, 102). Over time, this has led to the additional focus on the biomechanical properties, leading to the incorporation of 'physical stimulation' as the fourth essential domain (Figure 1.7).

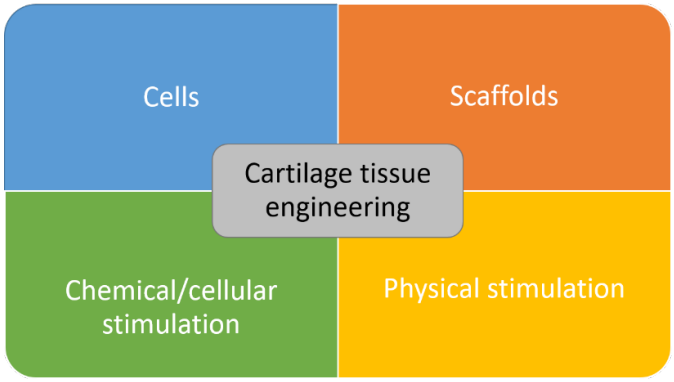


Figure 1.7 (Left). General components of cartilage tissue engineering.

Once the tissue is generated or constructed, the next step is to implant it into the host. The approach of transferring bench-made constructs to the host represented a significant

challenge due to the lack of precise integration into complex defect morphologies. The timely emergence of 3D bioprinting has opened exciting options for *in-situ* tissue delivery, as opposed to the manual transfer of constructs (pre-generated using a bench-based approach) into the defect. Furthermore, 3D bioprinting can be utilised to deliver constructs in an efficient and tailored approach, overcoming the unique and intricate morphological patterns associated with cartilage damage/defects. The combination of tissue engineering and bioprinting as an overall technique is referred to as 'biofabrication'. This concept will be discussed more in detail in section 1.5.1.

1.4.1 CELLS

Different cell potencies and types (Figure 1.8 and Table 1.3) from various sources have been utilised in cartilage tissue engineering. Early studies incorporated committed chondrocytes, with sources ranging from neonatal to adult tissue (103-106). Chondrogenesis has been shown *in vitro*; however, significant drawbacks include limited tissue availability, low cell numbers, donor site morbidity and cellular dedifferentiation *in vitro* (107, 108). Expanded autologous chondrocytes have been used as part autologous chondrocyte transplantation/implantation (ACI); however, no long term clinical improvement (>24 months) or superiority has been shown compared to microfracture (9).

Pluripotent stem cells (PSCs), including embryonic stem cells (ESCs) from the blastocyst and induced pluripotent stem cells (IPSCs), have also been used in cartilage tissue engineering (109-112). A significant chondrogenic potential is obtainable using ESCs with the added advantage of a theoretically unlimited ability to replicate. Issues with the use of ESCs include ethical concerns due to embryonic tissue utilisation, tumorigenicity risk and immune response activation leading to rejection (113-116). When sourced autologously, IPSCs, can overcome some of the issues associated with using ESCs, including ethical concerns and the activation of an immune response. Several IPSCs sources have been used, and the isolated primary cells need to be reprogrammed back into a stem cell-like lineage (117). Once reprogramed, they must be able to produce the following transcription factors: Oct3/4, Sox2, c-Myc, and Klf4, which are involved in cell proliferation, pluripotency, and differentiation (118, 119). Recently, Li et al (2016) induced peripheral blood cells to pluripotent stem cells, the abundance of blood compared to other tissue sources makes this a significant

development (120). Reprogramming IPSCs can be achieved using viral and non-viral vectors, which is a complex and time-consuming process.

Finally, Adult MSCs (121-123) have become a significant player in tissue engineering, particularly in forming chondrogenic tissue (124-126). Many sources of MSCs (Figure 1.8) have been identified and evaluated, irrespective of the source, MSCs can differentiate into mesodermal lineage such as chondrocytes, osteocytes, myocytes and adipocytes (127). Advantages of using MSCs include an abundance of source and cell numbers, readily harvestable and isolated (128). As they can be derived autologously, they carry less risk than embryonic stem cells, while still maintaining the ability to replicate for many phases.

Bone marrow (BM) was an early source of MSCs used; BM-derived MSCs are multipotent and produce tissue of mesodermal lineage (129). BM can be harvested autologously and doesn't pose the ethical, tumorigenic, or immunogenic risk associated with the use of pluripotent stem cells(129). The disadvantages of using BM include low tissue volume and low cell volume (130-132). BM-derived MSCs are comparable (133, 134), if not inferior, with respect to chondrogenic potential when compared to adipose-derived MSCs (ADSCS) (135-137). These factors, in addition to less invasive tissue harvesting techniques, make adipose tissue a more desirable source.

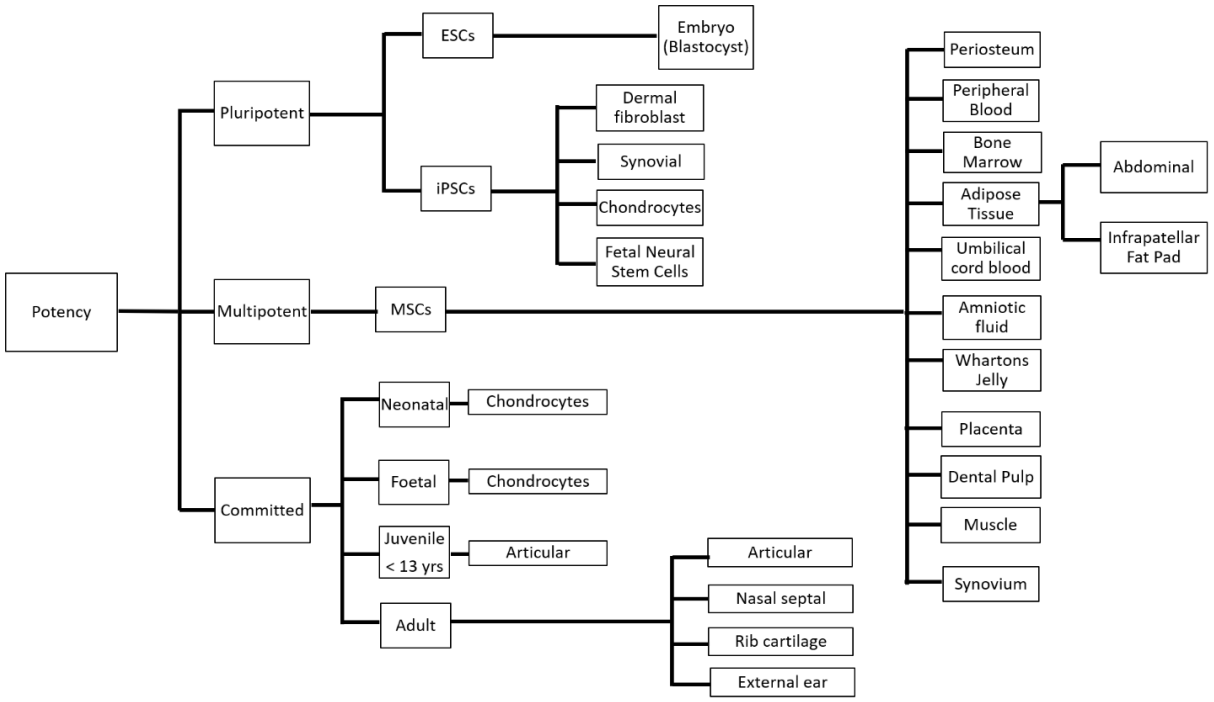


Figure 1.8. Different cells used in cartilage tissue engineering based on potency. Embryonic stem cells – ESCs, Induced pluripotent stem cells -IPSCs, and Mesenchymal stem cells – MSCs.

Cells	Types	Advantages	Disadvantages
Pluripotent stem cells	Embryonic stem cells	Indefinite self-renewal Multiple lineages	Ethical concerns Tumorigenicity Immune rejection
	Induced pluripotent stem cells	Autologous Indefinite self-renewal	Tumorigenicity Cellular reprogramming Instability
Mesenchymal stem cells	All	Autologous Abundant Easily harvested	Lower chondrogenic capacity compared to pluripotent stem cells
Chondrocytes	Foetal	Low immunogenicity	Limited availability
	Neonatal	Low immunogenicity	Limited availability
	Juvenile	Low immunogenicity	Limited availability
	Adult	Autologous	Limited availability Donor site morbidity De-differentiation

Table 1.3. Comparison of cell sources used in cartilage tissue engineering.

The two major sources of ADSCs are the abdominal fat and infrapatellar fat pad (IFP). The IFP is an emerging source of MSCs for cartilage tissue engineering (138), although there is less fat volume in the IFP compared to abdominal fat, chondrogenic potential has been shown to higher in ADSCs sourced from the IFP (139, 140). Compared to abdominal fat-derived ADSCs donor matched IFP-derived ADSCs displayed 5- and 8-fold higher levels of aggrecan (ACAN) and collagen 2 (Col 2) expression respectively (139). Dragoo et al (2003), initially used the infrapatellar fat pad (IFP) to source MSCs for tissue engineering (141). The IFP develops between the bones of the knee joint (Figure 1.9) and is located within the joint capsule, near the distal femur where knee defects commonly occur. It can be opportunistically harvested during knee arthroplasty or arthroscopy, and stem cells isolated from this tissue demonstrate high chondrogenic potential (138). Compared to arthroscopy, the entire IFP can be harvested using arthroplasty, leading to an increased number of cells; however, the percentage of live cells is the same using both techniques (138). Therefore, if enough infrapatellar fat can be harvested arthroscopically, this could pave the way for the minimally invasive harvest of tissue containing IFP-derived MSCS.

More recently, human articular cartilage progenitor cell (hAPCs), also known as cartilage progenitor cells (CPCs) or cartilage-derived stem/progenitor cells (CSPCs), have been isolated from articular cartilage with evidence of chondrogenic potential (142). These cells were first separated from chondrocytes by Dowthwaite et al (2004), by demonstrating that they selectively attach to fibronectin-coated tissue culture polystyrene (143). However, there is no specific biomarker panel to date which can clearly distinguish APCs from expression is thought to help characterise APCs. This effect of APCs raises the theory of whether they predominate in the superficial zone (SZ) of cartilage tissue. If so, this could lead to the creation of cartilage using different cell types in layers that can mimic the different depth ''zones'' of cartilage.

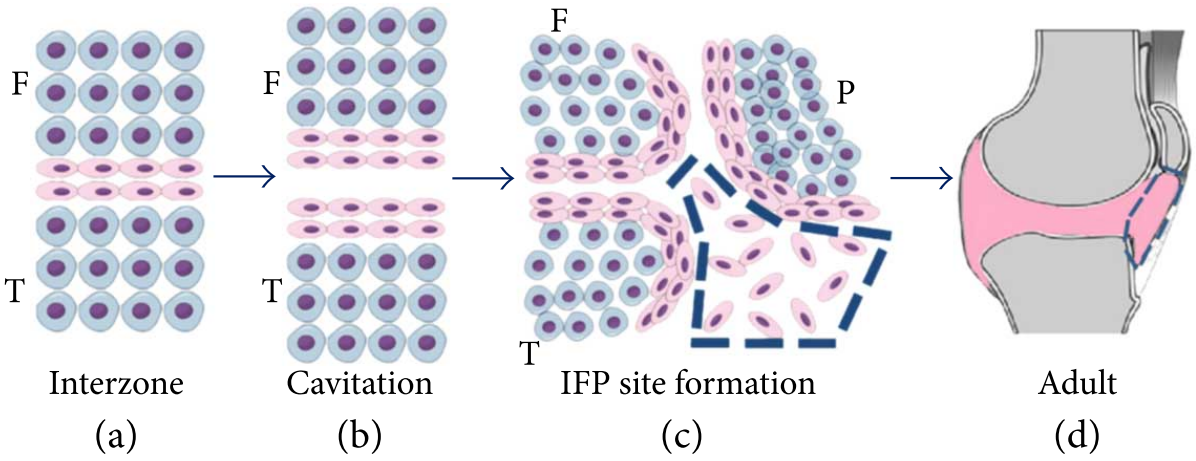


Figure 1.9. Ontogeny of the infrapatellar fat pad (IFP). During embryonic development, (a) a dense mesenchyme tissue arises between the chondrification of the femur (F) and tibia (T), the interzone (flattened cells in pink). (b) This is followed by cavitation in between this region. (c) By the 9th week of human development, a triangular space composed of a mesenchymal tissue becomes visible below the patella (P) (highlighted by the blue dashed). (d) In adulthood, interzone cells will have contributed to several joint structures (pink), including the IFP (highlighted by the blue dashed). Modified and used with permission from Stem Cells International under the Creative Commons Attribution 4.0 International License (144).

1.4.2 SCAFFOLDS

Scaffolds are primarily used in tissue engineering to provide structural support to native tissue (145, 146). Native cartilage contains structural proteins (e.g. collagen and elastin), adhesive proteins (e.g. fibrin and laminin) and proteoglycans (e.g. chondroitin sulphate and HA) (147). Cells must be able to attach to either ECM or be in close contact with other cells to function

(paracrine) (148). Scaffold-free designs can produce chondrogenesis; however, rely solely on cell-cell contact and require significant cell numbers (149). Without a scaffold, cells and their associated ECM lack mechanical and structural integrity leading to high levels of cytotoxicity.

Scaffolds can be classified as natural polymers, synthetic polymers or hybrid (Figure 1.10). Natural scaffolds are more biocompatible, display less degradation related toxicity and express native binding sites, thereby mimicking the natural ECM (145). They generally exhibit inferior mechanical properties compared to synthetic options (145, 150), which can be altered to control degradation and optimise biomechanical strength.

Several solid polymers and co-polymers have been investigated with respect to cartilage tissue engineering; their major drawback is the difficulty repairing irregular defects which exhibit complex morphologies. Softer polymers with the ability to fill defects and subsequently solidify show promise in cartilage tissue repair (151).

Hydrogels exhibit biomimetic properties like that of soft tissue, such as being printed into complex morphologies in a liquid state as a filler (152) which can subsequently be solidified using a cross-linking process. A major limitation is inferior mechanical stability (146, 153), which can be improved by cross-linking of the material (154); however, to date, no studied hydrogel has been able to closely match native human cartilage. Native human knee cartilage on average has a compressive Youngs modulus has been reported to range between 2.0 - 10.0 MPa shortly after loading and 0.4- 0.6 MPa long after loading (155, 156); however, is dependent on the level of stress (walking or running) and the specific location tested (femoral condyles or patellofemoral surface). Using prefabricated scaffolds up to 0.25-0.50 Mpa of compressive modulus has been achieved (155). Using high percentage by weight hydrogels (20%) up to 1 MPa in compressive strength has been achieved (157); however, such high weight compositions are detrimental to cellular and matrix maturation within constructs (157). Furthermore, using a higher crosslinking density have been shown to produce higher compressive properties in acellular scaffolds (158), but need to be balanced and optimised against cytotoxicity and genotoxicity (159). In fact, some studies investigating the effect of hydrogel crosslink density on matrix production by chondrocytes, show that the lowest crosslink density hydrogels (35-50 kPa) best supported matrix deposition (160, 161).

Therefore, a major consideration is to balance mechanical strength with matrix maturation and biology (162), which traditional regenerative approaches can't restore (163).

Crosslinking is necessary for the state change of hydrogels from liquid to a semi-solid, which enables cell-laden deposition in a 3D form. Crosslinking can be obtained using physical (reversible), chemical (irreversible) or light-associated reactions (irreversible) (164-167).

Specifically, gelatine-based hydrogels exhibit high cytocompatibility and biodegradability in physiological environments (168-170). The addition of the methacrylate/methacrylamide (MA) group to gelatin enables light assisted cross-linking of the material, thus mimicking the natural ECM of cartilage (171, 172). Further addition of Hyaluronic Acid (HA), a natural glycosaminoglycan found in cartilage can promote cell spreading (173). Notably, HA can also be methacrylated (HAMA) to increase overall material stiffness (173, 174); however, this has been shown to impede cartilage/matrix production unless used in a protective manner such as a core shell approach (175, 176). Among hydrogel-based scaffolds, Gelatin-Methacryloyl/Hyaluronic Acid (GelMA/HA) has been used for *in vitro* biofabrication (177) and for *in vivo* animal models of chondral repair (178).

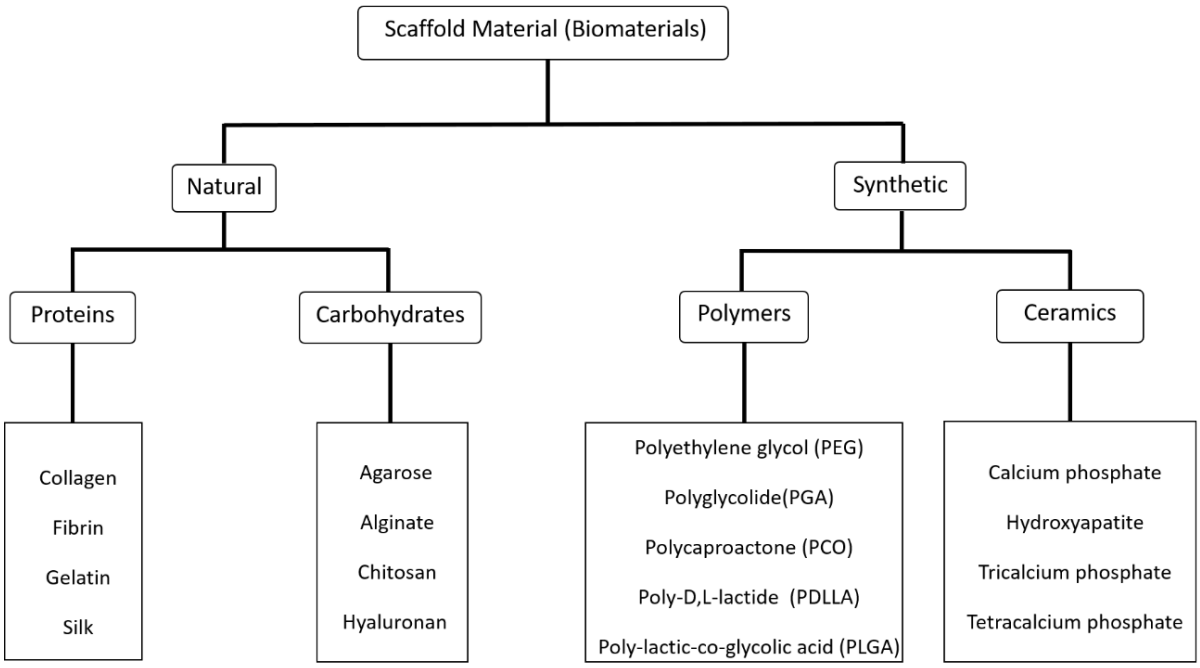


Figure 1.10. Different types of scaffold biomaterials used in cartilage tissue engineering

1.4.3 CHEMICAL STIMULATION: SIGNALLING MOLECULES

Molecules, including growth factors (GFs) and soluble non-protein chemical compounds, chemically regulate cell behaviour (Figure 1.11). Molecules bind to surface receptors on stem cells to activate intracellular signalling pathways controlling cellular proliferation, differentiation and synthesis (179, 180). MSCs have an important paracrine effect on cartilage formation and help regulate and control the environment with respect to inflammatory responses (181, 182). Chondrogenic differentiation can be achieved using growth factors individually or in combination, Sekiya et al (2005), demonstrated that the combination of transforming growth factor (TGF) -Beta 3 with bone morphogenetic protein (BMP)-2 induced more chondrogenesis in MSCs compared to using either TGF-B3 with BMP-4/BMP-6 or TGF –B3 by itself (183).

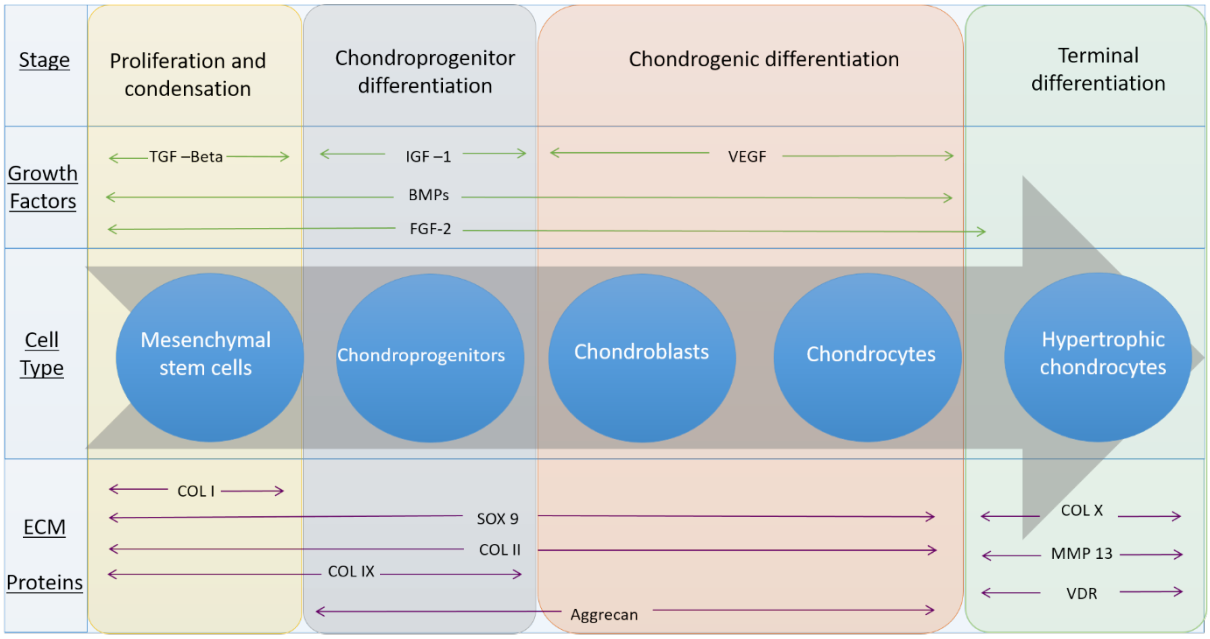


Figure 1.11. Mesenchymal stem cell expansion and chondrogenic differentiation pathway. Growth factors used for stimulation and ECM protein production is shown based on the stage of the pathway. Transforming growth factor-beta (TGF-Beta), Insulin-like growth factor 1 (IGF-1), Bone morphogenetic protein (BMP), Vascular endothelial growth factor (VEGF), Collagen (COL), Matrix metalloproteinase 13 (MMP-13) and Vitamin D receptor (VDR)

Emerging molecules that could be potential modulators of engineered cartilage include hyaluronic acid. which has been shown to stimulate chondrogenesis and reduce hypertrophy in BM-derived MSCs(184), ADSCs and chondrocytes(185). Similar effects have been

demonstrated using matrilin 3 to cultures of BM-derived MSCs(186). The addition of kartogenin has also induced chondrogenic differentiation in MSCs in a mouse model of OA(187); however, the therapeutic dose and long-term in vivo efficacy of kartogenin is yet to be determined, limiting its use(188). Biophysical stimuli such as glycosaminoglycan-depleting enzymes (such as chondroitinase ABC) or crosslinking agents (such as lysyl oxidase-like 2 (LOXL2)) have also been used to increase collagen content and to form collagen crosslinks, leading to improved tensile properties in neocartilage (189-191). The combination of TGFβ1, chondroitinase ABC and LOXL2 applied after aggregate redifferentiation generated neocartilage with tensile modulus and ultimate tensile strength values roughly 2 X those of untreated neocartilage(192). Overall, these emerging studies suggest that novel biochemical and biophysical stimuli could be used for effective neocartilage formation.

1.4.4 MECHANICAL/PHYSICAL AND ENVIRONMENTAL STIMULATION

Mechanical stimulation can be used to mimic the physical and environmental forces produced in the native joint can be strategically used to improve the formation and maturation of engineered cartilage. Proven stimuli that can be used to promote chondrogenesis include intermittent hydrostatic pressure (193), compressive loading (194-196), surface motion (shear) (197), oxygen tension (198, 199), electromagnetic (200, 201) and ultrasonic conduction (202).

Bioreactors are machines capable of providing biological and physical stimulation to the cell culture (203). Such systems provide a 3D environment that can improve the quality of engineered tissues. Various bioreactor designs (Figure 1.12) have been utilised, including constructs made of rotating vessels, spinner flasks and stirred double chambers (204). Ideal properties of bioreactors include easy and efficient assembly, sterility and low toxicity. Inbuilt sensors and precise systems can be incorporated to monitor and control operational conditions such as pH, temperature, oxygen tension and mechanical forces (205, 206).

In cartilage TE, bioreactors have been trialled specifically to induce perfusion, shear force, hydrostatic pressure, compression and the overall combined mechanical forces which are encountered by the human knee joint during daily activity. Zhao et al (2016), compared studies incorporating the factors as mentioned above; enhancement in both chondrogenic differentiation and proliferation was observed (204).

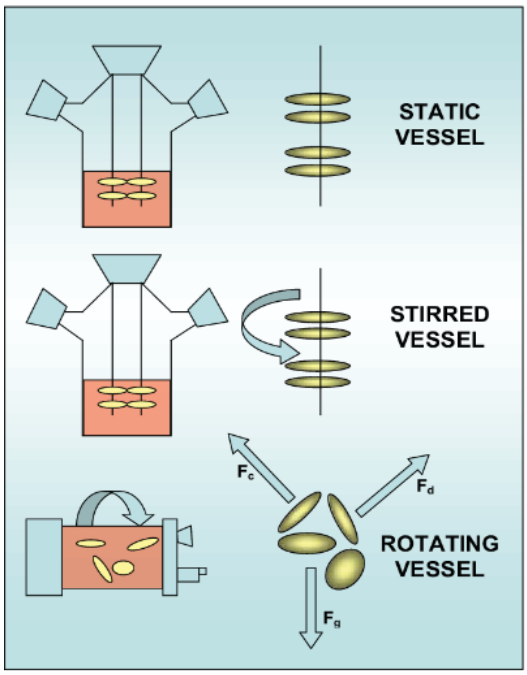


Figure 1.12 (Left) Bioreactor system designs. Representation of static, stirred and rotating vessels. Fc, Fd, Fg refer to centrifugal, drag and net forces respectively. Used with permission from J Orthop Res under the Creative Commons Attribution 4.0 International License (207).

1.5 GENERATION AND DELIVERY OF THE TISSUE CONSTRUCT

1.5.1 GAPS AND DOWNFALLS IN CARTILAGE TISSUE ENGINEERING

Historically with cartilage tissue engineering, prefabricated tissue at the bench side was transferred or implanted manually into a defect (25). An obvious limitation of this intended approach is the complexity involved with accurately replicating the complex morphologies associated with cartilage defects (25).

Preformed scaffolds must closely resemble the defect that they will be filling, meaning bioscaffolds need to be cultured to size *in vitro,* or the defects must be pre-contoured with debridement (208). Furthermore, unless sizing and orientation of the *in vitro* constructs are perfectly controlled, it is difficult to have any control over the zonal partitioning of engineered constructs, which remains difficult with modern biofabrication but much more conceivable (208) (209).

In order to truly control the ability to create zones and different regions (e.g., chondral, subchondral or osteochondral) using prefabricated tissue, multiple different *in vitro* cultures must be undertaken and tightly controlled (210) (209). This multizonal/anatomical notion can be more easily combated using different 'bioinks' composed of cells mixed with hydrogel scaffolds that can be loaded into a bioprinter and printed directly *in situ* (211).

1.5.2 THE CONCEPT OF BIOFABRICATION

The emergence of bioprinting over the past decade has enabled engineered tissue to be formed and delivered in an anatomically structured fashion (212). The combination of tissue engineering and controlled structural creation/delivery (bioprinting or bioassembly) is commonly referred to as 'Biofabrication' in the field of tissue engineering and regenerative medicine (Figure 1.13) (14). Bioprinting creates the ability to clinically deliver implants directly *in vivo*, whereas bioassembly technology is currently used as a tool for *in vitro* models (14). Therefore, bioprinting is used to form or deliver engineered tissue constructs in the biofabrication of cartilage (Figure 1.14).

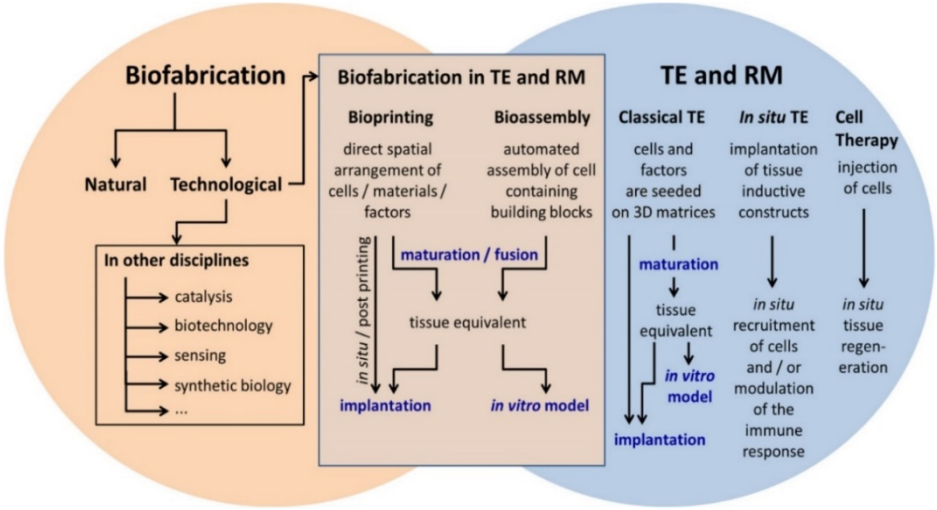


Figure 1.13. Biofabrication in tissue engineering (TE) and regenerative medicine (RM). Used with permission from Biofabrication under the Creative Commons Attribution 4.0 International License (14).

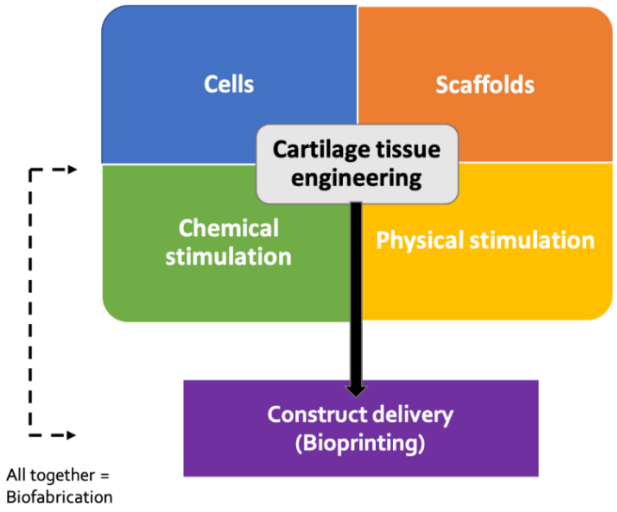


Figure 1.14. (Left) Concept of cartilage biofabrication. Biofabrication is the combination of tissue engineering with bioprinting technology.

1.5.3 3D BIOPRINTING

Bioprinting is the utilisation of 3D printing technology to produce living tissue for use in regenerative medicine and disease modelling (13). It allows for the accurate control of cell distribution, production of biomimetic geometry and the rapid production of a construct (25). Advanced systems can be used in conjunction with computer-aided design and can be regulated and optimised for precision (213). Several types of bioprinting mechanisms have been developed and evaluated with respect to cartilage tissue engineering, commonly used models are displayed (Figure 1.15) and compared in Tables 1.4 and 1.5.

INKJET PRINTING

Inkjet bioprinting relies on the pressure generated in the print head, fluid mechanics and gravity to extrude bioinks out of a cartridge (214, 215). Droplets are formed in either a continuous inkjet or drop-on-demand mode (216), with the latter achieving a much higher resolution and are generally used for biological applications. Common methods to generate drop-on-demand printing rely on thermal or piezoelectric effects (217). With thermal printing, a small part within the printhead is rapidly heated to generate vapour bubbles within the bioink (217), these bubbles coalesce and expand, generating a pressure pulse and finally, the bubbles shrink and collapse. Using piezoelectric methodology, a piezoelectric actuator converts the applied voltage into a mechanical deformation of a crystal, producing an acoustic wave which generates the pressure required for the drop ejection. To form droplets, a bioink must be liquid inside the cartridge and quickly crosslink after extrusion (218).

Consequently, various platforms for inkjet bioprinting were established, including shear-thinning bioinks (219). The thermal inkjet 3D bioprinter with simultaneous photopolymerization was used for precise positioning of encapsulated human chondrocytes during layer-by-layer deposition (220). Whereas the piezoelectric bioprinter was combined with $CaCl_2$ nebulizer to create alginate-based scaffolds (221). $CaCl_2$ at low concentrations was sprayed over printed constructed and washed out immediately after gelation.

EXTRUSION PRINTING

Extrusion bioprinting relies on pneumatic pressure or mechanical pistons to produce extrusion-based deposition (222). The constant generated force permits bioprinting of highly viscous bioinks. Co-axial printheads can be used in extrusion printers for simultaneous

delivery of the bioink through the core flow and the crosslinker trough the sheath flow (223), and this system is applicable for printing different types of bioinks (224, 225).

An emerging strategy is the handheld, 3D core/shell bioprinting device, 'Biopen', designed specifically for in *situ* 3D bioprinting of cartilage (176, 178, 226), more on this is detailed in section 1.5.3. A multiheaded deposition system (MHDS), can be used for complex bioprinting of multi-layered constructs for cartilage and osteochondral tissue regeneration (227). MHDS has been equipped with four heads that utilize pneumatic pressure for dispensing (227).

LASER-ASSISTED PRINTING

Laser-assisted bioprinting (LAB) is a nozzle-free, noncontact technique, where a laser is pulsed on a ribbon composed of three layers: laser-transparent layer, laser-absorbing layer, and bioink layer (228). The laser beam energy is absorbed by the ribbon what generates a local bubble on the opposite side. Rapid formation of the bubble ejects a desired amount of bioink on a receiving stage. LAB is applicable for high cell densities and high viscosity inks. The main three, laser-based techniques are 1) laser-induced forward transfer (LIFT), 2) absorbing film-assisted laser-induced forward transfer (AFA-LIFT), and 3) matrix-assisted pulsed laser evaporation direct writing (MAPLE-DW). LIFT has been successfully applied for *in situ* bioprinting of BMSCs on a bone defect in mice (229).

STEREOLITHOGRAPHY

Stereolithography (SLA) and digital light projection (DLP) are nozzle-free techniques that create 3D objects through layer-by-layer photopolymerization. In SLA, liquid resin is solidified by UV laser beam (230, 231), while in DLP, visible light is projected in the shape of the layer (230, 231). Final structures made of SLA or DLP are drained and washed. Scaffolds are often subjected to post-curing in order to improve their mechanical properties. These methods utilize photosensitive polymers or bioinks, usually requiring photoinitiators (231). Alternatively, if photoinitiators are undesirable, polymers with polymerization based on a thiolene reaction can be applied. SLA and DLP can be performed in two ways, i.e. bottom-up and top-down approach. In bottom-up fabrication, a layer of resin is cured by the light from above, and the structure is built on a support platform. While in the top-down approach, the source of the light is localized beneath the transparent plate.

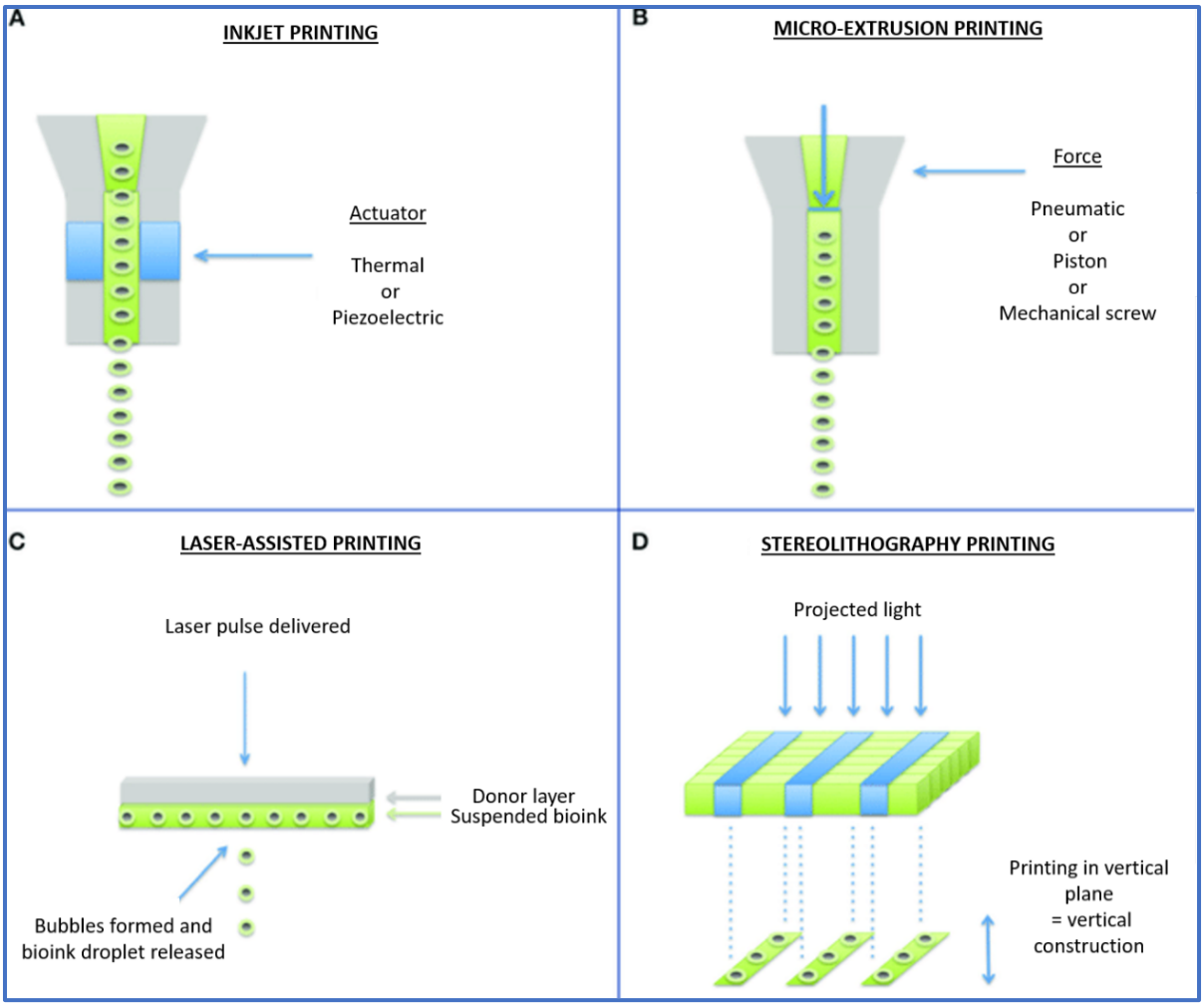


Figure 1.15. Different types of bioprinting mechanisms used in tissue engineering

Print method	**Cell viability**	**Viscosities (mPas)**	**Resolution**	**Speed**	**References**
Inkjet	80-90 %	3.5 - 12	50 µm	Fast	(213, 232, 233)
MEP	< 80 %	30 - 6.0 X 10^7	100 µm	Slow	(213, 232, 233)
LAP	> 90 %	1.0 - 300	50 µm	Medium	(213, 232, 233)
SLA	> 85 %	All	200 nm – 6 µm	Fast	(213, 232, 233)

Table 1.5. Comparison of 3D bioprinting methods. Millipascal seconds (mPas). MEP – Micro extrusion printing, LAP – Light assisted printing, SLA – Stereolithography.

Print method	Advantages	Disadvantages	References
Inkjet	Easily operated Cheap Quick print speed	Clogging of the head Settling effect of bioink	(234, 235)
ME	Easily operated Cheap High viscosities compatible	Large mechanical stressors Low cell viability	(236, 237)
LAP	High cell viability High viscosities compatible	Expensive Unknown effects of laser Scarce in vivo data	(238, 239)
SLA	Quick print speed High resolution High viscosities compatible	Poor compatibility with liquids and gels One material at a time UV light-related toxicity	(174, 232, 240-244)

Table 1.4. Advantages and disadvantages of different 3D bioprinting methods. Table 1.5. Comparison of 3D bioprinting methods. Millipascal seconds (mPas). MEP – Micro extrusion printing, LAP – Light assisted printing, SLA – Stereolithography.

1.5.4 SUITABLE CONSTRUCT DELIVERY METHODS FOR CARTILAGE TISSUE REPAIR

Cartilage damage can present in random and complex morphological patterns, and although damage can be appreciated grossly with magnetic resonance imaging (MRI), it is difficult to assess the exact nature and size of the defect (245). Therefore, the true quality of articular defect morphology can only be evaluated and visualised intraoperatively. To cater for such a situation, the ideal bioink composition would contain a hydrogel biomaterial that can fill a defect (151, 152). Once the appropriate void is filled, the top surface can be flattened and cross-linked to solidify.

The 'Axcelda ®pen' **(**formerly known as the biopen) is an example of a handheld pneumatic extrusion bioprinter (Figure 1.16) that has been developed for surgical use and is tailored specifically for *in vivo* cartilage repair, (Figure 1.17) (175, 246).

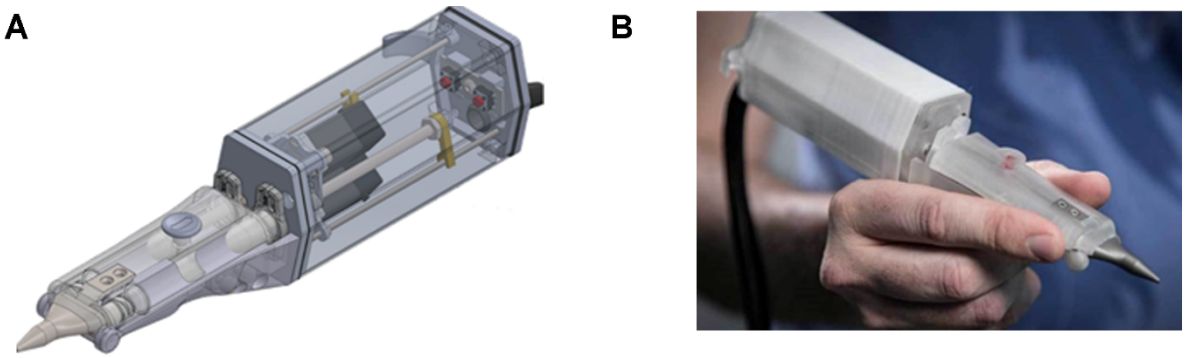


Figure 1.16. The 'Axcelda®pen' handheld extrusion-based 3D bioprinter. (A) Device Design representation and (B) Device prototype.



Figure 1.17 (Left). Intra-operative image of the Axcelda®pen being used in a sheep model. Modified and used with permission from Di Bella et al (25), under CC BL.

Engineered tissue using a portable hand-held device can be printed directly during surgery with the top of the construct being immediately cross-linked using methods mentioned earlier. This approach allows for implant stability within the lesion (247). However, when using non-portable printers and non-hydrogel-based scaffolds/materials, the formed implant will need to be manually positioned (requires precise geometry when initially created) into the lesion and then anchored with either sutures or a flap approach. *In vivo* animal delivery of engineered cartilage tissue has been performed to-date using large incisions over the knee, similar to those made in conventional knee replacement surgeries (247, 248). Larger incisions and increased operating time are associated with a higher risk of wound complications (e.g. infection and wound dehiscence) (249) and reduced cosmetic satisfaction, both of which are important to consider in the treatment of a young-middle aged population.

1.6 CURRENT MODELS USED FOR *IN VIVO* CARTILAGE REPAIR

Tissue engineering and biofabrication approaches *in vitro* are used to assess several aspects of regenerative medicine, such as the biocompatibility of the cell-scaffold interface and the effects of specific conditions/factors on cell proliferation and differentiation (250). However, an animal model is ultimately warranted to study the complex process of *in vivo* cartilage tissue formation and maturation; furthermore, this bridges the gap between i*n vitro* and clinical study in humans (250). The animal model provides an *in vivo* articular cartilage environment, appropriate for the study of the integration of engineered cartilage to the surrounding native tissue, and evaluation of the safety and efficacy of newly engineered cartilage (251).

Various animal models have been used for *in vivo* study, small and large animal models have been used to recapitulate/mimic disease and injury that can occur in humans, whereas, ectopic models have been used to test the biocompatibility of implants (252). Ultimately, the choice of animal depends on the purpose of the study, and specific animal models may not suit all the proposed study questions. Early-stage cartilage repair investigation can be performed using a small animal model to understand the pathophysiology of disease and to evaluate new therapeutic approaches (252, 253). Validation studies can then be performed to assess the clinical process and treatment of disease using a large animal model (254-257).

From a modelling perspective, the best animal model for translation to the clinic would be the non-human primate, which is the species most closely related to humans. However, there are important ethical and practical concerns with their use in research, which therefore significantly limits the use of these animals (258).

1.6.1 LARGE ANIMAL MODELS

Compared to smaller animal models, the joint size and cartilage thickness in larger animals are more like humans. Examples of large animal models used for cartilage repair research include the horse (equine), sheep (ovine), goat (caprine), pig (porcine) and dog (canine) (252). Cartilage thickness, formable defects sizes, advantages and disadvantages of each are summarised in Table 1.6.

Large Animal	Cartilage thickness	Formable Defect sizes	Advantages	Disadvantages
Horse (Equine)	1.75 mm	Large	Biochemically similar to humans High mechanical loading forces	Expensive Large facilities needed Ethical concerns
Sheep (ovine) and Goat (caprine)	0.4-1.0 mm 0.5-1.2 mm	Mid-Large	Relatively less expensive	Difficult positioning intraoperative Difficult post-op rehab
Pig (porcine)	1.5 mm	Mid- Large	Can use knockout pigs Easily bred	Expensive Rapid skeletal growth different from humans
Dog (canine)	0.95 mm	Small -Mid	Controlled weight bearing	Better rehab - Trainable Ethical concerns

Table 1.6. Common large animal models used in cartilage research

1.6.2 SMALL ANIMAL MODELS

While large animals better approximate the human joint size and cartilage thickness, they are relatively expensive and can be challenging to house and surgically facilitate due to positioning and size (252). It is generally well-accepted to utilise a small animal model for initial lines of investigation (259). Therefore, with pilot studies, the small animal model can be useful and practical in early screening and proof of concept experimentation (251). The major disadvantage of the small animal model is the small joint size and thin cartilage, which makes surgery challenging and is not fully representative of the clinical issue. Commonly used small animal models for cartilage research include the rabbit, mice and rat (Table 1.7).

Small Animal	Cartilage thickness	Formable Defect sizes	Advantages	Disadvantages
Rabbit (Lapine)	0.3 mm	Small	Cheap High mechanical loading forces	Thin cartilage Self-healing nature
Rat	0.1 -0.15 mm	Micro Bigger than Mice	Cheap Can use knockout rats	Thin cartilage Spontaneous healing Difficult to assess repair
Mice	0.1 mm	Micro	Cheap Can use knockout mice	Thin cartilage Difficult to assess repair

Table 1.7. Common small animal models used in cartilage research

1.6.3 ECTOPIC MODELS

Ectopic models, in which cartilage is grown outside the joint, are alternatives to the orthotopic models for cartilage repair (260). The most common ectopic model is subcutaneous implantation (261). The subcutaneous implantation model provides an *in vivo* physiological environment without the presence of mechanical loading conditions associated with the native joint (262). Therefore, it can be useful for study outcomes that are not associated with or influenced by joint forces, such as initial biocompatibility testing.

Although the model is more physiologically similar to the native joint environment compared to *in vitro* culture conditions, the overall lack of environmental influence is a significant limitation compared to a native *in vivo* model (261). These models can be used for a preliminary proof of concept and provide early information prior to engaging in an animal model which can be costly and time-consuming.

CHAPTER 2: KNOWLEDGE GAPS, HYPOTHESES AND RESEARCH AIMS

2.1 CHONDROGENIC POTENTIAL OF CELL SOURCES WITHIN THE KNEE JOINT AND OPTIMISATION OF THE CELL ISOLATION PROTOCOL

IDEAL CELL TYPE WITHIN THE KNEE JOINT FOR CARTILAGE REGENERATION

With a view of treating articular knee defects using tissue engineering strategies such as biofabrication with autologous cells, ideally, the cell source should be harvested from within the knee joint. The same harvest and treatment site can be used due to the proximity of such tissue to the defect, limiting the number and size of surgical incisions; and consequently, reducing associated risks (e.g. harvest site irritation or infection) (263).

Human adipose-derived mesenchymal stem cells (hADSCs) are a chondrogenic source (138) which can be isolated from the Infrapatellar fat pad (IFP), (Figure 2.1). Two other sources from within the knee joint with chondrogenic potential are the mature chondrocyte and articular progenitor cell (hAPCs) (142, 264). All three sources can be sourced autologously, which is an advantage given the inherent ethical and immunological risks associated with using commercial or allogenic cells (265). Both mature chondrocytes and hAPCs are isolated from the non-weight bearing zones of articular cartilage (Figure 2.1), where there is minimal tissue availability and low cell numbers (266, 267). Furthermore, the harvesting of articular cartilage carries some risk of damaging or removing healthy weight-bearing aspects of articular cartilage. On the other hand, hADSCs can be easily harvested from the IFP, which can be safely removed either arthroscopically or with a small open incision (138, 268). Despite these differences, all three cell sources are potentially applicable in cartilage tissue engineering; therefore, the first objective of this chapter is to verify and compare the chondrogenic differentiation potential of these three cell sources.

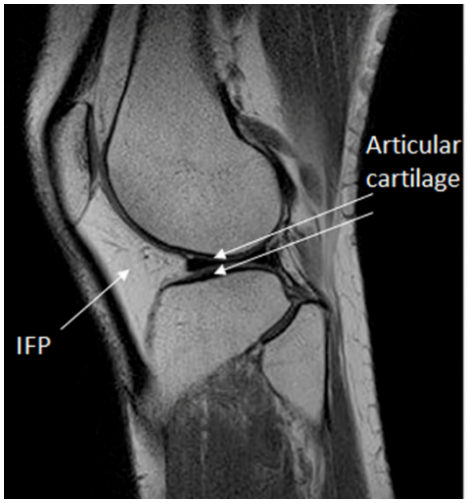


Figure 2.1 (Left). Sagittal magnetic resonance imaging scan of the knee joint showing the relationship of the IFP (arrow) to the articular cartilage (double arrow). Modified and used with permission from Wiley under CC BL, (138).

OPTIMISATION OF THE CURRENT IFP-DERIVED hADSCs ISOLATION PROTOCOL

The second objective of this chapter was to review and optimise the current IFP-derived hADSCs isolation protocol, with the intention of generating a rapid isolation protocol. Speeding up the isolation timeframe enables a quicker turnaround period of cell culture before reimplantation; furthermore, it can limit the timeframe in contact with animal-derived media and the risks associated with *in vitro* culture and sterility (265).

Obtaining a stem cell population requires several sequential steps (Figure 2.2) and overall current techniques take > 25 hours to isolate a pure stem population (269), although lengthy this is not a concern for *in vitro* study. With a view of clinical translation in humans, it is imperative to efficiently optimise the isolation timeframe, enabling a quicker turnaround period of cell culture before reimplantation and limiting the duration of cellular contact with animal-derived media and the sterility related risks (265).

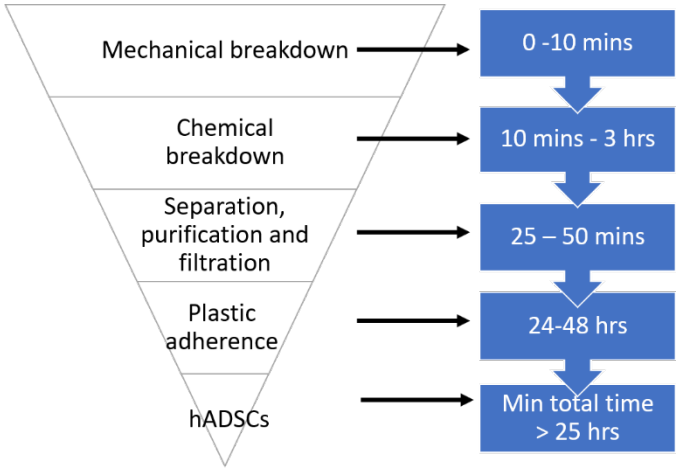


Figure 2.2 (Left). Human adipose-derived mesenchymal stem cell (hADSCs) isolation protocol from Infrapatellar fat tissue

Commercially available enzymatic and nonenzymatic isolation systems (270, 271) (272) are used to isolate cells rapidly; however, these systems isolate an SVF as opposed to a hADSC population. The use of SVF alone has been trialled as a therapeutic option for symptomatic benefit; however, there is no evidence of regenerative capacity (273).

Ahearne et al (2014), described the ability to rapidly isolate an adherent stem cells population within 5 hours by using only 30 minutes for cellular adherence to non-coated tissue culture polystyrene (TCPS). Cells were then combined with an agarose hydrogel to create tissue constructs (274). Contrary to the authors' analysis, a lack of true collagen 2 accumulation was evident and suggestive of a non-functional cell population. When using non-coated (TCPS), a period of at least 24 hours has been recommended for stem cell selection (275).

WHERE CAN WE SAVE TIME?

The two key steps that could be optimised for efficiency include chemical digestion of fat and cellular adherence to non-coated tissue culture polystyrene (TCPS).

Chemical Breakdown: The duration of chemical breakdown has been reported to range between 10 and 180 minutes (276). Insufficient collagenase breakdown time can reduce the cellular yield; whereas, increased time >30 minutes using collagenase digestion has been shown to reduce the number of viable cells (277). No minimal, let alone optimal timeframe has accurately been assessed in the literature.

Plastic Adherence: Coated-TCPS formulations have been reported to speed up the adherence of non-hADSCs populations. Matrigel-coated TCPS which have been used to obtained Sertoli cell adherence within 30 minutes (278) and have been optimised for 2D culture-expansion of neural and embryonic stem cells with no effect on molecular characteristics (279). Fibronectin has also been shown to accelerate cellular adherence of articular progenitor cells within 20 minutes (143); however, has a narrower ECM protein composition compared to Matrigel.

HYPOTHESES

1 – Human ADSCs isolated from the IFP are more chondrogenic than adult articular chondrocytes and hAPCs derived from knee cartilage

2 - The current IFP-derived hADSCs isolation timeframes could be optimised with respect to efficiency without affecting the cellular yield, phenotype and differentiation ability

AIMS

1 - Compare the chondrogenic potential of articular chondrocytes, human articular progenitor cells (hAPCs) and human Infrapatellar Fat Pad-derived Mesenchymal Stem Cells (IFP-derived hADSCs) to identify the most suitable source for cartilage repair

2 - Optimisation of the standard IFP-derived hADSCs isolation protocol leading to the generation of a rapid cell isolation protocol

3 - Validation of the rapid IFP-derived hADSCs isolation protocol against the standard isolation protocol

2.2 MINIMUM CHONDROGENIC REQUIREMENTS OF IFP-DERIVED HADSCS PRIOR TO REIMPLANTATION

THE EARLIEST TIMEPOINT DURING CULTURE EXPANSION AT WHICH hADSCs BECOME CHONDROGENIC AND THE NUMBER OF RELATIVE CELLS OBTAINABLE

Traditionally hADSCs are generously expanded in culture to reach an abundance of cells before being used *in vitro* and for reimplantation; furthermore, they can be passaged many times while maintaining their chondrogenic capacity and prior to developing significant levels of senescence (280). However, studies have shown that cells from lower passages are more ideal as therapeutic tools (90, 281) due to healthier immunomodulatory properties, cells from higher passages have been associated with higher levels of *in vivo* inflammation (90).

There is no literature indicating if expanded cells can be used before initial passaging (Passage 1) and how early expanded IFP-derived hADSCs can be induced towards differentiation. This is a crucial knowledge gap when envisioning future clinical translation, as an estimated turnaround timeframe for such a repair procedure should be identified. The earlier the timeline to reimplantation the less inherent risks involved with cell culture in a lab and exposure to animal-based serum products (282). Another key advantage of knowing when the earliest turnaround timeframe for reimplantation can occur is to identify and optimise the waiting time for patients between surgical procedures (Harvest and Reimplantation).

The first objective of this chapter is to determine the earliest time point during expansion in which hADSCs can be driven into chondrogenic differentiation. The relative number of cells obtainable post-expansion at this respective timeframe is identified.

THE MINIMUM STEM CELL CONCENTRATION REQUIRED TO PRODUCE NEOCARTILAGE

Cell-free articular repair techniques such as microfracture are indicated primarily based on the total surface area (TSA) of the defect (283, 284). Current cell-based implantation techniques such as autologous chondrocyte implantation (ACI) and matrix-assisted autologous chondrocyte implantation (MACI) are also indicated based on the TSA of defects; however, an extra factor needs to be considered which is the volume of the defect. The volume becomes crucial in cell-based repair, as adequate cell numbers need to be delivered for regeneration/repair to occur. In ACI and MACI, an expanded number of chondrocytes

based usually on surgeon preference or approximate physiological cartilage cell counts is used (285).

The use of higher chondrocyte concentrations *in vitro* can inhibit matrix synthesis, leading to reduced ECM production (286, 287) while using lower concentrations will not produce enough ECM *in vitro* (288, 289). Few *in vitro* and *in vivo* studies report the cell concentrations used, ultimately the use of higher concentrations are not superior to lower ones; therefore, no minimum let alone optimal cell concentrations range has been identified (290). The average chondrocyte cell count in healthy human knee cartilage is 10 million cells/mL (285), the inherent ability of stem cells to proliferate even during the differentiation needs to be considered when identifying the minimal concentration required to achieve adequate chondrogenesis (291). In line with producing an efficient therapy and minimising the associated risks with prolonged cell culture, the next objective in this chapter was to identify the minimum hADSCs concentration required to generate adequate neocartilage.

THE MAXIMUM DEFECT VOLUME REPAIRABLE USING A RAPIDLY ISOLATED hADSCs POPULATION WHICH IS EXPANDED FOR 5 DAYS

By identifying this minimum concentration and using it with the number of hADSCs obtained during a set-period of expansion, the maximum volume of defects repairable can be identified. This is a crucial link as it enables the indication range for a regenerative repair approach to be established; for example, the number of cells obtained from 3 days of expansion may be adequate to treat partial-thickness defects while 7 days of cellular expansion may be sufficient to treat full-thickness defects.

HYPOTHESES

1 - The overall hADSCs culture expansion timeframe could be minimised by identifying the earliest time frame in which cultured hADSCs can be driven into chondrogenesis

2 - The minimum hADSCs concentration required to produce neocartilage was lower than the native human chondrocyte cell count (10 million cells/mL)

3 - Linking the data from the first two aims, the maximum defect volume repairable and thereby, a treatment indication range could be established

AIMS

1 - Determine the earliest time point during *in vitro* culture expansion in which IFP-derived hADSCs can undergo chondrogenesis and the relative number of cells obtainable after the identified timeframe

2 - Identify the minimum IFP-derived hADSCs concentration required to produce *in vitro* neocartilage formation in a Gelatin-Methacryloyl/Hyaluronic Acid (GelMA/HA) hydrogel

3 - Determine the maximum defect volume repairable using a rapidly isolated IFP-derived hADSCs population expanded using the earliest chondrogenic timepoint and minimum chondrogenic hADSCs concentration

2.3 ESTABLISHING A BIOFABRICATION PROCEDURE FOR IN VIVO CHONDRAL REPAIR

To biofabricate tissue *in situ* during surgery, several critical components require selection and validation *in vitro* (Figure 2.3). In this chapter of work, essential aspects of the biofabrication approach are optimised and designed to enable a user-friendly, safe, sterile and efficient method that is compatible with the surgical environment.

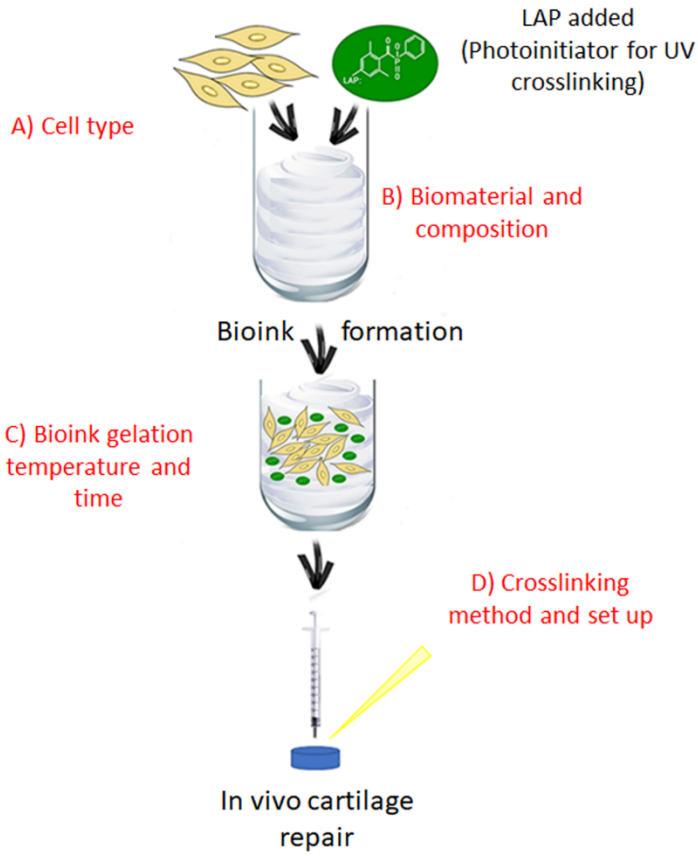


Figure 2.3 (Left). Set-up of an in situ biofabrication repair procedure for in vivo chondral defect repair. Highlighted in red are the parameters which need to be selected and identified before performing an intraoperative model.

A) Cell type

Given the proof of concept stage of this study, the model used downline in the next chapter is that of an *in vivo* small animal (rabbit), specific reasoning for this choice is detailed in the following research chapter.

The IFP can generally be harvested from a small animal model; however, the amount of tissue is small, leading to a minimal stem cell yield during isolation (292). The use of pooled IFPs from several animals as a starting point is generally used to overcome this issue (293); however is costly and wasteful; therefore, to better represent the model, in this study, a commercial MSCs animal cell line is used (Rabbit). Cartilage is an immune-privileged tissue,

meaning it is rare to have any host reaction to implanted tissue (294-298), nonetheless, to further minimise any inflammatory response, commercial cells were sourced from the same species and gender of rabbit to that used in the subsequent *in vivo* model (chapter 7). Therefore, as part of the procedural set up, the commercially sourced rabbit MSCs line was validated with a 3-week chondrogenic screening study.

B) Suitable hydrogel compositions

Gelatine-based hydrogels exhibit high cytocompatibility and biodegradability in physiological environments (168-170). The addition of methacrylate/methacrylamide (MA) groups to gelatin enables light-assisted cross-linking of the material, thus mimicking the natural ECM of cartilage (171, 172). Based on these advantageous factors and successful *in situ* delivery of GelMA *in vivo* (247), this material was selected as the ideal hydrogel for the subsequent *in vivo* model of cartilage repair in this thesis (chapter 7).

Depending on the percentage of the gelatine component in a GelMA hydrogel, the stiffness and strength can be tuned, by increasing the amount of gelatine the stiffer the hydrogel. Cells behave differently with different stiffnesses of the material (172); therefore, the overall downline aim of selecting a soft and hard hydrogel was to evaluate this difference *in vivo* for cartilage repair. Hence, the next step in the procedural set up was to validate the difference in mechanical strength (compression testing) using fabricated acellular 6% and 10% GelMA scaffolds.

C) Gelation time of the bioink

Aqueous solutions of gelatine solidify or 'gelate' when the temperature falls below the lower critical solution temperature (LCST) of 25°C, (299, 300). During *in situ* delivery, if the gelatine is too gelated, it becomes difficult to extrude and will not adequately fill the defect. Whereas if too liquified, then it will rapidly disperse and collapse (299, 300). Therefore, the control of gelation becomes crucial when using such thermoreversible hydrogels in cartilage repair (301). To optimally deliver a gelatin-based bioink composition, it should be printed in a semi-gelated form (302).

To achieve this, bioinks should be prepared and kept in a heated oven chamber or incubator, ideally between 35-40 °C which will preserve them in liquid form, and higher temperatures

can compromise cell viability (303). Prior to administration, bioinks should be allowed to gelate below the LSCT for a specific time, enabling them to reach the desired printability state before use. This duration is known as the 'gelation time', and it varies depending on the intrinsic compositions of the materials used and the environmental temperature of the room (304). Generally, gelation is performed at room temperature (23°C), which is below the lower end of the gelatine LCST (25°C). However, using the room temperature results in a less controlled and broad range of gelation times, likely due to the difficulty in precisely controlling the room temperature resulting from environmental influences (304).

Another method used to combat this challenge is to transfer the heated hydrogels (37°C incubator) into a colder than room temperature environment before printing (304). A convenient advantage of this method is that there is less waiting time required for the hydrogel to gelate before becoming printable (304). However, the risk associated with the quicker cooling of the gel is the potential for cell toxicity; therefore, the cooling temperature should be not be set below 0°C (211).

Gelation is expected to occur quicker with higher concentrations of gelatine (305); therefore, the harder (10% GelMA) should gelate quicker than the softer (6% GelMA) hydrogel-based bioink. The gelation time required for these two bioink compositions was evaluated *in vitro* using a filament formation test (ideal result is to extrude a homogenous string like gel) to identify the ideal gelation period before printing. This test was performed using gelation at both room temperature (23°C) and in a fridge (4°C).

D) Appropriate *in situ* cross-linking method

Poor thermostability of gelatine makes it challenging to cross-link physically, while chemical cross-linking is associated with a high risk of process-related toxicity (306). Using light-assisted cross-linking of GelMA, the cell viability has been reported as >85-90% (175, 307). Another advantage of using light-assisted cross-linking is the ease of surgical application (using a hand-held system) and lack of direct contact with the printed construct and healthy tissue. The distance required for adequate coverage of only the generated rabbit defect (size and details described later) without infringing on healthy tissue was identified as 1 cm. Therefore, in this chapter, a sterilisable 1 cm fixed distance probe cover was first designed, then 3D printed, and finally attached to the end of the light source enabling surgical use.

HYPOTHESES

1 - A novel surgical biofabrication approach to treat *in vivo* cartilage defects could be designed in a safe, operator friendly and compatible manner.

2 - This could be achieved by optimising the, cell source, hydrogel composition, hydrogel gelation times and crosslinking parameters.

AIMS

Set up of an *in vivo* surgical biofabrication model and procedure:

1 - Validate a commercially sourced rabbit MSCs line

2 - Identify suitable hydrogel-based bioink compositions

3 - Identify the respective gelation times of chosen bioinks

4 - Identify and set up a safe and appropriate intraoperative cross-linking method

2.4 CARTILAGE BIOFABRICATION USING THE MINIMUM CHONDROGENIC HADSCS CONCENTRATION – A PILOT *IN VIVO* RABBIT MODEL

This section serves as a novel pilot study assessing a novel biofabrication therapy for pure chondral repair *in vivo*, using the minimum chondrogenic stem cell concentration (chapter 5) and a novel intraoperative approach (chapter 6).

SELECTION OF THE RABBIT MODEL, DEFECT PARAMETERS AND TREATMENT GROUPS

The large animal model is commonly used in the later developmental stages of research associated with cartilage repair (252) and more closely resemble human cartilage compared to smaller animal models. However, given the fiscal feasibility, practicality and proof of concept nature of this study, the small animal is more suitable to the cost budgets and project timeframes of this thesis.

Within small animal models, the rabbit is the largest and most suited to relatively bigger defect sizes; furthermore, it can easily be managed, performed and evaluated. Rabbits have 2 knee joints (Hindlimbs) and therefore have 4 condyles (each knee has a lateral and medial femoral condyle). In the rabbit model, the lateral collateral ligament commonly traverses and is in contact with the under surface of the lateral femoral condyle, which can impede repair. Humans also have this ligament, but it is not so close in proximity with the lateral femoral condyle. To combat this, treatment groups should be evenly randomised to either condyle. Timepoints for study in rabbits are generally selected based on when early and mature cartilage formation is detectable, which is at around 3-4 and 6-8 weeks, respectively post-repair (308).

Literature shows that rabbit cartilage can spontaneously heal (309); however, several reports suggest using a minimum diameter of 3 mm as the critical-sized defect can prevent this natural revival (310-312). Rabbit articular knee cartilage, on average is approximately 0.3 mm thick (or deep) (313), the width of each condyle is roughly 5-6mm. (314, 315) Therefore based on current literature, to assess critical size defects (314, 315) in this model a 4 mm diameter circular defect with a depth of 0.3 mm was chosen, creating a volume of approximately 4 µL (mm^3). Beyond using a critical sized defect to avoid spontaneous regeneration, the specific size/volume of the defect is not a critical factor in this study since

the cellular treatment groups (highlighted below) rely on a cell concentration per volume as opposed to a certain number of cells.

HYPOTHESES

1 - The newly designed biofabrication approach could be implemented *in vivo* to repair cartilage defects using the minimum hADSCs concentration with either a soft or hard hydrogel composition

2 - The outcomes are hypothesised to be comparable if not better than those in the clinical standard (microfracture repair) group over an 8-week *in vivo* period

AIMS

Perform an *in vivo* rabbit model of cartilage repair using a biofabrication approach:

1 - Evaluate cartilage repair associated with using a minimum stem cell concentration and comparing it to microfracture treatment (clinical standard), by performing a macroscopic, microscopic and biomechanical assessment

2 - Evaluate cartilage repair associated with using a soft verse hard biocompatible hydrogel (6% verse 10% GelMA), by performing a macroscopic, microscopic and biomechanical assessment

CHAPTER 3: MATERIALS, PROTOCOLS AND METHODS

3.1 CELL HARVEST AND ISOLATION

3.1.1 HUMAN TISSUE HARVESTING - ETHICAL APPROVAL

Human Infrapatellar fat pat (IFP) and distal femoral bone cuts from the knee joint were opportunistically harvested from patients undergoing elective total knee arthroplasty with informed consent. This study was approved by the Human Research Ethics Committee Research Governance unit of St. Vincent's Hospital, Melbourne, Australia [HREC/16/SVHM/186]. Harvested tissue was used immediately or kept in a sterile container in phosphate-buffered saline 1X (PBS 1X) (Sigma-Aldrich, St. Louis, MO, USA) supplemented with antibiotics (Penicillin/Streptomycin 100X, Gibco, Thermo Fisher Scientific) overnight and used within 24 hours of harvest.

3.1.2 STANDARD IFP-DERIVED MESENCHYMAL STEM CELL ISOLATION PROTOCOL

Under a laminar flow hood, the IFP was placed in a sterile glass petri dish and 3 mL of complete hADSCs culture media [low glucose Dulbecco's modified eagle medium (DMEM) (Sigma Aldrich, St. Louis, LA, USA) supplemented with 10% (v/v) foetal bovine serum (FBS) (Gibco, Thermo Fisher Scientific Inc, Waltham, MA, USA), 100 U mL^{-1} Penicillin and 100 µL mL^{-1} Streptomycin solution (Gibco, Thermo Fisher Scientific Inc, Waltham, MA, USA), 2 mM L-Glutamine (Gibco), and 15 mM HEPES (Gibco), 20 ng mL^{-1} epidermal growth factor and 1 ng mL^{-1} fibroblast growth factor (R&D Systems Inc., Minneapolis, MN, USA)] was added. Using forceps and a scalpel fat was removed from the fibrous material and diced until only fat globules remained. Diced fat was collected with a sterile pipette and transferred to a 50 mL tube (BD Falcon). Next, 0.3 mL of 10 mg mL^{-1} collagenase type 1 (Worthington Biochemical, Lakewood, NJ, USA) was added, and chemical digestion was achieved with over 3 hours at 37 °C under constant agitation on a shaker at 250 revolutions per min (rpm). The sample was centrifuged at 2100×g for 10 minutes, and the resulting cell pellet was resuspended in PBS 1X before being filtered through a 100 µl nylon cell strainer (BD Falcon) and then centrifuged. The remaining pellet was then resuspended in 5 mL of red cell lysis buffer (160mM NH_4Cl; Sigma Aldrich) for 10 minutes and filtered through a 40 µl nylon cell strainer (BD Falcon). The sample was then centrifuged at 400×g for 5 minutes, and the cell pellet was resuspended in 500 µl of complete hADSCs culture media, a cell count and viability were calculated using a haemocytometer and trypan based live-dead staining. Cells were evenly plated on non-

coated TCPS wells and incubated for 24 hours, allowing for cellular adherence. Non-attached material was discarded, and the attached cells were washed once with PBS 1X before adding 500 µl of trypsin (Sigma Aldrich, St. Louis, LA, USA) and incubated for 3 minutes allowing for cellular de-attachment. Next 1 mL of complete hADSCs culture media was added to each well to neutralise the trypsin; samples were then centrifuged at 400×g for 5 minutes, the resulting pellet was resuspended in 500 µl of complete hADSCs culture media. The adherence percentage and hADSCs count was calculated using a haemocytometer and trypan based live-dead staining under light microscopy. Cells were replated at a density of 5000 cells/cm^2 onto non-coated TCPS wells and expanded for down line investigations.

3.1.3 MATURE ARTICULAR CHONDROCYTE ISOLATION PROTOCOL

Under a laminar flow hood, articular cartilage was dissected off the underlying subchondral bone of harvested bone cuts, and isolated pieces were then placed in a sterile glass petri dish and finely minced into 1–3-mm^3 pieces, using a scalpel. The pieces were rinsed once with PBS 1X solution and then transferred to a clean 6-well plate with 500 µl of trypsin solution added. The pieces were left for 30 minutes at 37°C in a 5% CO2 incubator. The trypsin was discarded, then the sample was washed once with PBS 1X and 4 mL of 1 mg mL^{-1}/well collagenase type 2 solution diluted in complete chondrocyte culture media [DMEM/HAMF 12 (Sigma Aldrich, St. Louis, LA, USA) supplemented with 10% FBS (Gibco, Thermo Fisher Scientific Inc, Waltham, MA, USA), 100 U mL^{-1} Penicillin and 100 µL mL^{-1} Streptomycin solution (Gibco, Thermo Fisher Scientific Inc, Waltham, MA, USA), and 2 mM L-Glutamine (Gibco)]. Samples were incubated for 48-72 hours at 37°C in a 5% CO2 incubator. The resulting suspension was aspirated, and the sample was centrifuged at 1500×g for 10 minutes, washed twice in PBS 1X using centrifugation at 1500×g for 3 minutes. The supernatant was removed, then the pellet was diluted in complete chondrocyte culture medium and passed through a 100 µm mesh nylon filter. The sample was then centrifuged at 400×g for 5 minutes, the supernatant removed, and the final resulting pellet was resuspended in 500 µl of complete chondrocyte culture medium, half of this solution was used for the hAPCs isolation as described below. A cell count was calculated on the remaining of the sample using a haemocytometer and trypan based live-dead staining under light microscopy and the solution was plated at a density of 10,000 cells/cm^2 onto non-coated TCPS and expanded for down line investigations.

3.1.4 ARTICULAR PROGENITOR CELL ISOLATION PROTOCOL

All steps are as per methods section 3.1.3 until half the final resuspended solution is obtained. At this stage, the already resuspended sample (in 250 µl of complete chondrocyte culture medium) is further diluted to a total of 9 mL with complete hAPCs medium [low glucose DMEM (Sigma Aldrich, St. Louis, LA, USA) supplemented with 10% FBS (Gibco, Thermo Fisher Scientific Inc, Waltham, MA, USA), 100 U mL^{-1} Penicillin and 100 µL mL^{-1} Streptomycin solution (Gibco, Thermo Fisher Scientific Inc, Waltham, MA, USA), 2 mM L-Glutamine (Gibco), and 15 mM HEPES (Gibco)]. Next, 3 mL of this solution was evenly distributed into three wells of premade fibronectin coated-well TCPS (6-well plate system, preparation method detailed below) and incubated for 20 minutes at 37°C. Non-attached cells were removed and 3 mL of new complete hAPCs culture medium added per well to allow cell expansion for down line investigations.

Fibronectin plate coating procedure (Sigma-Aldrich, St. Louis, MO, USA):

Lyophilised fibronectin powder is reconstituted with 2 mL of sterile water of protein (2 mg mL^{-1}, 2000X) and allowed to dissolve for 30 minutes at 37°C. Dilute the fibronectin to 10 mg mL^{-1} in sterile PBS 1X and coat the culture surface with a minimal volume (i.e. 500 µl for well of a 6-well plate). Plates were air-dried for 45 minutes at room temperature under a biosafety hood with the lid off. The excess was aspirated, and then plates stored at 4°C closed with parafilm until downline use.

3.1.5 CHEMICAL DIGESTION TIMEFRAMES

Under a laminar flow hood, the IFP was placed in a sterile glass petri dish, and 3 mL of complete hADSCs culture media is added. Using forceps and scalpel fat was removed from the fibrous material and diced until only the fat lobules are left. Diced fat was collected with a sterile pipette and transferred to a 50 mL tube with 0.3 mL of 10 mg mL^{-1} collagenase type 1 then added. Chemical digestion was then undertaken under constant agitation on a shaker at 250 rpm for timeframes of 10 minutes, 20 minutes, 30 minutes or 3 hours (Control). Samples were then centrifuged for 10 minutes at 2100×g, and the cell pellet was resuspended in 500 µl of complete hADSCs culture media, a cell count and viability were calculated using a haemocytometer and trypan based live-dead staining.

3.1.6 MATRIGEL-COATED TCPS WELLS FOR HADSCS ADHERENCE

Cell isolation was performed as per methods section 3.1.2 until the plating step. At this point, a cell count (Isolation cell count) was performed using a haemocytometer and trypan based live-dead staining. Cells were evenly split into two by volume and plated on non-coated TCPS wells (Control) or Matrigel-coated TCPS wells (Lifesciences, Corning, Tewksbury, MA, USA), the coating procedure is described below. All wells were tested for adherence at timeframes of 10 minutes, 20 minutes, 30 minutes, 1 hour, 6 hours, 12 hours and 24 hours. Adhesion at respective timeframes was tested by removing non-attached material and placing it in a 15 mL falcon tube, tubes were then centrifuged for 5 minutes at 300×g, the remaining pellet was resuspended, and a cell count (non-attached cells) performed.

Matrigel plate coating procedure, (Sigma-Aldrich, St. Louis, MO, USA):

12 mL of DMEM low glucose wasp placed in a 50 mL falcon tube, 880 µl of DMEM low glucose was removed and added and resuspended in a vial of Matrigel (120 µL). The total solution was immediately transferred and resuspended in the original falcon tube containing the remaining DMEM low glucose. 1 mL of solution was added to each desired well of a 6-well TCPS plate. The wells were air-dried for 1 hour with the lid off under a biosafety hood, and the excess was then aspirated. Plates were used immediately or stored wrapped in paraffin at 4°C for up to 7 days.

3.1.7 THE RAPID IFP-DERIVED MSCS (HADSCS) ISOLATION PROTOCOL

All steps were identical to the standard (control) isolation procedure detailed above in 3.1.2 apart from the following two changes which were shown to be optimisable for efficiency:

i) Chemical digestion was achieved in 30 minutes using 0.3 mL of 10mg mL^{-1} collagenase type 1 (Worthington Biochemical, Lakewood, NJ, USA),

ii) Cells were plated on Matrigel-coated TCPS wells (Lifesciences, Corning, Tewksbury, MA, USA) and incubated for 30 minutes to allow for cellular adherence. Wells were coated as per the manufacturer's protocol described above.

3.2 *IN VITRO* CELL CULTURE

3.2.1 CHONDROGENIC DIFFERENTIATION – PELLET CULTURE (HUMAN CELLS)

Chondrogenic differentiation was induced using the micro mass pellet culture technique, as described previously (140, 316): 2.5×10^5 confluent cells (Passage 3) mL^{-1} were placed in 1.5 mL tube (Sarstedt), centrifuged to form the pellets and initially cultivated with complete culture media. The next day, chondrogenic differentiation was commenced using DMEM high-glucose (Sigma), 100 U mL^{-1} penicillin and 100 µL mL^{-1} of streptomycin (Gibco), 2 mM L-Glutamine (Gibco), and 15 mM HEPES (Gibco), 1% insulin-transferring-selenium (Sigma), 100 nM dexamethasone (Sigma), 50 mg mL^{-1} ascorbate-2-phosphate (Sigma), 10 ng mL^{-1} TGFβ3 (Prepotech), and 10 ng mL^{-1} BMP6 (R&D Systems). Chondrogenic media was changed twice a week and pellets were collected and frozen at time points of 0 and 3 weeks.

3.2.2 CHONDROGENIC DIFFERENTIATION – 3D BIOSCAFFOLDS (HUMAN CELLS)

Biofabricated scaffolds were kept in 12 well TCPS plates, with chondrogenic media (formulation described in 3.2.1) changed twice a week, and samples were collected on day 0 and 3 weeks for analyses. The assessment was performed using GAG/DNA and qPCR methods as described later.

3.2.3 CHONDROGENIC DIFFERENTIATION – PELLET CULTURE (RABBIT CELLS)

Rabbit bone marrow derived MSCs (rBMSCs) isolated from New Zealand white rabbits were commercially sourced from Cyagen (Santa Clara, California). Cells were sourced at passage 2, expanded using the manufacturers MSCs growth medium (OriCell™, Cat. No. GUXMX-90011, Cyagen) and either used for *in vitro* chondrogenic analyses or frozen in liquid nitrogen for downline use. Cells (Passage 3) were pelleted at a number of 2.5×10^5 and then subject to 3 weeks of chondrogenic stimulation using the manufacturers' chondrogenic differentiation media (OriCell™, Cat. No. GUXMX-90041, Cyagen).

3.2.4 OSTEOGENIC DIFFERENTIATION – MONOLAYER 2D CULTURE (HUMAN CELLS)

Osteogenic differentiation was induced using cells at passage 3, by seeding hADSCs in 6-well TCPS plates at a seeding density of 5.0×10^5 cells per well with complete hADSCs culture media (Methods 3.1.2). The next day, osteogenic differentiation was commenced using DMEM low-glucose (Sigma), 2% FBS (Gibco), 100 U mL^{-1} penicillin and 100 µL mL^{-1} of

streptomycin (Gibco), 2 mM L-Glutamine (Gibco), 15 mM HEPES (Gibco), 10 mM β-glycerophosphate (Sigma), 50 µg mL^{-1} ascorbic acid (Sigma) and 100 nM dexamethasone (Sigma) was added. Osteogenic media was changed twice a week and samples were collected and frozen at time points of 0 and 3 weeks.

3.2.5 ADIPOGENIC DIFFERENTIATION – MONOLAYER 2D CULTURE (HUMAN CELLS)

Adipogenic differentiation was induced using cells at passage 3, by seeding hADSCs in six-well plates at a seeding density of 5.0×10^5 cells per well with complete hADSCs culture media (see methods 2.2.2). The next day, adipogenic differentiation was commenced using DMEM high glucose (Sigma), 2% FBS (Gibco), indomethacin 2^{-1} mM, 1 µM dexamethasone, 5^{-1} mM IBMX and 10 µM Insulin Bovine. Adipogenic media was changed twice a week and samples were collected and frozen at time points of 0 and 3 weeks.

3.3 PHENOTYPICAL *ANALYSIS*

3.3.1 HAEMATOXYLIN, FAST GREEN AND SAFRANIN 0 STAINING

Cells pellets were washed several times in PBS 1X, fixed in 1% paraformaldehyde (Santa Cruz Biotechnology, Dallas, TX, USA) for 4 hours at room temperature and then washed three times for 10 minutes each in PBS 1X. Next, they were embedded in Sucrose 30%-dH2O overnight at 4°C, embedded in O.C.T. TM Compound (Tissue-Tek, Sakura, Leiden, Netherlands) and flash-frozen in liquid nitrogen. Cryosections of 10 µm thickness were mounted onto glass slides and stained with Weigert's Haematoxylin (Sigma-Aldrich) for 5 minutes, washed in tap water, differentiated in Acid alcohol 1% (v/v) for 2 seconds and rinsed in dh_20 3 times. Next, they were stained with Aqueous Fast Green (Sigma-Aldrich) 0.05% (w/v) for 5 minutes and then rinsed in Acetic acid 1% (v/v) for 30 seconds. Finally, they were stained in Safranin O (Sigma-Aldrich) for 30 minutes, dipped in 95% (v/v) and 100% ethanol, cleaned three times for 1 minute each in Xylene (Chem-Supply, GILLMAN, SA, Australia) and then mounted in Pertex medium (Grale HDS, Ringwood, VIC, Australia). Samples were imaged using an epifluorescent inverted NikonTiE microscope equipped with a DSRi2 and NIS-Elements software using a Plan Fluor ELWD 10X DIC L NA 0.45 objective.

3.3.2 IMMUNOSTAINING – PELLET CULTURE

For fluorescence analysis, 10 µL thickness cryosections (for procedures see Safranin O staining paragraph) were washed three times in PBS1X and permeabilized for 15 minutes in PBS 1X-

0.1% TritonX-100 (PBT). Antigen retrieval was performed by adding 1 mg ml^{-1} Hyaluronidase (SIGMA, #H6254) diluted in PBS 1X and incubating 30 minutes at room temperature. After three washes 5 minutes each in PBS 1X, samples were dropped in blocking solution (10% goat serum diluted in PBT) for 60 minutes at room temperature and then incubated overnight at 4°C with mouse anti-human Collagen II (#II6B3, DSHB) diluted 1:250 in blocking solution. The day after, samples were washed, and the secondary antibody anti-mouse IgG Alexa Fluor-647 (#715-605-151, Jackson Immuno Research) diluted 1:100 in blocking solution was added and incubated for 2 hours at room temperature. After three washes 5 minutes each in PBS 1X, actin was labelled with Phalloidin FITC (#P5282 SIGMA) 1:500 diluted in PBT for 60 minutes, next nuclei were stained with DAPI (Thermo Fisher Scientific Inc.) 1:200 diluted in PBT for 60 minutes. Sections were washed 5 minutes each in PBS 1X and mounted with Fluoromount-G (Southern Biotech, Birmingham, AL, USA) onto glass slides. Samples were imaged with NikonA1R confocal microscope using a Nikon Plan VC 10× DIC N2 N.A. 0.75 objective lens and processed using NIS-Elements software and Large Image function (Nikon, Amsterdam, Netherlands).

3.3.3 IMMUNOSTAINING AND COLLAGEN 2 INTENSITY– 3D BIOSCAFFOLDS

For fluorescence analysis, 10 µL thickness cryosections (for procedures see Safranin O staining paragraph) were washed three times in PBS 1X and permeabilized for 15 minutes in PBS 1X-0.1% TritonX-100 (PBT). Antigen retrieval was performed by adding 1 mg ml^{-1} Hyaluronidase (SIGMA, #H6254) diluted in PBS 1X and incubating for 30 minutes at room temperature. After three washes 5 minutes each in PBS 1X, samples were dropped in blocking solution (10% goat serum diluted in PBT) for 60 minutes at room temperature and then incubated overnight at 4°C with mouse anti-human Collagen II (#II6B3, DSHB) and goat anti-human Collagen I (# sc8784, Santa Cruz) both diluted 1:250 in blocking solution. The day after, samples were washed and secondary antibodies anti-mouse IgG Alexa Fluor-647 (#715-605-151, Jackson Immuno Research) and anti-goat IgG Alexa Fluor-546 (# A11056, Thermo Fisher Scientific Inc.), both diluted 1:100 in blocking solution were added and incubated for 2 hours at room temperature. After three washes 5 minutes each in PBS 1X, actin was labelled with Phalloidin FITC (#P5282 SIGMA) 1:500 diluted in PBT for 60 minutes, next nuclei were stained with DAPI (Thermo Fisher Scientific Inc.) 1:200 diluted in PBT for 60 minutes. Sections were washed 5 minutes each in PBS 1X and mounted with Fluoromount-G (Southern Biotech, Birmingham,

AL, USA) onto glass slides. Samples were imaged with NikonA1R confocal microscope using a Nikon Plan VC 20× DIC N2 N.A. 0.75 objective lens and processed using NIS-Elements software and Large Image function (Nikon, Amsterdam, Netherlands). The Collagen II intensity fluorescence measurement analysis was performed with the ROI features plug-in of NIS-Element software.

3.3.4 IMMUNOPHENOTYPING – FLOW CYTOMETRY

Immunophenotypic characterisation of hADSCs, chondrocytes and hAPCs was performed by using a fluorescence-activated cell sorting (FACS) analysis of cell–surface markers at passage 3. Cells were labelled with monoclonal antibodies against CD31, CD34, CD45, CD73, CD90, CD146– FITC conjugates and CD44, CD49e—APC conjugated (Affimetrix bioscience, ThermoFisher Scientific). Control samples were labelled with isotype-matched control antibodies IgG1K-FITC and IgG1K-APC (Affimetrix bioscience). In brief, cells were trypsinised and aliquoted at a concentration of 2.5×10^5 cells mL^{-1}, fixed in 0.5% paraformaldehyde for 30 minutes at 4 °C, and washed once in PBS 1X. Next, samples were incubated with either conjugated specific antibodies or isotype-matched control at the manufacturer's recommended concentrations, diluted in PBS 1X supplemented with 5% FBS (FACS buffer). Labelled cells were washed, suspended in FACS buffer and analysed using a FC500 flow cytometer (Beckman Coulter).

3.4 MOLECULAR ANALYSIS

3.4.1 RNA EXTRACTION AND REVERSE TRANSCRIPTION

RNA was extracted and purified using Tri Reagent (Ambion, Austin, TX, USA) and the Direct zol-RNA miniprep kit (Zymo research) as per manufacturers protocol. RNA concentration and purity were measured using a NanoDrop spectrophotometer (Peqlab, Erlangen, Germany) and the Agilent 2100 BioAnalyzer (Agilent Technologies, Santa Clara, CA, USA). Complimentary DNA copies were reverse transcribed from 250 ng total RNA for all samples using oligo-dT primers and the Omniscript RT kit (Quiagen) as per manufacturer's protocol.

3.4.2 CHONDROGENIC GENE EXPRESSION (QPCR)

Relative amounts of RNA were evaluated with the TaqMan Gene expression assay (Applied Biosystems, Foster City, CA, USA) using the following probes: SOX9, ACAN, COL2A1, COL1A2, as target genes; GAPDH as the housekeeping gene, details shown in Table 3.1. RT-qPCR was

performed using the Quant Studio 6 Flex Real-Time PCR System (Thermo Fisher Scientific), relative quantification was calculated with the $2e^{-\Delta\Delta CT}$ method. The mean ΔCT value of the control sample was used in each experiment to calculate the ΔΔCT value of sample replicates by using the housekeeping gene (GAPDH).

TAQMAN gene markers	Applied biosystem reference number	Lineage of marker
Collagen 1 (COL 1A2)	Hs00164004_m1	Chondrogenic
Collagen 2 (COL 2A1)	Hs00264051_m1	Chondrogenic
Sex determining region Y-box9 (SOX-9)	Hs00165814_m1	Chondrogenic
Aggrecan (ACAN)	Hs00153936_m1	Chondrogenic
Glyceraldehyde 3-phosphate dehydrogenase (GAPDH)	Hs02786624_g1	House Keeping

Table 3.1. Probes used to assess chondrogenesis in RT- qPCR with the TAQMAN system.

3.4.3 OSTEOGENIC GENE EXPRESSION (QPCR)

Relative amounts of RNA were evaluated with the TaqMan Gene expression assay (Applied Biosystems, Foster City, CA, USA) using the following probes: osteocalcin (BGLAP), runX2 and ALP as target genes; GAPDH as the housekeeping gene, details shown in Table 3.2. RT-qPCR was performed using the Quant Studio 6 Flex Real-Time PCR System (Thermo Fisher Scientific), relative quantification was calculated with the $2e^{-\Delta\Delta CT}$ method. The mean ΔCT value of the control sample was used in each experiment to calculate the ΔΔCT value of sample replicates by using the housekeeping gene (GAPDH).

TAQMAN gene markers	Applied biosystem reference number	Lineage of marker
Osteocalcin (BGLAP)	Hs01587814_g1	Osteogenic
RUNX2	Hs01047973_m1	Osteogenic
Alkaline phosphatase (ALP)	Hs01029144_m1	Osteogenic
Glyceraldehyde 3-phosphate dehydrogenase (GAPDH)	Hs02786624_g1	House Keeping

Table 3.2. Probes used to assess osteogenesis in RT- qPCR with the TAQMAN system

3.4.4 ADIPOGENIC GENE EXPRESSION (QPCR)

Relative amounts of RNA were evaluated with the SYBR power up green Gene expression assay (Applied Biosystems, Foster City, CA, USA) using the following forward and reverse primers: CEBPα and FAB 4 as target genes; GAPDH as the housekeeping gene, details shown in Table 3.3. RT-qPCR was performed using the Quant Studio 6 Flex Real-Time PCR System (Thermo Fisher Scientific), relative quantification was calculated with the $2e^{-\Delta\Delta CT}$ method. The mean ΔCT value of the control sample was used in each experiment to calculate the ΔΔCT value of sample replicates by using the housekeeping gene (GAPDH).

SYBR green gene markers	Primer Sequence	Lineage of marker
CEBPα (CCAAT/enhancer-binding protein alpha)	FORWARD: TATAGGCTGGGCTTCCCCTT REVERSE: AGCTTTCTGGTGTGACTCGG	Adipogenic
FABP4 (Fatty Acid Binding Protein 4)	FORWARD: AACCTTAGATGGGGGTGTCCTG REVERSE: TCGTGGAAGTGACGCCTTTC	Adipogenic
Glyceraldehyde 3-phosphate dehydrogenase (GAPDH)	FORWARD: AATTCCATGGCACCGTCAAG REVERSE: AGGGATCTCGCTCCTGGAAG	House Keeping

Table 3.3. Probes used to assess adipogenesis in RT- qPCR with the SYBR green system.

3.4.5 CHONDROGENIC ASSESSMENT - GAG/DNA QUANTIFICATION (HUMAN AND RABBIT CELLS)

Cell pellets were collected and digested for 5 hours at 60°C using papaine extraction solution (250 μg mL^{-1} papaine, Sigma-Aldrich) and then centrifuged. Aliquots of the supernatant were assayed separately for glycosaminoglycan (GAG) and DNA content. Sulphated GAG content was determined with the dimethylmethylene blue (DMMB) method and chondroitin sulphate, while DNA content was determined with a Pico Green kit (Invitrogen). Synthetic GAG activity was calculated using a normalised GAG/DNA ratio in each sample.

3.5 *IN VITRO* BIOFABRICATION - 3D BIOSCAFFOLDS

3.5.1 BIOINK FORMULATIONS

Gelatin-Methacryloyl/Hyaluronic Acid (GelMA/HA) was synthesized, as previously described (175, 177). The material was dissolved to a final concentration of 100 mg mL^{-1} GelMA and 25 mg mL^{-1} HA (GelMA 10% /HA 2.5%) in sterile PBS 1X (Sigma-Aldrich). Cells (passage 3) were mixed into the hydrogel to form bioinks at 3 different cell concentrations: 1.25, 2.5 and 5.0 million hADSCs/mL. Next, 0.05% lithium phenyl-2,4,6-trimethylbenzoylphosphinate (LAP) was mixed into the bioink, which is a photoinitiator required for light assisted crosslinking.

*To enable the use of a consistent batch of GelMa material throughout all experiments, the MA degree of functionalisation amount was kept the same. Furthermore, changing the degree of methacrylation changes the rheological properties leading to higher viscosity (317).

3.5.2 GENERATION OF BIOSCAFFOLD MOULDS

Using AutoCAD fusion 360 software (Autodesk), 200 µL volume (200mm^3 = 1cm^2 TSA, 2 mm depth) mould templates were designed. Template were printed (Figure 3.1) using an Object30 Prime 3D polyjet printer (Stratasys) with MED610 (Stratasys) material. MED610 is an acrylic based transparent biocompatible photopolymer which is used in 3D printing (318). The resulting construct was cleaned and sterilised in 100% ethanol. Next, Platinum Silicone Rubber Part A and B (Solid Solutions, Solid Mould 550), (Figure 3.1B), were evenly mixed and stirred in a container. The mixture was then used to fill in the constructed template (Figure 3.1C) and covered with glass slides to contain the mixture without air bubbles. These were left overnight, and then the glass removed. The resulting PDMS (the negative) rubber construct was cut up into individual moulds (Figure 3.1D). Moulds were sterilised in an 80% ethanol bath for 30 minutes and subject to UV light for 10 minutes before use.

3.5.3 BIOFABRICATION PROCEDURE - GENERATION OF 3D BIOSCAFFOLDS

The above three bioinks (Methods 3.5.1) were loaded into 1 mL syringe cartridges and extruded into the individual PDMS scaffold moulds (described in Methods 3.5.2). Immediately after extrusion, samples were UV irradiated at room temperature for 10 seconds to both top and bottom using a 365 nm UV light source (Omnicure LX400 +, Lumen DynamixLDGI) with a light intensity of 700 mW cm^{-2}. The procedural workflow is visually represented in Figure 3.2.

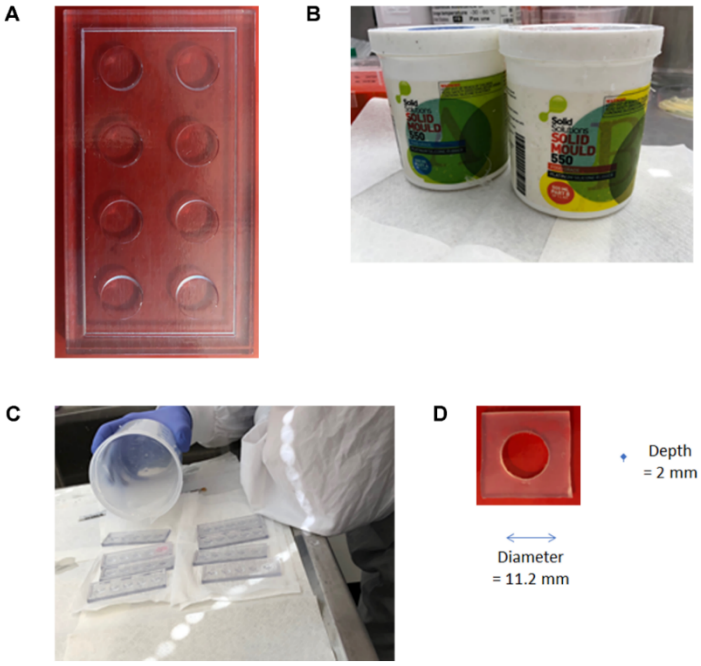


Figure 3.1. (Right) Design and preparation of scaffold template and moulds. A) Scaffold template, B) Silicone Rubber parts A and B, solid solutions, C) Filling of the template with rubber solution, D) Individual Bioscaffold mould.

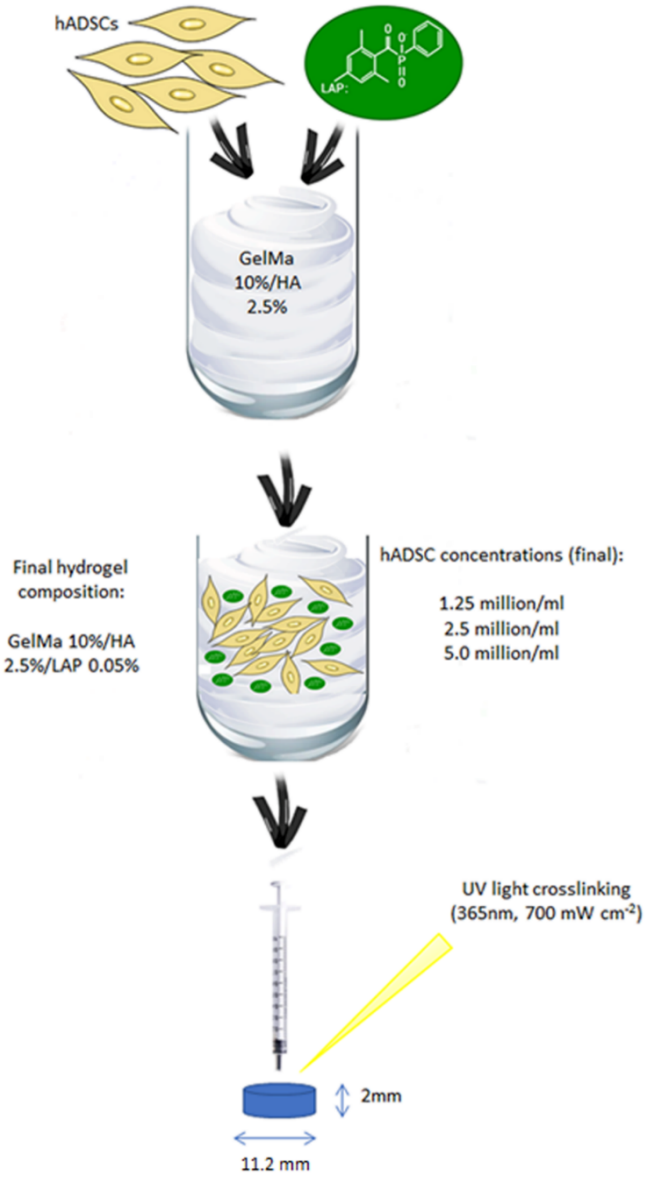


Figure 3.2. (Left) Graphical representation of the biofabrication procedure. Human adipose-derived mesenchymal stem cells (hADSCs), Gelatin-Methacryloyl/Hyaluronic acid (GelMA/HA) and UV light assisted photoinitiator (LAP).

3.6 DESIGN OF *IN VIVO* BIOFABRICATION PROCEDURE

3.6.1 BIOINK FORMULATIONS

Gelatin-Methacryloyl (GelMA) was synthesised, as previously described (175, 177). The material was dissolved to a final concentration of 60 mg or 100 mg mL^{-1} GelMA to form a soft and a hard hydrogel (Soft = 6% GelMA and Hard = 10% GelMA) in sterile PBS 1X (Sigma-Aldrich), containing 100 U mL^{-1} penicillin and 100 µL mL^{-1} of streptomycin (Gibco). Next, 0.1% lithium phenyl-2,4,6-trimethylbenzoylphosphinate (LAP) was added (photoinitiator required for light-assisted crosslinking). Notably, in comparison to the material used in section 3.5 - *In vitro* biofabrication, HA is not used combined with GelMa. In the *in vitro* experiments, both the top and bottom surfaces of the cylindrical bioscaffolds were crosslinked (described in 3.5.3) to enable full penetrance, which is more difficult to achieve with the addition of HA which increases the material opacity (319). This was shown by work performed in our broader lab in parallel (319), in the *in vivo* model only the top of the bioscaffolds construct can be exposed to crosslinking and therefore HA was removed from the composition to allow full penetrance of light.

3.6.2 MECHANICAL TESTING OF HYDROGELS– COMPRESSION TESTING

To validate the compressive strength of the two hydrogel formulations (Soft and Hard GelMA) described above, unconfined compression testing which is well accepted in cartilage engineering evaluation (320-322) was performed on triplicates of acellular scaffolds fabricated into 200 µL templates (Methods 3.5.2). Testing was performed at controlled room temperature (23°C) using a TA Electroforce 5500 mechanical loading device (TA Instruments, New Castle, USA) fitted with a calibrated 22 N load cell. The contact point between the two plates was recorded. Then, the sample was placed between two 4.2 cm diameter compression plates, in an unconfined setting, as previously described (171). A ramp function controlled the displacement of the upper plate, at a rate of 0.01 mm s^{-1}, until a total displacement of 25% of the sample height (0.5 mm). The contact area of the sample with the plate was measured by microscopy imaging before the test. Additionally, the point of inflexion of the load versus time curve showed the contact point between the sample surface and the compression plate to give the sample height. Load and displacement measurements were converted into stress (σ) and strain (ε) data using the sample surface area and height. The compressive modulus was then computed using stress data between 25% and 30% strain as follows: E_C = (σ30−

σ25)/(ε30−ε25). Three replicates for each of the formulations were tested and analysed. Data graphs were designed using Prism 8 software (GraphPad).

3.6.3 HYDROGEL GELATION TIME – FILAMENT FORMATION TEST

The printability of a hydrogel in a semi-gelated form can be easily evaluated using a filament formation test (177, 323, 324). Other recently described more elaborate methods that can be used to assess the shape fidelity of a hydrogel post printing, include the filament collapse and filament fusion tests (325). Using the filament formation test, 700 µl of each of the two chosen hydrogels (6% GelMA and 10 % GelMA) were loaded into 1 mL pneumatic cartridges and a 250 µm needle nozzle was attached. Next, the loaded system was kept in heater oven at 37°C to maintain them in a liquid state. Bioinks were removed and allowed to gelate for different time points using both a controlled room temperature of 23°C and a colder temperature of 4°C (Fridge). After respective gelation time points, cartridges (containing the bioinks) were loaded vertically onto the stand of a pneumatic piston device, (Figure 3.3A). The pneumatic piston device was set at an extrusion rate of 240 µL/min, which is the average controlled extrusion pressure of a hand-held syringe. Extrusion was performed, and the morphology of the bioinks as they emerged from the nozzle was observed using a fixed height video recording device. The formation of a liquid droplet, which drops from the nozzle (Figure 3.3B) was reported as a test failure, as the hydrogel is too liquefied for printing. The formation of gel that curls before hanging <5 mm from the tip of the nozzle or can't be continuously extruded for 5 seconds in a straight line indicated a failure of the test due to the hydrogel being hypergelated, (Figure 3.3D). The formation of a thin filament, hanging >5mm from the tip of the nozzle continuously over 5 seconds of extrusion indicated a test pass and meant that the bioink was printable, (Figure 3.3C). The results from both the bioink compositions using different gelation times and temperatures were then tabulated.

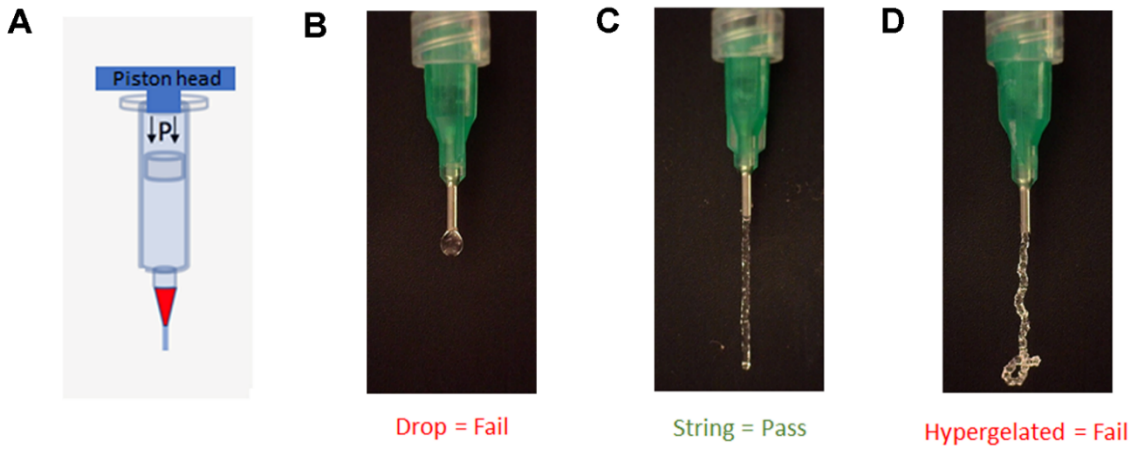


Figure 3.3. The filament formation test – assessment of hydrogel printability. A) Set-up, B) Formation of a liquid drop at the end of the nozzle – nonprintable, C) Formation of a continuous stringy filament upon extrusion, indicating a printable hydrogel composition. C) Formation of a non-continuous stringy filament that folds before 0.5mm or 5 secs of extrusion, hypergelated hydrogel. P – indicates the extrusion pressure.

3.6.4 SELECTION AND FIXATION OF THE LIGHT SOURCE (CROSSLINKING) AND DISTANCE

In view of being able to apply light-initiated cross-linking to bioscaffolds intraoperatively, a portable and easily operated light source attachment (BioLambda 405 nM wavelength, visible light, Sao Paulo, Brazil) was used. In this section a 405nM (visible light) source was used compared to the UV light source (365nM) used earlier in the *in vitro* bioscaffolds study (section 3.5.3). This transition was undertaken based on emergent findings in the literature, which showed more biocompatibility, penetrance and homogenous cross-linking when using visible light (>380Nm) assisted crosslinking for GelMa hydrogels in comparison to UV light (159, 326).The BioLambda (405 nM wavelength, visible light) hand-held device can be easily sterilised and surgically draped, enabling comfortable manoeuvring during surgery. Given the diameter of the defect model to be used (Figure 3.4), the optimal distance between the light source and the defect was identified as being 1 cm. This distance enables full coverage of the defect area (4 mm circular diameter) without affecting healthy surrounding tissue, (Figure 3.4); furthermore, the intensity of light is maintained at 10 mW/cm^2 over 60 seconds enabling adequate cross-linking of the hydrogel. To keep this distance fixed during the cross-linking procedure, a customised 3D fixed distance attachment cover was designed and printed using polylactic acid (PLA) material. This cover could be sterilised using ethanol and UV light, final design and intraoperative are shown in the results section of chapter 6.

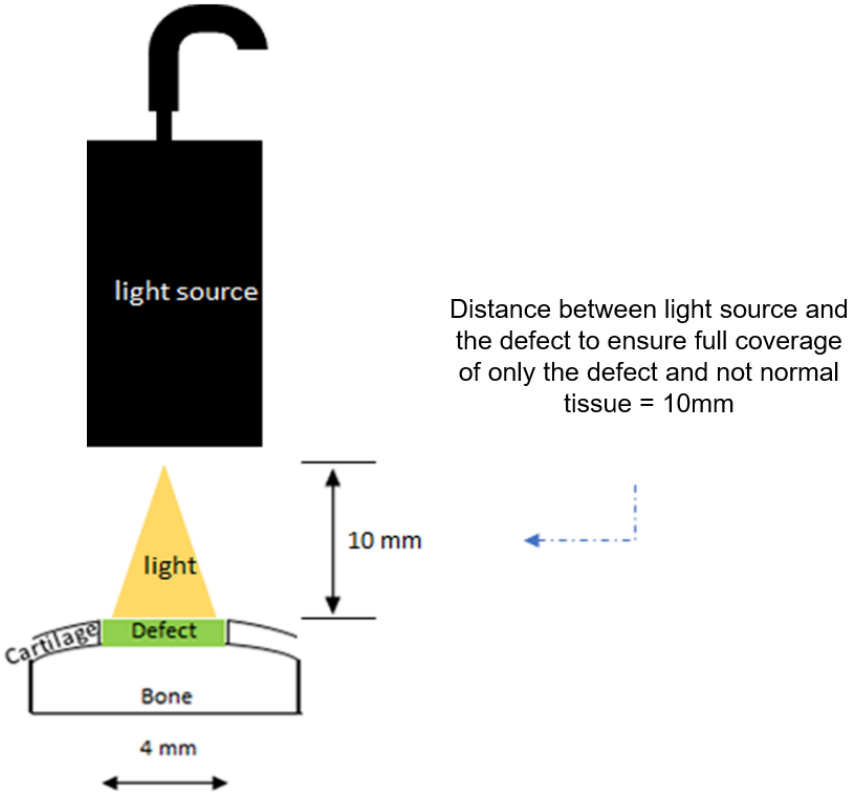


Figure 3.4. (Left) The distance required to cross-link the entire defect repair surface area safely. Green - Hydrogel based repair and Yellow –Visible light (405 nm).

3.7 *IN VIVO* BIOFABRICATION - RABBIT MODEL OF CARTILAGE REPAIR

3.7.1 ANIMAL ETHICS STATEMENT

This study was approved by the Animal Ethics Committee [AEC/002/19-r1] and the Experimental Medical and Surgical Unit (EMSU) of St. Vincent's Hospital, Melbourne, Australia. The animal study was conducted in accordance with the Australian Code for the Care and Use of Animals for Scientific Purposes (8th Edition).

3.7.2 SURGICAL MODEL OF CHONDRAL REPAIR

ANIMALS

Twelve New Zealand white male rabbits (Flinders, South Australia) between 3 and 4 months of age (Weight 2.7-3.0 kg) were used for the study (n=6 for each time point), an extra 2 were set aside based on the complication rates described in the literature (292). Rabbits were acclimatised and individually housed in cages.

In the rabbit model, the lateral collateral ligament commonly traverses and is in contact with the under surface of the lateral femoral condyle, to combat this, all treatment groups were evenly randomised to either condyle. In each rabbit, all four treatment groups were

performed, therefore utilising all the femoral condyles, Table 3.4. Timepoints were selected based on when early and mature cartilage formation is detectable, which is generally at 3-4 and 6-8 weeks, respectively post-repair (308).

Although rabbit cartilage can spontaneously heal (309), the literature suggests using a 3 mm diameter defect or larger as the critical-size to prevent this natural revival (310-312). Rabbit articular knee cartilage, on average is approximately 0.3 mm thick (or deep) (313), the width of each condyle is roughly 5-6mm. (314, 315) Therefore based on current literature, to assess critical size defects (314, 315) in this model a 4 mm diameter circular defect with a depth of 0.3 mm was chosen, this creates a volume of approximately 4 µL (mm^3), (Figure 3.5). A cylindrical defect is used as it can be easily manipulated using a twisting motion with a punch biopsy; in contrast, procedurally it is difficult to accurately create a cuboid type punch defect with such a small thickness.

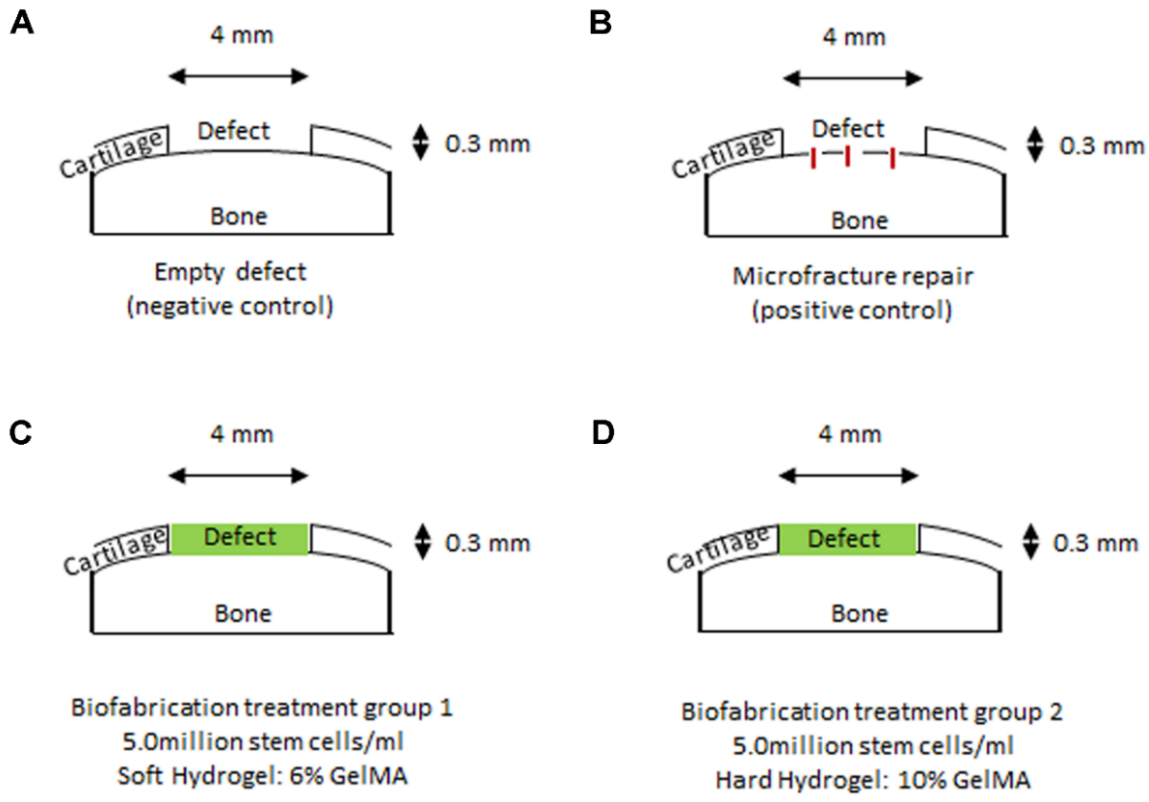


Figure 3.5. Graphical representation of treatments groups used in the rabbit model of cartilage repair. A) Empty, B) Microfracture repair and C-D) Biofabrication treatment groups. GelMA - Gelatin-Methacryloyl.

Treatment group	4-week timepoint	8-week timepoint
A) Empty (Negative control)	n=6	n=6
B) Microfracture (Positive control)	n=6	n=6
C) Biofabrication treatment group 1 5.0 million stem cells/mL Soft Hydrogel: 6% GelMA	n=6	n=6
D) Biofabrication treatment group 2 5.0 million stem cells/mL Hard Hydrogel: 10% GelMA	n=6	n=6
Total number of animals	12 animals (2 extras purchased, 14 in total)	

*Table 3.4. Distribution of rabbits and treatment groups. *Note each rabbit has 4 condyles.*

SURGICAL PROCEDURE

After subcutaneous injection of a pre-anaesthetic agent, general anaesthesia was induced using 35 mg/kg of ketamine (CEVA Animal Health Pty Ltd, Glenorie, NSW, Australia) and 5 mg/kg of xylazine (Troy Laboratories Pty Ltd, Glendenning, NSW, Australia). Anaesthesia was maintained intraoperatively using isoflurane/oxygen (AbbVie Pty Ltd, Botany, NSW, Australia). After successful induction of anaesthesia, knee and groin hair was shaved and the skin was prepped (decontaminated) using a 70% alcoholic chlorhexidine solution (Biotech Pharmaceuticals Pty Ltd, Laverton North, Victoria, Australia). A midline longitudinal incision was made over the knee joint followed by a medial parapatellar arthrotomy to access the joint. The patella was then dislocated laterally, and the infrapatellar fat pad was removed with a scalpel and discarded to help expose the femoral condyles. The knee was then flexed to reveal the weight-bearing regions of the femoral condyles. A cylindrical chondral defect in the centre of each of the femoral condyles was created using a 4 mm diameter biopsy punch and tissue was removed by scalpel dissection. This procedure was performed again on the contralateral knee, therefore, exposing both distal femurs (total of 4 femoral condyles per rabbit). Animals were randomly assigned to treatment groups, and treatment groups were evenly allocated to medial and lateral condyles. The four treatment groups performed were:

1) Empty defect -> No repair performed (Negative control).
2) Microfracture -> Subchondral bone in the defect was pierced with a micro awl several times to allow for bleeding and then clotting (Positive control).

3) Biofabrication treatment group 1 -> Stem cells at a concentration of 5.0 million MSCs /mL were mixed with 6% GelMA/0.05% LAP (Prepared before surgery, see 5.2.2) and into a 1 mL pneumatic syringe (250 µm needle nozzle attached). The syringe was then placed in a 4°C fridge for 9 minutes prior to use. Bioinks were then extruded using the hand-held syringe directly into the defect. The final construct was subject to visible light (405 nm wavelength) for 60 secs, held 1 cm away from the defect to allow for cross-linking of only the defect regions of focus (Treatment group 1).
4) Biofabrication treatment group 2: same as biofabrication treatment group 1 but using the harder hydrogel bioink composition of 10% GelMA/0.05% LAP and 3 minutes for gelation in a 4°C fridge (Treatment group 2).

Post-treatment, the patella was relocated, and the joint capsules were closed using 4–0 dexan sutures (Ethicon, Johnson & Johnson Medical, Somerville, NJ). The skin was closed using 5–0 monocryl subcuticular continuous stitch (Ethicon) and reinforced with interrupted horizontal sutures where necessary. The closed wound was then sprayed with wound fixation spray (Smith and Nephew, Australia).

Postoperative analgesia was subcutaneously administered as required using Carprofen 1.5 mg/kg (Carprofen Ventral TM, Sigma–Aldrich Corp., St Louis, MO). Animals recovered on a heat pad before being returned to their pens. Animals were monitored by animal technicians daily. Wound healing was monitored for 5-7 days. The rabbits could mobilise freely post-recovery in open pens (hay bedding) for the remainder of the tested time point, and access to food and drink was ad libitum. At respective time points, rabbits were humanely killed using inhalation anaesthesia followed by intracardiac injection of Lethobarb (Virbac Australia Pty Ltd, Milperra, NSW, Australia). The knee joint was exposed, disarticulated, and the femoral condyles were harvested.

3.7.3 MACROSCOPIC EVALUATION

The femoral joints were explanted, and then the distal femur and femoral condyles were exposed and cut using a hand-held rotary saw (Dremel, USA). The defects were macroscopically assessed using the International cartilage repair society (ICRS) macroscopic cartilage repair score, Table 3.5 (327). Four investigators with expertise in the field of

ICRS MACROSCOPIC SCORING SYSTEM OF CARTILAGE REPAIR			
PARAMETERS	**POINTS**	**PARAMETERS**	**POINTS**
Degree of defect repair		***Integration to the border zone***	
0% depth of defect repair	0	¼ of graft integrated, or no integration	0
25% depth of defect repair	1	½ of graft integrated (border > 1mm in ½)	1
50% depth of defect repair	2	¾ of graft integrated (border >1 mm in ¼)	2
75% depth of defect repair	3	Demarcating border < 1mm	3
level with surrounding cartilage	4	Complete integration	4
Macroscopic appearance		**MAXIMUM SCORE AVAILABLE**	12
Total degeneration of the grafted area	0	Grade I (normal)	12
		Grade II (nearly normal)	8-11
Several, small/few but large fissures	1	Grade III (abnormal)	4-7
		Grade IV (severely abnormal)	1-3
Small, scattered fissures or cracks	2	No repair	0
Fibrillated surface	3		
Intact smooth surface	4		

musculoskeletal disease and repair scored images of the defects and were blinded to the treatment type. Scores were collated and evaluated using Prism 8 (GraphPad) software.

Table 3.5. Macroscopic scoring system of cartilage repair. System according to the international cartilage repair society (ICRS) (327).

3.7.4 BIOMECHANICAL EVALUATION - ATOMIC FORCE MEASUREMENT

Following the macroscopic evaluation, 1 by 1 cm osteochondral blocks centred over the defect area (containing the defects and subchondral bone) were cut out using a hand-held rotary saw. The blocks were cute in such a way that there was a 3 mm bone and cartilage margin surrounding the original defect. The osteochondral blocks were then taken for atomic force measurement using a nanoindentation system. AFM nanoindentation was performed on an MFP-3D (Asylum Research) using the contact mode MLCT probe (Bruker Nano Inc). Force curves were presented to an indentation force of 5 nN at an approach rate of 2 ms^{-1}.

The sample Poisson's ratio was set at 0.31 based on literature describing the ratio in 4-month-old male New Zealand white rabbits (328). The Young's Modulus was obtained using the Hertz indentation model approximating the tip-shape as a 19.2° cone. Osteochondral defects were submerged in PBS 1X during measurement to preserve samples without drying. To enable the substantial representation of each defect, 100 indentations across three different regions were performed in a standardised fashion, making 300 force curves per sample. Three samples for each of the microfracture and two biofabrication treatment groups for both time points were measured. The same AFM probe was used for all measurements. Empty groups were not tested at these time points given the time-critical nature of getting samples though the AFM workflow and into formalin fixation for microscopic testing. However, the empty group and healthy rabbit knee cartilage were tested at time 0, using the extra/spare rabbits. As a reference, the youngs modulus reported in the literature for healthy 3 month-old male rabbit knee cartilage is roughly 600 kPa (329, 330).

3.7.5 MICROSCOPIC EVALUATION- HISTOLOGY AND SCORING

Following AFM analysis, osteochondral blocks were fixed in 10% neutral buffered formalin (Sigma Aldrich) for 48 hours. Subsequently, the samples were decalcified using ETDA as previously described for up to 48 hours (226, 331), then embedded in paraffin wax and allowed to cool for 60 minutes. Cryosections of 7 µm thickness were mounted onto glass slides and stained with Haematoxylin and Eosin as per the respective anatomical histopathology service protocol used (4-week samples -> University of Melbourne Histopathology Service, 8-week samples -> St Vincent's Public Hospital Melbourne Pathology department). Samples were imaged using a high-resolution mirax digital slide scanner (University of Melbourne, Australian Phenomics Networks Service) and subsequently processed using the caseviewer 2.3 software application (3d histotech, Budapest, Hungary). Stained samples (H&E) were collated and prepared. Subsequently, samples were blinded and scored by three different investigators from different backgrounds (Molecular biologist, Cellular biologist and Orthopaedic surgeon) using an adapted version of the modified O'Driscoll scoring system (Table 3.6), which was developed according to the Osteoarthritis Research Society International (OARSI) recommendations (18). Three parameters were removed from the original system, as they assess osteochondral repair: subchondral bone

formation, intactness of calcified layer and inflammation. Results were graphed and statistical evaluation performed using Prism 8 (GraphPad) software.

MODIFIED O'DRISCOLL MICROSCOPIC SCORING SYSTEM OF CARTILAGE REPAIR			
PARAMETERS	**POINTS**	**PARAMETERS**	**POINTS**
Tissue morphology		***Matrix staining***	
Exclusively non-cartilage	1	None	1
Mostly non-cartilage	2	Slight	2
Mostly fibrocartilage	3	Moderate	3
Mostly hyaline cartilage	4	Strong	4
Structural integrity		***Surface architecture***	
Severe disintegration	1	Severe fibrillation or disruption	1
Cysts or disruption	2	Moderate fibrillation or irregularity	2
No organisation of chondrocytes	3	Slight fibrillation or irregularity	3
Beginning of columnar organisation of chondrocytes	4	Normal	4
Normal, similar to healthy mature cartilage	5		
Chondrocyte clustering in implant		***Lateral integration***	
25-100% of cells clustered	1	Not bonded	1
<25% of cells clustered	2	Bonded at one end only/partially at both ends	2
No clusters	3	Fully bonded at both ends	3
Basal integration		***Defect filling***	
<50%	1	<25%	1
51-75%	2	26-50%	2
76-90%	3	51-75%	3
91-100%	4	76-90%	4
		91-110%	5
TOTAL MAXIMUM SCORE AVAILABLE			**32**

Table 3.6. Microscopic scoring system of cartilage repair. A system adapted from the Modified O'Driscoll histological score described by Nettles et al 2008, (332).

3.7.6 MICROSCOPIC EVALUATION- IMMUNOSTAINING

For fluorescence analysis, 7 µL thickness sections (for section preparation refer to Methods 3.7.5) were washed three times in PBS 1X and permeabilised for 15 minutes in PBS 1X-0.1% Triton X 100 (PBT). Antigen retrieval was performed by adding 1 mg mL^{-1} Hyaluronidase (SIGMA, #H6254) diluted in PBS 1X and incubating for 30 minutes at room temperature. After three 5 minute washes each in PBS 1X, samples were dropped in blocking solution (10% bovine serum albumin diluted in PBT) for 60 minutes at room temperature and then incubated overnight at 4°C with mouse anti-rabbit Collagen II (#II6B3, DSHB) and goat anti-rabbit Collagen I (# UNLB, Southern Biotech) both diluted 1:250 in blocking solution. The day after, samples were washed and secondary antibodies anti-mouse IgG Alexa Fluor-647 (#715-605-151, Jackson Immuno Research) and anti-goat IgG Alexa Fluor-546 (# A11056, Thermo Fisher Scientific Inc.), both diluted 1:100 in blocking solution were added and incubated for 2 hours at room temperature. After three washes 5 minutes each in PBS 1X, nuclei were stained with DAPI (Thermo Fisher Scientific Inc.) 1:200 diluted in PBT for 60 minutes. Sections were washed 5 minutes each in PBS 1X and mounted with Fluoromount-G (Southern Biotech, Birmingham, AL, USA) onto glass slides. Samples were imaged with a NikonA1R confocal microscope using a Nikon Plan VC 20× DIC N2 N.A. 0.75 objective lens and processed using NIS-Elements software and Large Image function (Nikon, Amsterdam, Netherlands).

3.8 THEOREMS

3.8.1 CELLULAR ADHERENCE

The percentage of adherence was calculated using the following equation:

$$\text{Adherence (\%)} = \frac{[(\text{Isolation cell count}) - \text{non-attached cell count}] \times 100}{(\text{Isolation cell count})}$$

3.8.2 GROWTH KINETICS - DOUBLING TIME

The proliferation rate of the cells between isolation and passage 1 (P0-1, i.e., never passaged) was evaluated by calculating their doubling time over 7 days. The cell population doubling time was calculated using the following equation (333):

$$\textit{Doubling time} = (t2 - t1) \times [\ln(2) / \ln(n2/n1)]$$

Theorem: Where *t*2-*t*1 is the number of days in culture, *n*2 is the number of cells recovered after the duration of expansion, and *n*1 is the total number of cells seeded.

3.8.3 THE MAXIMUM DEFECT VOLUME REPAIRABLE

Human IFP was opportunistically harvested from patients undergoing elective total knee arthroplasty with informed consent and used within 24 hours. Human ADSCs were then isolated using the rapid 85-minute isolation protocol and expanded. Using the average number of IFP-derived hADSCs obtainable after a set period of expansion, and the minimum cell concentration, the maximum repairable defect volume can be calculated (Figure 3.6). This maximum repairable defect volume forms the upper limit for the indication of treatment.

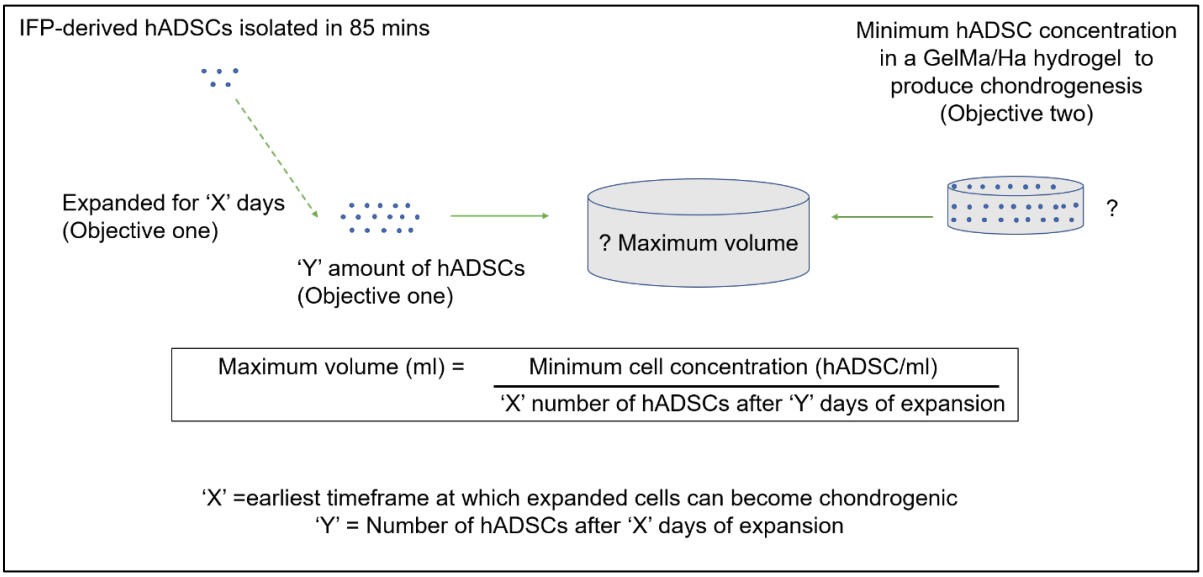


Figure 3.6. Graphical representation of how the maximal repairable chondral defect volume is calculated. Human adipose-derived mesenchymal stem cells (hADSCs), Gelatin-Methacryloyl/Hyaluronic acid (GelMA/HA).

3.9 STATISTICAL ANALYSIS

All statistical analyses were performed using Prism 8 (GraphPad) software. Differences between the experimental groups were determined using the unpaired t-test. Significance was represented as follows:

* = $p \leq 0.05$; ** = $p \leq 0.01$; *** = $p \leq 0.001$; not significant (n.s.) = $p > 0.05$.

Unless otherwise stated, data are presented as mean +/- standard error margin (SEM).

CHAPTER 4: CHONDROGENIC POTENTIAL OF CELL SOURCES WITHIN THE KNEE JOINT AND OPTIMISATION OF THE CELL ISOLATION PROTOCOL

4.1 INTRODUCTION

Numerous cell sources with chondrogenic potential have been used in in the field of cartilage tissue engineering. Such cells can be autologously harvested from different areas within the human body such as subcutaneous fat tissue, blood and the bone marrow (120, 129, 334). Ideally, with a view of clinical translation, the source used in chondral repair would display high chondrogenic potential, would be expandable and be isolatable from within the knee joint. This proximity of tissue harvest site to the defect region empowers future regenerative approaches in which the same harvest and reimplantation site could be utilised; this concept is described in a published review related to this work, Appendix 1 (335). Thus, we first identify the most chondrogenic cell from within the knee joint, which is hypothesised to be the human adipose-derived mesenchymal stem cell (hADSCs) originating from the infrapatellar fat pad (IFP). IFP-derived hADSCs were tested against two other chondrogenic sources from within the knee: the adult articular chondrocyte and the human articular progenitor cell (hAPCs).

Once an ideal tissue source is harvested, it is imperative to speed up the cellular isolation timeframe, this allows for an efficient downline reimplantation strategy and limits the duration of cellular exposure to *in vitro* environments and animal-based products. This is a crucial knowledge gap as current attention in the field is on *in vitro* optimisation and a lack of translative direction. A detailed review of how the isolation duration could be reduced has also been published in relation to this work, Appendix 2 (336). We hypothesised that this could be achieved by optimising the chemical breakdown and plastic adherence steps of the standard protocol with respect to efficiency. Considering our findings, a novel rapid isolation procedure was devised and validated by comparing it against the standard IFP-derived hADSCs isolation procedure.

4.2 RESULTS

CHONDROGENC POTENTIAL OF DIFFERENT CELL TYPES WITHIN THE KNEE JOINT

Chondrocytes (Cartilage-derived), hAPCs (Cartilage-derived) and hADSCs (IFP-derived), were isolated from respective tissue sources using the established isolation protocols described in the methods section. Cell populations were then culture-expanded for three passages before

undergoing immunophenotyping. Cells were then subject to three weeks of chondrogenic differentiation in pellet culture.

4.2.1 PHENOTYPICAL PROFILES OF THE THREE CELL TYPES TESTED

The phenotypes of the three different cell lines isolated were investigated using a cytofluorimetric analysis (Table 4.1 and Appendix 3), performed as described in the methods section. The expression of CD 44 and CD 105 is negative in hAPCs and positive for the other two cell types. However, there is no other clear delineating difference in marker expression to help differentiate these cell lines phenotypically. Given hADSCs reside in the IFP and the other two cell lines in articular cartilage, the major difficulty lies in phenotypically distinguishing between the chondrocyte and the hAPCs, which so far can only be characterised using CD 44 and 105 expression.

Marker	Description	hADSCs %	Chondrocytes %	hAPCs %
CD 44	Chondrogenic potency marker	100 (+)	98.94 (+)	0.60 (-)
CD 73	Extracellular adenosine production	99.03 (+)	97.80 (+)	98.50 (+)
CD 90	Cell-cell matrix interaction	94.67 (+)	100 (+)	97.40 (+)
CD 105	Modulates TGF-B function	99.88 (+)	99.83 (+)	0.8 (-)
Notch 1	Signalling pathway differentiation	0.13 (-)	0.09 (-)	0.6 (-)

Table 4.1. Flow cytometry results summary of key markers tested in hADSCs, chondrocytes and hAPCs. The expected phenotype is noted as positive/negative. Data are presented as a mean of three different patients (n=3); significant activity was calculated with unpaired t-test. An example of on the gating plots can be found attached in appendix 3.

4.2.2 CHONDROGENIC DIFFERENTIATION CAPACITY OF THE THREE CELL TYPES TESTED

To compare the chondrogenic potential between the three cell lines isolated, pellet culture was performed over three weeks and assessed. Pellet morphology was observed to evaluate the production of ECM. Also, a qPCR was performed to assess the expression of typical chondrogenic markers as described in the methods section.

With chondrogenic stimulation, it would be expected for pellet cultures to increase in size due to new extracellular matrix production. Pellet cultures (Figure 4.1A) demonstrate

substantial growth in the hADSCs group over three weeks, while hAPCs cultures remained the same size. Notably, chondrocytes cultures reduced in size over the three weeks, consistent with dedifferentiation in 3D culture. The gene expression assay (Figure 4.1B) represents chondrogenesis within the hADSCs group over three weeks, while a lack of chondrogenesis is evident in the chondrocyte group. The hAPCs group displayed a basal rate of chondrogenic gene expression; however, it was significantly less in comparison to the hADSCs.

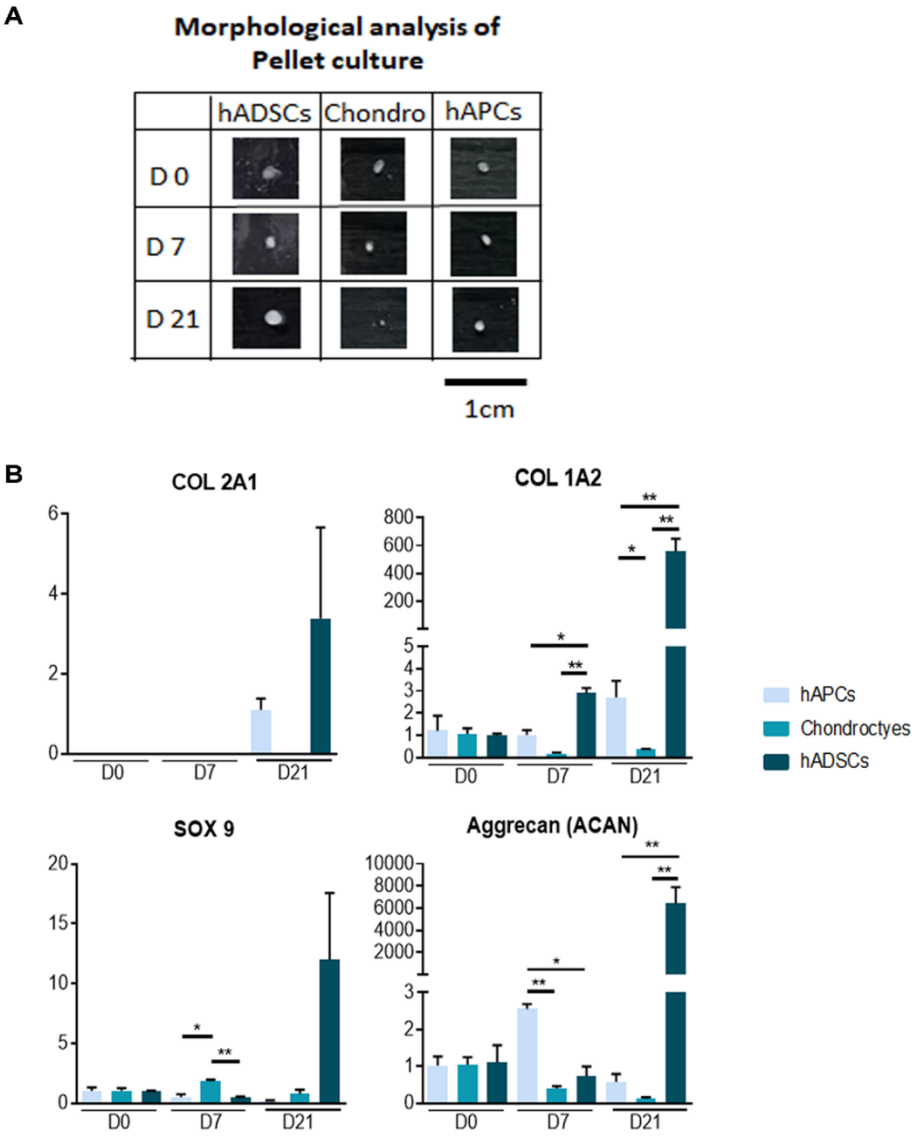


Figure 4.1. Chondrogenic assessment of hADSCs, chondrocytes and hAPCs. (A) Pellet morphology over three weeks of chondrogenic differentiation. (B) Bar graphs represent the expression of chondrogenic gene markers; Collagen type II (COL2A1, Collagen type I (COL1A2), Aggrecan (ACAN) and Sox-9 (SOX9) over three weeks. Data are presented as mean +/- standard error margin (SEM) between three biological replicates from two different patients (n=2), significant activity was calculated with an unpaired t-test.

OPTIMISATION OF THE CURRENT IFP-DERIVED HADSCS ISOLATION PROTOCOL

Results from aim 1 show that the IFP- derived hADSCs group displays the most chondrogenic potential. Given these findings, the next objective of this chapter focussed on the acceleration of the standard laboratory isolation protocol for IFP-derived hADSCs. The steps that could be optimised for efficiency included the chemical digestion of fat and cellular adherence to non-coated tissue culture polystyrene (TCPS). These aspects were individually assessed and optimised; then, based on successful findings, a rapid isolation protocol was generated.

4.2.3 REDUCTION IN CHEMICAL DIGESTION DURATION

To identify the quickest duration of chemical digestion required for adequate cell retrieval and viability, a range of collagenase assisted digestion durations were tested. As a reference, 3 hours(control) is used as per our standard laboratory isolation protocol (Figure 4.2).

Cell count and viability were then assessed as described in the methods section. At 10- and 20-minute digestion timeframes there were low cell counts of 5.0×10^3 and 4.0×10^4 respectively, furthermore, low cell viabilities of 7% and 20% respectively were observed. The 30-minute and 3-hour (Control) chemical digestion timeframes yielded a cell count of 2.25×10^5 and 2.5×10^5 cells, and cell viability of 83% and 75% respectively. Notably, there was no significant difference between the 30-minute and 3-hour (Control) groups for both features.

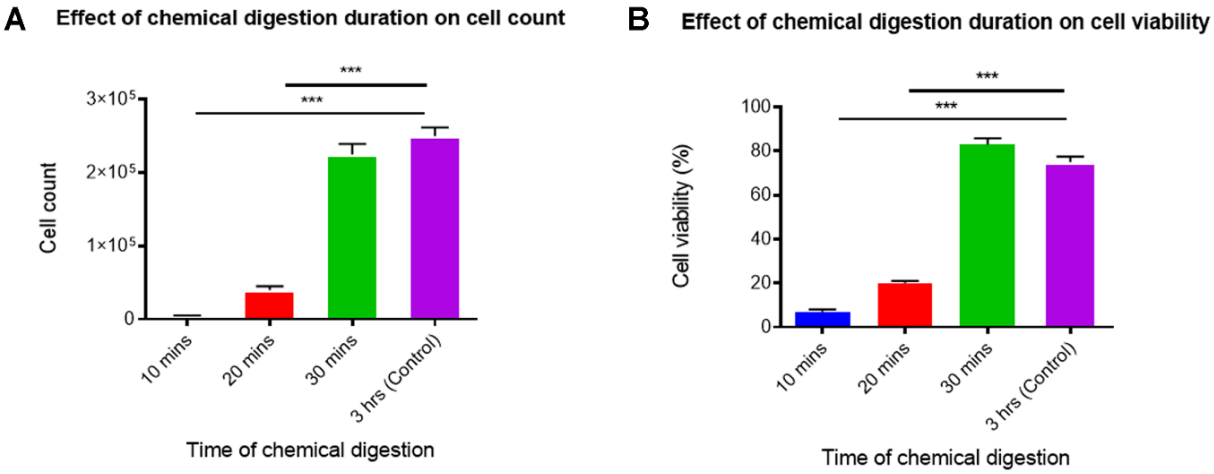


Figure 4.2. Effect of different durations of chemical digestion on cell yield and viability. Bar graphs representing the effect on cell count (A) and cell viability % (B). Data are presented as mean +/- SEM between three biological replicates from three different patients (n=3), significant activity was calculated with an unpaired t-test.

4.2.4 REDUCTION IN SELECTIVE TCPS ADHERENCE DURATION

To reduce the adherence duration associated with tissue culture polystyrene (TCPS), Matrigel-coated TCPS were compared to the non-coated TCPS (control) used in the standard isolation protocol. This coating formulation was chosen as it has been shown to speed up Sertoli cells adherence (30 minutes) (278) and has been optimised for 2D culture expansion of neural and embryonic stem cells with no effect on molecular characteristics (279).

Various adherence timepoints between 10 minutes and 24 hours were tested for both Matrigel-coated and non-coated TCPS groups. As expected, it took 24 hours to achieve reasonable adherence of cells to non-coated TCPS; however, it only took 30 minutes to obtain a similar level of cellular adhesion in the Matrigel-coated TCPS group, (Figure 4.3A). A comparable cellular adherence level of 60% is seen when 30 minutes of Matrigel-coated wells were used, compared to 58% seen when 24 hours of non-coated wells were used (Figure 4.3B). No significant difference was observed between these two groups at these timeframes.

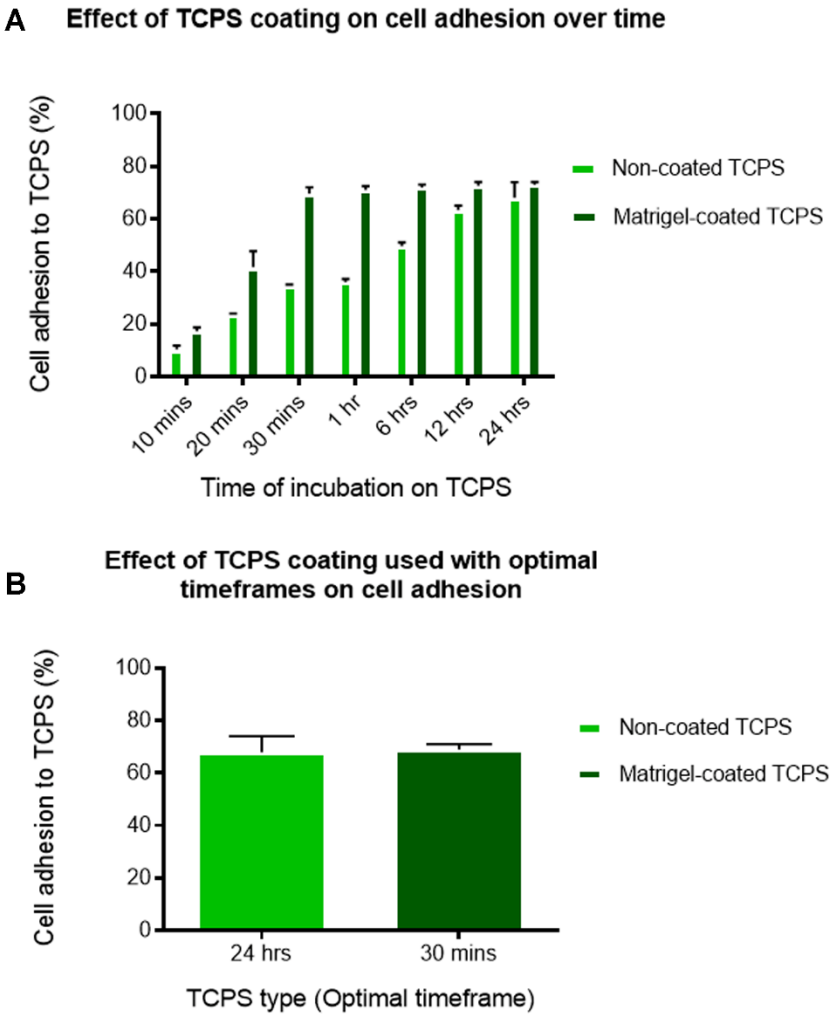


Figure 4.3. Cellular adherence on non-coated versus Matrigel-coated TCPS based on duration. Bar graph representing the effect of all timeframes tested (A) and non-coated TCPS at 24 hours compared to Matrigel-coated TCPS at 30 minutes. TCPS - Tissue culture polystyrene. Data are presented as mean +/- SEM between three biological replicates from three different patients (n=3), significant activity was calculated with unpaired t-test.

THE NEWLY GENERATED RAPID IFP-DERIVED HADSCS PROTOCOL

Based on these two key findings, a rapid IFP-derived hADSCs isolation protocol was devised. Two changes were implemented: 30 minutes of chemical digestion with collagenase and 30 minutes of cellular adherence using Matrigel-coated TCPS. This led to the generation of an 85-minute isolation procedure (Bottom pathway of Figure 4.4).

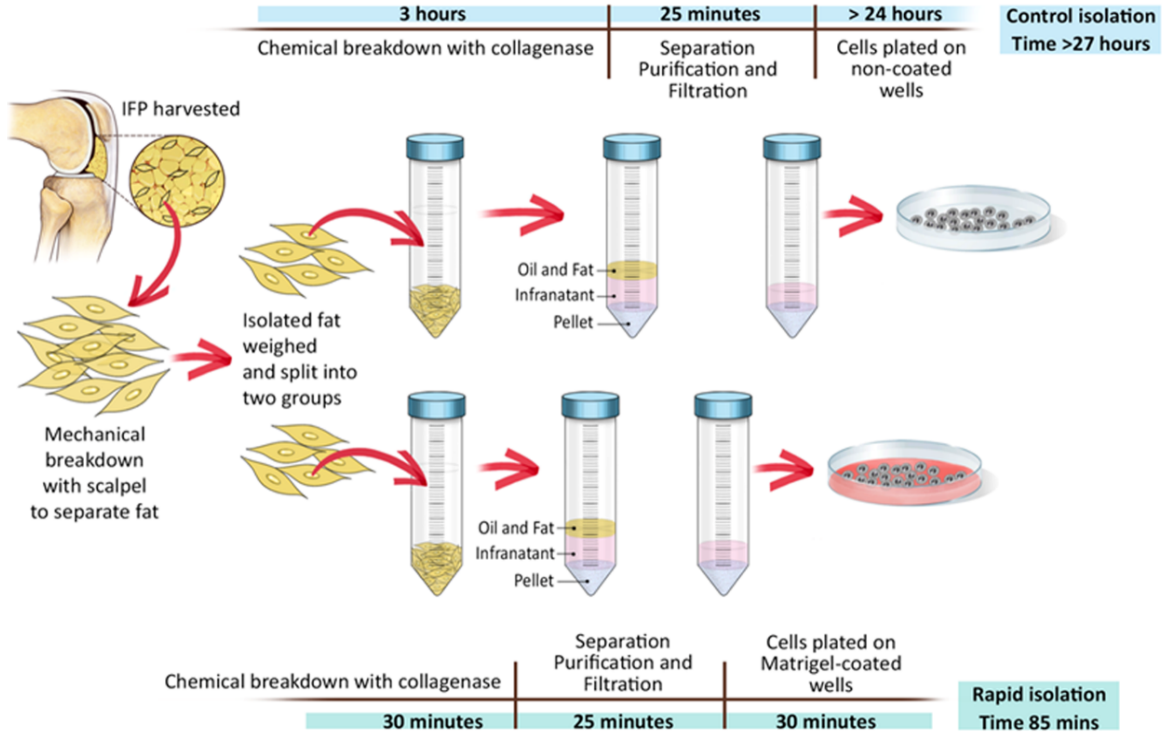


Figure 4.4. Graphical representation of the experimental design and timeframes of both rapid and control isolation groups.

VALIDATION OF THE RAPID ISOLATION PROTOCOL

To validate that the time required to isolate IFP-derived hADSCs can be reduced by modifying the chemical breakdown and cellular adherence steps (Figure 4.4), IFPs were isolated from three different patients. Each fat pad was weighed, divided equally into two, and then cell isolations were performed by following either the rapid or the control (standard) isolation protocols, the demographic characteristics are presented in Table 4.2.

Characteristic	Overall	Control isolation	Rapid isolation	p-value
Age (years)	60.67 +/- 5.81	n/a	n/a	n/a
Fat harvested (per IFP, grams)	2.09 +/- 0.04	1.05 used (50%)	1.05 used (50%)	n/a
Cell number (Pre selective adherence)	n/a	40.7 +/- 1.34 × 10^4	36.8 +/- 2.05 × 10^4	0.19
Selective adherence %	n/a	74.28 +/- 3.63	75.79 +/- 2.31	0.74
hADSCs number (Post selective adherence)	n/a	30.2 +/- 0.68 × 10^4	27.9 +/- 0.93 × 10^4	0.12

Table 4.2. Patient demographics of the three different patient lines tested. Data are presented as mean +/- SEM between three biological replicates from three different patients (n=3), significant activity was calculated with an unpaired t-test.

4.2.5 CELL RETRIEVAL EFFICIENCY

The cell count post isolation and cell viability using both isolation approaches were evaluated to assess if there was any reduction in cell yield or viability associated with using 30 minutes of collagenase digestion (Figure 4.5A-B). The rapid isolation approach yielded 3.68 × 10^5 (+/- 3.55 × 10^4) compared to 4.07 × 10^5 (+/- 2.32 × 10^4) live cells in the control isolation approach with no significant difference shown. Mean cell viability was 86.04 % (+/- 1.3) and 85.02 % (+/-1.42) for the rapid and control isolation groups, respectively, with no significant difference.

Next, to quantify how selective Matrigel-coated TCPS weer for adherence of a hADSCs population, the attachment percentage and post-attachment cell count was evaluated, comparing it to the non-coated TCPS control group (Figure 4.5C-D). Mean cell attachment was 75.79% (+/-2.31) in the rapid isolation group and 74.28% (+/- 3.63) in the control isolation group, with no significant difference. The number of hADSCs isolated post selective adherence in the rapid and control isolation groups was 2.79 × 10^5 (+/- 6.81 × 10^3) and 3.02 × 10^5 (+/- 9.28 × 10^3) respectively, with no significant difference. Notably, in all measures, there was no statistically significant difference observed between the two groups. Therefore, there

is no alteration in the ability to isolate a hADSCs population by reducing the chemical breakdown duration and using Matrigel-coating for adherence.

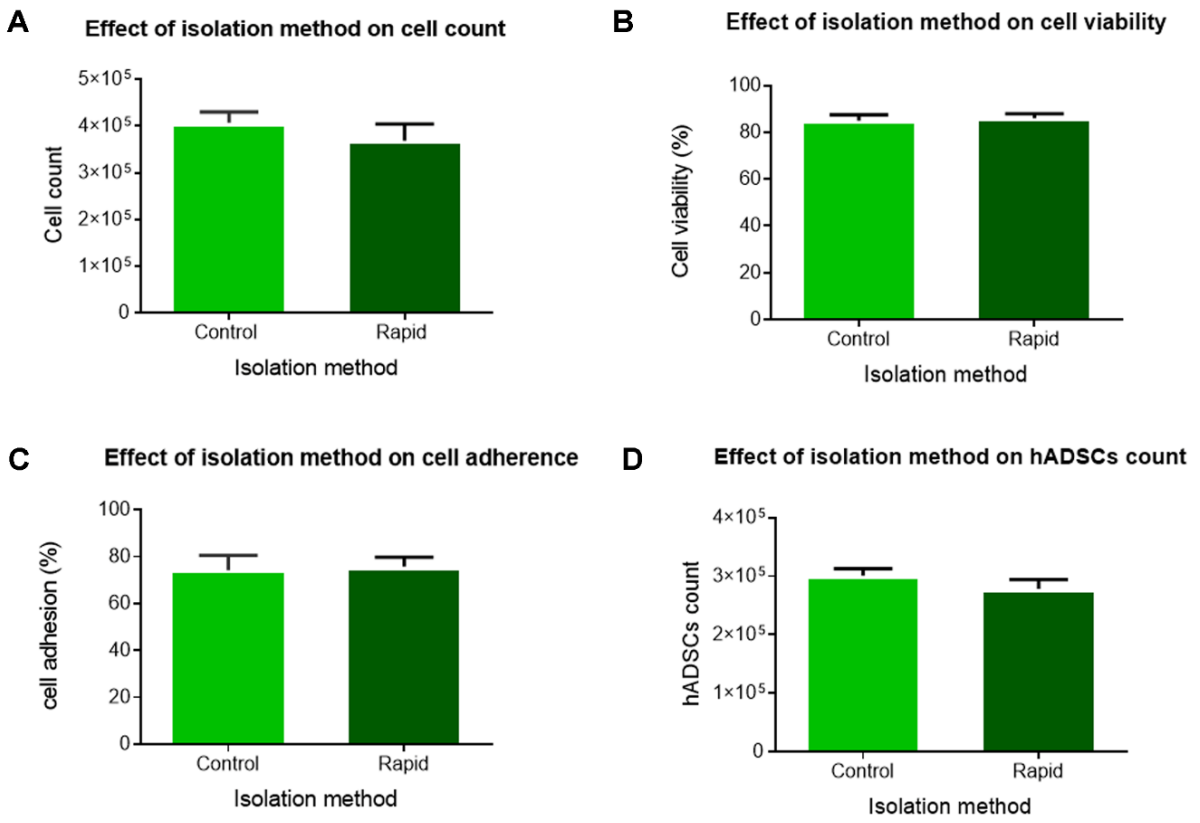


Figure 4.5. Comparison of rapid and control isolation groups for yield, viability, and adherence. Bar graphs representing the cell count (A), cell viability (B), cell adhesion (C) and hADSCs count post- adhesion (D). All data were calculated using trypan blue staining. Data are presented as mean +/- SEM between three biological replicates from three different patients (n=3), significant activity was calculated with an unpaired t-test.

4.2.6 IMMUNOPHENOTYPIC CHARACTERISATION

To assess if the reduction of the chemical breakdown phase and the adhesion to Matrigel-coated TCPS lead to the selection of a pure hADSCs population the immunophenotype of the cell populations isolated using both rapid and control isolation protocols were compared using morphological observation and flow cytometric analyses, Table 4.3.

Typically, hADSCs appear spindle-shaped early in expansion and then exhibit a smoothened morphology after long-term expansion, which was demonstrated in both isolation groups using bright-field microscopy (data not shown). After 3 weeks of expansion hADSCs typically express >90% positivity of the markers CD44, CD49c, CD73 and CD90 and <3% positivity of

CD31, CD34, CD45 and CD146, (337, 338). The immunophenotypic analysis showed that cells from both groups expressed the expected hADSCs profiles with no significant difference seen in any of the markers tested (Table 4.3).

Marker	hADSCs Phenotype	Description	Control group %	Rapid group %	p value
CD 31	-	Endothelial cell marker	0.66	0.83	0.60
CD 34	-	Hematopoietic/Endothelial marker	2.24	2.79	0.68
CD 44	+	Chondrogenic potency marker	99.86	99.82	0.57
CD 45	-	Leukocyte cell marker	1.05	0.89	0.53
CD 49c	+	Chondrogenic potency marker	95.43	95.52	0.98
CD 73	+	Extracellular adenosine production	98.61	98.34	0.79
CD 90	+	Cell-cell-matrix interactions	97.78	97.86	0.95
CD 146	-	Cell migration and angiogenesis	2.28	1.92	0.80

Table 4.3. Summary of flow cytometry results of markers tested in both isolation groups. A description of each type of marker tested is detailed. Data are presented as a mean between three different patients (n=3), significant activity was calculated with an unpaired t-test. Detailed gating imaging can be found attached in appendix 4.

4.2.7 TRILINEAGE DIFFERENTIATION OF RAPIDLY ISOLATED HADSCS

CHONDROGENIC DIFFERENTIATION

To evaluate if the use of the rapid isolation procedure affects the chondrogenic potential of the hADSCs population obtained, a 3-week differentiation study using pellet cultures of cells derived from both isolation groups was performed. Pellets grew from both groups grew in size and displayed a consistent white opaque macroscopic appearance consistent with ECM production, and validated with safranin O staining (Figure 4.6A). Next, the glycosaminoglycan/deoxyribonucleic acid (GAG/DNA) ratio (Figure 4.6B) and qPCR (Figure 4.6C) for chondrogenic gene expression (COL2A1, COL1A2, SOX-9 and ACAN) were tested. During chondrogenesis, the GAG/DNA ratio increases over three weeks as more ECM is produced, raising the GAG amount, which is seen in both rapid and control groups, p=0.004 and p=0.002. No significant difference is seen when comparing both groups after 21 days.

With chondrogenesis, gene expression of COL 2A1 and ACAN upregulates from no expression at day 0 to expression by day 21, while for COL 1A2 and SOX-9 there is a basal expression at day 0 which should significantly increase by week 3 (339). COL2A1 and ACAN expression in both rapid and control groups switched from no expression at day 0 to expression at day 21. COL1A2 expression in both rapid and control groups increased significantly from day 0 to day 21, p=0.046 and p=0.013, respectively. SOX-9 expression in both rapid and control groups increased significantly from day 0 to day 21, p=0.002 and p=0.008, respectively. Notably, for all genes, there was no significant difference in expression when comparing the rapid against the control groups at 21 days, suggesting successful chondrogenic differentiation of rapidly isolated hADSCs with no alteration in cell potency secondary to the modifications made.

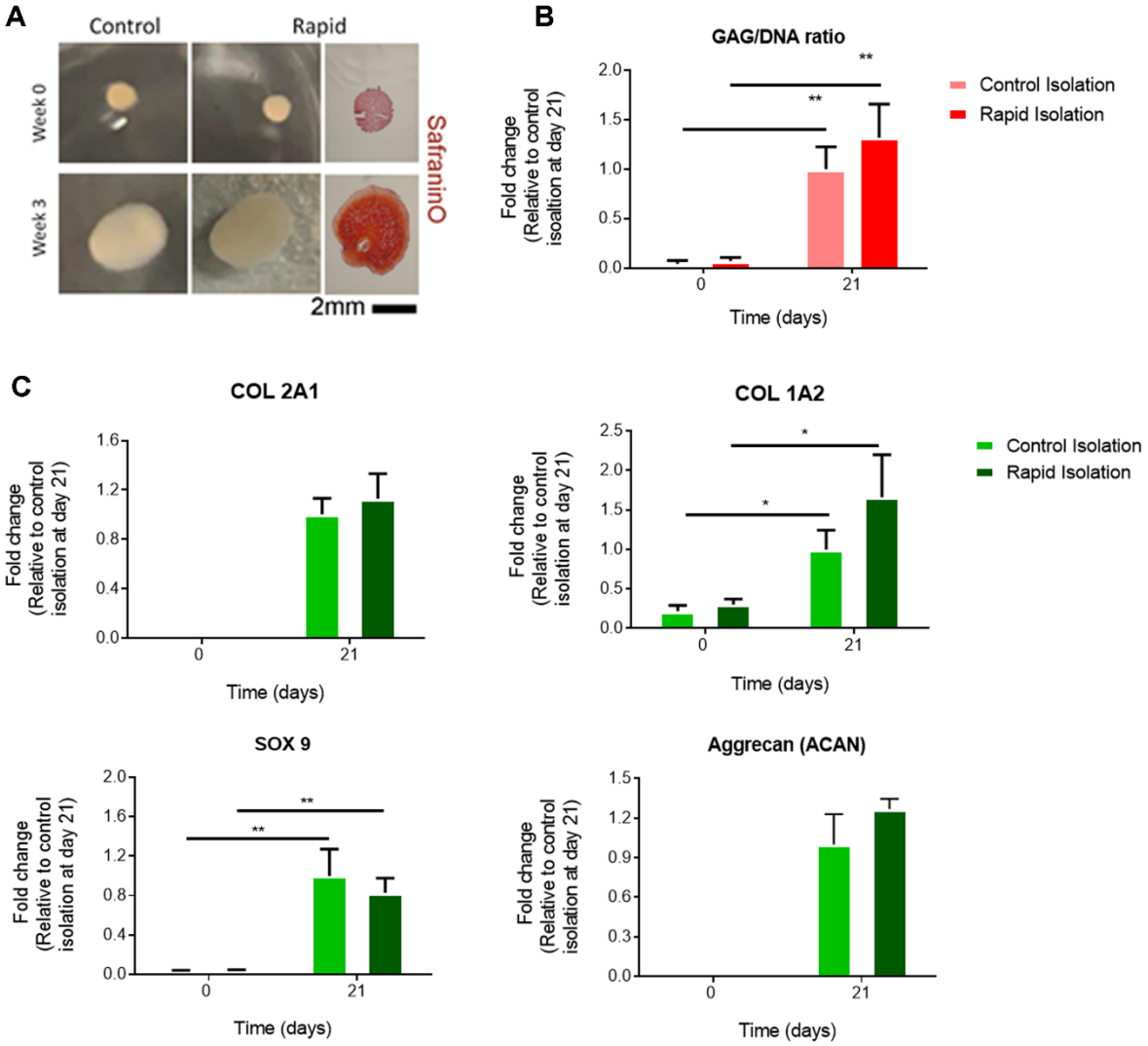


Figure 4.6. Chondrogenic assessment of rapidly isolated hADSCs. (A) The first two columns show images of pellet size over three weeks in both control and rapid groups. The third column represents the histological analysis of 10 µm cryosections stained with Safranin O, which

detects the accumulation of GAG in the ECM. (B) Bar graph representing the GAG/DNA ratio, showing the change in GAG production over 21 days, fold changes are calculated relative to the control isolation group at day 21. (C) Bar graphs represent fold changes relative to the control isolation group at day 21 for chondrogenic gene markers. Data are presented as mean +/- SEM between three biological replicates from three different patients (n=3), significant activity was calculated with an unpaired t-test.

OSTEOGENIC AND ADIPOGENIC DIFFERENTIATION

Both an osteogenic and adipogenic differentiation assay were performed with cells isolated using the rapid isolation, to confirm the trilineage capacity associated with a MSCs line. A 3-week osteogenic and adipogenic differentiation study was conducted using a 2D culture of cells obtained in both isolation groups as described in the methods section.

After three weeks of osteogenic differentiation, cells displayed morphology consistent with early osteogenic differentiation which is represented by structurally organised cellular clusters and early mineralisation visible with bright-field microscopy, (Figure 4.7A). Next, qPCR (Figure 4.7B) for osteogenic gene expression analysis (Osteocalcin, RUNX2, and ALP) was tested. With osteogenesis, gene expression of Osteocalcin, RUNX2, and ALP should increase from a basal state at day 0 significantly at day 21 (340). Although ALP expression in both rapid and control groups increased from day 0 to day 21, no statistical significance was seen. RUNX2 expression in both rapid and control groups increased significantly from day 0 to day 21, p=0.03 and p=0.005, respectively. Osteocalcin expression in both rapid and control groups increases considerably from day 0 to day 21, p=0.03 and p=0.04, respectively. Notably, no difference was observed in ALP, RUNX2 or Osteocalcin expression between both groups after day 21.

After three weeks of adipogenic differentiation, cells displayed morphology consistent with early adipogenic differentiation, and micro fat particles were visible using bright-field microscopy, (Figure 4.8A). Next, qPCR (Figure 4.8B) for adipogenic gene expression analysis (CEBPα and FABP4) was tested. In adipogenesis, gene expression of both CEBPα and FAB4 typically increases from a basal state at day 0 significantly by day 21 (341). CEBPα expression in both rapid and control groups increased significantly from day 0 to day 21, p=0.002 and p=0.0005, respectively. FABP4 expression in both rapid and control groups increased

significantly from day 0 to day 21, p=0.0002 and p=0.03, respectively. Notably, no difference was observed in both CEBPα and FABP4 expression after 21 days between both groups.

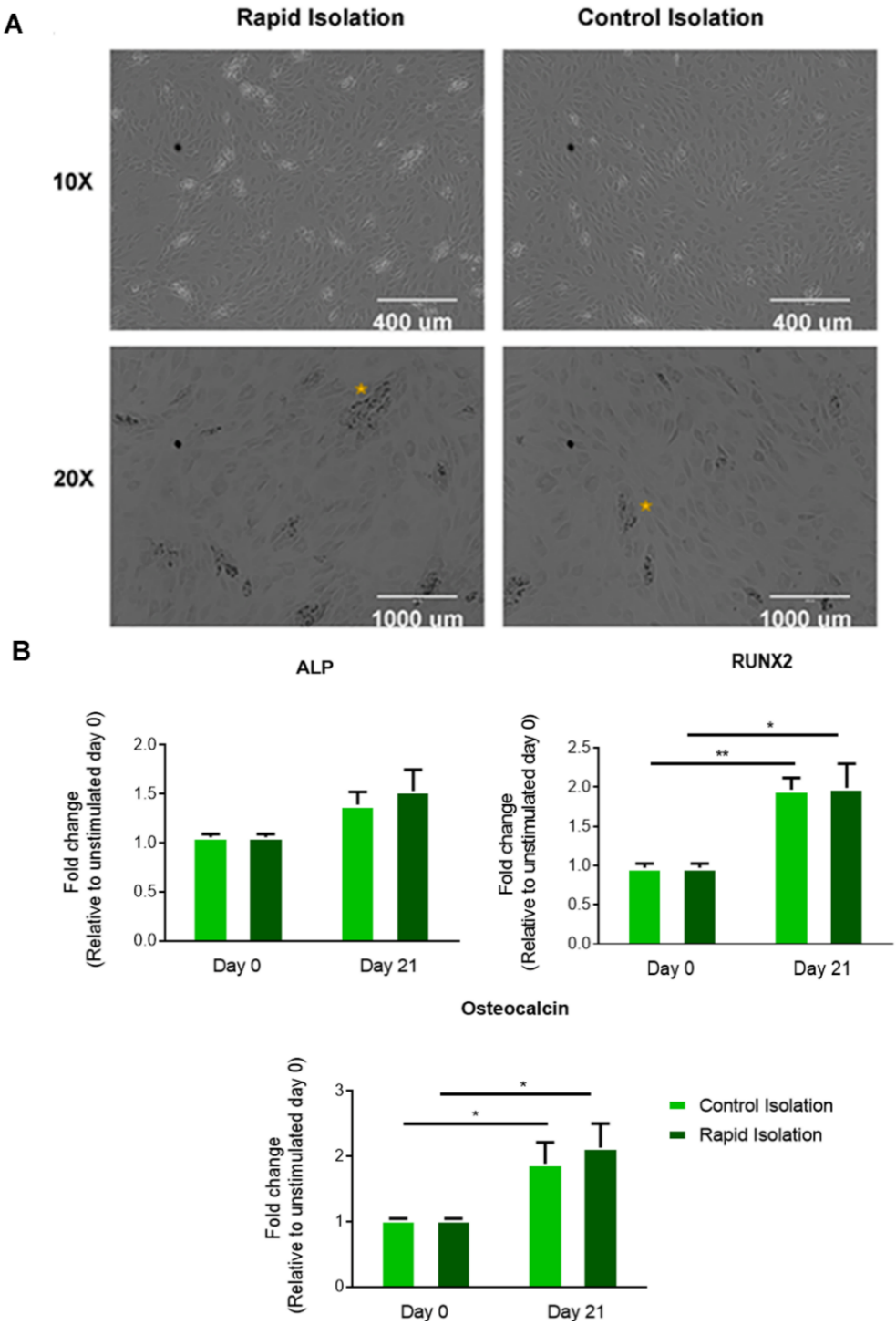


Figure 4.7. Osteogenic assessment of hADSCs. (A) Bright-field images of cells in monolayer from both control and rapid groups after 3 weeks of differentiation at 10X non-phase and 20X phase contrasts. Cell clusters with early mineralisation are highlighted with yellow stars. (B)

Bar graphs represent fold changes relative to day 0 for osteogenic gene markers. Data are presented as mean +/- SEM between three biological replicates from three different patients (n=3), significant activity was calculated with unpaired t-test

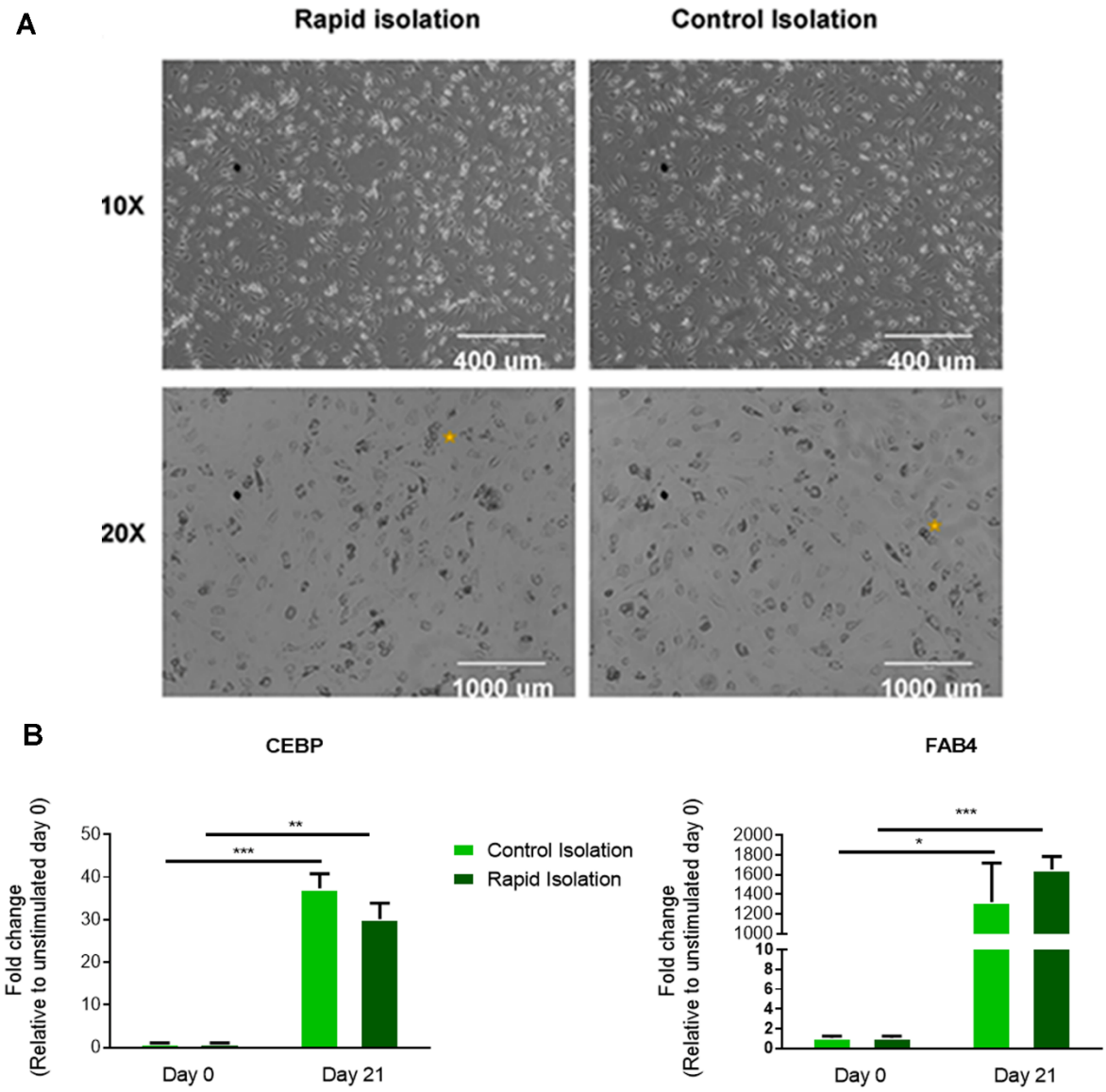


Figure 4.8. Adipogenic assessment of hADSCs. (A) Bright-field images of cells in monolayer from both control and rapid groups after 3 weeks of differentiation at 10X non-phase and 20X phase contrasts. Micro fat particles/lobules are highlighted with yellow stars. (B) Bar graphs represent fold changes relative to day 0 for adipogenic gene markers. Data are presented as mean +/- SEM between three biological replicates from three different patients (n=3), significant activity was calculated with unpaired t-test.

4.3 DISCUSSION

Cell types within the knee that have been reported to demonstrate chondrogenic potential include adult chondrocytes, IFP-derived hADSCs and hAPCs (138, 143, 264). In this study in comparison to adult chondrocytes and hAPCs, IFP-derived hADSCs are clearly demonstrated to be superior in chondrogenic potential. The use of chondrocytes from osteoarthritic donor knees may be a reason for failed chondrogenesis, although literature suggests there should be no significant effect on chondrogenic capacity (342). Given these results and chondrocytes displaying variable differentiation based on expansion time, multiple passaging (343) and the use of 2D vs 3D culture (344), this cell type would not be a suitable option for the engineering of cartilage tissue. These findings suggest that IFP-derived hADSCs are an ideal chondrogenic cell source from within the knee joint itself and should be used in regenerative therapies directed in relation to chondral knee defects. IFP-derived hADSCs can be harvested from the same site as the subsequent treatment site, thereby minimising incisions sites and surgical risk (345).

This chapter presents a rapid and efficient 85-minute method to isolate hADSCs from harvested IFP tissue, reducing the standard isolation timeframe by greater than 16-fold (336). To generate a rapid protocol, optimisation testing was first performed to identify areas within the current isolation protocol, which could be sped up. From this testing, two areas that could be sped up were identified: the chemical digestion phase could be reduced from 3 hours to 30 minutes, and the plastic adherence step could be reduced from 24 hours using non-coated TCPS to 30 minutes using Matrigel-coated TCPS. Notably a higher cell toxicity was associated with the lower collagenase assisted breakdown timeframes (<30 mins). During harvest there is likely to be dead tissue present secondary to the cauterisation technique that is used to remove IFP from the knee joint. Regardless of adequate cleaning and dilution, parts of dead tissue are likely to remain at the beginning of chemical digestion. Overtime with collagenase breakdown more of the healthy fat tissue is dissolved increasing the live cell count. Therefore, this phenomenon is not a collagenase associated cytotoxic effect, rather it is an artificial elevation from the beginning due to an initial pool of dead cells.

Then newly developed 85-minute rapid IFP-derived hADSCs isolation protocol yielded a cell count, cell viability, adherence percentage and total hADSCs count comparable to the control

group. Furthermore, flow cytometry results confirmed that the rapid protocol could be used to isolate and expand a pure homogenous stem cell population that is comparable to the control protocol. Cells initially isolated using the rapid protocol displayed an increase in the GAG/DNA ratio and chondrogenic gene expression over three weeks, which was comparable to cells initially isolated using the control protocol. Combining these investigations, we show that our 85-minute rapid isolation protocol is comparable to the control isolation protocol and the isolated hADSCs can undergo successful chondrogenesis with no impairment associated by reducing the chemical breakdown time and the use of Matrigel-coated wells to speed up adherence. The ability to rapidly derive an SVF population has been shown in the literature and commercially (270-272); however, there has never been an added step including a rapid selective adherence of ADSCs.

Furthermore, to prove the trilineage ability of hADSCs (346, 347), which is a type of mesenchymal stem cell, adipogenic and osteogenic differentiation studies were performed. The rapidly isolated hADSCs were able to undergo osteogenic and adipogenic differentiation as expected with the IFP-derived hADSCs phenotype after 3 weeks of respective differentiation (346-350). IFP-derived hADSCs have been shown to be comparable to bone marrow and subcutaneous adipose derived MSCs with respect to both osteogenic and adipogenic potential irrespective of the formula of differentiation used (351). Although proof of this trilineage capacity is not relevant directly to cartilage tissue engineering where only chondrogenic ability is required, this rapid isolation protocol can be extended to other fields of musculoskeletal tissue regeneration given the multilineage potential of MSCs. The rapid IFP-derived hADSCs protocol could; therefore, be extended to any field of medicine investigating the regeneration of cartilage, bone, muscle, tendon or fat tissue.

A limitation of this rapid protocol is the use of Matrigel-coated TCPS wells for selective cellular adherence, although commercially available for *in vitro* lab use (352) , this purified mouse tumour derived protein mixture is not approved for clinical use in humans. Furthermore, there are batch-batch variations associated with Matrigel, which presents concerns surrounding consistency (353). Therefore, either a synthetically similar composition or an autologous biological composition that can be consistently produced needs to be identified before any progression to clinical translation. Further work on synthetic and biological TCPS

coating options has been performed and is attached in appendix 5, elements of this work are still in progress and serve as part of an impending international patent application.

4.4 CONCLUSION

IFP-derived hADSCs are a promising chondrogenic source of cells which can be sourced from within the knee joint which is a commonly affected site for cartilage damage. This is the first study demonstrating the ability to isolated hADSCs from adipose tissue in a rapid manner. By isolating stem cells in 85 minutes, the isolation duration has not only been reduced by 16-fold but also enables the commencement of cellular expansion to occur one day earlier. This rapid IFP-derived hADSCs isolation procedure is efficient, allowing scientists to save valuable time for *in vitro* regenerative study involving mesodermal tissue and serves as the first successful step in achieving a quick turnaround biofabrication treatment approach for cartilage defects using a pure stem cell population.

CHAPTER 5: MINIMUM CHONDROGENIC REQUIREMENTS OF IFP-DERIVED hADSCs PRIOR TO REIMPLANTATION

5.1 INTRODUCTION

With a view of clinical translation, culture expansion of stem cells should be limited, thereby improving not only the efficiency and waiting time for subsequent repair but also reducing the duration of exposure to a laboratory environment and animal-based products. Risks such as sterility, contamination and inflammation are increased with longer durations of *in vitro* culture and the use of animal-based products (265, 282). Thus, we first evaluate the chondrogenic ability of culture-expanded hADSCs (rapidly isolated using the previously developed 85-minute protocol) and hypothesise that they can be driven into successful chondrogenesis prior to initial passaging (i.e. 0-7 days of expansion).

Few *in vitro* and *in vivo* studies report the cell concentrations used, and ultimately the use of higher concentrations are not reported to be superior to lower concentrations; therefore, no minimum let alone optimal cell concentrations range has been identified (290). To further improve the efficiency of therapy we aimed to identify the minimum hADSCs concentration required to generate adequate neocartilage, which is hypothesised to be less than the average chondrocyte concentration in healthy human knee cartilage (10 million cells/mL).

The defect or repair volume is crucial in cell-based therapies, as adequate cell numbers need to be delivered for regeneration/repair to occur, such volumes need to be symptomatically and functionally relevant. Hence, the final hypothesis was that by linking the data from the first two aims of this chapter, the volume and indication range applicable to our repair approach could cover a clinically relevant spectrum of defect sizes.

5.2 RESULTS

THE EARLIEST POINT WHEN IFP-DERIVED HADSCS CELLS BECOME CHONDROGENEIC

Rapidly isolated hADSCs were immediately pushed (0 days of expansion) into pellet culture or expanded for 3,5 and 7 days and then subject to pellet culture. For each group tested, the hADSCs count, doubling time and pellet formation ability was assessed, Table 5.1. Next, successfully formed pellets were subjected to 3 weeks of chondrogenesis and evaluated.

5.2.1 THE EARLIEST POINT DURING EXPANSION WHEN CELLS FORM 3D PELLETS

Immediately isolated cells and those used after 3 days of expansion were unable to form pellets and therefore screened out. Cells used after 5 and 7 days of expansion were able to

form 3D pellets successfully, and an average of 1.9 x 10^6 and 2.8 x 10^6 hADSCs were obtained after respective expansion timeframes (Table 5.1 and Figure 5.1A). The average doubling time (Passage 0-1) over 7 days was calculated to be 4.41 days, (Figure 5.1B),

Groups tested	Total samples	Average no. hADSCs	Average doubling time (days)	Pellet formation
Post isolation (day 0)	n=3	7.17. X 10^5	-	**Unsuccessful**
Expanded - 3 days	n=3	1.57. X 10^6	3.18	**Unsuccessful**
Expanded - 5 days	n=3	1.90 X 10^6	6.56	**Successful**
Expanded -7 days	n=3	2.80 X10^6	3.79	**Successful**

Table 5.1. Details of cell population groups tested, including sample size, number of cells, doubling time and ability to form 3D pellets. Data are presented as the mean of three cell lines (n=3). hADSCs- Human Adipose-Derived Mesenchymal Stem Cells.

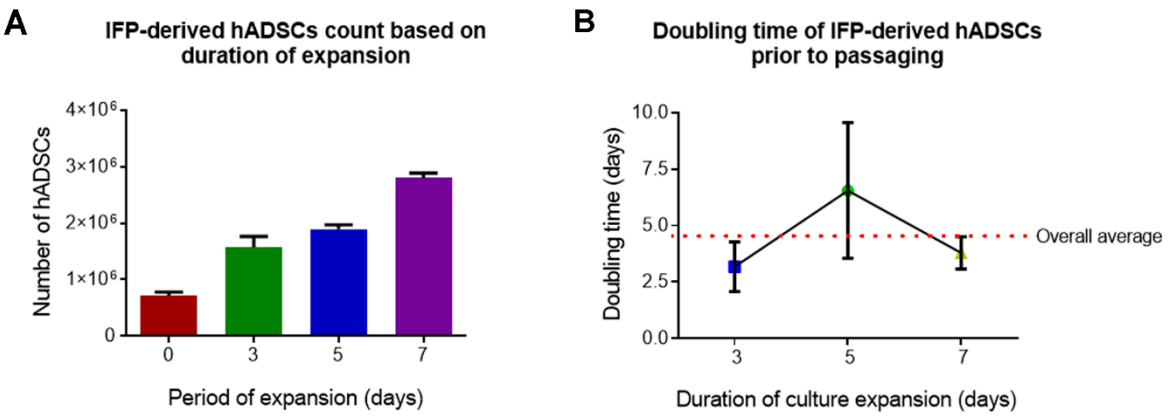


Figure 5.1. The growth kinetics of IFP-derived hADSCs during expansion prior to passaging. A) Bar graph showing the cell count over 7 days of culture expansion. B) Dot graph showing the doubling time of IFP-derived hADSCs prior to passaging. Data are presented for three separate lines (n=3). Human adipose-derived mesenchymal stem cells (hADSCs).

5.2.2 CHONDROGENIC ASSESSMENT OF 5 AND 7 DAY EXPANDED CELLS

Successfully formed pellets were subject to 3 weeks of chondrogenic differentiation and then assessed using histological staining and immunofluorescence imaging (Figure 5.2) Pellets from both 5 and 7-day expansion time points grew significantly in size over 3 weeks suggestive of an increase in ECM production, after 3 weeks the 5-day expansion group pellets were slightly smaller than the 7-day group. Safranin 0 staining was evident in pellets from both

groups after 3 weeks of chondrogenic stimulation, but not in the time 0 samples, confirming chondrogenic ECM production, (Figure 5.2A). Furthermore, collagen 2 staining (cyan) is well distributed and suggestive of chondrogenic formation in pellets originating from both the 5- and 7-day expansion populations over 3 weeks irrespective of pellet size (Figure 5.2D). Merged Dapi-Actin-Col II staining (Figure 5.2E) shows that Col II is both intracellularly and extracellularly deposited, indicative of mature neocartilage formation. DAPI (white) and Actin (red) staining represent the nuclei and cytoskeleton, respectively, (Figure 5.2B-C).

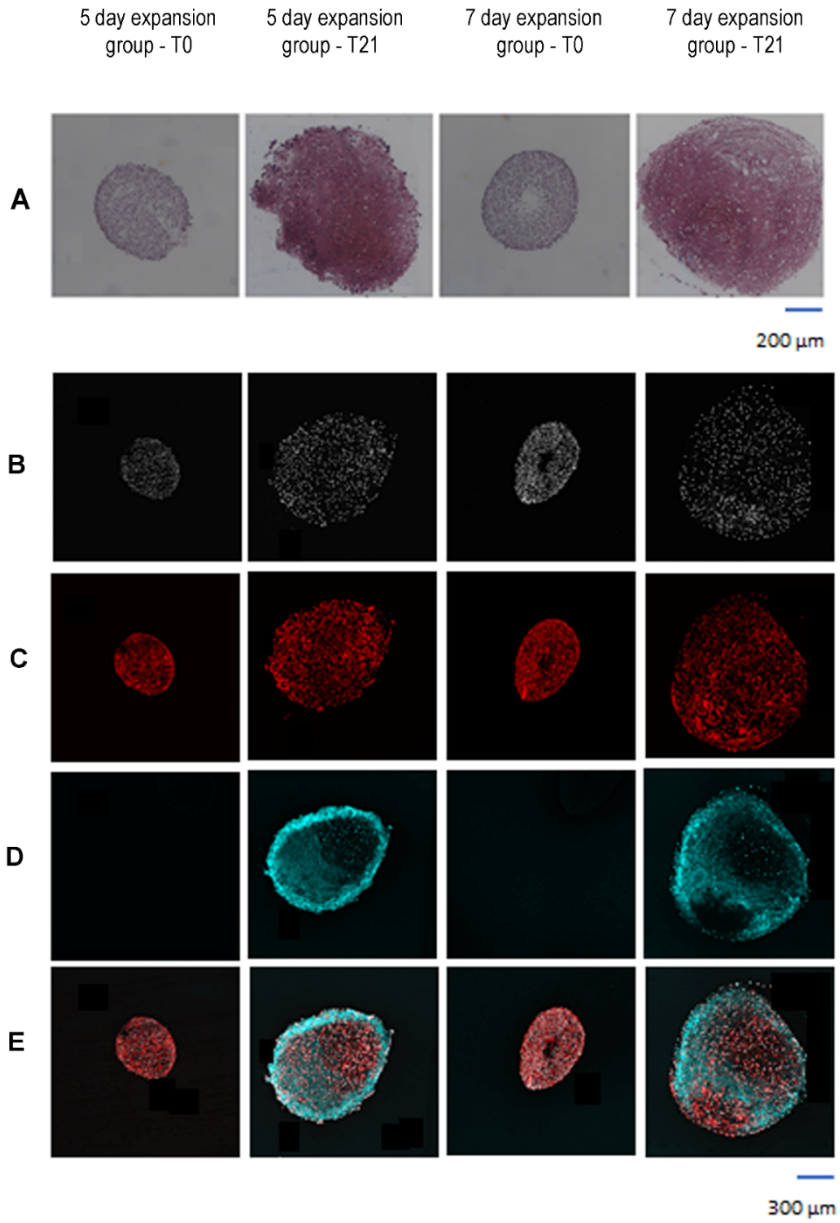


Figure 5.2. Chondrogenic assessment of 5- and 7-day expanded cell populations in pellet culture over 3 weeks using Safranin 0 and Immunostaining. A) Haematoxylin, Fast green and Safranin 0 staining, B) DAPI (white) – Cell nucleus, C) Actin (red) – cytoskeleton, D) Col II (cyan) – Collagen 2 and E) Merged DAPI, Actin and Col II.

THE MINIMUM HADSCS CONCENTRATION REQUIRED TO PRODUCE NEOCARTILAGE FORMATION IN A HYDROGEL

In the next objective, Gelatin-Methacryloyl/Hyaluronic acid (GelMA/HA) hydrogels were laden with three different hADSCs concentrations: 1.25, 2.5 and 5.0 million cells/mL to form 3 bioscaffolds compositions. To mimic a standardised 200 µL (200 mm^3 = 1 cm^2 TSA by 1 mm depth) modelled defect, bioscaffolds were cast into PDMS moulds (see methods for details). These bioscaffolds were subjected to *in vitro* chondrogenic differentiation for 3 weeks and evaluated using immunofluorescence imaging, GAG/DNA content and gene expression.

5.2.3 IMMUNOFLOURESCENCE IMAGING AND COLLAGEN 2 STAINING INTENSITY

To identify if areas of neocartilage formation were present, bioscaffolds were fixed, cut, stained and visualised using confocal microscopy to assess immunofluorescence of collagen I and II. Nuclear and Actin labelling were used to visualise cell distribution and morphology inside the bioscaffolds. Subsequently collagen type 2 staining intensity was quantified.

Confocal imaging of 10 µm sections cut along the z dimension was performed (Figure 5.3). The 1.25 million hADSCs/mL bioscaffolds were flatter, brittle and easily fell apart while constructs from the higher two concentrations maintained their shape and were rigid. Actin staining (red) shows appreciable cytoskeletal expression in all three groups, while Col I (cyan) expression shows basal collagen type I in all three concentrations groups.

Minimal Col II (cyan) is evident in the 1.25 million hADSCs/mL group, while appreciable Col II accumulation is visualised in both 2.5 and 5.0 million hADSCs/mL groups, (Figure 5.3). As expected, cell count represented by DAPI staining (white) increases proportionally with the hADSCs concentration, (Figure 5.3 and 5.4A). On closer observation (Figure 5.4B) it is evident that Collagen II expression is mostly intracellular in the 2.5 million hADSCs/mL group, while there is visibly more extracellular protein expression in the 5.0 million hADSCs/mL group, indicating a more advanced stage of chondrogenesis where the ECM is now being formed. Finally, collagen 2 staining intensity quantification (Figure 5.5) demonstrates a significantly higher amount of Col 2 in both the 2.5 million and 5.0 million groups compared to the 1.25 million hADSCs/mL group.

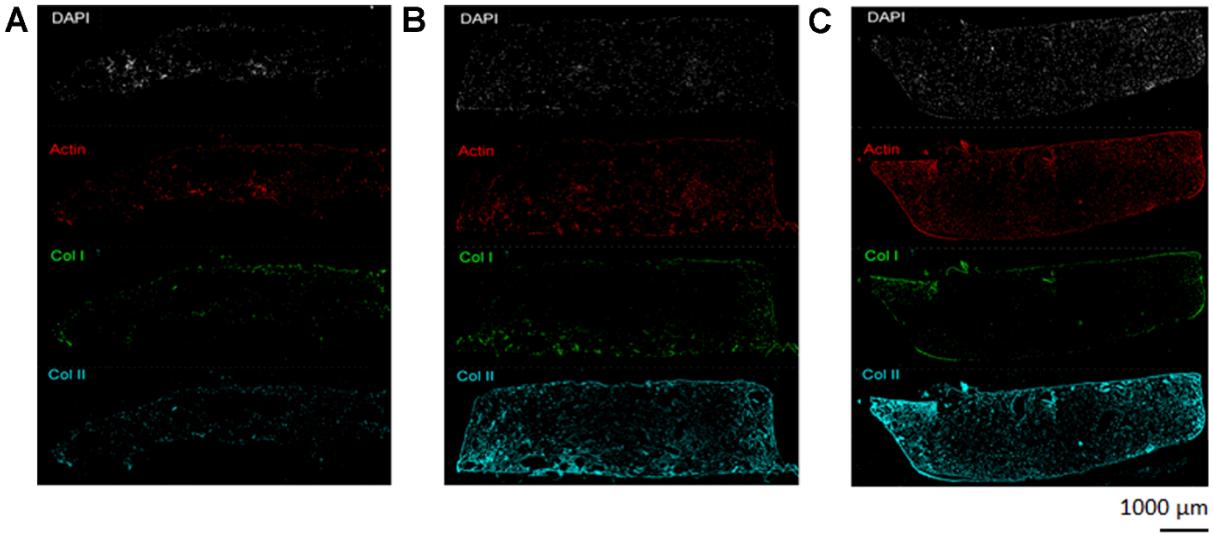


Figure 5.3. Confocal microscopy images of whole scaffold sections for the three different cell concentrations. Cross-sections of the A) 1.25 million hADSCs/mL, B) 2.5 million hADSCs/mL and C) 5.0 million hADSCs/mL concentration groups after 3 weeks. DAPI – Cell nucleus, Actin – cytoskeleton, Col I – Collagen 1 and Col II – Collagen 2.

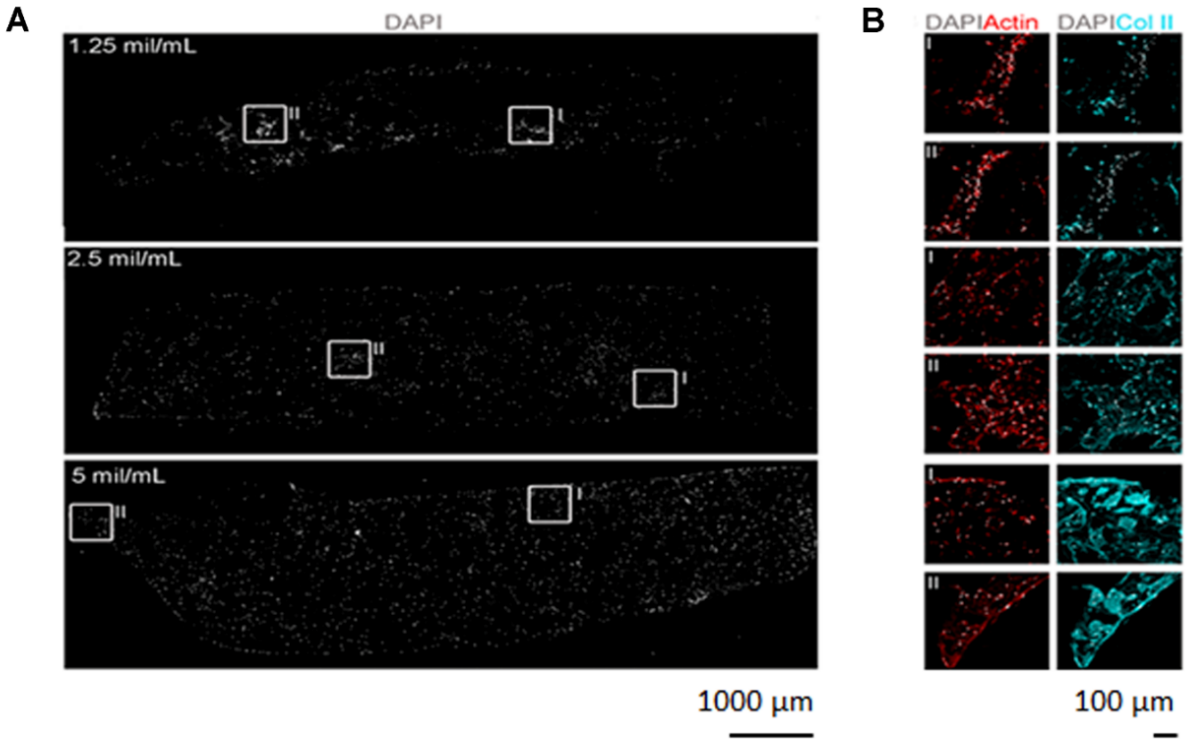


Figure 5.4. Neocartilage assessment of bioscaffolds generated using three different cell concentrations. Whole and 10X magnified sections. A) DAPI staining of whole transverse bioscaffold sections. Sections 1 and 11 are then further focused in section B) 10 X magnification with merged DAPI + Actin and DAPI + Col 11 images displayed. DAPI – Cell nucleus, Actin – cytoskeleton, and Col II – Collagen 2.

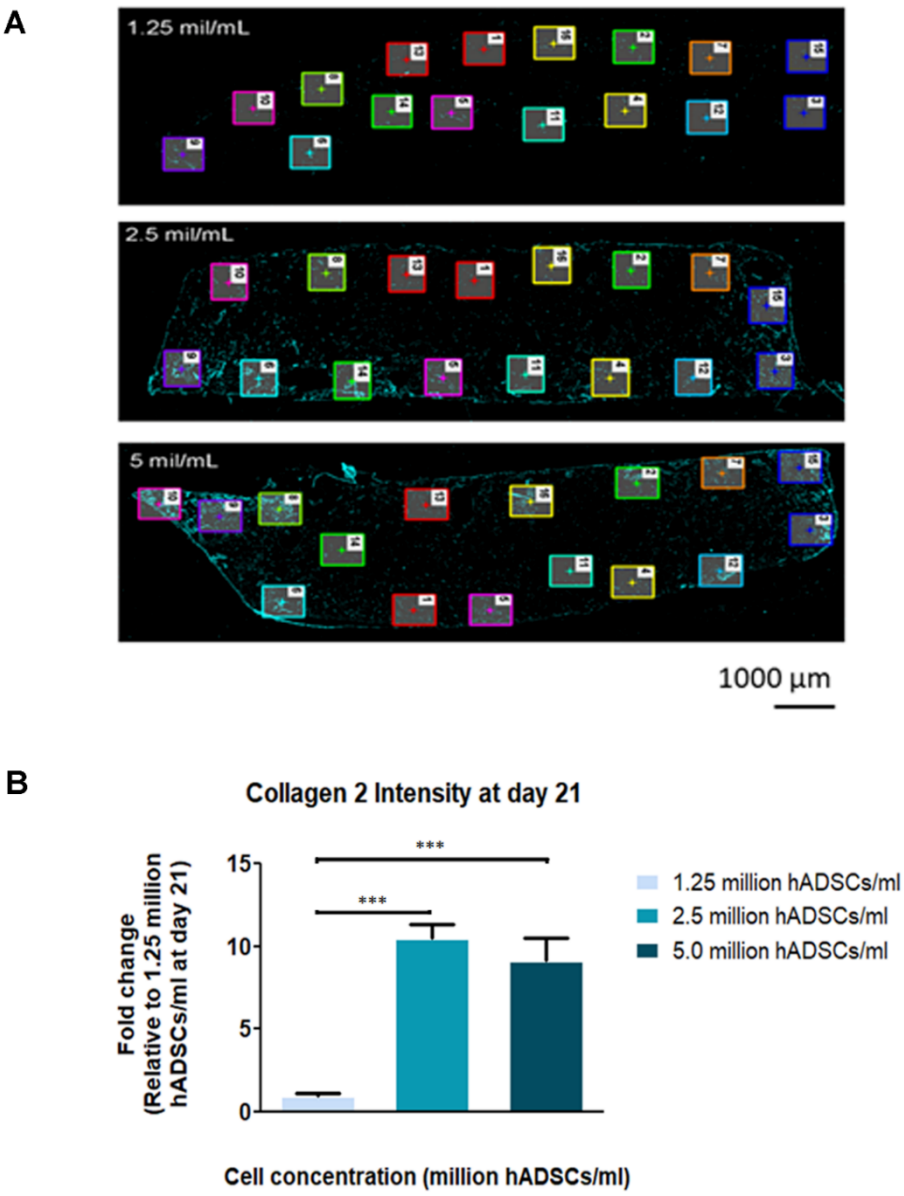


Figure 5.5. Collagen 2 (Col 2) staining intensity of bioscaffolds*. A) 16 evenly spaced Regions of interest (ROI) used in col 2 staining intensity (cyan) evaluation in the 1.25 million, 2.5 million and 5.0 million hADSCs/mL concentration groups, B) Bar graph summarising col 2 staining intensity results of the three groups, presented as expression relative to the 1.25 million hADSCs/mL group. Data are presented as mean +/- standard error margin (SEM) between three biological replicates using cells from two different patients (n=2), significant activity was calculated with unpaired t-test.*

5.2.4 GAG/DNA QUANTIFICATION AND GENE EXPRESSION (QPCR)

Bioscaffolds were analysed using GAG/DNA quantification (Figure 5.6A) and qPCR (Figure 5.6B) for chondrogenic gene analysis (COL2A1, COL1A2, SOX-9 and ACAN). Data is presented as a relative fold change compared to the 1.25 million hADSCs/mL group after 21 days.

The GAG/DNA ratio relative to the 1.25 million hADSCs/mL group at day 21 shows a 0.45- and 1.80-fold increase at day 21 in the 2.5 and 5.0 million hADSCs/mL groups respectively, with statistical difference seen between the 1.25 and 5.0 million hADSCs/mL groups, $p=0.037$.

Collagen 2A1 expression relative to the 1.25 million hADSCs/mL group at day 21 shows a 3.01- and 11.55-fold increase at day 21 in the 2.5 and 5.0 million hADSCs/mL groups respectively, with statistical difference seen between the 1.25 and 5.0 million hADSCs/mL groups, $p=0.007$, and between the 2.5 and 5.0 million hADSCs/mL groups, $p=0.04$. Collagen 1A2 expression relative to the 1.25 million hADSCs/mL group at day 21 shows a 0.02-fold decrease in the 2.5 million hADSCs/mL group and a 0.13-fold increase in the 5.0 million hADSCs/mL group, with no statistical difference seen between all groups. Sox – 9 expression relative to the 1.25 million hADSCs/mL group at day 21 shows a 0.32-fold decrease in the 2.5 million hADSCs/mL group and a 0.66-fold increase in the 5.0 million hADSCs/mL group, with no statistical difference seen between all groups. Aggrecan expression relative to the 1.25 million hADSCs/mL group at day 21 shows a 0.41- and 3.23-fold increase at day 21 in the 2.5 and 5.0 million hADSCs/mL groups respectively, with statistical difference seen between the 1.25 and 5.0 million hADSCs/mL groups, $p=0.003$, and between the 2.5 and 5.0 million hADSCs/mL groups, $p=0.006$.

The 5.0 million hADSCs/mL group produced a higher GAG/DNA ratio and significantly higher Collagen 2A1 (primary chondrogenic marker) expression, which is the principal constituent of chondrogenic ECM. This data supports the earlier findings showing extracellular Collagen 2 expression only in the 5.0 million hADSCs/mL concentration group (Figure 5.5B). In combination, these results suggest that the 5.0 million hADSCs/mL concentration is the minimum required to produce advanced neocartilage formation.

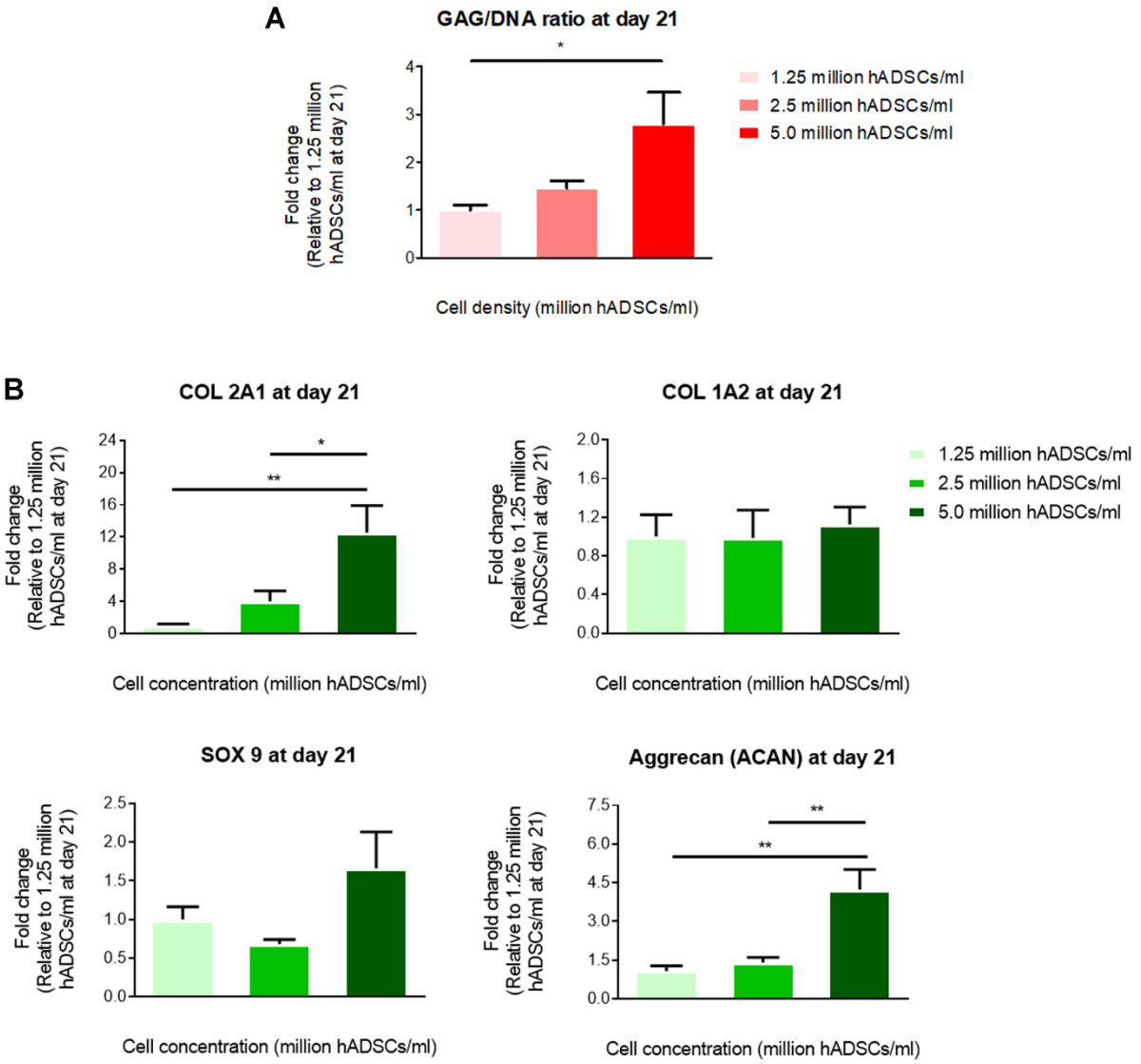


Figure 5.6. Chondrogenic assessment of GelMA/HA bioscaffolds generated using three different cell concentrations. A) Bar graph summarising the GAG/DNA ratio quantification after 21 days of chondrogenic stimulation, B) Bar graphs represent the quantification of chondrogenic gene marker expression. Data are presented relative to the 1.25 million hADSCs/mL concentration group. Represented as the mean +/- standard error margin (SEM) between three biological replicates from two different patients (n=2), significant activity was calculated with unpaired t-test. GAG/DNA - Glycosaminoglycan/Deoxyribonucleic acid. Collagen type 2 (COL2A1), Collagen type 1 (COL1A2), Aggrecan (ACAN) and Sox-9 (SOX9).

THE MAXIMUM DEFECT VOLUME REPAIRABLE USING A RAPIDLY ISOLATED HADSCS POPULATION WHICH IS EXPANDED FOR 5 DAYS

To identify the maximum defect volume repairable, the number of hADSCs obtainable after rapid isolation (85 minutes) and 5-days of expansion was correlated to the minimum chondrogenic hADSCs concentration, (Equation described in methods). This volume forms the upper limit for the defect volume range indicated for treatment.

From objective 1 the number of IFP-derived hADSCs obtainable after rapid isolation (85 minutes) and 5 days of subsequent expansion on average is: 1.90 X 10^6 hADSCs

From objective 2 the minimum identified hADSCs concentration required to produce neocartilage in a GelMA/HA laden bioscaffold is = 5.0 X 10^6 hADSCs/mL

As exhibited in Table 5.2, an extensive range of defect volumes can be treated using 1 or 2 IFPs (humans have 2, one in each knee). Furthermore, these defect sizes comfortably match the total surface area (TSA) of lesions indicated for microfracture repair, irrespective of the depth of cartilage (human knee cartilage 2-4mm)(61).

	Using expanded hADSCs for 5 days -> From 1 IFP	**Using expanded hADSCs for 5 days -> From 2 IFPs**
Maximum defect repairable (Volume)	380 µL (mm^3)	760 µL (mm^3)
Range of defect repairable (Volume)	<380 µL (mm^3)	<760 µL (mm^3)
Examples of correlating dimensions (*average human knee cartilage depth is 2-4mm)	3.80 cm^2 TSA x 1mm depth 1.90 cm^2 TSA x 2mm depth 1.27 cm^2 TSA x 3mm depth 0.95 cm^2 TSA x 4mm depth	7.60 cm^2 TSA by 1mm depth 3.80 cm^2 TSA x 2mm depth 2.53 cm^2 TSA x 3mm depth 1.90 cm^2 TSA x 4mm depth

Table 5.2. Defect volumes repairable using rapidly isolated hADSCs expanded for 5 days with the minimum required neocartilage forming concentration. IFP- Infrapatellar Fat Pad, hADSCs- human Adipose-Derived Mesenchymal Stem Cells, µL - Microlitres.

5.3 DISCUSSION

To create a quick turnaround biofabrication procedure, the minimum chondrogenic requirements of using expanded stem cells need to be identified, so that they can be reimplanted at the earliest possible timeframe.

To achieve this, the first investigation was to identify the earliest point during expansion in which hADSCs can successfully be induced into chondrogenesis. At time points 0 and after 3 days of expansion, cells were unable to be pushed into pellet culture suggesting they are unlikely to have matured into a more active stem cell phenotype which can be differentiated. Furthermore, chondrogenic differentiation can only be performed in 3D pellet culture, as a 2D culture of stem cells is traditionally weak. After 5- and 7-day expansion, timeframes cells were successfully able to be pelleted. This is the first study to demonstrate early cell growth kinetics (within 7 days, Passage 0-1, P0-1), with an average doubling time of 4.41 days reported and there was high variability seen which is likely due to the inability to perfectly control the starting number of cells. Growth kinetics are routinely calculated from Passage 1 onwards, and the average doubling rate of IFP-derived hADSCs has been demonstrated to be roughly 5-6 days at P1-2 which increases relative to the number of passages (333). Therefore, it is demonstrated that cell doubling time is rapid early in passaging even before the routine first assessment performed at P1-2.

Furthermore, these populations were both able to successfully undergo chondrogenesis over a 3-week timeframe. Therefore, the earliest turnaround time during expansion in which hADSCs can be pushed into chondrogenesis (used as therapy) is after 5 days, meaning the overall biofabrication treatment approach can be performed comfortably within < 1 week (85-minute harvest and isolation then 5 days of cellular expansion).

Another important consideration is the use of spare cells or pellets for biobanking procedures (354). For example, using 2 IFPs, on average between 1.43-1.72 x 10^6 cells can be collected based on results from chapters 4 and 5, this equates to roughly 6 pellets (each pellet 2.5x 10^5 cells). Looking ahead, the unused cells/pellets in the initial therapy could be stored and expanded using microspheres for bio banking (355, 356) which is an emerging field that can be used as a backup for failed initial therapy or as a storage for future therapy.

Given that the third step in the biofabrication process (Cellular reimplantation) can be performed using *in situ* bioprinting technology, effectively there is no addition to the overall turnaround duration as a result of this final phase. Therefore, with a known timeframe for the first two steps of the biofabrication process, treatment strategies can now be planned around a given turnaround timeframe.

The next objective in this body of work was to identify the minimum effective hADSCs concentration required to produce neocartilage in a GelMA-based biofabrication procedure. By identifying this concentration and correlating it to the number of cells isolatable over 5 days of expansion, the repairable defect volume can be calculated. After 3 weeks of chondrogenic stimulation, the 5.0 million hADSCs/mL concentration group demonstrated the most optimal GAG/DNA ratio, chondrogenic gene expression and hyaline-like ECM production visualised with immunostaining. Therefore, the 5.0 million hADSCs/mL concentration represents the minimum cell concentration required to trigger the chondrogenic pathway and produce advanced chondrogenesis in GelMA/HA-based bioscaffolds. A key limitation in this study is the inability to compare to higher concentrations, such as 10.0 million cells/mL which is commonly used (177). However, the key objective was to identify the minimum concentration required for chondrogenesis, a 10.0 million cells/mL concentration has already been validated; therefore, 5.0 million cells/mL was selected as the upper limit, it will be of further value to now test concentrations between 5.0 and 10.0 million. Another limitation to this part of the study is that we confined our experiments to GelMA/HA hydrogel, which may not be translatable to other hydrogel scaffold compositions which should have own cellular-interaction profiles examined separately.

Finally, using the data from the results obtained in the first two objectives, the maximal repairable volume using a 5-day expanded hADSCs population is calculated to be 380 µL (mm^3) using one IFP or 760 µL (mm^3) using both IFPs (two IFPs one in each knee). Based on these volumes, all lesion surface areas typically indicated for microfracture repair and most osteochondral defects (average 550 µL) (252, 357, 358) can be treated using the proposed biofabrication procedure. This calculation presented here opens up the possibility of personalised repair, which can be individually tailored to a patient based on their defect size. An obvious limitation in this step will be with identifying the exact dimensions of such defects

in advance. This can be assessed using preoperative magnetic resonance imaging or arthroscopic examination. Another limitation is that the cellular yield data collected is from patients in an elderly age group undergoing arthroplasty. To accurately represent the ideal treatment population, it would be beneficial to assess the IFP-derived hADSCs yield in patients below the age of 50.

5.4 CONCLUSION

In conclusion, this study demonstrated that a 1-week turnaround GelMA/HA-based biofabrication approach can be performed using rapidly isolated hADSCs (85 minutes), which are expanded for 5 days. Furthermore, this approach can comfortably treat defect sizes indicated for the current clinical standard repair option (microfracture). This paves the way for an *in vivo animal* model of cartilage defect repair using an optimised biofabrication procedure.

CHAPTER 6: ESTABLISHING A BIOFABRICATION PROCEDURE FOR *IN VIVO* CHONDRAL REPAIR

6.1 INTRODUCTION

To biofabricate tissue *in situ*, several components of our regenerative delivery method warrant optimisation and design; to enable a user-friendly, safe, sterile and efficient procedure that is compatible with the surgical environment.

The model selected for the next section of work (*in vivo* proof of concept) is a small animal (rabbit); hence, to fit within this model, a commercially sourced rabbit MSCs line was validated with a 3-week chondrogenic screening study.

GelMA, is a gelatin-based hydrogel which has excellent biocompatibility and a reliable biodegradability profile (168-170), it has been successfully used in *in vivo* models and delivered using an *in-situ* approach (247). The supplementation of methacrylate/methacrylamide (MA) groups to gelatin permits light-assisted cross-linking of the material, which helps boost the mechanical stability of the implant and aid in mimicking the natural ECM of cartilage (171, 172). The stiffness and strength of the GelMa hydrogel can be tuned, by increasing the percentage of gelatine. Fabricated tissue constructs behave differently with different material stiffnesses(172); therefore, next it was essential to validate the difference in mechanical strength using an acellular soft 6% and hard 10% GelMA scaffold.

Unlike *in vitro*, with *in vivo* study only the top of the bioscaffolds construct can be exposed to crosslinking and consequently Hyaluronic acid (HA) wasn't added to GelMA in the bioink formulation of this chapter. The addition of HA increases the material opacity (319); therefore, when only one side of the construct can be crosslinked, removing HA can maximise full penetrance of light as described in methods 3.6.1.

If the gelatine is too gelated during *in situ* delivery, it becomes difficult to extrude, whereas if too liquified, it rapidly disperses and collapses (299, 300). The control of gelation; therefore, becomes pivotal when using thermoreversible hydrogels for cartilage repair (301). Gelation is expected to occur quicker with higher concentrations of gelatine (305); therefore, we hypothesised that harder (10% GelMA) should gelate quicker than the softer (6% GelMA) hydrogel.

Light assisted cross-linking of GelMA is associated with a high cell viability, which is reported as >85-90% (175, 307). Compared to the *in vitro* work (chapter 5), in this chapter a transition

to visible light (405nM) was undertaken based on emergent findings in the literature reporting better biocompatibility and penetrance for GelMa hydrogels using visible light compared to UV light (159, 326). Surgical application is simple using a hand-held system, and the amount of visible light contact with healthy tissue can be limited. The distance required for adequate coverage of the generated rabbit defect (details in chapter 2) without infringing on healthy tissue is 1cm. Thus, the next step was to design, and 3D print a sterilisable 1 cm fixed distance cover that could be attached to the end of a light source enabling surgical use.

6.2 RESULTS

6.2.1 CHONDROGENIC VALIDATION OF A COMMERCIAL RABBIT MSCs LINE

A commercial MSCs line derived from the same species and gender of the rabbit that is to be used in the *in vivo* model (chapter 5) was sourced. The chondrogenic capacity of this cell line was then validated using a 3-week differentiation study by quantifying the GAG/DNA ratio (Figure 6.1). During the 3-week chondrogenic stimulation period, the GAG/DNA ratio increased significantly from 9.9 +/-1.1 to 15.1 +/-0.8, p=0.003. This increase in cartilage-specific glycosaminoglycan content over 3 weeks of stimulation indicates successful chondrogenic differentiation.

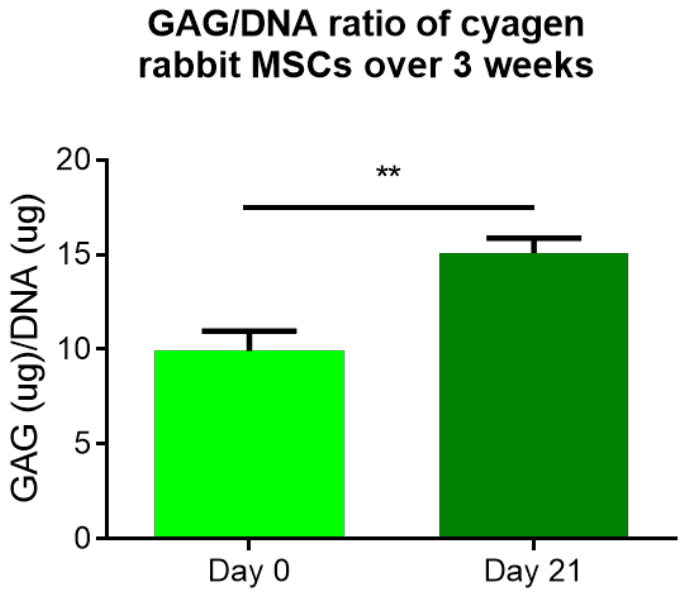


Figure 6.1. GAG/DNA ratio over 3-weeks of chondrogenic stimulation using a commercial (cyagen) rabbit MSCs line. ug – micrograms. GAG/DNA - Glycosaminoglycan/Deoxyribonucleic acid. Data are presented as mean +/- standard error margin (SEM) between three biological replicates of the same rabbit cell line, significant activity was calculated with unpaired t-test.

6.2.2 MECHANICAL ASSESSMENT OF A SOFT AND HARD GELATIN-BASED HYDROGEL

Next, two different compositions of GelMA (Gelatin-Methacryloyl), a soft and hard form (6% and 10% GelMA) were assessed using mechanical testing to confirm the difference in compressive strength, (Figure 6.2). Acellular scaffolds using these two hydrogel compositions were generated and cross-linked using visible light. The compressive strengths of these constructs were evaluated the next day as described in the methods.

The compressive moduli of the 6% and 10% GelMA hydrogel compositions were 23.2 +/-3.9 and 95.1 +/- 8.1 kPA (kilopascals) respectively, representing a 4.1 - fold difference. These results confirm that higher concentrations of gelatine within a GelMA-based hydrogel are associated with a higher compressive strength of printed scaffolds.

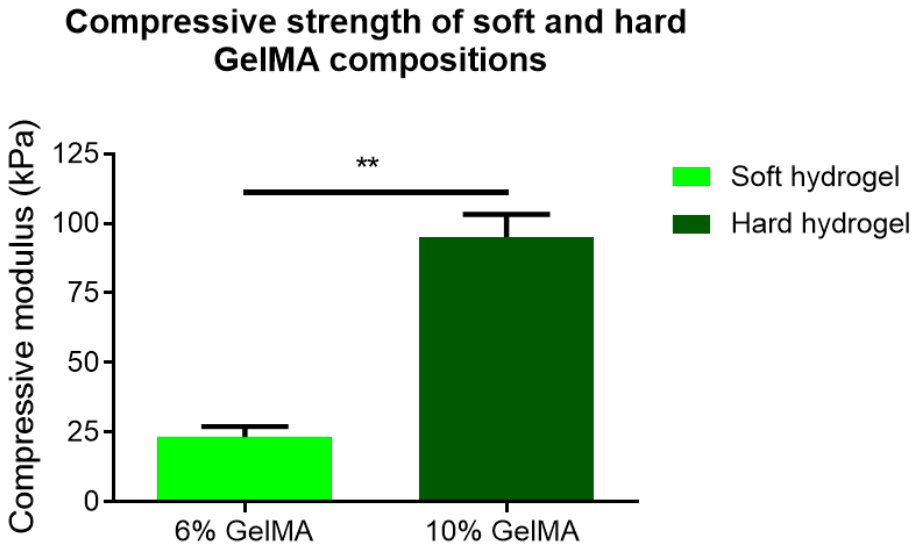


Figure 6.2. Compression testing of acellular GelMA scaffolds the day after printing. kPA – kilopascal and GelMA - Gelatin-Methacryloyl. Data are presented as mean +/- standard error margin (SEM) between three scaffold replicates, significant activity was calculated with unpaired t-test.

6.2.3 ASSESSMENT OF THE GELATION TIME OF CHOSEN HYDROGELS

The third step was to identify the appropriate gelation time of the two hydrogel compositions (6% GelMA and 10% GelMA) that is required prior to becoming printable. A filament formation test was performed to evaluate different time points of gelation associated with the use of the two different compositions and the use of two different temperatures (23°C and 4°C). Morphological observation of the hydrogels when gelation was performed at 23°C

showed that at least 15 minutes was required for the 6% GelMA group to gelate (positive test result) and become printable; whereas at least 10 minutes was needed for the GelMA 10% composition to become printable, Table 6.1. Morphological observation of the hydrogels when gelation was performed at 4°C showed that at least 6 minutes was required for the 6% GelMA group to gelate (positive test result) and become printable; whereas at least 1 minute was needed for the GelMA 10% composition to become printable, Table 6.2.

These results confirm that higher concentrations of gelatine in a GelMA hydrogel are associated with quicker gelation times. Furthermore, when gelated at a cooler temperature of at 4°C, the gelation of the GelMA occurred faster. Taking into consideration the effect of the heat that would emanate from the wound, it was decided that 9 minutes of gelation at 4°C would be used for the GelMA 6% group, and 3 minutes of gelation at 4°C would be used for the GelMA 10% group.

Bioink composition	**Extrusion Flow (kept constant)**	**Minutes at room temperature (23°C)**	**Morphological observation**
GelMA 6%	240 µL/minute	0	drop
		1	drop
		3	drop
		5	drop
		10	drop
		15	string
GelMA 10%	240 µL/minute	0	drop
		1	drop
		3	drop
		5	drop
		10	string
		15	string

Table 6.1. Assessment of the gelation time required for hydrogel printability (Filament formation test) using the room temperature of 23°C. GelMA - Gelatin-Methacryloyl.

Bioink composition	Extrusion Flow (kept constant)	Minutes in a cooled temperature (4°C)	Morphological observation
GelMA 6%	240 µL/minute	0	drop
		1	drop
		3	drop
		6	string
		9	string
GelMA 10%	240 µL/minute	0	drop
		1	string
		3	string
		6	hypergelated
		9	Non-extrudable

Table 6.2. Assessment of the gelation time required for hydrogel printability (filament formation test) using a cooled temperature of 4°C. GelMA - Gelatin-Methacryloyl.

6.2.4 DESIGN OF A SAFE INTRAOPERATIVE CROSSLINKING METHOD

Finally, a visible light source (405 nm) for cross-linking was established and set-up to fit within a surgical setting. To cover the whole defect and not affect any healthy native tissue, a 1 cm distance interval is required from the tip of the light source. Given that a hand-held cross-linking device (LEDsaber, Biolambda, Sao Paulo, Brazil), is most suitable for an intraoperative approach, a sterilisable attachment probe cover was designed to fix this distance and provide consistent cross-linking to all the repair defects, shown in Figure 6.3.

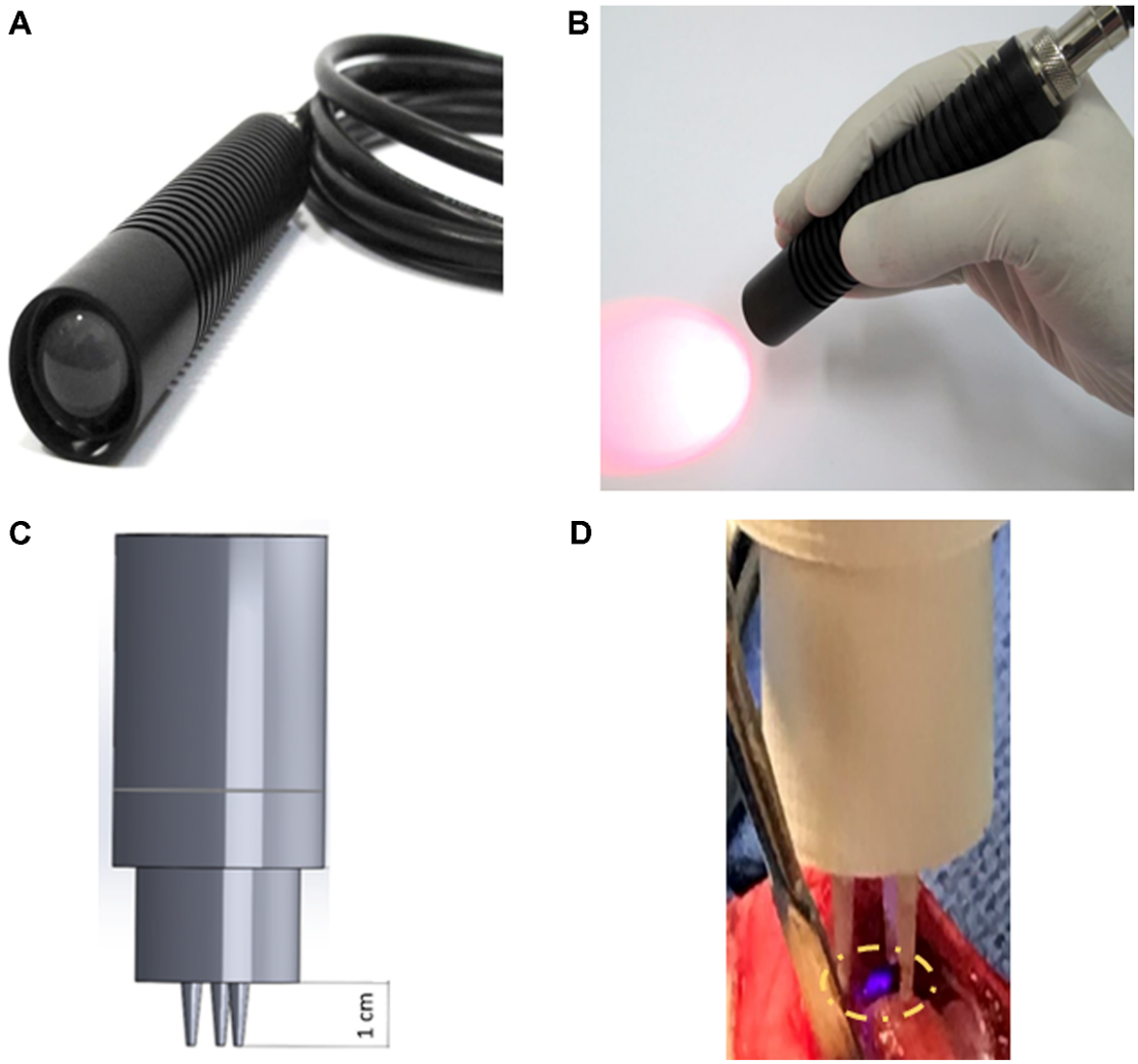


Figure 6.3. Light source adapter set-up at a fixed distance of 1cm. A-B) Handheld light source (LEDsaber, Biolambda, Sao Paulo, Brazil), C) Design of fixed distance probe attachment, D) Intraoperative use of the light source and probe cover system, the yellow dotted circle shows the light (blue) hitting only the defect, and the three prongs gently stabilising the device.

FINAL SET-UP OF THE *IN VIVO* BIOFABRICATION REPAIR PROCEDURE

Before performing an *in vivo* rabbit model of cartilage repair several components of the biofabrication procedure required selection and validation. A summary of all these design selections and validations performed in this chapter of work are shown highlighted in green in Figure 6.4.

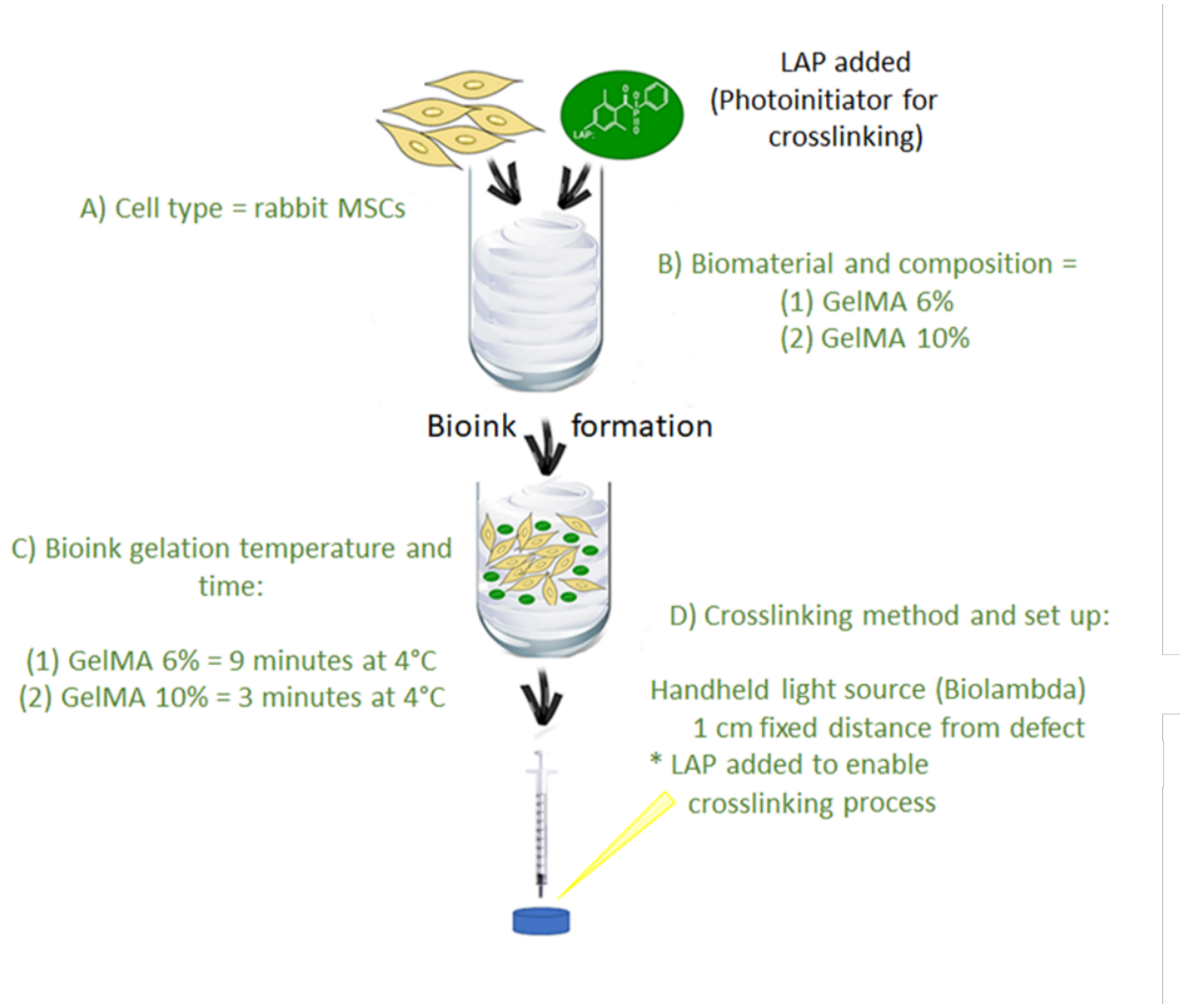


Figure 6.4. Summary of final biofabrication procedure. Highlighted in green are the components which have been selected and validated for use in this in situ applicable surgical procedure. LAP - Lithium phenyl-2,4,6-trimethylbenzoylphosphinate and GelMA - Gelatin-Methacryloyl.

6.3 DISCUSSION

As part of the biofabrication set-up and design, several aspects of the procedure were first selected and validated in this chapter. First, the cell source selected (commercial rabbit BMSCs) was verified and confirmed to show *in vitro* chondrogenic differentiation capacity. A limitation to this aspect of the design is in the inability to use rabbit MSCs isolated from the Infrapatellar Fat Pad (IFP), in chapters 4 and 5 of this thesis testing was performed using human IFP-derived MSCs (hADSCs). The rabbit (largest small animal model) was chosen to suit the feasibility of this proof of concept project, in which the native IFP and MSCs yield is too low and variable.

Next, two different compositions of a GelMA hydrogel (soft and hard) were tested to evaluate their respective baseline compressive strength. Then the individual gelation time required before printing for each composition was identified. As expected, the lower concentration (6% GelMA) had less compressive strength compared to the higher concentration (10% GelMA) group with a >4-fold difference.

Using the filament formation test, it was determined that gelation times were quicker for both 6% and 10% GelMA hydrogel concentrations when cooled at 4°C compared to 23°C. Overcooling of bioinks is associated with cytotoxicity when temperatures < 0°C are used; therefore, at 4°C, minimal effects on cytocompatibility is expected (211). Therefore, for the 6% and 10% GelMA-based hydrogels, gelation times of 9 and 3 minutes (cooled prior at 4°C) respectively were chosen and subsequently utilised during the *in vivo* rabbit model of cartilage repair (Chapter 7).

A limitation to this aspect of work is that testing was only performed on two different GelMA compositions. The purpose of this study was to choose two different composition extremes that could subsequently be used to evaluate the effect of *in vivo* cellular repair. Thus, the aim was not to conduct a broad investigation on the strength of varying GelMA concentrations, but rather to assess the difference between soft and hard GelMA-based bioinks on cartilage repair.

Finally, a 1 cm fixed distance light-assisted cross-linking system was designed using an easily operatable hand-held device and a sterilisable attachment cover. This distance ensured that only the defect area of interest was exposed to visible light and cross-linked, and no healthy tissue was affected in the process.

6.4 CONCLUSION

In this chapter of work, a biofabrication treatment approach to cartilage repair in a rabbit model was designed. This novel approach is safe, user friendly, and has been devised to suit the intraoperative environment. The design processes and framework embodied in this chapter should serve as a guideline for future proposals of biofabrication therapy in larger animal models and human clinical trials.

CHAPTER 7: CARTILAGE BIOFABRICATION USING THE MINIMUM CHONDROGENIC HADSCs CONCENTRATION – A PILOT *IN VIVO* RABBIT MODEL

7.1 INTRODUCTION

Biofabrication approaches can be used *in vitro* to investigate select aspects of regenerative medicine, such as the biocompatibility of scaffolds and the effects of specific conditions on cell proliferation and differentiation (250). However, an animal model is ultimately warranted to study the complex process of *in vivo* cartilage tissue formation and maturation; furthermore, this bridges the gap between i*n vitro* and clinical study in humans (250).

Given the fiscal feasibility, practicality and proof of concept nature of this study, the small animal is more suitable to the cost budgets and project timeframes of this thesis. Based on current literature, to assess critical size defects (314, 315) in this model a 4 mm diameter circular defect with a depth of 0.3 mm was chosen, which creates a volume of approximately 4 µL (mm^3). The four treatment groups selected were empty defect (Negative control), microfracture (Positive control), biofabrication treatment group 1 (5.0 million MSCs /mL of 6% GelMA) and biofabrication treatment group 2 (5.0 million MSCs /mL of 6% GelMA). Timepoints were selected based on when early and mature cartilage formation is detectable, which is at around 3-4 and 6-8 weeks, respectively post-repair (308).

This section serves as a pilot study assessing a novel biofabrication therapy for pure chondral repair *in vivo*. This new approach utilises the minimum chondrogenic stem cell concentration (chapter 5) with a soft or hard hydrogel (6% or 10% a Gelatin-Methacryloyl) and an innovative intraoperative method (chapter 6). The outcomes of which are hypothesised to be comparable if not better than those in the clinical standard (microfracture repair) group.

7.2 RESULTS

CARTILAGE REPAIR USING A NOVEL BIOFABRICATION PROCEDURE *IN VIVO*

7.2.1 POSTOPERATIVE OUTCOMES

All rabbits survived the 4- and 8-week time points. One rabbit required reclosure of the proximal capsule and skin for wound dehiscence postoperatively at day 3, after 7 days of monitoring the wound healed with no further complications. One rabbit developed bilateral swelling over the knee joint after 5 days, sterile examination with needle aspiration revealed serous fluid consistent with a postoperative seroma. After needle aspiration and drainage, no further recollection or complications were observed.

7.2.2 MACROSCOPIC ASSESSMENT

To macroscopically evaluate cartilage repair, harvested condyles were visually inspected (Figure 7.1A) and then scored based on the international cartilage repair society (ICRS) morphological evaluation system (Figure 7.1B-C), as described in the methods section. Post femoral harvest, one rabbit femur from the 8-week group showed signs of inflammatory change over the proximal trochlea notch region; however, the remaining femur, condyles and treatment regions were unaffected.

4 WEEK GROUP

After 4 weeks, the defect border could still be visualised on close inspection of the empty treatment group with hypertrophic tissue. The fracture holes were still evident within the defects formed as part of microfracture treatment. Defect areas in both the biofabrication treatment groups were harder to discriminate from nearby healthy cartilage and were less demarcated compared to the other treatment groups.

Repair in the empty group on average was scored 6.0 +/- 0.7 (n=6) which are consistent with a grade III ICRS macroscopic score which indicates abnormal tissue repair. Repair in the microfracture treatment group on average scored 6.6 +/- 0.9 (n=6) which is consistent with a grade III ICRS macroscopic score which indicates abnormal tissue repair.

Repair in the biofabrication treatment group 1 (5 million MSCs/mL of 6% GelMA) on average scored 8.8 +/- 0.5 (n=6) which was consistent with a grade II ICRS macroscopic score which indicates nearly normal tissue repair. Repair in the biofabrication treatment group, 2 (5 million MSCs/mL of 10% GelMA) on average, scored 6.6 +/- 0.5 (n=6) which was consistent with a grade II-III ICRS macroscopic score which indicates between abnormal and nearly normal tissue repair.

When comparing all the treatment group scores at 4 weeks, the biofabrication treatment group 1 score was significantly higher than all the other groups. When laterality was assessed (Figure 7.1C), irrespective of the treatment type, repair of the lateral condyle scored on average 7.0 +/- 0.4 and the medial condyle scored on average 8.0 +/-0.4 after 4-weeks, no significant change was observed between groups.

8 WEEK GROUP

After 8 weeks, the defect border could still be visualised on close inspection of the empty treatment group with hypertrophic tissue still visible similar to the 4-week group. The fracture holes were still evident within the defects formed as part of microfracture treatment, similar to the 4-week observations. In both the biofabrication treatment groups defect areas were harder to discriminate when compared to surrounding healthy cartilage and looked more integrated and less demarcated compared to the empty and microfracture groups.

Repair in the empty group on average was scored 6.0 +/- 0.5 (n = 6), this score is consistent with a grade III ICRS macroscopic score which indicates abnormal tissue repair. No significant change was observed between the 4- and 8-weeks scores of the empty group. Repair in the microfracture treatment group on average scored 6.46 +/- 0.47 (n = 6), this score is consistent with a grade III ICRS macroscopic score which indicates abnormal tissue repair. No significant change was observed between the 4- and 8-weeks scores of the microfracture group.

Repair in the biofabrication treatment group 1 (5 million MSCs/mL of 6% GelMA) on average scored 8.8 +/- 0.5 (n=6), this score was consistent with a grade II ICRS macroscopic score which indicates nearly normal tissue repair. No significant change was observed between the 4- and 8-weeks scores of the biofabrication treatment group 1. Repair in the biofabrication treatment group 2 (5 million MSCs/mL of 10% GelMA) on average scored 7.6 +/- 0.4 (n = 6), this score is consistent with a grade II-III ICRS macroscopic score which indicates between abnormal and nearly normal tissue repair. No significant change was observed between the 4- and 8-weeks scores of the biofabrication treatment group 2.

The biofabrication treatment group 1 and 2 scores were significantly higher than both the empty and microfracture groups after 8 weeks. When laterality was assessed (Figure 7.1C), irrespective of the treatment type, repair of the lateral condyle scored on average 6.5 +/- 0.4 and the medial condyle scored on average 7.2 +/- 0.4 after 8-weeks., no significant change was observed over this interval. Furthermore, no significant difference was observed between the 4- and 8-weeks scores of treatments in both medial and lateral condyles.

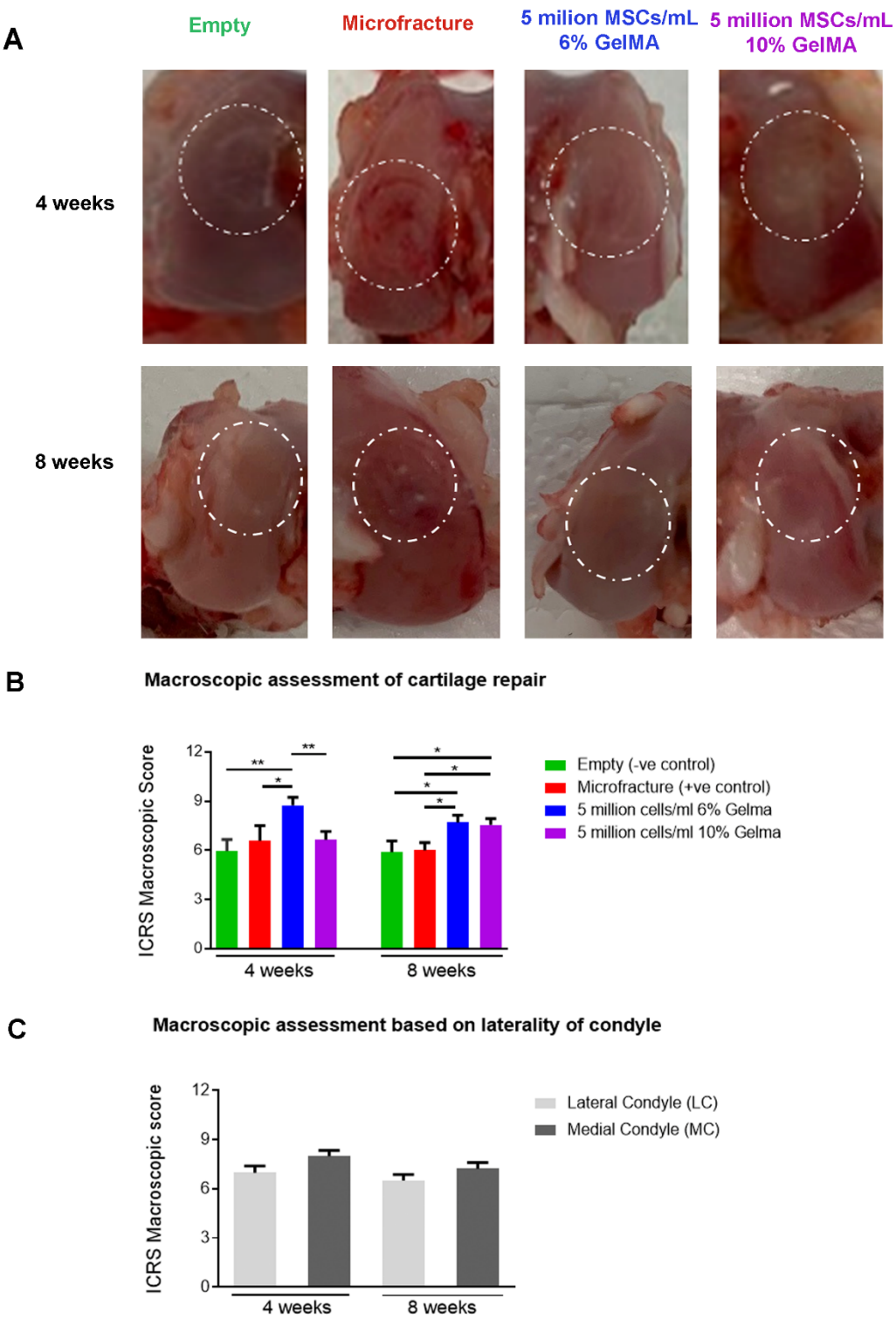


Figure 7.1. Cartilage morphology and macroscopic scoring. A) Representative Defects after 4 and 8 weeks of treatment, area of repair highlighted as a dotted white circle, B) Macroscopic scoring of cartilage repair (n=6) and C) Macroscopic scoring of cartilage based on the laterality of the condyle, (n=12). GelMA - Gelatin-Methacryloyl and MSCs -Mesenchymal stem cells. Data are presented as mean +/- standard error margin (SEM); significant activity was calculated with unpaired t-test.

7.2.3 BIOMECHANICAL ASSESSMENT – ATOMIC FORCE MICROSCOPY

The biomechanical properties of the performed treatment groups were assessed using atomic force microscopy (AFM), as described in the methods (Figure 7.2). As a reference point, the youngs modulus of articular knee cartilage in healthy 12 weeks old, male, New Zealand white rabbits are reported in the literature to be 600 kPa on average (329, 330).

Healthy (normal) rabbit cartilage and empty defects were tested using AFM on the spare rabbits once the treated rabbits had survived the postoperative period. The normal rabbit condyles on average had a young's modulus of 598 +/- 57 kPA (kilopascals). The empty defects had on average a youngs modulus of 1155 +/- 179 kPA.

4 WEEK GROUP

In the microfracture group, the youngs modulus was 55.1 +/- 5.0 kPA. In the biofabrication treatment group 1, the youngs modulus was 162 +/- 11 kPA. In the biofabrication treatment group 2, the youngs modulus was 215 +/- 25 kPA at 4 and 8 weeks respectively.

After 4 weeks, the youngs modulus of the biofabrication treatment group 2 was significantly higher than both the microfracture and biofabrication 1 treatment groups, $p < 0.001$ and $p = 0.03$ respectively. The biofabrication treatment group 2 had a significantly higher youngs modulus compared to microfracture at week 4, $p < 0.0001$.

8 WEEK GROUP

In the microfracture group, the youngs modulus significantly increased to 249 +/- 37 kPA by 8 weeks, $p<0.0001$. In the biofabrication treatment group 1, the youngs modulus significantly decreased to 55 +/- 5 kPA by 8 weeks, $p<0.0001$. In the biofabrication treatment group 2, the youngs modulus increased to 278 +/- 26 kPA, no statistical difference was detected over the 4-8-week interval.

After 8 weeks, the youngs moduli of both the microfracture and biofabrication treatment group 2 were significantly higher than the biofabrication 1 treatment group, $p < 0.0001$ and $p<0.0001$ respectively.

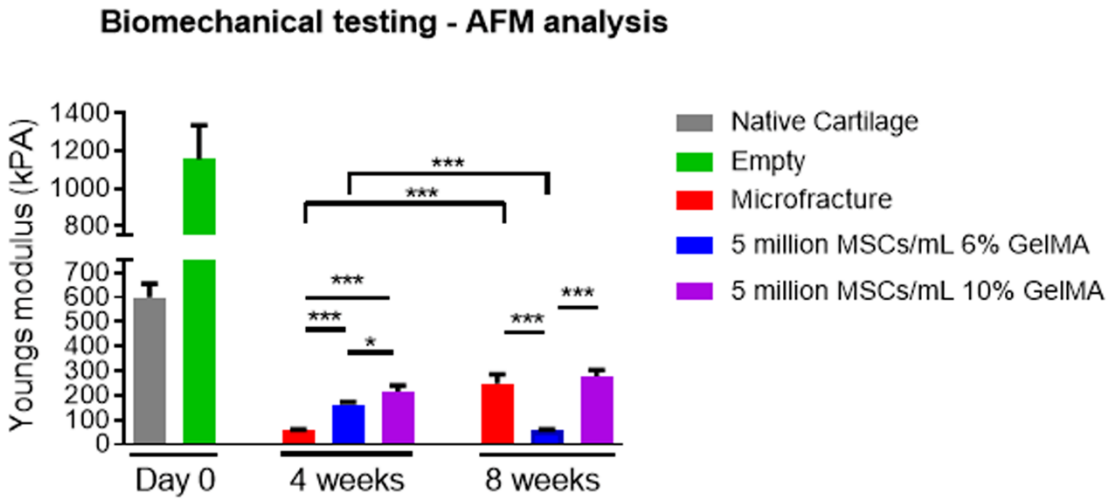


Figure 7.2. Atomic Force Microscopy (AFM) mechanical testing. For each group samples from three different rabbits were tested (n=3). Day 0 reference measurements performed on healthy cartilage and empty groups (n=2). GelMA - Gelatin-Methacryloyl and MSCs - Mesenchymal stem cells. Data are presented as mean +/- standard error margin (SEM); significant activity was calculated with unpaired t-test

7.2.4 MICROSCOPIC ASSESSMENT

Microscopical evaluation of cartilage repair was performed by assessing the histology and immunofluorescence of collagen 1 and 2 in harvested tissue (Figure 7.3A). Microscopic scoring of the repair was then conducted using an adapted version of the modified O' Driscoll scoring system, as described in the methods, Figure 7.3B.

4 WEEK GROUP

On the visual observation of histology (Figure 7.3, 4 weeks first row), spontaneous regeneration was seen in the empty defect group, tissue was fibrillated and hypertrophic, with extension beyond the native cartilage surface. The microfracture group showed no-minimal recovery, with the fracturing of subchondral bone still visible after 4 weeks. Both the biofabrication treatment groups (5 million MSCs/mL of 6% and 10% GelMA) showed regenerative repair at week 4, inadequate lateral integration to native tissue was evident in both.

Next, immunostaining for collagen 1 and 2 was performed to evaluate further the type of tissue that was produced (Figure 7.3, rows 2-4). Collagen 2 should predominate in hyaline

cartilage, while collagen 1 is associated with fibrocartilage. In general, the results were consistent with the histological examination.

In the empty group, there was adequate collagen 2 expression at week 4 with a layer of collagen 1 evident on top. There was a lack of collagen 2 staining and consistency observed in the microfracture repair group and minimal expression of collagen 1 staining indicating the absence of tissue regeneration/formation.

Collagen 2 staining after 4 weeks in both biofabrication treatment groups was detected, with a higher signal observed in the 5 million MSCs/mL of 10% GelMA group. At the 4-week time point, there are points of disruption visible in both groups which corresponded to the defect borders; furthermore, collagen 1 staining was present within these regions

Finally, as part of the microscopic assessment, the sectioned cartilage tissue was scored using an adapted form of an established system for chondral repair/regeneration. The modified O' Driscoll score is a validated (359) marking system which is adapted from two different classifications, enabling a more comprehensive assessment of cartilage repair using implanted tissue. In addition to all the parameters found in the original O'driscoll scoring system; subchondral bone formation, basal integration and inflammation are added from the international cartilage repair visual assessment scale (ICRS 11 – VAS) (360). For this study, three parameters were removed, which were subchondral bone formation, intactness of the calcified layer and inflammation. These parameters are more specific osteochondral repair as opposed to the isolated chondral repair mimicked in this study.

The empty group was scored 22.7 +/- 2.4 at. The microfracture group was scored 9.9 +/- 0.7. The biofabrication treatment group 1 (5 million MSCs/mL of 6% GelMA) was scored 20.1 +/- 1.5. In the biofabrication treatment group 2 (5 million MSCs/mL of 10% GelMA) the score was 24.7 +/- 1.5. At the 4-week time point, the microfracture group was scored significantly lower than all other treatment groups.

8 WEEK GROUP

On the visual observation of histology (Figure 5.3, 8 weeks first row), spontaneous regeneration was seen in the empty defect group and the tissue is fibrillated and hypertrophic, extending beyond the native cartilage surface similar to the 4-week group. The

microfracture group showed no-minimal regeneration with the fracturing of subchondral bone still visible, similar to the 4-week group. Both the biofabrication treatment groups (5 million MSCs/mL of 6% and 10% GelMA) showed regenerative repair after 8 weeks, with significantly improved lateral integration to native tissue compared to the 4-week group.

In general, the results were consistent with the histological examination. In the empty group, compared to the 4-week time point, there was reduced collagen 2 expression with increased regions of collagen 1 compatible with prevailing hypertrophic tissue. There was a lack of collagen 2 staining and consistency observed in the microfracture repair group; furthermore, minimal expression of collagen 1 staining also indicated the absence of tissue regeneration/formation, similar to that observed in the 4-week group.

After 8 weeks in both the biofabrication treatment groups, there was a more homogenous expression of collagen 2 throughout the cartilage surface, with no apparent gaps or breaks visible. Furthermore, the staining intensity was similar between both groups, and collagen 1 staining was mostly evident in the subchondral bone regions, with no-minimal expression seen at the cartilage surface in both groups.

The empty group decreased to 20.3 +/- 2.0 after 8 weeks, no significant statistical difference was observed over the 4-8-week interval. The microfracture group significantly increased to 17.9 +/- 2.3 after 8 weeks, $p = 0.005$. The biofabrication treatment group 1 (5 million MSCs/mL of 6% GelMA) score significantly increased at 8 weeks with a score of 26.3 +/- 1.3, $p = 0.04$. In the biofabrication treatment group 2 (5 million MSCs/mL of 10% GelMA) the score increased to 26.0 +/-1.6, no significant statistical difference was observed over the 4-8-week interval.
At the 8-week time point, both empty and microfracture groups were scored significantly less than both the biofabrication treatment groups.

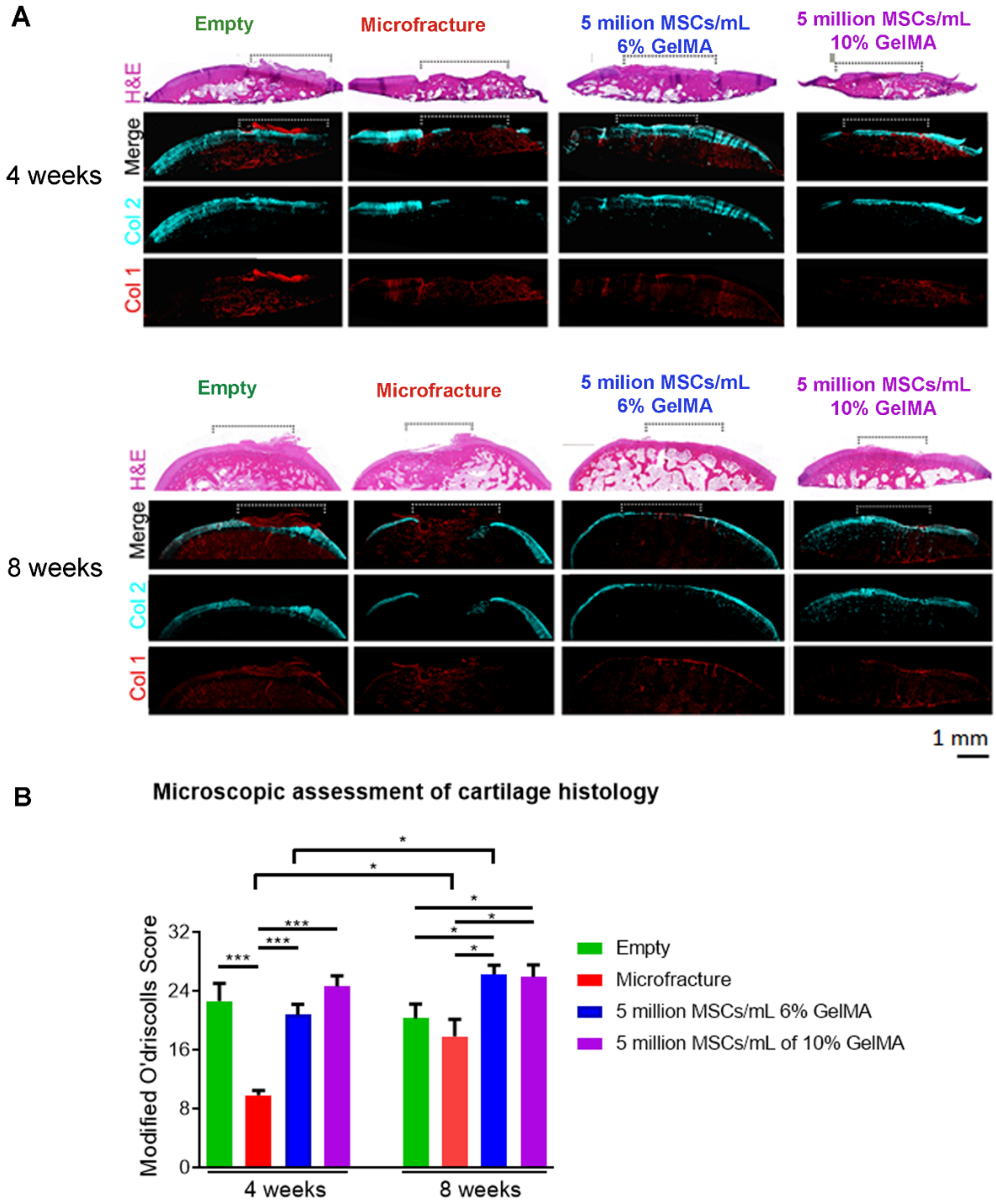


Figure 7.3. Histology, immunostaining and microscopic scoring of cartilage repair. A) Histology and immunostaining in 4-week and 8-week treatment groups, B) Microscopic scoring of treatment groups after 4 and 8 weeks. Scoring of cartilage repair based on an adapted form of the modified o' Driscoll score, (n=3) for each treatment group and (n=3) for each time point. Haematoxylin and Eosin (H &E), Col 2 (cyan) and Col 1 (red). GelMA - Gelatin-Methacryloyl and MSCs -Mesenchymal stem cells. Data are presented as mean +/- standard error margin (SEM); significant activity was calculated with unpaired t-test.

7.3 DISCUSSION

An *in vivo* rabbit model of cartilage repair was performed using 4- and 8-week endpoints for harvest. In each rabbit condyle one of the 4 treatment groups were performed: empty defect, microfracture, biofabrication treatment group 1 (5 million MSCs/mL of 6% GelMA) and biofabrication treatment group 2 (5 million MSCs/mL of 10% GelMA).

The biofabrication procedure was simply and efficiently implemented in the *in vivo* rabbit model. The intraoperative printing of the hydrogel was well controlled. A limitation that was associated with the bioprinting aspect of the procedure was the presence of blood over the defect; this diluted the implant and made it difficult to control the homogenous formation of the construct. Macroscopic scoring showed significantly higher results in both the biofabrication treatment groups when compared to the empty group and microfracture repair. Both biofabrication groups had scores consistent with nearly normal tissue repair, whereas empty and microfracture repairs both showed abnormal tissue repair. Notably, no difference was seen individually between biofabrication groups over 8 weeks, suggesting no difference in repairability between the 4-8-week interval.

Microscopic repair scoring was generally consistent with the macroscopic results. Notably, spontaneous regeneration was seen in the empty treatment group, even though a critical-sized defect was generated based on past literature. However, this regeneration at both timepoints was consistent with hypertrophic fibrocartilage production, which is reflected by the significant amount of collagen 1 staining evident. The microfracture group demonstrated weak regeneration/formation of tissue over 8 weeks. However, with microfracture repair, extensive fibrocartilage formation is expected; therefore, the time points tested may be too early in this model to see any significant tissue repair associated with this technique. Alternatively, these results may be consistent with the formation of a critical-sized defect. Both biofabrication treatment groups performed better with respect to chondral repair in comparison to the empty and microfracture groups by 8 weeks, with no significant difference between the softer and harder biofabrication treatment compositions.

The mechanical (AFM) results were consistent with the microscopic scoring. The empty defect group tested at day 0 (using the spare rabbits) had a high youngs modulus, consistent with that of subchondral bone, which is expected immediately after a full-thickness cartilage

defect is formed. The modulus in the microfracture group was low at week 4 and increased significantly by week 8; however, overall, the modulus was still half that of native rabbit tissue. This is consistent with the lack of fibrocartilage formation seen with microscopic evaluation; significant fibrocartilage formation should produce very stiff tissue resulting in high youngs modulus. In the softer hydrogel (5 million MSCs/mL in 6% GelMA) biofabrication group the modulus significantly decreases during the 4-8-week interval, at 8 weeks the modulus is about 10-fold less than that of normal healthy cartilage. Whereas, in the harder hydrogel (5 million MSCs/mL in 10% GelMA) biofabrication group, the modulus is much higher at week 4 and increases slightly by week 8.

Overall, these results suggest that the softer hydrogel is likely being degraded quicker than new matrix formation by the cells. In contrast, in the harder hydrogel, the degradation rate is slower than new matrix formation. The ideal hydrogel composition aims to provide adequate chondrogenesis and structural strength; therefore, considering the equivalent chondral repair capacity demonstrated in both soft and hard GelMa groups after 8 weeks, the harder 10% GelMA composition best satisfies these requirements.

A limitation associated with using the rabbit model was the evidence of spontaneous regeneration seen within the empty defect group. This regeneration is a well-known drawback of the model; however, the use of a critical-sized defect has been reported to overcome this issue. In this study the critical-sized cartilage defect did not deter this phenomenon of spontaneous regeneration; however, the repair was histologically shown to be fibrous tissue as opposed to hyaline after 8 weeks, and therefore unlikely to confound the results observed in the biofabrication treatment groups.

Several studies using a rabbit model combined with ADSCs have shown chondrogenic potential with respect to macroscopic and microscopic scoring (361-365). In these studies, traditional cartilage engineering methods using premade constructs/tissue combined with flaps or glue are utilised (363, 366-368) which are slow and cumbersome. A hallmark study performed in a sheep model using a extrusion printer-based approach and a periosteal flap demonstrated some evidence of chondral repair, albeit with poor implant stability (178). The lack of light assisted crosslinking (164, 165) is likely to have contributed to this poor implant retention/integration (178) The study presented in this chapter of work is the first *in vivo*

model to show a streamlined, efficient *in situ* biofabrication-based therapy for pure chondral repair; furthermore, this study uses suitable controls and sufficiently examines the macroscopic, microscopic and biomechanical function of repaired tissue. Moreover, this is the first study to report the effect of different GelMA compositions in a rabbit model using ADSCs and biofabrication technology.

7.4 CONCLUSION

In this body of work, a biofabrication treatment approach to *in vivo* cartilage repair using stem cells was performed safely in an operative setting, validating the procedural setup which was designed in chapter 6. This the first *in vivo* study to prove that a concentration of 5 million MSCs/mL is enough to produce neocartilage and outperform the current clinical standard (microfracture repair). Furthermore, this is the first study to show that the use of soft verse hard GelMA plays no difference in the ability to create hyaline-like tissue. Therefore, the use of a harder GelMA composition may be preferable, given that it provides better mechanical strength to the repair. The next step in validating this treatment approach is to perform a larger animal model in which long-term outcome can be assessed, and if successful, will pave the way to human clinical trials.

CHAPTER 8: DISCUSSION, FUTURE DIRECTIONS AND CONCLUSIONS

The avascular nature of articular cartilage (2) makes chondral repair a significant challenge in the field of musculoskeletal medicine. Biofabrication approaches have become prominent in the research field, particularly for cartilage (Chondral) repair (176, 369). The advances in 3D bioprinting technology have enabled a more translational outlook towards repair using stem cells and biomaterials (175). However, several barriers and concerns surround the use of such therapies in humans.

With a view of treating articular knee defects using tissue engineering strategies such as biofabrication with autologous cells, ideally, the cell source should be harvested from within the knee joint. The same harvest and treatment site can be used due to the proximity of such tissue to the defect, limiting the number and size of surgical incisions; and consequently, reducing associated risks (e.g. harvest site irritation or infection) (345). Three cell sources potentially applicable in cartilage tissue engineering are the adult chondrocyte, human articular progenitor cell (hAPC), and human adipose-derived mesenchymal stem cell isolated from the Infrapatellar fat pad (IFP-derived hADSC). The first objective of chapter 4 was to verify and compare the chondrogenic differentiation potential of these three cell sources.

Compared to adult chondrocytes and hAPCs, IFP-derived hADSCs displayed superior chondrogenic gene expression. The hAPCs group revealed a basal rate of chondrogenic gene expression; however, were significantly less chondrogenic in comparison to the hADSCs. There was a failure in chondrogenesis observed using chondrocytes, which could be attributed to the use of IFP tissue from osteoarthritic donor knees. However, the literature suggests there should be no significant effect on chondrogenic capacity (342). Chondrocytes display variable differentiation effects based on expansion time, multiple passaging (343) and the use of 2D vs 3D culture (344). Furthermore, hAPCs and chondrocytes would need to be harvested from non-weight bearing regions of articular cartilage which is scarce and poses a risk of damage to weight-bearing cartilage. Given these results, the most suitable cell type from within the knee for the regeneration of cartilage tissue would be the hADSCs.

The second objective of this chapter was to review and optimise the current IFP-derived hADSCs isolation protocol, intending to generate a rapid isolation protocol. Speeding up the isolation timeframe enables a quicker turnaround period of cell culture before reimplantation; furthermore, it can limit the timeframe in contact with animal-derived media

and sterility related risks associated with *in vitro* culture (265). Past attempts at developing rapid hADSCs protocols have failed to adequately isolate a functioning stem cell population with proven chondrogenic potential; furthermore, the analysis of these populations has been weak (274).

Here we developed a rapid and straightforward 85-minute method to isolate hADSCs from harvested IFP tissue, reducing the standard isolation timeframe by over 16-fold. The two areas that were sped up were: the chemical digestion phase (reduced from 3 hours to 30 minutes) and the plastic adherence step (reduced from 24 hours using non-coated TCPS to 30 minutes using Matrigel-coated TCPS).

Then newly developed 85-minute rapid IFP-derived hADSCs isolation protocol yielded a cell count, cell viability, adherence percentage and total hADSCs count comparable to the control group. Furthermore, flow cytometry results confirmed that the rapid protocol could be used to isolate and expand a pure homogenous stem cell population that is comparable to the control protocol. Cells isolated using the rapid protocol displayed an increase in the GAG/DNA ratio and chondrogenic gene expression over three weeks, which was comparable to cells initially isolated using the control protocol. Combining these investigations, we show that our 85-minute rapid isolation protocol is comparable to the control isolation protocol and the isolated hADSCs can undergo successful chondrogenesis with no impairment associated with the two abovementioned modifications. Furthermore, to prove the trilineage ability of hADSCs, which is a type of mesenchymal stem cell, adipogenic and osteogenic differentiation studies were performed. Rapidly isolated hADSCs were able to differentiate into adipocytes and osteocytes as expected with the hADSCs phenotype; therefore, this protocol can be extended to other fields of musculoskeletal tissue regeneration given the multilineage potential of MSCs.

A limitation of this rapid protocol is the use of Matrigel-coated wells for selective cellular adherence, although commercially approved for *in vitro* lab use, this mouse tumour derived purified protein mixture is not approved for clinical use in humans. Therefore, either a synthetically similar composition or an autologous biological composition needs to be identified before any progression to clinical translation. Further work on different TCPS

coatings has been performed (appendix 5), elements of this work are still in progress and serve as part of an impending international patent application.

Traditionally hADSCs are generously expanded in culture to reach an abundance of cells before being used *in vitro* and for reimplantation. There is no literature indicating if expanded cells can be used before initial passaging (Passage 1) and how early expanded IFP-derived hADSCs can be induced towards differentiation. The earlier the timeline to reimplantation the less inherent risks involved with cell culture in a lab and exposure to animal-based serum products (282). Another key advantage of knowing when the earliest turnaround timeframe for reimplantation can occur is to identify and optimise the patient waiting time between surgical procedures (Harvest and Reimplantation).

The first objective of chapter 5 was to determine the earliest time point during expansion in which hADSCs can be driven into chondrogenesis. At time points 0 and after 3 days of expansion, cells were unable to be pushed into pellet culture suggesting they are unlikely to have matured into a more active stem cell phenotype which can be differentiated. After 5- and 7-day expansion, timeframes cells were successfully pelleted. Furthermore, these populations were both able to successfully undergo chondrogenesis over a 3-week timeframe. Therefore, the earliest turnaround time during expansion in which hADSCs can be pushed into chondrogenesis (used as therapy) is after 5 days.

The next objective of this chapter was to identify the minimum effective hADSCs concentration required to produce neocartilage in a GelMA-based biofabrication procedure. By identifying this concentration and correlating it to the number of cells isolatable over 5 days of expansion, the repairable defect volume can be calculated. Three hADSCs concentrations representing 12.5, 25 and 50% of the average chondrocyte concentration in knee cartilage, were biofabricated with GelMA/HA and cast into standardised cylindrical models. After 3 weeks of chondrogenic stimulation, the 5.0 million hADSCs/mL concentration group demonstrated the most optimal GAG/DNA ratio, chondrogenic gene expression and hyaline-like ECM production visualised with immunostaining. Therefore, the 5.0 million hADSCs/mL concentration represents the minimum cell concentration required to trigger the chondrogenic pathway and produce advanced chondrogenesis in GelMA/HA-based bioscaffolds. A limitation to this part of the study is that experiments were confined to our

desired hydrogel which is GelMA/HA, the results of which may not be translatable to the use of other hydrogels which should have own cellular-interaction profiles examined separately.

Finally, using the data from the results obtained in the first two objectives of chapter 5, the maximal repairable volume using a 5-day expanded hADSCs population is calculated, which is 380 µL (mm^3) using one IFP or 760 µL (mm^3) using both IFPs (two IFPs one in each knee). Based on these volumes, all lesion surface areas typically indicated for microfracture repair and most osteochondral defects (average 550 µL) (252, 357, 358) can be treated using the proposed biofabrication procedure irrespective of the depth of the lesion if both IFPs are utilised.

Patients present with unique defect morphologies and sizes, by knowing the number of cells that can be obtained after a 5-days of expansion and the minimum chondrogenic hADSCs concentration, we can now decide how much of the IFP needs to be harvested per patient. For example, a patient with a 1.5 cm^2 TSA defect with a depth of 1 mm will have a volume repair indication of 150 µL (mm^3), which means harvesting of half an IFP will sufficiently enable a 1-week turnaround biofabrication treatment approach. The data presented in this chapter not only optimises the expansion aspect of a biofabrication treatment approach but also makes it a personalised repair option which can be individually tailored. An obvious limitation in this step will be with identifying the exact dimensions of such defects in advance, which could be overcome by utilising preoperative magnetic resonance imaging or arthroscopic examination. Another limitation is that the cellular yield data collected is from patients in an elderly age group undergoing arthroplasty. To accurately represent the ideal treatment population, it would be beneficial to assess the IFP-derived hADSCs yield in younger patients.

As part of the biofabrication set-up and design in chapter 6, several aspects of the procedure were selected and validated. The rabbit (largest small animal model) was chosen to suit the feasibility of this proof of concept project, in which the IFP and MSCs yield is too low and variable. Therefore, first, an appropriate commercial cell source was selected (rabbit BMSCs) and validated to show *in vitro* chondrogenic differentiation capacity. Next, two different compositions of a GelMA hydrogel (soft and hard) were tested to evaluate their respective baseline compressive strength. Then the individual gelation time required before printing for

each composition was identified. As expected, the lower concentration (6% GelMA) had less compressive strength compared to the higher concentration (10% GelMA) group with a >4-fold difference. Using the filament formation test, it was determined that gelation times of 9 and 3 minutes of a temperature of 4°C were best suited to reach a printable hydrogel state in the 6% and 10% GelMA hydrogels respectively. A limitation to this aspect of work is the testing of only two different GelMA compositions. However, this study aimed to subsequently evaluate the effect of *in vivo* cellular repair using a soft versus hard bioink, rather than conducting a broad investigation into the strength of different GelMA concentrations. Finally, in the first objective, a 1 cm fixed distance hand-held UV cross-linking system was designed using an easily operatable device and a sterilisable attachment cover. This distance ensured that only the defect area of interest was cross-linked, and no healthy tissue was affected in the process.

The final element of this thesis (chapter 7) was to assess if the minimum chondrogenic hADSCs concentration could be used with the newly developed biofabrication procedure to repair cartilage. An *in vivo* rabbit model of cartilage repair was performed using 4- and 8-week endpoints for harvest. In each rabbit condyle one of the 4 treatment groups were performed: empty defect, microfracture (clinical standard), biofabrication treatment group 1 (5 million MSCs/mL of 6% GelMA) and biofabrication treatment group 2 (5 million MSCs/mL of 10% GelMA).

The biofabrication procedure was easily and efficiently implemented in the *in vivo* rabbit model. The intraoperative printing of the hydrogel was well controlled. The gelation timeframes of 9 and 3 minutes (cooled at 4°C) used for the 6% and 10% hydrogels respectively, achieved similar printability levels to that identified *in vitro* in chapter 6 (filament formation test). A limitation associated with the bioprinting aspect of the procedure was the presence of blood over the defect; this diluted the implant and made it difficult to control the homogenous formation of the construct. An approach adapted to limit this was to dry the defect with surgical cloth for a few minutes, to obtain a period of haemostatic control, before construct delivery. The perioperative outcomes in all rabbits used in the study were well controlled, with only minor wound complications encountered, which were easily resolved.

Macroscopic scoring showed significantly higher results in both the biofabrication treatment groups when compared to the empty group and microfracture repair. Both biofabrication groups had scores consistent with nearly normal tissue repair, whereas empty and microfracture repairs both showed abnormal tissue repair. Notably, no difference was seen between both biofabrication groups over 8 weeks, suggesting no difference in repairability between the 4-8-week interval. When the laterality of the condyle (medial or lateral) was assessed, a higher score of the repair was evident for the medial femoral condyle at both 4 and 8-week time points compared to the lateral femoral condyle; however, there was no statistical significance. This was an expected finding given the lateral collateral ligament in the rabbit is near the lateral femoral condyle and likely to impede repair.

Microscopic repair scoring was generally consistent with the macroscopic results. Notably, spontaneous regeneration was seen in the empty treatment group, even though a critical-sized defect was generated based on past literature (308, 315). However, this regeneration was consistent with hypertrophic fibrocartilage production, which is reflected by the significant amount of collagen 1 staining evident. The microfracture group demonstrated weak regeneration/formation of tissue over 8 weeks. However, with microfracture repair, extensive fibrocartilage formation is expected; therefore, the time points tested may be too early in this model to see any significant tissue repair associated with this technique; alternatively, these results may be consistent with the formation of a critical-sized defect. In both the biofabrication treatment groups, hyaline cartilage regeneration was evident after 8 weeks. At the 4-week checkpoint, there were disruptions seen at the defect interface in both groups; however, these were overcome by 8 weeks with a more homogenous distribution of collagen 2 observed throughout the surface. Staining of collagen 2 was similar in both the 5 million MSCs/mL of 6% GelMA and 5 million MSCs/mL of 10% GelMA groups at both 4 and 8-week time points, suggesting no significant difference in the ability to form hyaline tissue after 8 weeks *in vivo* between the two groups.

The mechanical (AFM) results were consistent with the microscopic scoring. Healthy rabbit cartilage tested at day 0 (using the spare rabbits) showed a similar youngs modulus to that reported with 3-month-old male rabbits in the literature. The empty defect group tested at day 0 (using the spare rabbits) had a high youngs modulus, consistent with that of

subchondral bone, which is expected immediately after a full-thickness cartilage defect is formed. The modulus in the microfracture group was low at week 4 and increased significantly by week 8; however, overall, the modulus was still half that of native tissue. This is consistent with the lack of fibrocartilage formation seen with microscopic evaluation; significant fibrocartilage formation should produce stiff tissue resulting in high compressive modulus.

In the softer hydrogel (5 million MSCs/mL in 6% GelMA) biofabrication group the modulus significantly decreases during the 4-8-week interval, at 8 weeks the modulus is about 10-fold less than that of normal healthy cartilage. Whereas, in the harder hydrogel (5 million MSCs/mL in 10% GelMA) biofabrication group, the modulus is much higher at week 4 and increases slightly by week 8. These results suggest that the softer hydrogel is likely being degraded quicker than the new matrix formation by the cells. In contrast, in the harder hydrogel, the degradation rate is slower than the formation of the new matrix.

When combined with the microscopic results, it is evident that by 8 weeks the biofabrication treatment groups show similar hyaline-like cartilage repair; however, the harder hydrogel provided roughly 5 x more mechanical strength compared to the softer hydrogel group. Furthermore, in chapter 6, it is shown the gelation time of the harder 10% hydrogel is much quicker and therefore more efficient for operative use. Uniting all these results it is clear the 10% GelMa group is more suitable for *in vivo* cartilage repair using the described approach.

A limitation associated with using the rabbit model was the evidence of spontaneous regeneration seen within the empty defect group. This regeneration is a well-known drawback of the model; however, the use of a critical-sized defect has been reported to overcome this issue. In this study the critical-sized cartilage defect did not deter this phenomenon of spontaneous regeneration; however, the repair was histologically shown to be fibrous tissue as opposed to hyaline after 8 weeks, and therefore unlikely to confound the results observed in the biofabrication treatment groups.

In conclusion, a rapid <1-week cell isolation and expansion technique has been developed, enabling an efficient turnaround to treatment using autologously harvested stem cells from the infrapatellar fat pad. Furthermore, the minimum chondrogenic stem cell concentration needed to produce neocartilage has been validated both *in vitro* and *in vivo*. The newly

devised surgical biofabrication approach used in conjunction with the minimum chondrogenic hADSCs concentration showed better outcomes compared to microfracture treatment (clinical standard).

A key limitation to translating such therapies to clinical human trials for the treatment of post-traumatic arthritis will be the need for regulatory approval (282). The complex nature of mixing cellular therapy along with materials such as hydrogels is yet to be trialled in vivo with humans and ongoing interaction and consensus with regulatory boards such as the FDA and TGA will be imperative for future success (282, 370). Large *in vivo* animal trials looking at mid-long-term outcomes of post-traumatic arthritis will be pivotal in receiving such approvals (335). Clinical trials to examine the safety and efficacy of engineered cartilage in large patient populations are costly and time-consuming. Recognizing this, the FDA has announced a new policy outline to expedite the approval of new therapies, the Regenerative Medicine Advanced Therapy (RMAT) designation, which has been created to expedite the approval process (371). Advantages of the RMAT designation include FDA assistance as early as the phase I trial stage, the discussion of potential surrogate or intermediate end points to accelerate approval and eligibility for priority review of marketing applications (371). The RMAT designation might be a solution to reducing the cost and time required to gain marketing approval for engineered articular cartilage products .

The results from this thesis pave the way for future large animal studies targeted at cartilage regeneration with the use of efficient and innovative biofabrication procedures. Utilising such models, mid-long-term outcomes can be assessed, which if successful will promote the progression to human clinical studies

CHAPTER 9: REFERENCES

1. Fox SA, Bedi A, Rodeo SA. The basic science of articular cartilage: structure, composition, and function. Sports Health. 2009;1:461-8.
2. Hunter W. On the structure and diseases of articulating cartilage. Phil Trans Roy Soc. 1743;42B:514-21.
3. Craig W, David JW, Ming HZ. A current review on the biology and treatment of the articular cartilage defects (part I & part II). J Musculoskelet Res. 2003;7:157–81.
4. Spasovski D, Spasovski V, Bascarevic, Z, Stojiljkovic, M, Vreca, M, Andelkovic, M et al. Intra-articular injection of autologous adipose-derived mesenchymal stem cells in the treatment of knee osteoarthritis. J Gene Med. 2018;20:e3002.
5. Kim S, Ha CW, Park YB, Nam E, Lee JE, Lee HJ. Intra-articular injection of mesenchymal stem cells for clinical outcomes and cartilage repair in osteoarthritis of the knee: a meta-analysis of randomized controlled trials. Archives of orthopaedic and trauma surgery. 2019;139(7):971-80.
6. Tetteh ES, Bajaj S, Ghodadra NS. Basic science and surgical treatment options for articular cartilage injuries of the knee. J Orthop Sports Phys Ther. 2012;42(3):11.
7. Steadman J, Rodkey WG, Singleton SB, Briggs KK,. Microfracture technique forfull-thickness chondral defects: Technique and clinical results. Operative Techniques in Orthopaedics. 1997;7(4):300-4.
8. Mithoefer K, McAdams T, Williams RJ, Kreuz PC, Mandelbaum BR. Clinical efficacy of the microfracture technique for articular cartilage repair in the knee: an evidence-based systematic analysis. Am J Sports Med. 2009;37(10):2053-63.
9. Knutsen G, Drogset JO, Engebretsen L, Grontvedt T, Isaksen V, Ludvigsen TC, et al. A randomized trial comparing autologous chondrocyte implantation with microfracture. Findings at five years. J Bone Joint Surg Am. 2007;89(10):2105-12.
10. Bartlett W, Skinner J.A, Gooding C.R, Carrington R.W.J, Flanagan A.M, Briggs T.W.R, et al. Autologous chondrocyte implantation versus matrix-induced autologous chondrocyte implantation for osteochondral defects of the knee: a prospective, randomised study. J Bone Joint Surg Br. 2005;87(5):640-5.
11. Langer R, and Vacanti JP Tissue engineering. Science. 1993;260:920-6.
12. Giannoudis PV, Einhorn TA, Marsh D. Fracture healing: the diamond conceptt. Injury. 2007;38(Suppl 4):S3-6.
13. Guillemot F, Mironov V, Nakamura M. Bioprinting is coming of age: Report from the International Conference on Bioprinting and Biofabrication in Bordeaux (3B'09). Biofabrication. 2010;2(1):010201.
14. Groll J, Boland T, Blunk T, Burdick JA, Cho DW, Dalton PD, et al. Biofabrication: reappraising the definition of an evolving field. Biofabrication. 2016;8(1):013001.
15. Buckwalter JA, Hunziker EB, Rosenberg LC, Coutts R, Adams M, Eyre D. Articular cartilage: composition and structure. In: Woo SLY, Buckwalter JA, editors, eds. Injury and Repair of the Musculoskeletal Soft Tissues. Park Ridge, IL. American Academy of Orthopaedic Surgeons. 1988:405-25.
16. Carlson B. Chapter 10 - Limb Development. Human Embryology and Developmental Biology (Fifth Edition). 2014:193-215.
17. Sadler T, Langman J. Langman's Medical Embryology (12th ed). Lippincott Williams & Wilkins/Wolters Kluwer Health. 2015.
18. DeLise A, Fischer L, Tuan R. Cellular interactions and signaling in cartilage development. Osteoarthritis and cartilage. 2000;8:309-34.

19. Green J, Tollemar V, Dougherty MC, Yan Z, Yin L et al. Multifaceted signaling regulators of chondrogenesis: Implications in cartilage regeneration and tissue engineering. Genes & Diseases. 2015;2(4):307-27.
20. Karaplis A. Embryonic development of bone and regulation of intramembranous and endochondral bone formation. Principles of Bone Biology, 3rd ed New York: Academic Press. 2008:53-84.
21. Hunziker EB. Articular cartilage repair: basic science and clinical progress. A review of the current status and prospects. Osteoarthritis and Cartilage. 2002;10(6):432-63.
22. Eyre D. Collagen of articular cartilage. Arthritis Res. 2001;4(1):30-5.
23. Roughley PJ. The structure and function of cartilage proteoglycans. Eur Cell Mater. 2006;12:92-101.
24. Buckwalter JA, Mankin HJ. Articular cartilage: tissue design and chondrocyte-matrix interactions. Instr Course Lect 1998;47:477-86.
25. Di Bella C, Fosang A, Donati DM, Wallace GG, Choong PF. 3D Bioprinting of Cartilage for Orthopedic Surgeons: Reading between the Lines. Front Surg. 2015;2:39.
26. Bhosale A, Richardson JB. Articular cartilage: structure, injuries and review of management. British Medical Bulletin. 2008;87(1):77–95.
27. Lyons T, McClure SF, Stoddart, RW, McClure J. The normal human chondro-osseous junctional region: evidence for contact of uncalcified cartilage with subchondral bone and marrow spaces. BMC Musculoskelet Disord 2006;7(52).
28. Mow VC, Ateshian GA, Ratcliffe A. Anatomic form and biomechanical properties of articular cartilage of the knee joint. In: Finerman GAM, Noyes FR, editors, eds. Biology and Biomechanics of the Traumatized Synovial Joint: The Knee as a Model. 2nd ed. Rosemont, IL. American Academy of Orthopaedic Surgeons. 1992:55-81.
29. Mow V, Kuei SC, Lai WM, Armstrong CG. Biphasic creep and stress relaxation of articular cartilage in compression? Theory and experiments, Journal of biomechanical engineering. 1980:73-84.
30. Maroudas A. Physiochemical properties of articular cartilage. In: Freeman MAR, editor, eds. Adult Articular Cartilage. Kent, United Kingdom: Cambridge University Press. 1979:215-90.
31. Mow VC, Holmes MH, Lai WM. Fluid transport and mechanical properties of articular cartilage: a review. J Biomech. 1984;17:377-94.
32. Hayes W, Bodine AJ. Flow-independent viscoelastic properties of articular cartilage matrix. 1978 11:407-19.
33. Woo S, Mow VC, Lai WM. Biomechanical properties of articular cartilage. In: Skalak R, Chen S, eds. Handbook of Bioengineering. New York, NY: McGraw-Hill Book Co. 1987:4.1-4.44.
34. Lu XL, Mow VC. Biomechanics of articular cartilage and determination of material properties. 2008;40(2):193-9.
35. Wong B, Bae WC, Gratz KR, Sah RL. . Shear deformation kinematics during cartilage articulation: effect of lubrication, degeneration, and stress relaxation. Mol Cell Biomech. 2008;5(3):197-206.
36. McNickle A, Provencher MT, Cole BJ. . Overview of existing cartilage repair technology. Sports Med Arthrosc Rev. 2008;16(4):196-201.
37. Dowson D, Jin ZM. . Micro-elastohydrodynamic lubrication of synovial joints. Eng Med. 1986;15(2):63-5.

38. Hou J, Mow VC, Lai WM, Holmes MH. An analysis of the squeeze-film lubrication mechanism for articular cartilage,. Journal of Biomechanics. 1992;25(3):247-59.
39. J. C. The lubrication of animal joints in relation to surgical reconstruction by arthroplasty. Ann Rheum Dis. 1960;19(1):10-9.
40. Coles J, Blum JJ, Jay GD, Darling EM, Guilak F, Zauscher S. In situ friction measurement on murine cartilage by atomic force microscopy. J Biomech. 2008;41(3):541-8.
41. Ateshian G. The role of interstitial fluid pressurization in articular cartilage lubrication. J Biomech. 2009;42(9):1163-76.
42. Krishnan R, Kopacz M, Ateshian GA. . Experimental verification of the role of interstitial fluid pressurization in cartilage lubrication. J Orthop Res. 2004;22(3):565-70.
43. Forster H, Fisher J. . The influence of loading time and lubricant on the friction of articular cartilage. Proc Inst Mech Eng H. 1996;210(2):109-19.
44. Schmidt T, Sah RL. Effect of synovial fluid on boundary lubrication of articular cartilage. Osteoarthritis and Cartilage. 2007;15(1):35-47.
45. Coles J, Zhang L, Blum JJ, Warman ML, Jay GD, Guilak F, Zauscher S. . Loss of cartilage structure, stiffness, and frictional properties in mice lacking PRG4. Arthritis Rheum. 2010;62(6):1666-74.
46. Teeple E, Elsaid KA, Fleming BC, Jay GD, Aslani K, Crisco JJ, Mechrefe AP. . Coefficients of friction, lubricin, and cartilage damage in the anterior cruciate ligament-deficient guinea pig knee. J Orthop Res. 2008;26(2):231-7.
47. McNary S, Athanasiou KA, Reddi AH. . Engineering lubrication in articular cartilage. Tissue Eng Part B Rev. 2012;18(2):88-100.
48. Lotz M, Loeser RF. Effects of aging on articular cartilage homeostasis. Bone. 2012;51(2):241-8.
49. Martin J, Buckwalter JA. Roles of articular cartilage aging and chondrocyte senescence in the pathogenesis of osteoarthritis. The Iowa orthopaedic journal 2001;21:1-7.
50. Pelletier JP, Jovanovic DV, Lascau-Coman V, Fernandes JC, Manning PT, Connor JR, et al. Selective inhibition of inducible nitric oxide synthase reduces progression of experimental osteoarthritis in vivo: possible link with the reduction in chondrocyte apoptosis and caspase 3 level. Arthritis and Rheum. 2000;43:1290-9.
51. Punzi L, Galozzi, P., Luisetto, R., Favero, M., Ramonda, R., Oliviero, F., & Scanu, A. . Post-traumatic arthritis: overview on pathogenic mechanisms and role of inflammation. RMD open. 2016;2(2):e000279.
52. Brown T, Johnston RC, Saltzman CL, Marsh JL, Buckwalter JA. Posttraumatic osteoarthritis: a first estimate of incidence, prevalence, and burden of disease. J Orthop Trauma. 2006;20(10):739-44.
53. Lohmander L, Englund PM, Dahl LL, Roos EM. The long-term consequence of anterior cruciate ligament and meniscus injuries: osteoarthritis. AJSM. 2007;35(10):1756-69.
54. Favero M RR, Goldring MB, Goldring SR, Punzi L. Early knee osteoarthritis. RMD Open. 2015;1(Suppl 1):e000062.
55. Lotz M, Kraus VB. Posttraumatic osteoarthritis: pathogenesis and pharmacological treatment options. Arthritis Res Ther. 2010;12(3):211.
56. Armiento A, Alini M, Stoddart MJ. Articular fibrocartilage - Why does hyaline cartilage fail to repair? Adv Drug Deliv Rev. 2019;146:289-305.
57. Zhang L, Hu J, Athanasiou KA. The Role of Tissue Engineering in Articular Cartilage Repair and Regeneration. Critical Reviews™ in Biomedical Engineering. 2009;37(1-2):1-57.

58. Valderrabano V, Horisberger, M., Russell, I., Dougall, H., & Hintermann, B. Etiology of ankle osteoarthritis. Clinical orthopaedics and related research. 2009;467(7):1800-06.
59. Gage B, McIlvain NM, Collins CL, Fields SK, Comstock RD. Epidemiology of 6.6 million knee injuries presenting to United States emergency departments from 1999 through 2008. Acad Emerg Med. 2012;19(4):378-85.
60. Curl W, Krome J, Gordon ES, Rushing J, Smith BP, Poehling GG. Cartilage injuries: a review of 31,516 knee arthroscopies. Arthroscopy. 1997;13(4):456-60.
61. Moyad T. Cartilage injuries in the adult knee: Evaluation and management. Cartilage. 2011;2:11.
62. Pate RR, Pratt M, Blair SN, Haskell WL, Macera CA, Bouchard C, et al. Physical activity and public health. A recommendation from the Centers for Disease Control and Prevention and the American College of Sports Medicine. JAMA 1995;273:402-7.
63. Hochberg MC, Altman RD, Brandt KD, Clark BM, Dieppe P, Griffin MR, et al. Guidelines for the medical management of osteoarthritis. Part II. Osteoarthritis of the knee. American College of Rheumatology. Arthritis Rheum. 1995;38(11):1541-6.
64. Zhang W, Ouyang H, Dass C, Xu J. Current research on pharmacologic and regenerative therapies for osteoarthritis. . Bone Research. 2016;4:15040.
65. Clouet J, Vinatier C, Merceron C, Pot-vaucel M, Maugars Y, Weiss P, et al. From osteoarthritis treatments to future regenerative therapies for cartilage. Drug Discov Today. 2009;14(19-20):913-25.
66. Tanveer E, Anastassiades T. Glucosamine and chondroitin for treating symptoms of osteoarthritis: evidence is widely touted but incomplete. JAMA 2000;283:1483-4.
67. Hellingman C, Davidson ENB, Koevoet W, Vitters EL, van den Berg WB, van Osch GJVM, et al. Smad Signaling Determines Chondrogenic Differentiation of Bone-Marrow-Derived Mesenchymal Stem Cells: Inhibition of Smad1/5/8P Prevents Terminal Differentiation and Calcification.67. Tissue Engineering Part A. 2011;17:1157-67.
68. Joosten L, Crisan TO, Azam T, Cleophas MC, Koenders MI, van de Veerdonk FL, et al. Alpha-1-anti-trypsin-Fc fusion protein ameliorates gouty arthritis by reducing release and extracellular processing of IL-1beta and by the induction of endogenous IL-1Ra. Annals of Rheumatic Diseases. 2016;75:1219-27.
69. Fischer J, Hueber AJ, Wilson S, Galm M, Baum W, Kitson C, et al. Combined Inhibition of Tumor Necrosis Factor α and Interleukin-17 As a Therapeutic Opportunity in Rheumatoid Arthritis: Development and Characterization of a Novel Bispecific Antibody. Arthritis & Rheumatology. 2015;67:51-62.
70. Lee C, Cook JL, Mendelson A, Moioli EK, Yao H, Mao JJ. Regeneration of the articular surface of the rabbit synovial joint by cell homing: a proof of concept study. Lancet. 2010;376:440-8.
71. Karimi T, Barati D, Karaman O, Moeinzadeh S, Jabbari E. A developmentally inspired combined mechanical and biochemical signaling approach on zonal lineage commitment of mesenchymal stem cells in articular cartilage regeneration. Integrative Biology. 2015;7:112-27.
72. Madry H, Orth P, Kaul G, Zurakowski D, Menger MD, Kohn D, et al. Acceleration of articular cartilage repair by combined gene transfer of human insulin-like growth factor I and fibroblast growth factor-2 in vivo. Archives of Orthopaedic and Trauma Surgery. 2010;130:1311-22.

73. Kraus V, Birmingham J, Stabler TV, Feng S, Taylor DC, Moorman CT 3rd, Garrett WE, Toth AP. Effects of intraarticular IL1-Ra for acute anterior cruciate ligament knee injury: a randomized controlled pilot trial (NCT00332254). Osteoarthritis Cartilage. 2012;20(4):271-8.
74. Ayhan E, Kesmezacar H, Akgun I. Intraarticular injections (corticosteroid, hyaluronic acid, platelet rich plasma) for the knee osteoarthritis. World J Orthop. 2014;5(3):351-61.
75. Martin C, Browne J. Intra-articular Corticosteroid Injections for Symptomatic Knee Osteoarthritis: What the Orthopaedic Provider Needs to Know. The Journal of the American Academy of Orthopaedic Surgeons. 2019;27(17):e758-e66.
76. Dieppe PA, Sathapatayavongs B, Jones HE, Bacon PA, Ring EF. Intra-articular steroids in osteoarthritis. Rheumatol Rehabil 1980;19:212-7.
77. Cohen S, Proudman S, Kivitz AJ, Birch FX, Donohue JP et al. A randomized, double-blind study of AMG 108 (a fully human monoclonal antibody to IL-1R1) in patients with osteoarthritis of the knee. Arthritis Res Ther. 2011;13(4):R125.
78. Fransson L. Mammalian glycosaminoglycans. In: Aspinall GO (ed) The Polysaccharides Academic Press, Inc; St Louis, Missouri, USA. 1985.
79. Prieto J, Pulido MM, Zapico J, Molina AJ, Gimeno M et al. Comparative study of hyaluronic derivatives: rheological behavior, mechanical and chemical degradation. Int J Biol Macromol. 2005;35(1-2):43-9.
80. Legre-Boyer V. viscosupplementation: Techniques, indications, results. Orthop Traumatol Surg Res. 2015;101(1 Suppl):S101-8.
81. D'Agostino A, Stellavato A, Corsuto L, Diana P, Filosa, R et al. Is molecular size a discriminating factor in hyaluronan interaction with human cells? Carbohydr Polym. 2017;157:21-30.
82. Altman R, Manjoo A, Fierlinger A, Niazi F, Nicholls M. The mechanism of action for hyaluronic acid treatment in the osteoarthritic knee: a systematic review. BMC Musculoskelet Disord. 2015;16:321.
83. Marshall KW. Viscosupplementation for osteoarthritis: current status, unresolved issues, and future directions. J Rheumatol 1998;25:2056-8.
84. Lane N, Corr M. Osteoarthritis in 2016: Anti-NGF treatments for pain - two steps forward, one step back? Nat Rev Rheumatol. 2017;13(2):76-8.
85. Guideline for the management of knee and hip osteoarthritis, 2nd edition, RACGP website. [Internet-PDF],(Cited 19/12/2019),https://www.racgp.org.au/FSDEDEV/media/documents/Clinical%20Resources/Guidelines/Joint%20replacement/Guideline-for-the-management-of-knee-and-hip-OA-2nd-edition.pdf. 2018.
86. Middleton K, Barro V, Muller B, Terada S, Fu FH. Evaluation of the Effects of Platelet-Rich Plasma (PRP) Therapy Involved in the Healing of Sports-Related Soft Tissue Injuries. Iowa Orthop J. 2012;32:150-63.
87. Dragoo J, Braun HJ, Durham JL, Ridley BA, Odegaard JI, Luong R, Arnoczky SP. Comparison of the acute inflammatory response of two commercial platelet-rich plasma systems in healthy rabbit tendons. AJSM. 2012;40:1274-81.
88. McCarrel T, Minas T, Fortier LA. Optimization of leukocyte concentration in platelet-rich plasma for the treatment of tendinopathy. JBJS. 2012;94:e143.
89. Mishra A HK, Woodall J, Vieira A. Sports Medicine Applications of Platelet Rich Plasma. Sports Medicine Applications of Platelet Rich Plasma. Curr Pharm Biotechnol. 2012;13:1185–95.

90. Wang X, Liu C, Li S, Xu Y, Chen P ea. Effects of continuous passage on immunomodulatory properties of human adipose-derived stem cells. Cell Tissue Bank. 2015;16(1):143-50.
91. Jevotovsky D, Alfonso AR, Einhorn TA, Chiu ES et al. Osteoarthritis and stem cell therapy in humans: a systematic review. Osteoarthritis Cartilage. 2018;26(6):711-29.
92. Australian orthopaedic association (AOA) and rheumatology association (ARA) joint position statment on stem cell therapies Aw, [Internet-PDF], 2014, (cited 20/12/2019),, https://www.aoa.org.au/docs/default-source/Advocacy/aoa-australian-rheumatology-association-stem-cell-therapies.pdf?sfvrsn=de19c404_6.
93. Camp C, Stuart MJ, Krych AJ. Current concepts of articular cartilage restoration techniques in the knee. Sports health. 2014;6(3):265–73.
94. Cole B, Pascual-Garrido C, Grumet RC. Surgical management of articular cartilage defects in the knee. J Bone Joint Surg Am. 2009;91(7):1778-90.
95. Brittberg M, Lindahl A, Nilsson A, Ohlsson C, Isaksson O, Peterson L. Treatment of deep cartilage defects in the knee with autologous chondrocyte transplantation. N Engl J Med. 1994(14):7.
96. Steadman J, Rodkey WG, Briggs KK, Rodrigo JJ. Orthopade. The microfracture technic in the management of complete cartilage defects in the knee joint. Orthopade. 1999;28(1):7.
97. Bartlett W, Skinner JA, Gooding CR, Carrington RWJ, Flanagan AM, Briggs TWR, et al. Autologous chondrocyte implantation versus matrix-induced autologous chondrocyte implantation for osteochondral defects of the knee: a prospective, randomised study. J Bone Joint Surg Br. 2005;87(5):640-5.
98. Kreuz P, Steinwachs MR, Erggelet C, Krause SJ, Konrad G, Uhl M, and Südkamp N. Results after microfracture of full-thickness chondral defects in different compartments in the knee. Osteoarthritis and Cartilage. 2006;14(11):7.
99. Redman SN, Oldfield SF, Archer CW. Current strategies for articular cartilage repair. Eur Cell Mater. 2005;9:23-32.
100. Steadman JR, Briggs KK, Rodrigo JJ, Rodkey WG. Outcomes of microfracture for traumatic chondral defects of the knee: Average 11-year follow-up. Arthroscopy. The Journal of Arthroscopic & Related Surgery. 2003;19(5):477-84.
101. Grad S, Eglin D, Alini M, Stoddart MJ. Physical stimulation of chondrogenic cells in vitro: a review. Clin Orthop Relat Res. 2011;469(10):2764-72.
102. Schulz RM, Bader A. Cartilage tissue engineering and bioreactor systems for the cultivation and stimulation of chondrocytes. Eur Biophys J. 2007;36(4-5):539-68.
103. Adkisson HD, Martin JA, Amendola RL, Milliman C, Mauch KA, Katwal AB, et al. The potential of human allogeneic juvenile chondrocytes for restoration of articular cartilage. Am J Sports Med. 2010;38(7):1324-33.
104. Mahmoudifar N, Doran PM. Tissue engineering of human cartilage and osteochondral composites using recirculation bioreactors. Biomaterials. 2005;26(34):7012-24.
105. Jakob M, Démarteau O, Suetterlin R, Heberer M, Martin I. Chondrogenesis of expanded adult human articular chondrocytes is enhanced by specific prostaglandins 2004;43(7):852-7.
106. Saha S, Kirkham J, Wood D, Curran S, Yang X. Comparative study of the chondrogenic potential of human bone marrow stromal cells, neonatal chondrocytes and adult chondrocytes. Biochem Biophys Res Commun. 2010;401:333-8.

107. Aulthouse AL, Beck M, Griffey E, Sanford J, Arden K, Machado MA, et al. Expression of the human chondrocyte phenotype in vitro. In Vitro Cell Dev Biol. 1989;25:659-68.
108. Hardingham T, Tew S, Murdoch A. Tissue engineering: chondrocytes and cartilage. Arthritis Res. 2002;4(Suppl 3):S63-8.
109. Gao J, Yao JQ, Caplan, AI. Stem cells for tissue engineering of articular cartilage. Proceedings of the Institution of Mechanical Engineers, Part H:Journal of Engineering in Medicine. 2007;221(5):441-50.
110. Medvedev SP, Grigoreva EV, Shevchenko A. Human induced pluripotent stem cells derived from fetal neural stem cells successfully undergo directed differentiation into cartilage. Stem Cells Dev. 2011;20(6):1099-112.
111. Wei Y, Wen Zeng Wan R, Wang J, Zhou Q, Qiu S, Singh, . Chondrogenic differentiation of induced pluripotent stem cells from osteoarthritic chondrocytes in alginate matrix. Eur Cell Mater. 2012;23:1-12.
112. Park S, Im GI. Embryonic stem cells and induced pluripotent stem cells for skeletal regeneration. Tissue Eng Part B Rev. 2014;20(5):381-91.
113. Lui K, Waldmann H, Fairchild, PJ. Embryonic stem cells: overcoming the immunological barriers to cell replacement therapy. Curr Stem Cell Res Ther 2009;4:70-80.
114. Ben-David U, Benvenisty N. The tumorigenicity of human embryonic and induced pluripotent stem cells. Nat Rev Cancer. 2011;11:268-77.
115. Ghosh Z, Huang M, Hu S, Wilsin KD, Dey D, Wu, JC. Dissecting the oncogenic and tumorigenic potential of differentiated human induced pluripotent stem cells and human embryonic stem cells. Cancer Res. 2011;71:5030-9.
116. English K, Wood KJ. Immunogenicity of embryonic stem cell-derived progenitors after transplantation. Curr Opin Organ Transplant. 2011;16:90-5.
117. Takahashi K, Yamanaka S. Induction of pluripotent stem cells from mouse embryonic and adult fibroblast cultures by defined factors. Cell. 2006;126(6):663-76.
118. Stadtfeld M, Hochedlinger K. Induced pluripotency: history, mechanisms, and applications. Genes & Dev. 2010;24:2239-63.
119. Schmidt R, Plath K. The roles of the reprogramming factors Oct4, Sox2 and Klf4 in resetting the somatic cell epigenome during induced pluripotent stem cell generation. Genome Biol. 2012;13(10):251.
120. Li Y, Liu T, Van Halm-Lutterodt N, Chen J, Su Q, Hai Y. Reprogramming of blood cells into induced pluripotent stem cells as a new cell source for cartilage repair. Stem Cell Research & Therapy. 2016;7(1):31.
121. Becker AJ, Mc Culloch CE, Till JE. Cytological demonstration of the clonal nature of spleen colonies derived from transplanted mouse marrow cells. Nature. 1963;197:3.
122. Friedenstein AJ, Deriglasova UF, Kulagina NN, Panasuk AF, Rudakowa SF, Luriá EA, et al. Precursors for fibroblasts in different populations of hematopoietic cells as detected by the in vitro colony assay method. Exp Hematol. 1974:83-92.
123. Pittenger MF, Mackay AM, Beck SC, Jaiswal RK, Douglas R, Mosca JD, et al. Multilineage Potential of Adult Human Mesenchymal Stem Cells. Science. 1999;284(5411):5.
124. Im G. Chondrogenesis from mesenchymal stem cells derived from adipose issue on the fibrin scaffold. Current Applied Physics. 2005;5(5):438-43.
125. Bosnakovski D, Mizuno M, Kim G, Takagi S, Okumura M, Fujinaga T. Chondrogenic differentiation of bovine bone marrow mesenchymal stem cells (MSCs) in different hydrogels: Influence of collagen type II extracellular matrix on MSC chondrogenesis. Biotechnology and Bioengineering. 2006;93(6):1152-63.

126. Wollenweber M, Domaschke H, Hanke T, Boxberger S, Schmack G, Gliesche, K, et al. Mimicked bioartificial matrix containing chondroitin sulphate on a textile scaffold of poly(3-hydroxybutyrate) alters the differentiation of adult human mesenchymal stem cells. Tissue Eng. 2006;12(2).
127. Ullah I, Subbarao RB, Rho GJ. Human mesenchymal stem cells - current trends and future prospective. Biosci Rep. 2015;35(2):e00191.
128. Bunnell BA, Flaat M, Gagliardi C, Patel B, Ripoll C. Adipose-derived stem cells: Isolation, expansion and differentiation. Methods. 2008;45(2):6.
129. Sheng G. The developmental basis of mesenchymal stem/stromal cells (MSCs). BMC Dev Biol. 2015;15:44.
130. Zuk PA, Zhu M, Mizuno H, Huang J, Futrell JW, Katz AJ, et al. Multilineage Cells from Human Adipose Tissue: Implications for Cell-Based Therapies. Tissue Engineering. 2001;7(2):211-28.
131. Kastrinaki MCA, I. Charbord, P. and Papadaki. H.A. Isolation of human bone marrow mesenchymal stem cells using different membrane markers: comparison of colony/cloning efficiency, differentiation potential, and molecular profile. Tissue Eng Part C Methods. 2008;14:7.
132. Ronziere MC, Perrier E, Mallein-Gerin F, Freyria AM. Chondrogenic potential of bone marrow- and adipose tissue-derived adult human mesenchymal stem cells. Biomed Mater Eng. 2010;20(3):145-58.
133. Strioga M, Viswanathan S, Darinskas A.,Slaby O, Michalek J. Same or Not the Same? Comparison of Adipose Tissue-Derived Versus Bone Marrow-Derived Mesenchymal Stem and Stromal Cells. STEM CELLS AND DEVELOPMENT. 2012;21(14):29.
134. Ude C, Sulaiman SB, Min-Hwei N, Hui-Cheng C, Ahmad J, Yahaya NM, Saim AB, Idrus RB. . Cartilage regeneration by chondrogenic induced adult stem cells in osteoarthritic sheep model. PLoS One. 2014;9(6):e98770.
135. Jang Y, Koh YG, Choi YJ, Kim SH, Yoon DS, Lee M, Lee JW. Characterization of adipose tissue-derived stromal vascular fraction for clinical application to cartilage regeneration. In Vitro Cell Dev Biol Anim. 2015;51(2):9.
136. Zhu Y, Liu T, Song K, Fan X, Ma X, Cui Z. . Adipose-derived stem cell: a better stem cell than BMSC. Cell Biochem Funct. 2008;26(6):664-75.
137. Zuk P. Adipose-Derived Stem Cells in Tissue Regeneration: A Review. ISRN Stem Cells. 2013;2013:713959.
138. Hindle P, Khan N, Biant L, Péault B. The Infrapatellar Fat Pad as a Source of Perivascular Stem Cells with Increased Chondrogenic Potential for Regenerative Medicine. STEM CELLS Translational Medicine. 2017;6(1):77-87.
139. Lopa S, Colombini A, Stanco D, de Girolamo L, Sansone V, Moretti M. Eur Cell Mater. 2014;27:298-311.
140. Felimban R, Ye K, Traianedes K, Di Bella C, Crook J, Wallace GG, et al. Differentiation of stem cells from human infrapatellar fat pad: characterization of cells undergoing chondrogenesis. Tissue Eng Part A. 2014;20(15-16):2213-23.
141. Dragoo JL SB, Zhu M, Hame SL, Thomas BJ, Lieberman JR, Hedrick MH, Benhaim P. Tissue-engineered cartilage and bone using stem cells from human infrapatellar fat pads. J Bone Joint Surg Br. 2003;85(5):8.
142. Neumann AJ, Gardner OFW, Williams R, Alin M, Archer CW, Stoddart MJ. Human Articular Cartilage Progenitor Cells Are Responsive to Mechanical Stimulation and

Adenoviral-Mediated Overexpression of Bone-Morphogenetic Protein 2. PLOS ONE 2015;10(8):e0136229.
143. Dowthwaite GP, Bishop JC, Redman SN, Khan IM, Rooney P, Evans DJ, et al. The surface of articular cartilage contains a progenitor cell population. J Cell Sci. 2004;117(Pt 6):889-97.
144. Do Amaral R, Almeida HV, Kelly DJ, O brien FJ, CJ K. Infrapatellar fat pad stem cells: from developmental biology to cell therapy. Stem Cells Int. 2017.
145. Chen G, Ushida, T, Tateishi T. Scaffold Design for Tissue Engineering. Macromolecular Bioscience. 2002;2(2):67-77.
146. Drury JL, Mooney DJ. Hydrogels for tissue engineering: scaffold design variables and applications. Biomaterials. 2003;24(24):4337-51.
147. Frantz C, Stewart KM, Weaver VM. The extracellular matrix at a glance. Journal of Cell Science 2013;123:4195-200.
148. Baraniak P, McDevitt TC. Stem cell paracrine actions and tissue regeneration. Regen Med. 2010;5(1):121-43.
149. Yu Y, Moncal KK, Li J, Peng W, Rivero I, Martin JA, et al. Three-dimensional bioprinting using self-assembling scalable scaffold-free "tissue strands" as a new bioink. Sci Rep. 2016;6:28714.
150. Raghunath J, Rollo J, Sales K, Seifalian A. Biomaterials and scaffold design: key to tissue- engineering cartilage. Biotechnol Appl Biochem. 2007;46(2):73-84.
151. Kim IL, Mauck RL, Burdick JA. Hydrogel design for cartilage tissue engineering: a case study with hyaluronic acid. Biomaterials. 2011;32:8771-82.
152. Mandal A, Clegg JR, Anselmo AC, Mitragotri S. Hydrogels in the clinic. Bioengineering and Translational Medicine. 2020;5(2):e10158.
153. Villanueva I, Weigel CA, Bryant SJ. Cell-matrix interactions and dynamic mechanical loading influence chondrocyte gene expression and bioactivity in PEG-RGD hydrogels. Acta Biomater. 2009;5(8):2832-46.
154. Ying-chun C, Chen M, Gaffney AE, Brown CP. Effect of crosslinking in cartilage-like collagen microstructures. Journal of the Mechanical Behaviour of Biomedical Materials. 2017;66(October 2016):138-43.
155. Cigan A, Roach BL, Nims RJ, Tan AR, Albro MB, Stoker AM, Cook JL, Vunjak-Novakovic G, Hung CT, Ateshian GA. High seeding density of human chondrocytes in agarose produces tissue-engineered cartilage approaching native mechanical and biochemical properties. J Biomech. 2016;49(9):1909-17.
156. Setton L, Elliott DM, Mow VC. Altered mechanics of cartilage with osteoarthritis: human osteoarthritis and an experimental model of joint degeneration. Osteoarthritis Cartilage. 1999;7(1):2-14.
157. Beck EC, Barragan, M., Tadros, M. H., Gehrke, S. H., & Detamore, M. S. Approaching the compressive modulus of articular cartilage with a decellularized cartilage-based hydrogel. Acta biomaterialia. 2016;38:94-105.
158. S Lin LG. Influence of crosslink density and stiffness on mechanical properties of type I collagen gel. Materials. 2015;8:551-60.
159. Lee C, O'Connell, C. D., Onofrillo, C., Choong, P., Di Bella, C., & Duchi, S. Human articular cartilage repair: Sources and detection of cytotoxicity and genotoxicity in photo-crosslinkable hydrogel bioscaffolds. Stem cells translational medicine. 2020;9(3):302-15.
160. Bryant S, Anseth KS. Hydrogel properties influence ECM production by chondrocytes photoencapsulated in poly(ethylene glycol) hydrogels. J Biomed Mater Res. 2002;59:63-72.

161. Nicodemus G, Skaalure SC, Bryant SJ. Gel structure has an impact on pericellular and extracellular matrix deposition, which subsequently alters metabolic activities in chondrocyte-laden PEG hydrogels. Acta Biomateriala. 2011;7:492–504.
162. Onofrillo C, Duchi S, Francis S, O'Connell CD, Caballero Aguilar LM, Doyle S, Yue Z, Wallace GG, Choong PF, Di Bella C. FLASH: Fluorescently LAbelled Sensitive Hydrogel to monitor bioscaffolds degradation during neocartilage generation. Biomaterials. 2021;264:120383.
163. Malda J, Groll J, van Weeren PR. Rethinking articular cartilage regeneration based on a 250-year-old statement. Nat Rev Rheumatol. 2019;15(10):571-2.
164. Sung HW, Huang DM, Chang WH, Huang RN, Hsu JC. Evaluation of gelatin hydrogel crosslinked with various crosslinking agents as bioadhesives: in vitro study. J Biomed Mater Res. 1999;46:520-30.
165. Bartnikowski M, Wellard R, Woodruff M, Klein T. Tailoring Hydrogel Viscoelasticity with Physical and Chemical Crosslinking. Polymers (Basel). 2015;7:2650–69.
166. Choi J, Yong KW, Choi JY, Cowie AC. Recent advances in photo-crosslinkable hydrogels for biomedical applications. BioTechniques. 2019;66(1):40-53.
167. Pfeiffer E, Vickers SM, Frank E, Grodzinsky AJ, Spector M. The effects of glycosaminoglycan content on the compressive modulus of cartilage engineered in type II collagen scaffolds. Osteoarthritis Cartilage. 2008;16(10):1237-44.
168. Song K, Li L, Li W, Zhu Y, Jiao Z, et al. Three-dimensional dynamic fabrication of engineered cartilage based on chitosan/gelatin hybrid hydrogel scaffold in a spinner flask with a special designed steel frame. Mater Sci Eng C. 2015;55:384-92.
169. Suvarnapathakiab S, Nguyen MA, Wu X, Nukavarapu SP, Camci-Unal G. Synthesis and characterization of photocrosslinkable hydrogels from bovine skin gelatin. RSC Adv. 2019;9:13016-25.
170. Santoro M, Tatara AM, Mikos AG. Gelatin carriers for drug and cell delivery in tissue engineering. J Control Release. 2014;190:210-8.
171. Loessner D, Meinert C, Kaemmerer E, Martine LC, Yue K, Levett PA, et al. Functionalization, preparation and use of cell-laden gelatin methacryloyl-based hydrogels as modular tissue culture platforms. Nat Protoc. 2016;11(4):727-46.
172. Klotz BJ, Gawlitta, D, Rosenberg AJWP, Malda J, Melchels FPW. Gelatin-Methacryloyl Hydrogels: Towards Biofabrication-Based Tissue Repair. Trends in Biotechnology,. 2016;34(5):394-407.
173. Camci-Unal G, Cuttica D, Annabi N, Demarchi D, Khademhosseini A. . Synthesis and Characterization of Hybrid Hyaluronic Acid-Gelatin Hydrogels. Biomacromolecules. 2013;814(4):1085-92.
174. Yue K, Trujillo-de Santiago G, Alvarez MM, Tamayol A, Annabi N, Khademhosseini A. Synthesis, properties, and biomedical applications of gelatin methacryloyl (GelMA) hydrogels. Biomaterials. 2015;73:254-71.
175. Duchi S, Onofrillo C, O'Connell CD, Blanchard R, Augustine C, Quigley AF, et al. Handheld Co-Axial Bioprinting: Application to in situ surgical cartilage repair. Sci Rep. 2017;7(1):5837.
176. Onofrillo C, Duchi S, O'Connell CD, Blanchard R, O'Connor AJ, Scott M, Wallace GG, Choong PFM, Di Bella C. Biofabrication of human articular cartilage: a path towards the development of a clinical treatment. Biofabrication. 2018;10(4):045006.

177. Schuurman W, Levett PA, Pot MW, van Weeren PR, Dhert WJ, Hutmacher DW, et al. Gelatin-methacrylamide hydrogels as potential biomaterials for fabrication of tissue-engineered cartilage constructs. Macromol Biosci. 2013;13(5):551-61.
178. Di Bella C, Duchi S., O'Connell C.D., Blanchard R., Augustine C., Yue Z., et al. In situ handheld three-dimensional bioprinting for cartilage regeneration. J Tissue Eng Regen Med. 2018;12(3):11.
179. Hynes R. Extracellular matrix: not just pretty fibrils. Science. 2009;326(5957):1216-9.
180. Bonnans C, Chou J, Werb Z. Remodelling the extracellular matrix in development and disease. Nat Rev Mol Cell Biol. 2014;15(12):786-801.
181. van Buul GM, Villafuertes E, Bos PK, Waarsing JH, Kops N, Narcisi R, et al. Mesenchymal stem cells secrete factors that inhibit inflammatory processes in short-term osteoarthritic synovium and cartilage explant culture. Osteoarthritis Cartilage. 2012;20(10):1186-96.
182. Linero I, Chaparro O. Paracrine Effect of Mesenchymal Stem Cells Derived from Human Adipose Tissue in Bone Regeneration. PLoS ONE. 2014;9(9):1-12.
183. Sekiya I, Colter DC, Prockop DJ. Comparison of effect of BMP-2, -4, and -6 on in vitro cartilage formation of human adult stem cells from bone marrow stroma. Cell and Tissue Research. 2005;320(2):269-76.
184. Feng Q, Lin S, Zhang K, Dong C, Wu T, Huang H, Yan X, Zhang L, Li G, Bian L. Sulfated hyaluronic acid hydrogels with retarded degradation and enhanced growth factor retention promote hMSC chondrogenesis and articular cartilage integrity with reduced hypertrophy. Acta Biomater. 2017;53:329-34.
185. Amann E, Wolff P, Breel E, van Griensven M & Balmayor ER. Hyaluronic acid facilitates chondrogenesis and matrix deposition of human adipose derived mesenchymal stem cells and human chondrocytes co-cultures. Acta Biomater. 2017;52:130-44.
186. Liu Q, Wang J, Chen Y, Zhang Z, Saunders L, Schipani E, Chen Q, Ma PX. Suppressing mesenchymal stem cell hypertrophy and endochondral ossification in 3D cartilage regeneration with nanofibrous poly(l-lactic acid) scaffold and matrilin-3. Acta Biomater. 2018;76:29-38.
187. Johnson K, Zhu S, Tremblay MS, Payette JN, Wang J, Bouchez LC, Meeusen S, Althage A, Cho CY, Wu X, Schultz PG. A stem cell-based approach to cartilage repair. Science. 2012;336(6082):717-21.
188. Cai G LW, He Y, Huang J, Duan L, Xiong J, Liu L, Wang D. Recent advances in kartogenin for cartilage regeneration. J Drug Target. 2019;27(1):28-32.
189. Bian L, Crivello KM, Ng KW, Xu D, Williams DY, Ateshian GA, Hung CT. Influence of temporary chondroitinase ABC-induced glycosaminoglycan suppression on maturation of tissue-engineered cartilage. Tissue Eng Part A. 2009;15(8):2065-72.
190. Natoli R, Revell CM & Athanasiou KA. Chondroitinase ABC treatment results in greater tensile properties of self-assembled tissue-engineered articular cartilage. Tissue Eng Part A.15:3119–28.
191. Makris E, Responte DJ, Paschos NK, Hu JC & Athanasiou KA. Developing functional musculoskeletal tissues through hypoxia and lysyl oxidase-induced collagen cross-linking. Proc Natl Acad Sci U S A. 2014;111:4832–41.
192. Lee J, Huwe LW, Paschos N, Aryaei A, Gegg CA, Hu JC, Athanasiou KA. Tension stimulation drives tissue formation in scaffold-free systems. Nat Mater. 2017;16(8):864-73.
193. Miyanishi K, Trindade MC, Lindsey DP, Beaupré GS, Carter DR, Goodman SB, et al. Dose and time dependent effects of cyclic hydrostatic pressure on transforming growth

factor-beta3-induced chondrogenesis by adult human mesenchymal stem cells in vitro. Tissue Eng. 2006;12(8):2253-62.
194. Huang CYC, Hagar KL, Frost LE, Sun Y, Cheung HS. Effects of Cyclic Compressive Loading on Chondrogenesis of Rabbit Bone-Marrow Derived Mesenchymal Stem Cells. STEM CELLS. 2004;22(3):313-23.
195. Bian L, Zhai DY, Zhang EC, Mauck RL, Burdick JA. Dynamic compressive loading enhances cartilage matrix synthesis and distribution and suppresses hypertrophy in hMSC-laden hyaluronic acid hydrogels. Tissue Eng Part A. 2012;18(7-8):715-24.
196. Bian L, Fong JV, Lima EG, Stoker AM, Ateshian GA, Cook JL, et al. Dynamic mechanical loading enhances functional properties of tissue-engineered cartilage using mature canine chondrocytes. Tissue Eng Part A. 2010;16(5):1781-90.
197. Grad S, Lee CR, Wimmer MA, Alini M. Chondrocyte gene expression under applied surface motion. Biorheology 2006;43:259-60.
198. Buckley C, Vinardell T, Kelly DJ. Oxygen tension differentially regulates the functional properties of cartilaginous tissues engineered from infrapatellar fat pad derived MSCs and articular chondrocytes. Osteoarthritis and cartilage. 2010;18(10):1345-54.
199. Sheehy E, Buckley CT, Kelly DJ. Oxygen tension regulates the osteogenic, chondrogenic and endochondral phenotype of bone marrow derived mesenchymal stem cells. Biochemical and Biophysical Research Communications. 2012;417(1).
200. Maziarz A, Kocan B, Bester M, Budzik S, Cholewa M, Ochiya T, et al. How electromagnetic fields can influence adult stem cells: positive and negative impacts. Stem Cell Res Ther. 2016;7(1):54.
201. Luciani N, Du V, Gazeau F, Richert A, Letourneur D, Le Visage C, et al. Successful chondrogenesis within scaffolds, using magnetic stem cell confinement and bioreactor maturation. Acta Biomater. 2016;37:101-10.
202. Choi JW, Choi BH, Park SH, Pai KS, Li TZ, Min BH, et al. Mechanical stimulation by ultrasound enhances chondrogenic differentiation of mesenchymal stem cells in a fibrin-hyaluronic acid hydrogel. Artif Organs. 2013;37:648-55.
203. Salehi-Nik N, Amoabediny G, Pouran B, Tabesh H, Shokrgozar MA, Haghighipour N, et al. Engineering parameters in bioreactor's design: a critical aspect in tissue engineering. BioMed research international. 2013;2013:762132.
204. Zhao J, Griffin M, Cai J, Li S, Bulter PEM, Kalaskar DM. Bioreactors for tissue engineering: An update. Biochemical Engineering Journal. 2016;109:268-81.
205. Shahin K, Doran PM. Strategies for enhancing the accumulation and retention of extracellular matrix in tissue-engineered cartilage cultured in bioreactors. PLoS One. 2011;6.
206. Yoon HH, Bhang SH,Shin JY,Shin J,Kim BS. Enhanced cartilage formation via three-dimensional cell engineering of human adipose-derived stem cells. Tissue Eng Part A 2012;18:1949-56.
207. Vunjak-Novakovic G, Martin I, Obradovic B, Treppo S, Grodzinsky AJ, Langer R, et al. Bioreactor cultivation conditions modulate the composition and mechanical properties of tissue-engineered cartilage. J Orthop Res. 1999;17(1):130-8.
208. Groen W, Diloksumpan P, van Weeren PR, Levato R, Malda J. From intricate to integrated: Biofabrication of articulating joints. J Orthop Res. 2017;35(10):289-97.
209. Klein T, Rizzi SC, Reichert JC, Georgi N, Malda J, Schuurman W, Crawford RW, Hutmacher DW. Strategies for zonal cartilage repair using hydrogels. Macromol Biosci. 2009;9(11).

210. Ren X, Wang, F., Chen, C. et al. . Engineering zonal cartilage through bioprinting collagen type II hydrogel constructs with biomimetic chondrocyte density gradient. . BMC Musculoskelet Disord 2016;17:301.
211. Gungor-Ozkerim P, Inci I, Zhang YS, Khademhosseini A, Dokmeci MR. Bioinks for 3D bioprinting: an overview. Biomaterials science. 2018;6(5):915-46.
212. Roseti L, Cavallo C, Desando G, Parisi V, Petretta M. Three-Dimensional Bioprinting of Cartilage by the Use of Stem Cells: A Strategy to Improve Regeneration. Materials (Basel). 2018;11(9):1749.
213. Murphy SV, Atala A. 3D bioprinting of tissues and organs. Nat Biotechnol. 2014;32(8).
214. Boland T, Xu T, Damon B, Cui X. Application of inkjet printing to tissue engineering. Biotechnol J. 2006;1:910-7.
215. Semba J, Mieloch AA, Rybka JD. Introduction to the state-of-the-art 3D bioprinting methods, design, and applications in orthopedics. Bioprinting. 2020;18:e00070.
216. Nakamura M, Kobayashi A, Takagi F, Watanabe A, Hiruma Y, Ohuchi K, et al. Biocompatible Inkjet Printing Technique for Designed Seeding of Individual Living Cells. Tissue Eng. 2005;11:1658-66.
217. Morita N, Khalate AA, van Buul AM, Wijshoff H. Inkjet Printheads. Fundam Inkjet Print. 2016:57-92.
218. Skardal A. Principles and applications of bioprinting. A Khademhosseini, G Camci-Una (Eds), 3D Bioprinting Regen Eng Princ Appl, CRC Press. 2018:1-24.
219. Gargus E, Lewis P, Shah R. Bioinks for 3D printing. 3D Bioprinting Regen Eng Princ Appl. 2018:25-50.
220. Cui X, Gao G, Yonezawa T, Dai G. . Human cartilage tissue fabrication using three-dimensional inkjet printing technology. J Vis Exp. 2014(88):51294.
221. Raddatz L, Lavrentieva A, Pepelanova I, Bahnemann J, Geier D, Becker T, Scheper T, Beutel S. . Development and Application of an Additively Manufactured Calcium Chloride Nebulizer for Alginate 3D-Bioprinting Purposes. J Funct Biomater. 2018;9(4):63.
222. Huang Y, Zhang XF, Gao G, Yonezawa T, Cui X. . 3D bioprinting and the current applications in tissue engineering. Biotechnol J. 2017;12(8).
223. Zhang Y, Pi Q, van Genderen AM. . Microfluidic Bioprinting for Engineering Vascularized Tissues and Organoids. J Vis Exp 2017. 2017(126):55957.
224. Zhu W, Cui H, Boualam B, Masood F, Flynn E, Rao RD, Zhang ZY, Zhang LG. . 3D bioprinting mesenchymal stem cell-laden construct with core-shell nanospheres for cartilage tissue engineering. Nanotechnology. 2018;29(18):185101.
225. Naren R, Hui-Suk Y. A simultaneous 3D printing process for the fabrication of bioceramic and cell-laden hydrogel core/shell scaffolds with potential application in bone tissue regeneration. J Mater Chem B. 2016:4707-16.
226. Duchi S, Doyle S, Eekel T, O'Connel C, Augustine C, et al. Protocols for Culturing and Imaging a Human Ex Vivo Osteochondral Model for Cartilage Biomanufacturing Applications. Materials (Basel). 2019;12(4).
227. Kundu J, Shim JH, Jang J, Kim SW, Cho DW. . An additive manufacturing-based PCL-alginate-chondrocyte bioprinted scaffold for cartilage tissue engineering. J Tissue Eng Regen Med. 2013;9(11):1286-97.
228. Vinson B, Sklare SC, Huang Y, Chrisey DB. Laser-based 3D bioprinting. A Khademhosseini, G Camci-Unal (Eds), 3D Bioprinting Regen Eng Princ Appl, Taylor & Francis Group. 2018:77098.

229. Keriquel V, Oliveira H, Rémy M, Ziane S, Delmond S, Rousseau B, Rey S, Catros S, Amédée J, Guillemot F, Fricain JC. . In situ printing of mesenchymal stromal cells, by laser-assisted bioprinting, for in vivo bone regeneration applications. Sci Rep. 2017;7(1):1778.
230. Melchels F, Feijen J, Grijpma DW. . A review on stereolithography and its applications in biomedical engineering. Biomaterials. 2010;31(24):6121-30.
231. Kačarević Ž, Rider PM, Alkildani S, Retnasingh S, Smeets R, Jung O, Ivanišević Z, Barbeck M. . An Introduction to 3D Bioprinting: Possibilities, Challenges and Future Aspects. Materials. 2018;11(11):2199.
232. Yue Z, Liu, Xiao, Coates, Patrick & Wallace, Gordon Advances in printing biomaterials and living cells: implications for islet cell transplantation. Current Opinion in Organ Transplantation. 2016;21:467-75.
233. Vijayavenkataraman S YW, Lu WF, Wang CH, Fuh JYH. 3D bioprinting of tissues and organs for regenerative medicine. Adv Drug Deliv Rev. 2018;132:296-332.
234. Guillotin B, Souquet A, Catros S, Duocastella M, Pippenger B, Bellance S, et al. Laser assisted bioprinting of engineered tissue with high cell density and microscale organization. Biomaterials 31 2010;31(28):7250-6.
235. Pepper ME, Seshadri V, Burg T, Booth BW, Burg KJ, Groff RE. Cell settling effects on a thermal inkjet bioprinter. Proc Annu Int Conf IEEE Eng Med Biol Soc EMBS. 2011:3609-12.
236. Bishop E, Mostafa S, Pakvasa M, Luu HH, Lee MJ, Wolf JM, et al. 3D bioprinting technologies in tissue engineering and regenerative medicine: Current and future trends. Genes Dis. 2017;4:185-95.
237. Khalil S, Sun W. Biopolymer deposition for freeformfabrication of hydrogel tissue constructs. Mater Sci Eng. 2007;27(3):469-78.
238. Catros S, Guillotin B, Bačáková M, Fricain JC, Guillemot F. Effect of laser energy, substrate film thickness and bioink viscosity on viability of endothelial cells printed by laser-assisted bioprinting. Appl Surf Sci. 2011:5142-7.
239. Duarte Campos D, Blaeser A,Weber M, Jäkel J, Neuss S, Jahnen-Dechent W, et al. Three-dimensional printing of stem cell-laden hydrogels submerged in a hydrophobic high-density fluid. Biofabrication 2013;5(1).
240. Tumbleston JR, Shirvanyants D, Ermoshkin N, Janusziewicz R, Johnson AR, Kelly D, et al. Continuous liquid interface production of 3D objects. Science 2015;347(6228):1349-52.
241. Wang Z, Abdulla R, Parker B, Samanipour R, Ghosh S, Kim K. A simple and high-resolution stereolithography-based 3D bioprinting system using visible light crosslinkable bioinks. Biofabrication 2015;7(4).
242. Raman R, Bhaduri B, Mir M, Shkumatov A, Lee MK, Popescu G, et al. High-Resolution Projection Microstereolithography for Patterning of Neovasculature. Adv Healthc Mater. 2016;5:610-9.
243. Hull CW. US Patent: 4,575,330. Filed: August 08, 1984. Issued: March 11, Database: USPTO Patent Grants. 1986.
244. Donderwinkel I, van Hest JCM, Cameron NR. Bio-inks for 3D bioprinting: recent advances and future prospects. Polymer Chemistry. 2017;8(31):4451-71.
245. Eckstein F, Cicuttini F, Raynauld JP, Waterton JC, C P. Magnetic resonance imaging (MRI) of articular cartilage in knee osteoarthritis (OA): morphological assessment. Osteoarthritis Cartilage. 2006;14 Suppl A:A46-75.
246. O'Connell CD, Di Bella C, Thompson F, Augustine C, Beirne S, Cornock R, et al. Development of the Biopen: a handheld device for surgical printing of adipose stem cells at a chondral wound site. Biofabrication. 2016;8(1):015019.

247. Di Bella C, Duchi S, O'Connell CD, Blanchard R, Augustine C, Yue Z, et al. In situ handheld three-dimensional bioprinting for cartilage regeneration. Journal of tissue engineering and regenerative medicine. 2018;12(3):611-21.
248. Holland TA, Bodde EW, Cuijpers VM, Baggett LS, Tabata Y, Mikos AG, et al. Degradable hydrogel scaffolds for in vivo delivery of single and dual growth factors in cartilage repair. Osteoarthritis Cartilage. 2007;15(2):187-97.
249. Sørensen L, Hemmingsen U, Kallehave F, Wille-Jørgensen P, Kjaergaard J, Møller LN, Jørgensen T. Risk factors for tissue and wound complications in gastrointestinal surgery. . Ann Surg. 2005;241(4):654-8.
250. Gotterbarm T, Breusch SJ, Schneider U, Jung M. The minipig model for experimental chondral and osteochondral defect repair in tissue engineering: retrospective analysis of 180 defects. Lab Anim. 2008;42(1):71-82.
251. Chu C, Szczodry M, Bruno S. Animal models for cartilage regeneration and repair. Tissue Eng Part B Rev. 2010;16(1):105-15.
252. Ahern B, Parvizi J, Boston R, Schaer TP. Preclinical animal models in single site cartilage defect testing: a systematic review. Osteoarthritis Cartilage. 2009;17(6):705-13.
253. Pelletier J, Boileau C, Altman RD, Pelletier JM. Experimental models of osteoarthritis: usefulness in the development of disease-modifying osteoarthritis drugs/agents. Therapy. 2010;7(6):621-34.
254. McCoy A. Animal models of osteoarthritis: comparisons and key considerations. Vet Pathol. 2015;52(5):803-18.
255. Teeple E, Jay GD, Elsaid KA, Fleming BC. Animal models of osteoarthritis: challenges of model selection and analysis. The AAPS journal. 2013;15(2):438-46.
256. Kuyinu E, Narayanan G, Nair LS, Laurencin CT. Animal models of osteoarthritis: classification, update, and measurement of outcomes. Journal of orthopaedic surgery and research. 2016;11:19.
257. Aigner T, Lohmander S. OAC histopathology supplement. Osteoarthritis Cartilage. 2010;18(Suppl 3):S1-S122.
258. Chatfield K, Morton D. The Use of Non-human Primates in Research. In: Schroeder D, Cook J, Hirsch F, Fenet S, Muthuswamy V. (eds) Ethics Dumping. SpringerBriefs in Research and Innovation Governance. Springer, Cham. 2018.
259. An Y, Freidman FJ. Animal Models in Orthopaedic Research. CRC Press LLC. 1999.
260. Scotti C, Piccinini E, Takizawa H, Todorov A, Bourgine P, et al. Engineering of a functional bone organ through endochondral ossification. Proc Natl Acad Sci USA. 2013;110(10):3997-4002.
261. Scott M, Levi B, Askarinam A, Nguyen A, Rackohn T, et al. Brief review of models of ectopic bone formation. Stem Cells and Development. 2011;21:655-67.
262. Abarrategi A, Perez-Tavarez R, Rodriguez-Milla MA, Cubillo I, Mulero F, et al. In vivo ectopic implantation model to assess human mesenchymal progenitor cell potential. Stem Cell Rev Rep. 2013;9(6):833-46.
263. Cheng H CB, Soleas IM, Ferko NC, Cameron CG, Hinoul P. Prolonged Operative Duration Increases Risk of Surgical Site Infections: A Systematic Review. Surg Infect (Larchmt). 2017;18(6):722-35.
264. Williams R, Khan IM, Richardson K, Nelson L, McCarthy HE, Analbelsi T, et al. Identification and clonal characterisation of a progenitor cell sub-population in normal human articular cartilage. PLoSONE. 2010;5(10):e13246.

265. Pigeau G, Csaszar E, Dulgar-Tulloch A. Commercial Scale Manufacturing of Allogeneic Cell Therapy. Front Med (Lausanne). 2018;5:233.
266. Johnstone B, Alini M, Cucchiarini M, Dodge GR, Eglin D, al. GFe. Tissue engineering for articular cartilage repair--the state of the art. Eur Cell Mater. 2013;25:248-67.
267. Zhang L, Hu J, Athanasiou KA. The role of tissue engineering in articular cartilage repair and regeneration. Crit Rev Biomed Eng. 2009;37(1-2):1-57.
268. Dragoo J, Chang W. Arthroscopic Harvest of Adipose-Derived Mesenchymal Stem Cells From the Infrapatellar Fat Pad. Am J Sports Med. 2017;45(13):3119-27.
269. Nae S, Bordeianu IB, Stancioiu AT, Antohi N. Human adipose-derived stem cells: definition, isolation, tissue-engineering applications. Rom J Morphol Embryol. 2013;54(4):919-24.
270. Oberbauer E, Steffenhagen C, Wurzer C, Gabriel C, Redl H, Wolbank S. Enzymatic and non-enzymatic isolation systems for adipose tissue-derived cells: current state of the art. Cell Regen (Lond). 2015;4:7.
271. Raposio E, Simonacci F, Perrotta RE. Adipose-derived stem cells: Comparison between two methods of isolation for clinical applications. Ann Med Surg (Lond). 2017;20:87-91.
272. Francis MP, Sachs PC, Elmore LW, Holt SE. Isolating adipose-derived mesenchymal stem cells from lipoaspirate blood and saline fraction. organogenesis. 2010;6(1):4.
273. Sridharan B, Lin SM, Hwu AT, Laflin AD, Detamore MS. Stem Cells in Aggregate Form to Enhance Chondrogenesis in Hydrogels. PLoS One. 2015;10(12):e0141479.
274. Ahearne M, Liu Y, Kelly DJ. Combining freshly isolated chondroprogenitor cells from the infrapatellar fat pad with a growth factor delivery hydrogel as a putative single stage therapy for articular cartilage repair. Tissue Eng Part A. 2014;20((5-6)):930-9.
275. Colter D, Class R, Digirolamo CM, Prockop DJ. Rapid expansion of recycling stem cells in cultures of plastic-adherent cells from human bone marrow. Proc Natl Acad Sci USA. 2000;97:6.
276. Rodriguez AM, Pisani D, Dechesne CA, Turc-Carel C, Kurzenne JY, Wdziekonski B, et al. Transplantation of a multipotent cell population from human adipose tissue induces dystrophin expression in the immunocompetent mdx mouse. J Exp Med. 2005;201(9):1397-405.
277. Seaman SA, Tannan SC, Cao Y, Peirce SM, Lin KY. Differential Effects of Processing Time and Duration of Collagenase Digestion on Human and Murine Fat Grafts. Plast Reconstr Surg. 2015;136(2):189e-99e.
278. Papadopoulos V, Dym M. Sertoli cell differentiation on basement membrane is mediated by the c-fos protooncogene Proc Natl Acad Sci USA. 1994;99:5.
279. Lee SW, Lee HJ,Hwang HS, Ko K, Han DW, Ko K. Optimization of Matrigel-based culture for expansion of neural stem cells. Animal Cells and System. 2015;19(3):6.
280. Gruber H, Somayaji S, Riley F, Hoelscher GL, Norton HJ, Ingram J, et al. Human adipose-derived mesenchymal stem cells: serial passaging, doubling time and cell senescence. Biotechnic & histochemistry : official publication of the Biological Stain Commission. 2012;87(4):303-11.
281. Faghih H, Javeri A, Taha MF. Impact of early subcultures on stemness, migration and angiogenic potential of adipose tissue-derived stem cells and their resistance to in vitro ischemic condition Cytotechnology. 2017;69(6):885-900.
282. Halme D, Kessler D. FDA regulation of stem-cell-based therapies. N Engl J Med. 2006;355(16):6.

283. Steadman J, Rodkey W, Briggs K, Cole B, Kercher J. Microfracture: Its History and Experience of the Developing Surgeon. . Cartilage. 2010;1(2):78-86.
284. Williams R, Harnly H. Microfracture: indications, technique, and results. Instr Course Lect. 2007;56:419-28.
285. Hunziker E, Quinn T, Häuselmann H. Quantitative structural organization of normal adult human articular cartilage. Osteoarthritis Cartilage. 2002;10(7):564-72.
286. Bernstein P, Dong M, Graupner S, Corbeil D, Gelinsky M, et al. Sox9 expression of alginate-encapsulated chondrocytes is stimulated by low cell density. J Biomed Mater Res A. 2009;91A:910-9.
287. Abbott J, Holtzer H. The loss of phenotypic traits by differentiated cells, The reversible behavior of chondrocytes in primary cultures. J Cell Biol. 1966;28:473-87.
288. Handley C, Bateman J, Oakes B, Lowther D. Characterization of the collagen synthesized by cultured cartilage cells. Biochim Biophys Acta 1975;386(2):444-50.
289. Francioli S, Candrian C, Martin K, Heberer M, Martin I, Barbero A. Effect of three-dimensional expansion and cell seeding density on the cartilage-forming capacity of human articular chondrocytes in type II collagen sponges. J Biomed Mater Res A 2010;95A(3):924-31.
290. Foldager C, Gomoll A, Lind M, Spector M. Cell Seeding Densities in Autologous Chondrocyte Implantation Techniques for Cartilage Repair. Cartilage. 2012;3(2):108-17.
291. Cooper G, Sunderland MA The Cell: A Molecular Approach. 2nd edition. Cell Proliferation in Development and Differentiation. Sunderland (MA): Sinauer Associates, https://wwwncbinlmnihgov/books/NBK9906/. 2000.
292. Ye K, Traianedes K, Robins SA, Choong PFM, Myers DE. Osteochondral repair using an acellular dermal matrix-pilot in vivo study in a rabbit osteochondral defect model. J Orthop Res. 2018;36(7):1919-28.
293. Almeida F, Nobre YT, Leite KR, Bruschini H. Autologous transplantation of adult adipose derived stem cells into rabbit urethral wall. Int Urogynecol J. 2010;21(6):743-8.
294. Balanescu A, Radu E, Nat R, Regalia T, Bojinca V, et al. Co-stimulatory and adhesion molecules of dendritic cells in rheumatoid arthritis. J Cell Mol Med. 2002;6:415-25.
295. Fox D. The role of T cells in the immunopathogenesis of rheumatoid arthritis: new perspectives. Arthritis Rheum. 1997;40:598-609.
296. Chesterman P, Smith AU. Homotransplantation of articular cartilage and isolated chondrocytes. An experimental study in rabbits. J Bone Joint Surg 1968;50:184-97.
297. Elves M, Zervas J. An investigation into the immunogenicity of various components of osteoarticular grafts. Br J Exp Pathol. 1974;55:344-51.
298. Lance E, Fisher RL. Transplantation of the rabbit's patella. J Bone Joint Surg. 1970;52:145-56.
299. Gupta A, Mohanty B, Bohidar HB. Flory temperature and upper critical solution temperature of gelatin solutions. Biomacromolecules. 2005;6(3):1623-7.
300. Mohanty B, Bohidar HB. Microscopic structure of gelatin coacervates. International journal of biological macromolecules. 2005;36(1-2):39-46.
301. Liu M, Zeng X, Ma CX, Yi H, Ali Z, et al. Injectable hydrogels for cartilage and bone tissue engineering. Bone Res 2017;5:17014
302. Pepelanova I, Kruppa K, Scheper T, Lavrentieva A. Gelatin-Methacryloyl (GelMA) Hydrogels with Defined Degree of Functionalization as a Versatile Toolkit for 3D Cell Culture and Extrusion Bioprinting. Bioengineering (Basel). 2018;5(3):55.

303. Panwar A, Tan LP. Current Status of Bioinks for Micro-Extrusion-Based 3D Bioprinting. Molecules. 2016;21(6):685.
304. Liu W, Heinrich MA, Zhou Y, Akpep A, Hu N, et al. Extrusion Bioprinting of Shear-Thinning Gelatin Methacryloyl Bioinks. Adv Healthc Mater. 2017;6(12):10.
305. Sun X, Holley RA. Factors Influencing Gel Formation by Myofibrillar Proteins in Muscle Foods. Comprehensive reviews in food science and safety.10(1):33-51.
306. Billiet T, Vandenhaute M, Schelfhout J, Van Vlierberghe S, Dubruel P. A review of trends and limitations in hydrogel-rapid prototyping for tissue engineering. Biomaterials. 2012;33:6020-41.
307. Wang Z, Jin X, Dai R, Holzman J, Kim K. An ultrafast hydrogel photocrosslinking method for direct laser bioprinting RSC ADVANCES. 2016;6(25):21099-104.
308. Oliveira J, Gardel LS, Rada T, Martins L, Gomes ME, Reis RL. Injectable gellan gum hydrogels with autologous cells for the treatment of rabbit articular cartilage defects. J Orthop Res. 2010;28(9):1193-9.
309. Wei X, Messner K. Maturation-dependent durability of spontaneous cartilage repair in rabbit knee joint. J Biomed Mater Res. 1999;46(4):539-48.
310. Cellular Products for Joint Surface Repair – Briefing Document. Cellular T, and Gene Therapies Advisory Committee, 2005, Meeting 38, March 3–4.
311. Tamai N, Myoui A, Hirao M, Kaito T,Ochi T, et al. A new biotechnology for articular cartilage repair: subchondral implantation of a composite of interconnected porous hydroxyapatite, synthetic polymer (PLA–PEG), and bone morphogenetic protein-2 (rhBMP-2). Osteoarthritis Cartilage. 2005:405-17.
312. Trzeciak T, Kruczynski J, Jaroszewski J, Lubiatowski P. Evaluation of cartilage reconstruction by means of autologous chondrocyte versus periosteal graft transplantation: an animal study. Transplant Proc. 2006;38:305-11.
313. Frisbie D, Cross MW, McIlwraith CW. A comparative study of articular cartilage thickness in the stifle of animal species used in human pre-clinical studies compared to articular cartilage thickness in the human knee. Vet Comp Orthop Traumatol. 2006;19:142-6.
314. Shao X, Hutmacher DW , Ho TS, Goh J, Lee EH. Evaluation of a hybrid scaffold/cell construct in repair of high-load-bearing osteochondral defects in rabbits. Biomaterials,. 2006;27:1071-80.
315. Chuma H, Mizuta H, Kudo S, Takagi K, Hiraki Y. One day exposure to FGF-2 was sufficient for the regenerative repair of full-thickness defects of articular cartilage in rabbits. Osteoarthritis Cartilage. 2004;12:834-42.
316. Estes B, Diekman BO, Gimble JM, Guilak F. Isolation of adipose-derived stem cells and their induction to a chondrogenic phenotype. Nat Protoc. 2010;5(7):18.
317. O'Connell CD, Zhang B, Onofrillo C, Duchi S, Blanchard R, Quigley A, et al. Tailoring the mechanical properties of gelatin methacryloyl hydrogels through manipulation of the photocrosslinking conditions. Soft Matter. 2018;14(11):2142-51.
318. Stratasys. Biocompatible Clear MED610 datasheet [Internet]. 2018 [cited 2019 Septemebr 31]. Available from: http://www.stratasys.com/materials/search/biocompatible.
319. O'Connell C, Konate S, Onofrillo C, Kapsa R, Baker C, Duchi S, Eekel T, Yue Z, Beirne S, Barnsley G, Di Bella C, Choong PF, Wallace GG. Free-form co-axial bioprinting of a gelatin methacryloyl bio-ink by direct in situ photo-crosslinking during extrusion. Bioprinting. 2020;19:e00087.

320. Visser J, Melchels FP, Jeon JE, van Bussel EM, Kimpton LS, Byrne HM, Dhert WJ, Dalton PD, Hutmacher DW, Malda J. Reinforcement of hydrogels using three-dimensionally printed microfibres. Nat Commun. 2015;6:6933.
321. Xiao Y, Friis EA, Gehrke SH, Detamore MS. . Mechanical testing of hydrogels in cartilage tissue engineering: beyond the compressive modulus. Tissue Eng Part B Rev. 2013;19(5):403-12.
322. Patel J, Wise BC, Bonnevie ED, Mauck RL. . A Systematic Review and Guide to Mechanical Testing for Articular Cartilage Tissue Engineering. Tissue Eng Part C Methods. 2019;25(10):593-608.
323. Paxton N, Smolan W, Bock T, Melchels F, Groll J, Jungst T. Proposal to assess printability of bioinks for extrusion-based bioprinting and evaluation of rheological properties governing bioprintability. Biofabrication. 2017;9(4):044107.
324. O'Connell C, Ren J, Pope L, Li Y, Mohandas A, Blanchard R et al. Characterizing Bioinks for Extrusion Bioprinting: Printability and Rheology. In: Crook J. (eds) 3D Bioprinting. Methods in Molecular Biology (Springer protocols). 2020;2140.
325. Ribeiro A, Blokzijl MM, Levato R, Visser CW, Castilho M, Hennink WE, Vermonden T, Malda J. Assessing bioink shape fidelity to aid material development in 3D bioprinting. Biofabrication. 2017;30(10):014102.
326. Lim K, Klotz BJ, Lindberg GCJ, Melchels FPW, Hooper GJ, Malda J, Gawlitta D, Woodfield TBF. Visible Light Cross-Linking of Gelatin Hydrogels Offers an Enhanced Cell Microenvironment with Improved Light Penetration Depth. Macromol Biosci. 2019;19(6):e1900098.
327. Brittberg M, Peterson L. Introduction of an articular cartilage classification. ICRS Newsletter. 1998;1:5-8.
328. Roemhildt M, Coughlin KM, Peura GD, Fleming BC, Beynnon BD. Material properties of articular cartilage in the rabbit tibial plateau. J Biomech. 2006;39(12):2331-7.
329. Jia S, Zhang T, Xiong Z, Pan W, Liu J, et al. In Vivo Evaluation of a Novel Oriented Scaffold-BMSC Construct for Enhancing Full-Thickness Articular Cartilage Repair in a Rabbit Model PLOS ONE 2015;10(12):e0145667.
330. Julkunen P, Harjula T, Iivarinen J, Marjanen J, Seppanen K, et al. Biomechanical, biochemical and structural correlations in immature and mature rabbit articular cartilage. Osteoarthritis Cartilage. 2009;17(12):1628-38.
331. Castania V, Silveira JW, Issy AC, Pitol DL, Castania ML, et al. Advantages of a combined method of decalcification compared to EDTA. Microscopy Research and Techniqu. 2015;78(2):111-8.
332. Nettles D, Kitaoka K, Hanson NA, Flahiff CM, Mata BA, et al. In situ crosslinking elastin-like polypeptide gels for application to articular cartilage repair in a goat osteochondral defect model. Tissue Eng Part A. 2008;14(7):1133-40.
333. Garcia J, Wright K, Roberts S, Kuiper JH, Mangham C, Richardson J, et al. Characterisation of synovial fluid and infrapatellar fat pad derived mesenchymal stromal cells: The influence of tissue source and inflammatory stimulus. Scientific reports. 2016;6:24295.
334. Jang Y KY, Choi YJ, Kim SH, Yoon DS, Lee M, Lee JW. Characterization of adipose tissue-derived stromal vascular fraction for clinical application to cartilage regeneration. In Vitro Cell Dev Biol Anim. 2015;51(2):9.
335. Francis S, Di Bella C, Wallace GG, Choong PFM. Cartilage Tissue Engineering Using Stem Cells and Bioprinting Technology—Barriers to Clinical Translation. Front Surg. 2018;5.

336. Francis SL, Duchi S, Onofrillo C, Di Bella C, Choong PFM. Adipose-Derived Mesenchymal Stem Cells in the Use of Cartilage Tissue Engineering: The Need for a Rapid Isolation Procedure. Stem Cells International. 2018;2018:9.
337. Dominici M, Le Blanc K, Mueller I, Slaper-Cortenbach I, Marini F, Krause D, et al. Minimal criteria for defining multipotent mesenchymal stromal cells. The International Society for Cellular Therapy position statement. Cytotherapy. 2006;8(4):315-7.
338. Lv FJ, Tuan RS, Cheung KM, Leung VY. Concise review: The surface markers and identity of human mesenchymal stem cells. Stem Cells. 2014;32:1408-19.
339. Lefebvre V, Smits P. Transcriptional control of chondrocyte fate and differentiation. Birth Defects Res C Embryo Today. 2005;75(3):200-12.
340. Javed A, Chen H, Ghori FY. Genetic and transcriptional control of bone formation. Oral Maxillofac Surg Clin North Am. 2010;22(3):283-5.
341. Lowe C, O'Rahilly S, Rochford JJ. Adipogenesis at a glance. J Cell Sci. 2011;124:2681-6.
342. Dehne T, Karlsson C, Ringe J, Sittinger M, A L. Chondrogenic differentiation potential of osteoarthritic chondrocytes and their possible use in matrix-associated autologous chondrocyte transplantation. Arthritis research & therapy. 2009;11(5):R133.
343. Kang SW, Yoo SP, Kim BS. Effect of chondrocyte passage number on histological aspects of tissue-engineered cartilage. Biomed Mater Eng. 2007;17:269-76.
344. Lin Z, Willers C, Xu, J, Zheng MH. The chondrocyte: biology and clinical application. Tissue Eng. 2006;12:1971-84.
345. Cheng H, Chen BP, Soleas IM, Ferko NC, Cameron CG, Hinoul P. Prolonged Operative Duration Increases Risk of Surgical Site Infections: A Systematic Review. Surg Infect (Larchmt). 2017;18(6):722-35.
346. Mochizuki T, Muneta T, Sakaguchi Y et al. Higher chondrogenic potential of fibrous synovium- and adipose synovium-derived cells compared with subcutaneous fat-derived cells: distinguishing properties of mesenchymal stem cells in humans. Arthritis Rheum. 2006;54:843-53.
347. Wickham M, Erickson GR, Gimble JM, Vail TP, Guilak F. Multipotent stromal cells derived from the infrapatellar fat pad of the knee. Clin Orthop Relat Res. 2003;412:196-212.
348. Hopper N, Wardale J, Howard D et al. Peripheral blood derived mononuclear cells enhance the migration and chondrogenic differentiation of multipotent mesenchymal stromal cells. Stem Cells Int. 2015:323454.
349. Vinardell T, Buckley CT, Thorpe SD, Kelly DJ. Composition-function relations of cartilaginous tissues engineered from chondrocytes and mesenchymal stem cells isolated from bone marrow and infrapatellar fat pad. J Tissue Eng Regen Med. 2011;5:673-83.
350. Ding D, Wu KC, Chou HL et al. Human infrapatellar fat pad-derived stromal cells have more potent differentiation capacity than other mesenchymal cells and can be enhanced by hyaluronan. Cell Transplant. 2015;24:1221–32.
351. Sun Y, Chen S, Pei M. Comparative advantages of infrapatellar fat pad: an emerging stem cell source for regenerative medicine. Rheumatology. 2018;57(12):2072–86.
352. Vukicevic S, Kleinman HK, Luyten FP, Roberts AB, Roche NS, Reddi AH. Identification of multiple active growth factors in basement membrane matrigel suggests caution in interpretation of cellular activity related to extracellular matrix components. Exp Cell Res. 1992;202:1-8.
353. Hughes C, Postovit LM, Lajoie GA. Matrigel: a complex protein mixture required for optimal growth of cell culture. Proteomics. 2010;10(9):1886-90.

354. Yong K, Choi JR, Wan Safwani WK. Biobanking of Human Mesenchymal Stem Cells: Future Strategy to Facilitate Clinical Applications. Adv Exp Med Biol. 2016;951:99-110.
355. Kodali A, Lim TC, Leong DT, Tong YW. Cell-microsphere constructs formed with human adipose-derived stem cells and gelatin microspheres promotes stemness, differentiation, and controlled pro-angiogenic potential. Macromol Biosci. 2014;14(10):1458-68.
356. Natesan S, Baer DG, Walters TJ, Babu M, Christy RJ. Adipose-derived stem cell delivery into collagen gels using chitosan microspheres. Tissue Eng Part A. 2010;16(4):1369-84.
357. Bouwmeester P, Kuijer R, Homminga GN, Bulstra SK, Geesink R. A retrospective analysis of two independent prospective cartilage repair studies: autogenous perichondrial grafting versus subchondral drilling 10 years post-surgery. J Orthop Res. 2002;20:267-73.
358. Hjelle K, Solheim E, Strand T, Muri R, Brittberg M. Articular cartilage defects in 1,000 knee arthroscopies. Arthroscopy. 2002;18:730-4.
359. Mainil-Varlet P, Kandel R, Roberts S. In: 8th World Congress of the International Cartilage Repair Society. Miami, Florida. 2009;60.
360. Mainil-Varlet P, Kandel R, Roberts S. ICRS II histology score for the assessment of the quality of human cartilage repair. Osteoarthritis Cartilage. 2009;38(5):880-90.
361. Perdisa F, Gostyńska, N., Roffi, A., Filardo, G., Marcacci, M., & Kon, E. Adipose-Derived Mesenchymal Stem Cells for the Treatment of Articular Cartilage: A Systematic Review on Preclinical and Clinical Evidence. Stem cells international. 2015:597652.
362. Dai N, Fan GY, Liou NH, Wang YW, Fu KY, Ma KH, Liu JC, Chang SC, Huang KL, Dai LG, Chen SG, Chen TM. Histochemical and functional improvement of adipose-derived stem cell-based tissue-engineered cartilage by hyperbaric oxygen/air treatment in a rabbit articular defect model. Ann Plast Surg. 2015;74(Suppl 2):S139-45.
363. Dragoo JL, Carlson G., McCormick F., et al. Healing full-thickness cartilage defects using adipose-derived stem cells. Tissue Engineering. 2007;13(7):1615–21.
364. Nathan S, De S. D., Thambyah A., Fen C., Goh J., Lee E. H. Cell-based therapy in the repair of osteochondral defects: a novel use for adipose tissue. Tissue Engineering. 2003;9(4):733-44.
365. Toghraie F, Chenari N, Gholipour MA, Faghih Z, Torabinejad S, Dehghani S, Ghaderi A. Treatment of osteoarthritis with infrapatellar fat pad derived mesenchymal stem cells in Rabbit. Knee. 2011;18(2):71-5.
366. Zhang K, Zhang Y., Yan S., et al. chitosan. Repair of an articular cartilage defect using adipose-derived stem cells loaded on a polyelectrolyte complex scaffold based on poly(l-glutamic acid) and. Acta Biomaterialia. 2013;9(7):7276–88.
367. Wang Z, An RZ, Zhao JY, Zhang Q, Yang J, Wang JB, Wen GY, Yuan XH, Qi XW, Li SJ, Ye XC. Repair of articular cartilage defects by tissue-engineered cartilage constructed with adipose-derived stem cells and acellular cartilaginous matrix in rabbits. Genet Mol Res. 2014;13(2):4599-606.
368. Cao Z, Hou S., Sun D., Wang X., Tang J. Osteochondral regeneration by a bilayered construct in a cell-free or cell-based approach. Biotechnology Letters. 2012;34(6):1151-57.
369. Levato R, Visser J, Planell JA, Engel E, Malda J, Mateos-Timoneda MA. Biofabrication of tissue constructs by 3D bioprinting of cell-laden microcarriers. Biofabrication. 2014;6(3):035020.

370. Kwon H, Brown, W. E., Lee, C. A., Wang, D., Paschos, N., Hu, J. C., & Athanasiou, K. A. . Surgical and tissue engineering strategies for articular cartilage and meniscus repair. Nature reviews Rheumatology. 2019;15(9):550–70.
371. 2017 [US Food and Drug Administration. Guidance for Industry: Expedited Programs for Regenerative Medicine Therapies for Serious Conditions. https://www.fda.gov/media/120267/download].

CHAPTER 10: APPENDICES

APPENDIX 1: CARTILAGE TISSUE ENGINEERING USING STEM CELS AND BIOPRINTING TECHNOLOGY - BARRIERS TO CLINICAL TRANSLATION

frontiers in Surgery

REVIEW
published: 27 November 2018
doi: 10.3389/fsurg.2018.00070



Cartilage Tissue Engineering Using Stem Cells and Bioprinting Technology—Barriers to Clinical Translation

Sam L. Francis[1,2,3], Claudia Di Bella[1,2,3], Gordon G. Wallace[3,4] and Peter F. M. Choong[1,2,3]*

[1] Department of Surgery, University of Melbourne, Melbourne, VIC, Australia, [2] Department of Orthopaedics, St Vincent's Hospital, Melbourne, VIC, Australia, [3] Biolab 3D, Alfanhead Centre for Medical Discovery, Melbourne, VIC, Australia, [4] Australian Research Council, Centre of Excellence for Electromaterials Science, Intelligent Polymer Research Institute, University of Wollongong, Wollongong, NSW, Australia

There is no long-term treatment strategy for young and active patients with cartilage defects. Early and effective joint preserving treatments in these patients are crucial in preventing the development of osteoarthritis. Tissue engineering over the past few decades has presented hope in overcoming the issues involved with current treatment strategies. Novel advances in 3D bioprinting technology have promoted more focus on efficient delivery of engineered tissue constructs. There have been promising *in-vitro* studies and several animal studies looking at 3D bioprinting of engineered cartilage tissue. However, to date there are still no human clinical trials using 3D printed engineered cartilage tissue. This review begins with discussion surrounding the difficulties with articular cartilage repair and the limitations of current clinical management options which have led to research in cartilage tissue engineering. Next, the major barriers in each of the 4 components of cartilage tissue engineering; cells, scaffolds, chemical, and physical stimulation will be reviewed. Strategies that may overcome these barriers will be discussed. Finally, we will discuss the barriers surrounding intraoperative delivery of engineered tissue constructs and possible solutions.

Keywords: cartilage, stem cells, scaffolds, hydrogels, tissue engineering, bioprinting, bio fabrication

OPEN ACCESS

Edited by:
Zsolt J. Balogh,
University of Newcastle, Australia

Reviewed by:
Konstantinos Markatos,
Biomedical Research Foundation of the Academy of Athens, Greece
Holly Tyler-Faris Pilson,
Wake Forest Baptist Medical Center, Winston-Salem, United States

****Correspondence:***
Sam L. Francis
sfrancis1@student.unimelb.edu.au

Specialty section:
This article was submitted to Orthopedic Surgery, a section of the journal Frontiers in Surgery

Received: *31 August 2018*
Accepted: *08 November 2018*
Published: *27 November 2018*

Citation:
Francis SL, Di Bella C, Wallace GG and Choong PFM (2018) Cartilage Tissue Engineering Using Stem Cells and Bioprinting Technology—Barriers to Clinical Translation. Front. Surg. 5:70. doi: 10.3389/fsurg.2018.00070

INTRODUCTION

Articular cartilage defects pose a significant burden to patients both symptomatically and functionally, leading to reduced quality of life. Younger patients particularly have no long-term treatment strategy and face multiple operations and possible complications in their lifetime due to the inevitable development of osteoarthritis (1, 2).

Several surgical options exist in current practice (Discussed in detail under the current treatment strategies section); however, they only provide short-term benefit in certain subsets of patients based on the nature of the defect and host factors. Fibrocartilage production is the major barrier in long-term viability of these methods and is detrimental to joint function (3).

Treatment strategies currently being pursued in research, focus on the development of 3D bioprinting of engineered cartilage tissue. This is a diverse field with many factors warranting optimization and integration to deliver the ultimate 3D tissue structure. However, there are several obstacles with each individual component, collectively leading to a barrier with respect to clinical

use of cartilage tissue engineering and 3D bioprinting for cartilage repair. These hurdles will need to be addressed prior to any design of a human clinical trial.

ARTICULAR CARTILAGE: STRUCTURE AND REPAIR

Articular cartilage is primarily composed of hyaline tissue. Hyaline cartilage is a specialized tissue found in most joints and provides low friction and shock absorption. It also provides a structural and biological barrier between two bone surfaces leading to smooth uniform range of motion (4).

Articular cartilage has unique biomechanical properties stemming from its structure (**Figure 1**) and composition. The lubricated surface provides low friction for articular motion. The extracellular matrix (ECM) and large water content from the effect of proteoglycans provides resistance to strong and repetitive loads of compression and shear. Variations of structure and composition in the different zones allow articular cartilage to resist complex loads and forces encountered in daily activity (4).

Damaged hyaline cartilage is unable to self-repair (5) due to its avascular nature. This characteristic of articular cartilage represents a major challenge in the field of orthopedics. Overtime, either with or without treatment the defect is filled with fibrocartilage, which represents a stiff tissue that doesn't provide the specialized properties of hyaline cartilage (3).

CURRENT TREATMENT STRATEGIES

Surgically many techniques have been developed in an attempt to repair/regenerate cartilage. These can be classified into bone marrow stimulation techniques (drilling, abrasion, and microfracture), direct chondral replacement (mosaicplasty and osteochondral allograft transplantation) and cell culture-based treatment (Autologous Chondrocyte Implantation and Matrix-induced Autologous Chondrocyte Implantation).

Microfracture is the most commonly used technique whilst Autologous Chondrocyte Implantation (ACI) and Matrix-induced Autologous Chondrocyte Implantation (MACI) are used by some surgeons in specific cases. Microfracture is an arthroscopic technique in which holes are created in the subchondral bone to allow blood and bone marrow to proximate, clot, and stimulate cartilage repair (6). ACI involves cartilage being harvested from non/low-weight bearing regions from which chondrocytes are isolated and expanded over 6–8 weeks, after which the cells are implanted back in surgically (7). MACI is a progression of the ACI technique characterized by the delivery of cells in association with a scaffold (8).

Comparison between all three methods have shown no superiority of the newer techniques compared to the less expensive microfractures. A randomized control trial comparing ACI to microfracture showed no significant improvement in cartilage repair outcomes (9), furthermore, no difference was shown comparing ACI to MACI (10). With no significant difference prevailing amongst the three techniques the general surgical inclination has been to opt for microfracture which is a simpler and cheaper option.

Studies involving microfracture show better outcome in patients <40 years old with isolated lesions averaging 2 cm^2 in size, however at 36 months follow up there was significant reduction in clinical outcome (11). This technique can therefore only be provided to a small subset of patients and lacks long-term outcome data. Reasons for poor long-term outcomes include fibrocartilage production, patient age, functional level, location, and size of the defect (3, 11–13).

THE EMERGENCE OF CARTILAGE TISSUE ENGINEERING

Poor long-term results and outcomes from bone marrow stimulation techniques like microfracture introduced the field of cartilage tissue engineering (**Figure 2**). The general principle of tissue engineering involves the use of cells, scaffolds, growth factors, and physical stimulation (diamond concept) to regenerate living tissue (13).

In the field of cartilage, the aim is to develop biomimetic tissue that can reliably perform, both biologically and biomechanically, as hyaline cartilage. There is a long history of cartilage tissue engineering attempts with initially engineered components resembling hyaline cartilage, however compared to native cartilage they lacked in mechanical properties (14, 15). Over time there has been additional focus on the biomechanical properties and cell-matrix/scaffold properties. The biomechanical forces being replicated in cartilage engineering include shear, tension, and compression which are endured in day to day activity within native joints (16).

3D bioprinting has emerged as a new technique to overcome some of the difficulties encountered in standard tissue engineering strategies, thanks to its speed, reliability, and precision (17). With respect to cartilage regeneration, the potential superiority of 3D bioprinting is in the ability to provide an efficient and tailored approach in the treatment of unique defect patterns.

Cartilage engineering-based techniques would be indicated in those with pure chondral lesions. If stem cells are used for such a repair approach, then any size of isolated chondral injury can be repaired due to the high replicative ability of these cells, meaning an abundant cell number can be obtained with expansion. With research progression osteochondral defects could theoretically be repaired by building distinct layers with cells differentiated into cartilage or bone.

Cells–Barriers

Many different cell lineages of various potencies and sources (**Figure 3**) have been studied; advantages and disadvantages of the types are outlined in **Table 1**. Mesenchymal stem cells (MSC) have emerged as a major line with respect to cartilage engineering and show excellent chondrogenic potential (18, 19).

Abbreviations: 3D, Three dimensional; ACI, Autologous Chondrocyte Implantation; MACI, Matrix-induced Autologous Chondrocyte Implantation; MSC, Mesenchymal Stem Cell; TGF, Transforming Growth Factor; BMP, Bone Morphogenetic Protein.

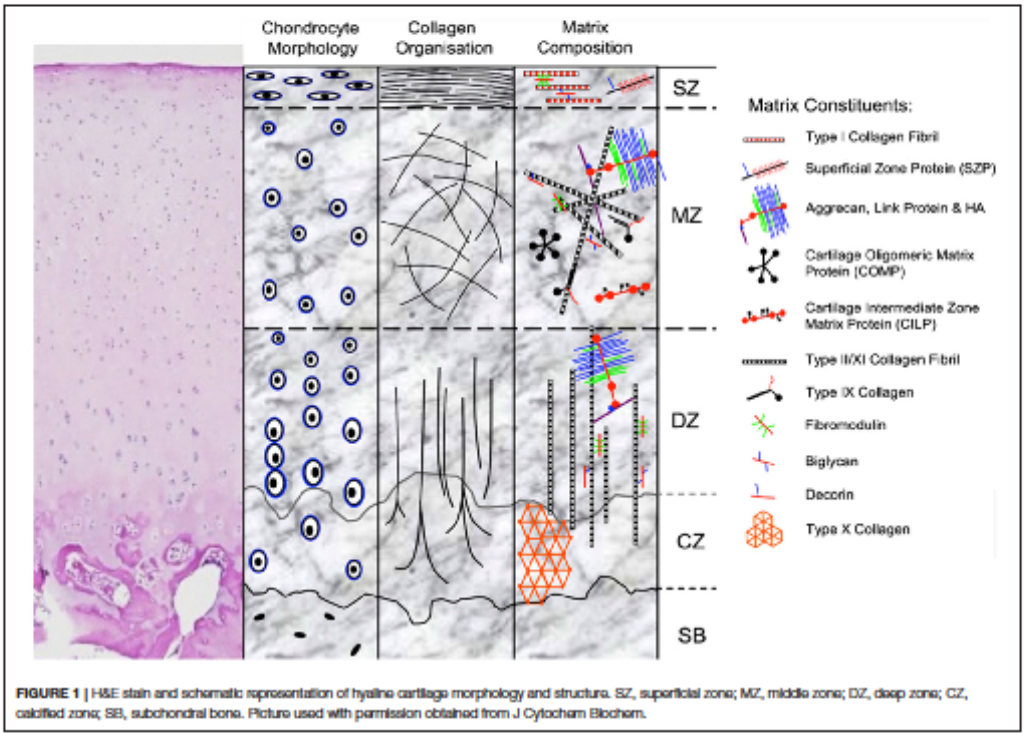


FIGURE 1 | H&E stain and schematic representation of hyaline cartilage morphology and structure. SZ, superficial zone; MZ, middle zone; DZ, deep zone; CZ, calcified zone; SB, subchondral bone. Picture used with permission obtained from J Cytochem Biochem.

The optimal tissue sources for harvesting MSCs has traditionally been the bone marrow and adipose tissue, due to easier access and the amount of tissue available. Adipose derived MSCs has been shown to produce superior chondrogenic differentiation when compared to bone marrow derived MSCs (20, 21), furthermore, more MSCs can be isolated per tissue volume when using adipose compared to bone. Abdominal subcutaneous tissue and the infrapatellar fat pad (IFP) are the most commonly used adipose tissue harvest sites for MSC isolation. Although abdominal subcutaneous fat is more abundant, IFP tissue has been shown to be more superior with respect to chondrogenic potential (22).

Irrespective of final cell choice and source there are several key barriers that need to be addressed for clinical translation using cell-based cartilage engineering.

Concerns Around *in-vitro* Lab-Based Cell Expansion

Cell expansion systems are timely and currently require *in-vitro* lab-based cell culture. This opens up concerns with respect to lab sterility, ethics, and risks associated with the use of animal serum-based media products (23–26). Development of a rapid isolation approach may allow avoidance of any *in-vitro* lab-based cell culture if enough cells can be isolated and implanted directly in theater (27, 28), eliminating concerns surrounding sterility and limiting the exposure to animal serum-based media.

Irrespective of isolation timeframes it will be critical to establish protocols for cell culture without animal serum-based media products in view of human clinical translation. The development of animal serum-free culture media using human derived growth supplements for MSC expansion, such as human platelet lysates (29–33) presents a promising solution. Furthermore, development of animal and human serum-free culture media for the expansion of MSC toward clinical applications is another promising strategy (34–36).

How Many Cells Are Needed Based on Defect Size?

Cell-free cartilage repair techniques such as microfracture are based primarily on lesion thickness (37, 38). Current cell implantation techniques such as ACI and MACI use an expanded number of chondrocytes based on either surgeon preference or rough physiological cartilage cell counts with preference leaning toward higher than normal cell densities (39). The use of higher chondrocyte densities *in-vitro* can inhibit matrix synthesis leading to reduced ECM production (40, 41), whilst using lower densities will not produce enough ECM *in-vitro* (42, 43). Only a few *in-vivo* and *in-vitro* studies report cell densities used and

the use of higher cell densities has not been shown to be superior to lower densities, therefore, no optimal clinical cell density has been identified (39).

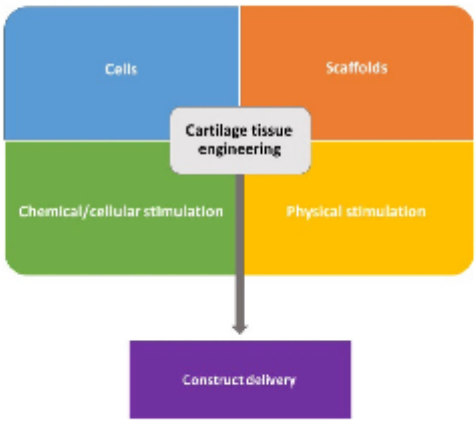


FIGURE 2 | General components used in cartilage tissue engineering.

There is no data on the desired stem cell density in the literature, with research groups tending to use cell counts based on anatomical human data which shows roughly 1×10^4 chondrocytes in 1 mm^3 of tissue (44). Stem cells have a higher proliferate ability compared to chondrocytes (45), therefore, use of chondrocyte based cell numbers with stem cells will not be an accurate measure of the optimal cell density needed at time of repair. It will be imperative to investigate the optimal cell density per defect volume when using stem cells and taking into consideration other factors such as the matrix type and volumes used.

Scaffold Materials–Barriers

The vast majority of cartilage tissue engineering techniques use scaffolds, which help support and create 3D structures of the cellular matrix. Successful scaffold designs optimize certain requirements (46–48) including; biocompatibility, environment, toxicity, degradation rate, pore size, pore geometry, and scaffold stiffness.

Scaffolds can be classified as natural polymers, synthetic polymers, or a hybrid. In cartilage engineering softer polymers, which can initially fill in defects and then solidify at later stages, are the bio-scaffolds that show most promise for clinical application due to their ability to fill complex morphologies which present at the time of surgical repair (49). Soft polymers such as hydrogels have biomimetic properties similar to soft

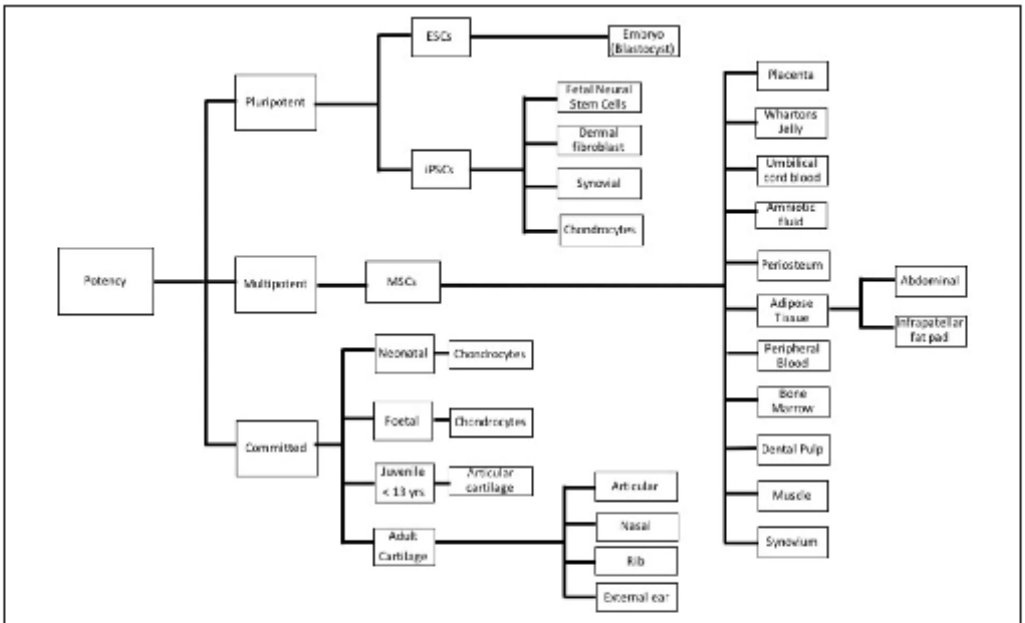


FIGURE 3 | Different cell types used in cartilage tissue engineering based on potency. ESC, Embryonic stem cell; IPSC, Induced pluripotent stem cell; and MSC, Mesenchymal stem cell.

TABLE 1 | Advantages and disadvantages of different cell potencies that have been used in cartilage tissue engineering.

Potency	Types	Advantages	Disadvantages
Pluripotent stem cells	ESCs	Indefinite self-renewal Multiple cell/tissue lineages	Ethical concerns Tumorigenicity Immune rejection
	IPSCs	Autologous Indefinite self-renewal	Tumorigenicity Cellular reprogramming
Mesenchymal stem cells	–	Autologous Abundant Easily accessible/harvested	Donor site morbidity
Chondrocytes	Fetal	Low immunogenicity	Limited availability
	Neonatal	Low immunogenicity	Limited availability
	Juvenile	Low immunogenicity	Limited availability
	Adult	Autologous	Limited availability Donor site morbidity De-differentiation

ESC, Embryonic stem cell; IPSC, Induced pluripotent stem cells.

tissue (50), however, at their starting point, i.e., liquid phase, hydrogels have relatively poor mechanical stability, which represents a limitation of their use in this state (51).

Can Hydrogels Provide Biomimetic Mechanical Strength?

Normally hydrogels are printed in a liquid state, which can then solidify after a phase transformation induced by chemical or non-chemical reactions. Cross-linking can be undertaken via photo, thermal or chemical induction (52). This process allows molecules to crosslink and provides increased mechanical stability to the tissue (53, 54).

Over time tunable hydrogel composites have been formulated which can be tweaked to enhance the mechanical properties of the material (55–57) and allow vertical construction of a 3D shape which was another initial limitation of hydrogel use (57). However, each addition or modification that is made can interact and effect the biocompatibility and therefore needs to be thoroughly tested.

Can Cross-Linking of the Scaffold Be Incorporated Intraoperatively?

Cross linking can be performed prior to implantation, meaning the engineered construct is made on a bench then implanted separately. This will prevent normal human tissue from being affected directly by cross-linking reactions and the sources used. To date, most *in-vivo* animal models have utilized bench-based formation of cross-linked pre-formed cartilage tissue, with subsequent implantation into simple non-complex defect morphologies which are man-made at time of surgery (58–60).

However, as mentioned earlier implanting pre-formed tissue will be difficult due to the complexity associated with cartilage defect morphology and therefore if at time surgical printing is preferred then the ability to cross link needs to be performed during surgery also leading to the issue of safe intraoperative cross-linking.

A recent pilot study (61) showed an intraoperative direct hand-held repair technique in a sheep model where tissue was formed and cross-linked directly into a defect at time of repair, thus avoiding any pre-printed bench-based tissue engineering techniques. In this study an ultraviolet light was used to cross link the hydrogel material which was preloaded with a photo initiating material, the light source was used as a separate component to the hand-held bioprinter. Macroscopically the use of the light source didn't affect surrounding healthy tissue. This study also used simple man-made defects and therefore doesn't confirm the ability to directly bio-print engineered cartilage into complex morphologies, however, if validated with more complex lesion patterns provides a more suitable option compared to implanting pre-formed cartilage tissue.

In future studies it will be ideal to directly add such a source to a hand-held printing device limiting the need for additional components and complexity to the surgical approach.

Chondrogenic Stimulation–Barriers

Molecules including growth factors and soluble non-protein chemical compounds chemically regulate cell behavior. Molecules bind to surface receptors on stem cells to activate intracellular signal pathways controlling cellular proliferation, differentiation, and synthesis. Mesenchymal stem cells have an important paracrine effect on cartilage formation and promoting an anti-inflammatory environment (62, 63).

Many combinations such as transforming growth factor (TGF) beta-3 with bone morphogenetic protein (BMP) 2 have induced chondrogenesis in adult stem cell use (64). Irrespective of the combination used, during *in-vitro* experimentation chemical stimulants can be provided (via culture media) periodically, producing consistent chondrogenic differentiation.

However, regular delivery and monitoring of stimulation can't be translated into an *in-vivo* setting as the native knee synovium must take over nutritional control. The native synovium in an adult is not catered to newly growing cartilage, meaning the desired growth factors and respective concentrations provided in *in-vitro* studies will not be present *in-vivo*, therefore, synovial take-over of nutritional regulation becomes an unknown obstacle in the way of human clinical trials.

Can Engineered Cartilage Tissue Be Maintained in the Body in the Long Term?

With a view of translating tissue engineered cartilage into the human knee, a major barrier will be with the formation of reliable and consistent chondrogenic tissue over time. Human blood supply will have growth factors and chemical stimulants that can assist with chondrogenic stimulation, however, highest activity is during fetal/young stages of life with increasing age associated with less stimulation and organization of chondrocytes and extracellular matrix (65). Therefore, theoretically if engineered tissue (composed of newly forming cartilage cells from a stem cell base) is used in adolescent cartilage repair we have no certainty of cellular control and regulation *in-vivo*.

Short term results are promising with respect to the use of cartilage tissue engineering methods in an *in-vivo* animal model (58, 59, 61). However, no mid/long-term (>12 weeks) *in-vivo* animal studies using cartilage tissue engineering and 3D bioprinting methods have been performed, therefore, no superiority compared to current clinical techniques such as microfracture and ACI can be ascertained. Mid/long-term *in-vivo* animal studies using tissue engineering techniques will be crucial in validating the ability of the native synovium in nourishing and maintaining engineered cartilage over large periods of time, this data will be pivotal to obtain prior to any progression to human clinical trials.

Physical/Environmental Stimulation–Barriers

With respect to mechanical and environmental stimulation, if tissue is to be printed directly *in-vivo* then native forces encountered by the knee in conjunction with synovial nourishment should directly take over adequate stimulation. Therefore, with an approach avoiding lab-based tissue growth there is no major concern with the ability to mimic the environment of the human knee.

The replication and delivery of such an environment is only important when trying to maintain a bench based *in-vitro* model of repair research where a bio-printed piece of tissue is maintained in a lab for *in-vitro* investigation or for *in-vivo* models using pre-formed tissue which is maintained in a lab then implanted at a later date. In these studies, tissue will need to be maintained as close to the native *in-vivo* environment as possible whilst in the lab. Therefore, ideally these cartilage constructs should be exposed to the different types of mechanical forces encountered by the native knee, such as shear stress, perfusion, hydrostatic pressure, and compression (16, 66).

Recreating the Properties of the Human Knee in a 3D Culture Environment–3D Bioreactors

Well-designed bioreactor systems can provide stimulation in one consistent and regular setting therefore providing a culture environment that promotes cartilage growth (67).

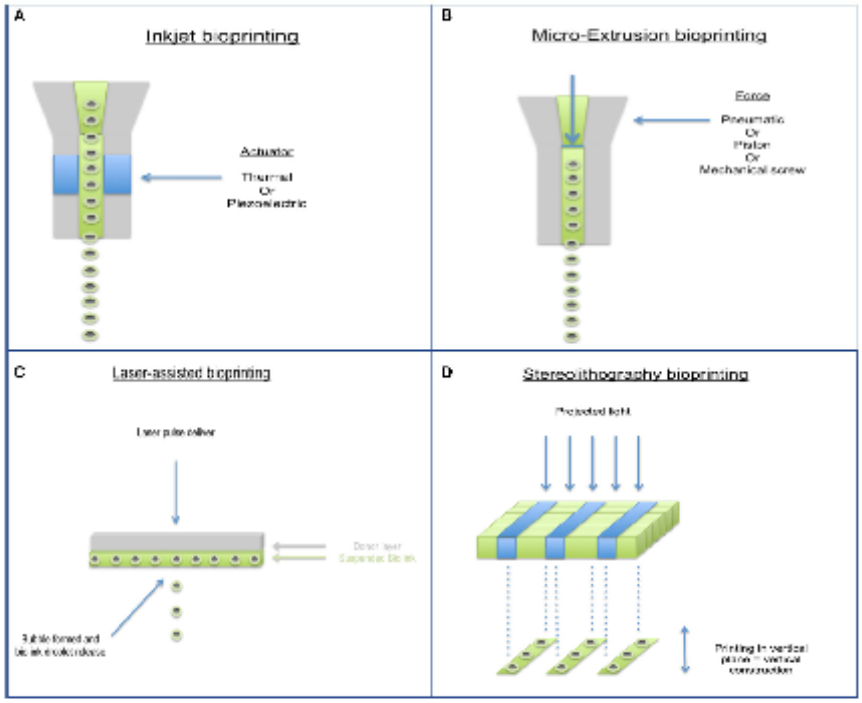


FIGURE 4 | Different types of 3D Bioprinting methods. **(A)** Inkjet bioprinter, **(B)** Micro-extrusion bioprinter, **(C)** Laser-assisted bioprinter, and **(D)** Stereolithography bioprinter.

Single stimulation bioreactor environments

Induction of shear force to promote cartilage growth has been demonstrated using rotating vessels (68–70), spinner flasks (71, 72), and stirred double chambers (73). Induction of perfusion to promote cartilage growth has been demonstrated using fluid perfusion bioreactor systems either using a unidirectional (74) or a bidirectional (75) bioreactor. Induction of hydrostatic pressure to promote cartilage growth has been demonstrated using fluid filled chambers with water pumps (76, 77). Induction of compression to promote cartilage growth has been widely demonstrated (78).

TABLE 2 | Characteristics and disadvantages of the different 3D Bioprinting methods.

Bioprinter type	Cell viability %	Resolution	Speed	Disadvantages
Inkjet	80–90	High	Fast	Clogging of head Settling effect of bio ink
Micro extrusion	<80	Moderate	Slow	Large mechanical stressors
Laser assisted	>90	High	Medium	Expensive Immature field Unknown effects of laser on cells
Stereolithography	>85	High	Fast	Limited compatibility with liquid/gel biomaterials



FIGURE 5 | Intra-operative photograph of the Biopen in action in a sheep model. [Modified from and used with permission from Di Bella et al. (81), under CC BL].

Bioreactors for inducing multiple/combined mechanical force

Bioreactors applying multiple mechanical properties are currently being developed. One study combining intermittent unconfined shear and compressive loading for 2.5 weeks showed increase in glycosaminoglycan and collagen type II production in human chondrocytes by 5.3- and 10-fold, respectively, after simultaneous stimulation (74).

More development is warranted into the application of multiple mechanical forces within bioreactor systems with respect to *in-vitro* cartilage tissue engineering.

Construct Delivery—Barriers

Modern advancement in 3D bioprinting technology opens up novel techniques with respect to the delivery of engineered human tissue. As mentioned earlier with respect to cartilage tissue engineering the ideal materials for printing are hydrogels given their ability to accommodate complex morphologies (49). With respect to 3D bioprinting of engineered cartilage tissue the ideal printing device would need to be small, portable, and operator friendly to allow for direct intraoperative printing into defects.

Bioprinting has largely come about to combat the limitations of past tissue engineering methods and allows for accurate control of cell distribution, production of biomimetic geometry, and rapid production of construct (79, 80). With respect to cartilage tissue repair, it is impossible to accurately characterize defects even with current advances in medical imaging, therefore bioprinting techniques in this field need to be focused more on flexibility rather than computer aided precision. Several different types of bioprinters have been developed (**Figure 4**), characteristics and disadvantages of each type are shown in **Table 2**. Hand-held bioprinting used in conjunction with hydrogels are best suited to achieve this as they can plug defects of any nature easily like using a glue stick/gel, avoiding the need for large and heavy machinery in the operating theater (81).

The most suitable mechanism to fit a portable hand-held type device would be extrusion printing given the compactable nature of the mechanism, an example of this is the "bio pen" which uses pneumatic extrusion-based technology to allow printing of hydrogels (82), **Figure 5** shows the intraoperative use of the bio pen in an sheep model. This device can be loaded with two cartridges allowing for a co-axial based printing method (**Figures 6A–D**) which can concentrate cells in the middle core with an outer hydrogel shell layer that can be crosslinked and protect the inner cellular tissue (83).

Engineered tissue using a portable hand-held device can be printed directly during surgery on the spot with the top of the construct being immediately crosslinked using methods mentioned earlier. This approach allows for implant stability within the lesion (61). However, when using non-portable printers and non-hydrogel-based scaffolds/materials the formed implant will need to be manually positioned (requires precise geometry when initially created) into the lesion and then anchored with either sutures or a flap approach.

In-vivo animal delivery of engineered cartilage tissue has been performed to-date using large incisions over the knee, similar to those made in conventional knee replacement surgeries

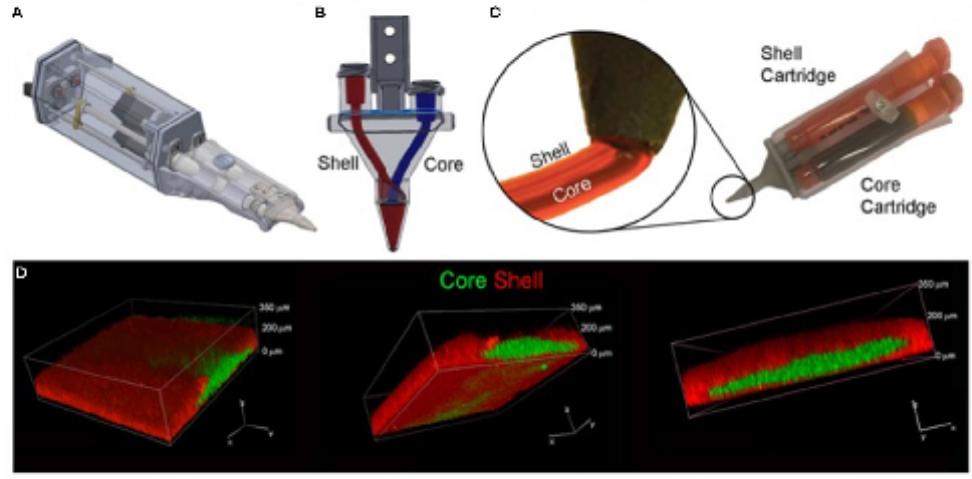


FIGURE 6 | Core/Shell 3D printing by co-axial extrusion. **(A)** Schematic representation of the 3D co-axial handheld printer. **(B)** Schematic representation of the co-axial nozzle. **(C)** Picture of the cartridges dedicated to Core and Shell loading in the printer, with relative magnification of the nozzle during co-axial deposition. **(D)** Representative 3D rendered confocal images of Core/Shell printed sample labeled with fluorescent beads. The hydrogel shell is shown in red channel, while the cellular/hydrogel core is shown in green channel. The panel shows the same image representative of 3D rendered of superimposed green and red channels in three different orientations. [Modified from and used with permission from Duchi et al. (83) under CC BL].

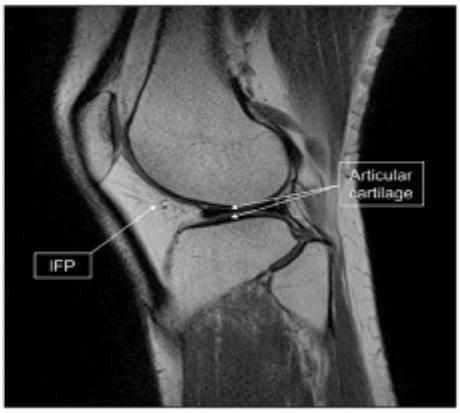


FIGURE 7 | Infrapatellar fat pad (IFP) location and harvested tissue. Sagittal magnetic resonance imaging scan of the knee showing the relationship of the IFP (arrow) to the articular cartilage (double arrow). [Modified from and used with permission from Hindle et al. (22) under CC BL].

(61, 84). Larger incisions, however, increase the risk of wound complications (e.g., infection and wound dehiscence) and reduce cosmetic satisfaction, both of which are important factors to consider in treatment of a young-middle aged population.

Can Engineered Cartilage Tissue Be Provided Using Less Risk Adverse Minimally Invasive Techniques?

Arthroscopic knee surgery (85) (key-hole surgery) can provide such a solution and is performed in a day surgery setting allowing patients to return to daily activity almost immediately. Technically speaking the desired bioprinting device would therefore be incorporated as an attachment into an arthroscopic kit, once again the most suited to this would be a small hand-held bioprinter. This microsurgical kit/device will need adequate valdiation and training prior to use.

If as mentioned earlier a rapid stem cell isolation can be established to fit within a surgical time frame (28) then this will open up the ability to harvest tissue, isolate stem cells then directly re-implant a cell/scaffold interface into knee joint in one single operation. Furthermore, if stem cells can be harvested from a source like the infrapatellar fat pad (IFP) (86) which is in close proximity to the knee joint (**Figure 7**) the operation can be performed using one surgical site. Arthroscopic harvest of the IFP for adipose-derived mesenchymal stem cells isolation has been performed successfully in a rabbit model (22).

Will the Delivered Construct Integrate Effectively With Host Tissue?

Another uncertainty is the ability of engineered cartilage tissue to integrate with healthy tissue. It is evident that superior cartilage repair can be achieved using a hand-held printing method, however both hand-held and bench-based printing methods can

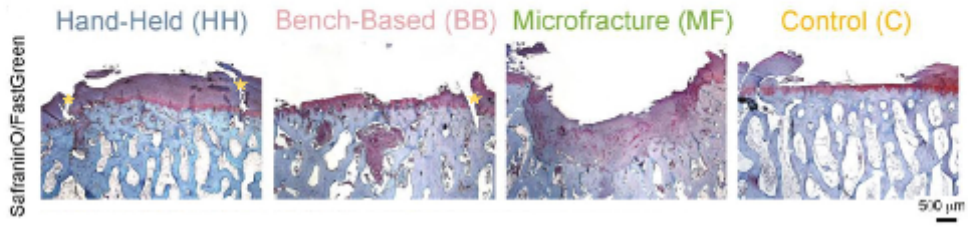


FIGURE 8 | Histology (Safranin/Fast green staining) showing better new cartilage formation in the HH group compared to the other groups. Subchondral cysts and collapse are seen in the BB and MF group, with fibrocartilage formation. Voids at the implanted/native tissue interfaces are seen in the HH and BB groups indicated by the yellow stars. HH, Hand held Biopen printed scaffold; BB, Bench Based 3D printed scaffold; MF, Microfractures; C, Negative Control (defect left empty). Voids at the implanted/native tissue interfaces are seen in the HH and BB groups. [Modified from and used with permission from Di Bella et al. (81), under CC BL].

produce the development of voids (**Figure 8**) between the edges of the implanted tissue and health native tissue (61).

A possible solution to overcome this would be to apply an initial coat of biocompatible adhesive (87) into the defect prior to implantation allowing better proximation of tissue. Subsequently it will be pivotal to investigate if such a method then allows interaction of the implanted tissue with the healthy tissue, this could be investigated adding tracking materials/dyes to the constructed tissue, and then assessing movement/integration at different time points (88, 89).

CONCLUSION–HUMAN CLINICAL TRANSLATION

Cartilage repair techniques using stem cells and 3D bioprinting technology still remains elusive with respect to human clinical translation. Many challenges remain to be addressed and overcome as described in this review. More focus on *in-vivo* animal studies will be essential to investigate many of these barriers. Whilst continued progress is made on such issues it is important to begin setting up larger scale *in-vivo* animal trials which will be the next step toward human clinical translation.

AUTHOR CONTRIBUTIONS

SF completed a literature search, contributed to the preparation of the manuscript, and critically revised the manuscript. CD, GW, and PC contributed ideas, content to the manuscript, and critically revised the manuscript.

ACKNOWLEDGMENTS

The cartilage research group is currently supported by funding from the Royal Australian College of Surgeons (RACS), The Australian Research Council Industrial Transformation Training Centre (ARC-ITTC) in Additive Biomanufacturing and the Medical Technologies and Pharmaceuticals (MTPConnect) BioMedTech Horizons program.

REFERENCES

1. Robertsson O, Stefánsdóttir A, Lidgren L, Ranstam J. Increased long-term mortality in patients less than 55 years old who have undergone knee replacement for osteoarthritis: results from the swedish knee arthroplasty register. *J Bone Joint Surg.* (2007) 89:599–603. doi: 10.1302/0301-620X.89B5.18355
2. Julin J, Jämsen E, Puolakka T, Konttinen YT, Moilanen T. Younger age increases the risk of early prosthesis failure following primary total knee replacement for osteoarthritis: a follow-up study of 32,019 total knee replacements in the Finnish Arthroplasty Register. *Acta Ortho Scand.* (2010) 81:413–9. doi: 10.3109/17453674.2010.501747
3. Redman SN, Oldfield SF, Archer CW. Current strategies for articular cartilage repair. *Eur Cell Mater.* (2005) 9:23–32. doi: 10.22203/eCM.v009a04
4. Fox SA, Bedi A, Rodeo SA. The basic science of articular cartilage: structure, composition, and function. *Sports Health* (2009) 1:461–8. doi: 10.1177/1941738109350438
5. Hunter W. On the structure and diseases of articulating cartilage. *Phil Trans R Soc.* (1743) 42B:514–21.
6. Steadman Jr, Briggs KK, Rodrigo JJ. The microfracture technic in the management of complete cartilage defects in the knee joint. *Orthopade* (1999) 28:26–32.
7. Brittberg M, Lindahl A, Nilsson A, Ohlsson C, Isaksson O, Peterson L. Treatment of deep cartilage defects in the knee with autologous chondrocyte transplantation. *N Engl J Med.* (1994) 331:889–95. doi: 10.1056/NEJM199410063311401
8. Frenceschi F, Longo UG, Ruzzini L, Marinozzi A, Maffulli N, Denaro V. Simultaneous arthroscopic implantation of autologous chondrocytes and high tibial osteotomy for tibial chondral defects in the varus knee. *Knee* (2008) 15:309–13. doi: 10.1016/j.knee.2008.04.007
9. Knutsen G, Drogset JO, Engebretsen L, Grontvedt T, Isaksen V, Ludvigsen TC, et al. A randomized trial comparing autologous chondrocyte implantation with microfracture. Findings at five years. *J Bone Joint Surg Am.* (2007) 89:2105–12. doi: 10.2106/JBJS.G.00003
10. Bartlett W, Skinner JA, Gooding CR, Carrington RW, Flanagan AM, Briggs TW, et al. Autologous chondrocyte implantation versus matrix-induced autologous chondrocyte implantation for osteochondral defects of the knee:

a prospective, randomised study. *J Bone Joint Surg Br.* (2005) 87:640–5. doi: 10.1302/0301-620X.87B5.15905
11. Kreuz PCSMR, Erggelet C, Krause SJ, Konrad G, Uhl M, Südkamp N. Results after microfracture of full-thickness chondral defects in different compartments in the knee. *Osteoarthritis Cartilage* (2006) 14:119–25. doi: 10.1016/j.joca.2006.05.003
12. Steadman JR, Briggs KK, Rodrigo JJ, Rodkey WG. Outcomes of microfracture for traumatic chondral defects of the knee: average 11-year follow-up. Arthroscopy. *J Arthroscopic Relat Surg.* (2003) 19:477–84. doi: 10.1053/jars.2003.50112
13. Giannoudis PV, Einhorn TA, Marsh D. Fracture healing: the diamond concept1. *Injury* (2007) 38(Suppl. 4):S3–6. doi: 10.1016/S0020-1383(08)70003-2
14. Grad S, Eglin D, Alini M, Stoddart MJ. Physical stimulation of chondrogenic cells *in vitro*: a review. *Clin Orthop Relat Res.* (2011) 469:2764–72. doi: 10.1007/s11999-011-1819-9
15. Schulz RM, Bader A. Cartilage tissue engineering and bioreactor systems for the cultivation and stimulation of chondrocytes. *Eur Biophys J.* (2007) 36:539–68. doi: 10.1007/s00249-007-0139-1
16. Lai JH Levenston ME. Meniscus and cartilage exhibit distinct intra-tissue strain distributions under unconfined compression. *Osteoarthritis Cartilage* (2010) 18:1291–9. doi: 10.1016/j.joca.2010.05.020
17. Mandrycky C, Wang Z, Kim K, Kim DH. 3D bioprinting for engineering complex tissues. *Biotechnol Adv.* (2016) 34:422–34. doi: 10.1016/j.biotechadv.2015.12.011
18. Ronziere MC, Perrier E, Mallein-Gerin F, Freyria AM. Chondrogenic potential of bone marrow- and adipose tissue-derived adult human mesenchymal stem cells. *Biomed Mater Eng.* (2010) 20:145–58. doi: 10.3233/BME-2010-0626
19. Rada T, Reis RL, Gomes ME. Adipose tissue-derived stem cells and their application in bone and cartilage tissue engineering. *Tissue Eng.* (2009) 15:113–25. doi: 10.1089/ten.teb.2008.0423
20. Strioga M, Viswanathan S, Darinskas A, Slaby O, Michalek J. Same or not the same? comparison of adipose tissue-derived versus bone marrow-derived mesenchymal stem and stromal cells. *Stem Cells Dev.* (2012) 21:2724–52. doi: 10.1089/scd.2011.0722
21. Jang Y Koh YG, Choi YJ, Kim SH, Yoon DS, Lee M, et al. Characterization of adipose tissue-derived stromal vascular fraction for clinical application to cartilage regeneration. *In Vitro Cell Dev Biol Anim.* (2015) 51:142–50. doi: 10.1007/s11626-014-9814-6
22. Hindle P, Khan N, Biant L, Péault B. The infrapatellar fat pad as a source of perivascular stem cells with increased chondrogenic potential for regenerative medicine. *Stem Cells Transl Med.* (2017) 6:77–87. doi: 10.5966/sctm.2016-0040
23. Herberts CA Kwa MSG, Hermsen HP. Risk factors in the development of stem cell therapy. *J Transl Med.* (2011) 9:29. doi: 10.1186/1479-5876-9-29
24. Halme DG, Kessler DA. FDA regulation of stem-cell-based therapies. *N Engl J Med.* (2006) 355:1730–5. doi: 10.1056/NEJMhpr063086
25. Heiskanen A, Satomaa T, Tiitinen S, Laitinen A, Mannelin S, Impola U, et al. N-glycolylneuraminic acid xenoantigen contamination of human embryonic and mesenchymal stem cells is substantially reversible. *Stem Cells* (2007) 25:197–202. doi: 10.1634/stemcells.2006-0444
26. Shih DT, Burnouf T. Preparation, quality criteria, and properties of human blood platelet lysate supplements for *ex vivo* stem cell expansion. *N Biotechnol.* (2015) 32:199–211. doi: 10.1016/j.nbt.2014.06.001
27. .Francis MP, Sachs PC, Elmore LW, Holt SE. Isolating adipose-derived mesenchymal stem cells from lipoaspirate blood and saline fraction. *Organogenesis* (2010) 6:11–4. doi: 10.4161/org.6.1.10019
28. Francis SL, Duchi S, Onofrillo C, Di Bella C, Choong PFM. Adipose-derived mesenchymal stem cells in the use of cartilage tissue engineering: the need for a rapid isolation procedure. *Stem Cells Int.* (2018) 2018:8947548. doi: 10.1155/2018/8947548
29. Hemeda H, Giebel B, Wagner W. Evaluation of human platelet lysate versus fetal bovine serum for culture of mesenchymal stromal cells. *Cytotherapy* (2014) 16:170–80. doi: 10.1016/j.jcyt.2013.11.004
30. Bieback K, Hecker A, Kocaömer A, Lannert H, Schallmoser K, Strunk D, et al. Human alternatives to fetal bovine serum for the expansion of mesenchymal stromal cells from bone marrow. *Stem Cells* (2009) 27:2331–41. doi: 10.1002/stem.139
31. Crespo-Diaz R, Behfar A, Butler GW, Padley DJ, Sarr MG, Bartunek J, et al. Platelet lysate consisting of a natural repair proteome supports human mesenchymal stem cell proliferation and chromosomal stability. *Cell Trans.* (2011) 20:797–812. doi: 10.3727/096368910X543376
32. Schallmoser K, Strunk D. Preparation of pooled human platelet lysate (pHPL) as an efficient supplement for animal serum-free human stem cell cultures. *J Vis Exp.* (2009) 32:1523. doi: 10.3791/1523
33. Walenda G, Hemeda H, Schneider RK, Merkel R, Hoffmann B, Wagner W. Human platelet lysate gel provides a novel three dimensional-matrix for enhanced culture expansion of mesenchymal stromal cells. *Tissue Eng Part C* (2012) 18:924–34. doi: 10.1089/ten.tec.2011.0541
34. Chase LG, Lakshmipathy U, Solchaga LA, Rao MS, Vemuri MC. A novel serum-free medium for the expansion of human mesenchymal stem cells. *Stem Cell Res Ther.* (2010) 1:8. doi: 10.1186/scrt8
35. Lindroos B, Boucher S, Chase L, Kuokkanen H, Huhtala H, Haataja R., et al. Serum-free, xeno-free culture media maintain the proliferation rate and multipotentiality of adipose stem cells *in vitro*. *Cytotherapy* (2009) 11:958–72. doi: 10.3109/14653240903233081
36. Patrikoski M, Juntunen M, Boucher S, Campbell A, Vemuri MC, Mannerström B, et al. Development of fully defined xeno-free culture system for the preparation and propagation of cell therapy-compliant human adipose stem cells. *Stem Cell Res Ther.* (2013) 4:27. doi: 10.1186/scrt175
37. Steadman JR, Rodkey WG, Briggs KK, (eds.). Microfracture: its history and experience of the developing surgeon. *Cartilage* (2010) 1:78–86. doi: 10.1177/1947603510365533
38. Williams RJ, Hamly HW III. Microfracture: indications, technique, and results. *Instr Course Lect. Am. Acad. Orthop. Surg.* (2007) 56:419–28.
39. Foldager CB, Gomoll AH, Lind M, Spector M. Cell seeding densities in autologous chondrocyte implantation techniques for cartilage repair. *Cartilage* (2012) 3:108–17. doi: 10.1177/1947603511435522
40. Abbott J, Holtzer H. The loss of phenotypic traits by differentiated cells. 3. The reversible behavior of chondrocytes in primary cultures. *J Cell Biol.* (1966) 28:473–87. doi: 10.1083/jcb.28.3.473
41. Bernstein P, Dong M, Graupner S, Corbeil D, Gelinsky M, Günther KP, et al. Sox9 expression of alginate-encapsulated chondrocytes is stimulated by low cell density. *J Biomed Mater Res A* (2009) 91A:910–9. doi: 10.1002/jbm.a.32308
42. Handley CJ, Bateman JF, Oakes BW, Lowther DA. Characterization of the collagen synthesized by cultured cartilage cells. *Biochim Biophys Acta* (1975) 386:444–50. doi: 10.1016/0005-2795(75)90287-1
43. Francioli SE, Candrian C, Martin K, Heberer M, Martin I, Barbero A. Effect of three-dimensional expansion and cell seeding density on the cartilage-forming capacity of human articular chondrocytes in type II collagen sponges. *J Biomed Mater Res A* (2010) 95A:924–31. doi: 10.1002/jbm.a.32917
44. Hunziker EB, Quinn TM, Häuselmann HJ. Quantitative structural organization of normal adult human articular cartilage. *Osteoarthritis Cartilage* (2002) 10:564–72. doi: 10.1053/joca.2002.0814
45. Mobasheri A, Kalamegam G, Musumeci G, Batt ME. Chondrocyte and mesenchymal stem cell-based therapies for cartilage repair in osteoarthritis and related orthopaedic conditions. *Maturitas* (2014) 78:188–98. doi: 10.1016/j.maturitas.2014.04.017
46. Stoop R. Smart biomaterials for tissue engineering of cartilage. *Injury* (2008) 39:S77–87. doi: 10.1016/j.injury.2008.01.036
47. Nava MM, Draghi L, Giordano C, Pietrabissa R. The effect of scaffold pore size in cartilage tissue engineering. *J Appl Biomater Funct Mater.* (2016) 14:e223–9. doi: 10.5301/jabfm.5000302
48. Arora A, Kothari A, Katti DS. Pore orientation mediated control of mechanical behavior of scaffolds and its application in cartilage-mimetic scaffold design. *J Mech Behav Biomed Mater.* (2015) 51:169–83. doi: 10.1016/j.jmbbm.2015.06.033

49. Kim IL, Mauck RL, Burdick JA. Hydrogel design for cartilage tissue engineering: a case study with hyaluronic acid. *Biomaterials* (2011) 32:8771–82. doi: 10.1016/j.biomaterials.2011.08.073
50. Peppas NA, Kavimandan NJ. Nanoscale analysis of protein and peptide absorption: insulin absorption using complexation and pH-sensitive hydrogels as delivery vehicles. *Eur J Pharm Sci.* (2005) 29:183–97. doi: 10.1016/j.ejps.2006.04.014
51. Drury JL, Mooney DJ. Hydrogels for tissue engineering: scaffold design variables and applications. *Biomaterials* (2003) 24:4337–51. doi: 10.1016/S0142-9612(03)00340-5
52. Drury JL, Mooney DJ. The effects of crosslinking of scaffolds engineered from cartilage ECM on the chondrogenic differentiation of MSCs. *Biomaterials* (2013) 34:5802–12. doi: 10.1016/j.biomaterials.2013.04.027
53. Chen YC, Chen M, Gaffney EA, Brown CP. Effect of crosslinking in cartilage-like collagen microstructures. *J Mech Behav Biomed Mater.* (2017) 66:138–43. doi: 10.1016/j.jmbbm.2016.10.006
54. D'Este M, Eglin D. Hydrogels in calcium phosphate moldable and injectable bone substitutes: sticky excipients or advanced 3-D carriers. *Acta Biomater.* (2013) 9:5421–30. doi: 10.1016/j.actbio.2012.11.022
55. Huang CC, Ravindran S, Yin Z, George A. 3-D self-assembling leucine zipper hydrogel with tunable properties for tissue engineering. *Biomaterials* (2014) 35:5316–26. doi: 10.1016/j.biomaterials.2014.03.035
56. Fathi A, Mithieux SM, Wei H, Chrzanowski W, Valtchev P, Weiss AS, et al. Elastin based cell-laden injectable hydrogels with tunable gelation, mechanical and biodegradation properties. Elastin based cell-laden injectable hydrogels with tunable gelation, mechanical and biodegradation properties. *Biomaterials* (2014) 35:5425–35. doi: 10.1016/j.biomaterials.2014.03.026
57. Discher DE, Janmey P, Wang Y-L. Tissue cells feel and respond to the stiffness of their substrate. *Science* (2005) 310:1139–43. doi: 10.1126/science.1116995
58. Guo X, Park H, Young S, Kretlow JD, van den Beucken JJ, Baggett LS, et al. Repair of osteochondral defects with biodegradable hydrogel composites encapsulating marrow mesenchymal stem cells in a rabbit model. *Acta Biomater.* (2010) 6:39–47. doi: 10.1016/j.actbio.2009.07.041
59. Nehrer S, Breinan HA, Ramappa A, Hsu HP, Minas T, Shortkroff S, et al. Chondrocyte-seeded collagen matrices implanted in a chondral defect in a canine model. *Biomaterials* (1998) 19:2313–28. doi: 10.1016/S0142-9612(98)00143-4
60. Nehrer S, Breinan HA, Ramappa A, Hsu HP, Minas T, Shortkroff S, et al. Evaluation of a hybrid scaffold/cell construct in repair of high-load-bearing osteochondral defects in rabbits. *Biomaterials* (2006) 27:1071–80. doi: 10.1016/j.biomaterials.2005.07.040
61. Di Bella C, Duchi S, O'Connell CD, Blanchard R, Augustine C, Yue Z, et al. *In situ* handheld three-dimensional bioprinting for cartilage regeneration. *J Tissue Eng Regen Med.* (2018) 12:611–21. doi: 10.1002/term.2476
62. van Buul GM, Villafuertes E, Bos PK, Waarsing JH, Kops N, Narcisi R, et al. Mesenchymal stem cells secrete factors that inhibit inflammatory processes in short-term osteoarthritic synovium and cartilage explant culture. *Osteoarthritis Cartilage* (2012) 20:1186–96. doi: 10.1016/j.joca.2012.06.003
63. Linero I, Chaparro O. Paracrine effect of mesenchymal stem cells derived from human adipose tissue in bone regeneration. *PLoS ONE* (2014) 9:e107001. doi: 10.1371/journal.pone.0107001
64. Sekiya I, Larson BL, Vuoristo JT, Reger RL, Prockop DJ. Comparison of effect of BMP-2,–4, and–6 on *in vitro* cartilage formation of human adult stem cells from bone marrow stroma. *Cell Tissue Res.* (2005) 320:269–76. doi: 10.1007/s00441-004-1075-3
65. Hardingham T, Bayliss M. Proteoglycans of articular cartilage: changes in aging and in joint disease. *Semin Arthritis Rheum.* (1990) 20(3 Suppl. 1):12–33.
66. Zhao J, Griffin M, Cai J, Li S, Bulter PEM, Kalaskar DM. Bioreactors for tissue engineering: an update. *Biochem Eng J.* (2016) 109:268–81. doi: 10.1016/j.bej.2016.01.018
67. Griffin DJ, Vicari J, Buckley MR, Silverberg JL, Cohen I, Bonassar LJ. Effects of enzymatic treatments on the depth-dependent viscoelastic shear properties of articular cartilage. *J Orthop Res.* (2014) 32:1652–7. doi: 10.1002/jor.22713
68. Takebe T, Kobayashi S, Kan H, Suzuki H, Yabuki Y, Mizuno M, et al. Human elastic cartilage engineering from cartilage progenitor cells using rotating wall vessel bioreactor. *Transplant Proc.* (2012) 44:1158–61. doi: 10.1016/j.transproceed.2012.03.038
69. Marlovits S, Tichy B, Truppe M, Gruber D, Schlegel W. Collagen expression in tissue engineered cartilage of aged human articular chondrocytes in a rotating bioreactor. *Int J Artif Organs* (2003) 26:319–30. doi: 10.1177/039139880302600407
70. Ohyabu Y, Kida N, Kojima H, Taguchi T, Tanaka J, Uemura T. Cartilaginous tissue formation from bone marrow cells using rotating wall vessel (RWV) bioreactor. *Biotechnol Bioeng.* (2006) 95:1003–8. doi: 10.1002/bit.20892
71. Liu L, Wu W, Tuo X, Geng W, Zhao J, Wei J, et al. Novel strategy to engineer trachea cartilage graft with marrow mesenchymal stem cell macroaggregate and hydrolyzable scaffold. *Artif Organs* (2010) 34:426–33. doi: 10.1111/j.1525-1594.2009.00884.x
72. Khonsky DJ, Abdelmohsen K, Abe A, Abedin MJ, Abelovich H, Acevedo Arozena A, et al. Enhanced cartilage formation via three-dimensional cell engineering of human adipose-derived stem cells. *Tissue Eng A* (2012) 18:1949–56. doi: 10.1089/ten.TEA.2011.0647
73. Chang C-H, Lin F-H, Lin CC, Chou C-H, Liu H-C. Cartilage tissue engineering on the surface of a novel gelatin–calcium–phosphate biphasic scaffold in a double-chamber bioreactor. *Biomed Mater Res B Appl Biomater.* (2004) 71B:313–21. doi: 10.1002/jbm.b.30090
74. Santoro R, Olivares AL, Brans G, Wirz D, Longinotti C, Lacroix D, et al. Bioreactor based engineering of large-scale human cartilage grafts for joint resurfacing. *Biomaterials* (2010) 31:8946–52. doi: 10.1016/j.biomaterials.2010.08.009
75. Wendt D, Marsano A, Jakob M, Heberer M, Martin I. Oscillating perfusion of cell suspensions through three-dimensional scaffolds enhances cell seeding efficiency and uniformity. *Biotechnol Bioeng.* (2003) 84:205–14. doi: 10.1002/bit.10759
76. Candiani G, Raimondi MT, Aurora R, Lagana' K, Dubini G. Chondrocyte response to high regimens of cyclic hydrostatic pressure in 3-dimensional engineered constructs. *Int J Artif Organs* (2008) 31:690–9. doi: 10.1177/039139880803100604
77. Correia C, Pereira AL, Duarte AR, Frias AM, Pedro AJ, Oliveira JT. Dynamic culturing of cartilage tissue: the significance of hydrostatic pressure. *Tissue Eng Part A* (2012) 18:1979–91. doi: 10.1089/ten.TEA.2012.0083
78. Hoenig E, Winkler T, Mielke G, Paetzold H, Schuettler D, Goepfert C, et al. High amplitude direct compressive strain enhances mechanical properties of scaffold-free tissue-engineered cartilage. *Tissue Eng Part A* (2011) 17:1401–10. doi: 10.1089/ten.TEA.2010.0395
79. Murphy SV, Atala A. 3D bioprinting of tissues and organs. *Nat Biotechnol.* (2014) 32:773–85. doi: 10.1038/nbt.2958
80. Collins SF. Bioprinting is changing regenerative medicine forever. *Stem Cells Dev.* (2014) 23(Suppl. 1):79–82. doi: 10.1089/scd.2014.0322
81. Di Bella C, Fosang A, Donati DM, Wallace GG, Choong PF. 3D bioprinting of cartilage for orthopedic surgeons: reading between the lines. *Front Surg.* (2015) 2:39. doi: 10.3389/fsurg.2015.00039
82. O'Connell CD, Di Bella C, Thompson F, Augustine C, Beirne S, Cornock R, et al. Development of the Biopen: a handheld device for surgical printing of adipose stem cells at a chondral wound site. *Biofabrication* (2016) 8:015019. doi: 10.1088/1758-5090/8/1/015019
83. Duchi S, Onofrillo C, O'Connell CD, Blanchard R, Augustine C, Quigley AF, et al. Handheld co-axial bioprinting: application to *in situ* surgical cartilage repair. *Sci Rep.* (2017) 7:5837. doi: 10.1038/s41598-017-05699-x
84. Holland TA, Bodde EW, Cuijpers VM, Baggett LS, Tabata Y, Mikos AG, et al. Degradable hydrogel scaffolds for *in vivo* delivery of single and dual growth factors in cartilage repair. *Osteoarthritis Cartilage* (2007) 15:187–97. doi: 10.1016/j.joca.2006.07.006
85. Watanabe M. Memories of the early days of arthroscopy. *Arthroscopy* (1986) 2:209–14. doi: 10.1016/S0749-8063(86)80073-1
86. Dragoo JL, Samimi B, Zhu M, Hame SL, Thomas BJ, Lieberman JR, et al. Tissue-engineered cartilage and bone using stem cells from

human infrapatellar fat pads. *J Bone Joint Surg Br.* (2003) 85:740–7. doi: 10.1302/0301-620X.85B5.13587

87. Bhagat V, Becker ML. Degradable adhesives for surgery and tissue engineering. *Biomacromolecules* (2017) 18:3009–39. doi: 10.1021/acs.biomac.7b00969
88. Allen AB, Gazit Z, Su S, Stevens HY, Guldberg RE. *In vivo* bioluminescent tracking of mesenchymal stem cells within large hydrogel constructs. (2014) 20:806–16. doi: 10.1089/ten.TEC.2013.0587
89. Hachani R, Lowdell M, Birchall M, Thanh NT. Tracking stem cells in tissue-engineered organs using magnetic nanoparticles. *Nanoscale* (2013) 5:11362. doi: 10.1039/c3nr03861k

Conflict of Interest Statement: The authors declare that the research was conducted in the absence of any commercial or financial relationships that could be construed as a potential conflict of interest.

Copyright © 2018 Francis, Di Bella, Wallace and Choong. This is an open-access article distributed under the terms of the Creative Commons Attribution License (CC BY). The use, distribution or reproduction in other forums is permitted, provided the original author(s) and the copyright owner(s) are credited and that the original publication in this journal is cited, in accordance with accepted academic practice. No use, distribution or reproduction is permitted which does not comply with these terms.

APPENDIX 2: ADIPOSE-DERIVED MESENCHYMAL STEM CELLS IN THE USE OF CARTILAGE TISSUE ENGINEERING: THE NEED FOR A RAPID ISOLATION PROCEDURE

Hindawi
Stem Cells International
Volume 2018, Article ID 8947548, 9 pages
https://doi.org/10.1155/2018/8947548

Review Article

Adipose-Derived Mesenchymal Stem Cells in the Use of Cartilage Tissue Engineering: The Need for a Rapid Isolation Procedure

Sam L. Francis,[1,2] **Serena Duchi**,[1,2] **Carmine Onofrillo**,[1,2] **Claudia Di Bella**,[1,2] **and Peter F. M. Choong**[1,2]

[1]*Department of Surgery, The University of Melbourne, Melbourne, VIC, Australia*
[2]*Department of Orthopaedics, St. Vincent's Hospital, Melbourne, VIC, Australia*

Correspondence should be addressed to Sam L. Francis; sfrancis1@student.unimelb.edu.au

Received 19 December 2017; Accepted 1 March 2018; Published 3 April 2018

Academic Editor: Jianying Zhang

Copyright © 2018 Sam L. Francis et al. This is an open access article distributed under the Creative Commons Attribution License, which permits unrestricted use, distribution, and reproduction in any medium, provided the original work is properly cited.

Mesenchymal stem cells (MSCs) have shown much promise with respect to their use in cartilage tissue engineering. MSCs can be obtained from many different tissue sources. Among these, adipose tissue can provide an abundant source of adipose-derived mesenchymal stem cells (ADMSCs). The infrapatellar fat pad (IFP) is a promising source of ADMSCs with respect to producing a cartilage lineage. Cell isolation protocols to date are time-consuming and follow conservative approaches that rely on a long incubation period of 24–48 hours. The different types of ADMSC isolation techniques used for cartilage repair will be reviewed and compared with the view of developing a rapid one-step isolation protocol that can be applied in the context of a surgical procedure.

1. Introduction

Cartilage tissue engineering has become a major research interest in the past few decades, primarily due to the inability of native human cartilage to self-repair [1, 2]. There is no reliable long-term joint preserving management option for early onset arthritis secondary to cartilage defects, and this may potentially lead to joint replacement (arthroplasty) and associated short- and long-term risks and sequelae [3, 4]. Fibrocartilage formation is the major barrier in the long-term viability of currently used clinical methods and is detrimental to joint function [5, 6].

The diamond concept [7] embodies the 4 major strategies that underpin tissue engineering, namely, cells, scaffolds, growth factor/cytokines, and environmental stimulation.

This review will focus specifically on ADMSC isolation techniques and their efficiency with respect to driving cartilage formation.

Current isolation procedures in cartilage tissue engineering are in vitro and laboratory-based. These are primarily complex two-step procedures that also raise ethical concerns with respect to human tissue culture in a laboratory setting [8].

Translating these techniques into the clinical setting will require the development of a rapid, sterile, one-step technique that could fit into a day surgery timeframe. To date, rapid isolation of bone marrow-derived MSCs [9, 10] and their therapeutical potential has been studied [11], but an important barrier to adoption has been the low number of stem cells requiring a period of cell expansion in the laboratory. There is only one published study assessing a rapid isolation protocol (<30 minutes) for ADMSCs from abdominal lipoaspirate [12], but even this technique relies on a minimum of 24 hours for plastic adherence.

2. Adipose-Derived Mesenchymal Stem Cells

ADMSCs have the ability to differentiate into mesodermal tissue lineages, that is, bone, cartilage, muscle, and adipose [6, 13–16]. They have been incorporated into many different scaffold-based systems and have an established role in cartilage tissue engineering [17, 18].

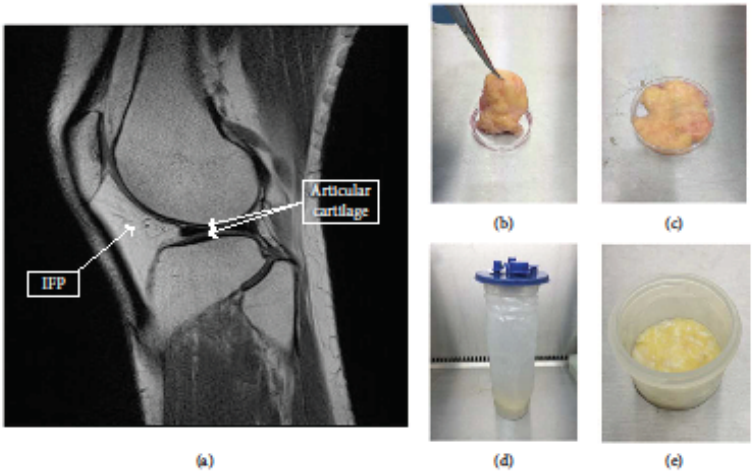


Figure 1: (Modified and used with permission from Wiley under CCBL). Infrapatellar fat pad (IFP) location and harvested tissue. (a) Sagittal magnetic resonance imaging scan of the knee showing the relationship of the IFP (arrow) to the articular cartilage (double arrow). (b, c) Excised IFP from a patient undergoing knee arthroplasty (b) has the fat removed from the fibrous tissue (c). (d, e) The arthroscopically harvested fat pad (d) was separated from the irrigation fluid before enzymatic digestion (e).

Initially, bone marrow (BM) was the most commonly used source of MSCs. Like ADMSCs, BM-derived MSCs are multipotent in nature and can produce tissue of mesodermal lineage [19]. Tissue can be harvested autologously and does not pose the ethical, tumorigenic, or immunogenic risk as presented by pluripotent stem cells. The disadvantages of using BM include low tissue volume and low cell volume [13, 20, 21]. BM-derived MSCs are comparable [22], if not inferior, in respect to chondrogenic potential when compared to ADMSCs [22, 23]. These factors, in addition to less invasive tissue harvesting techniques, make adipose tissue a more desirable source.

3. Tissue Sources and Harvesting Techniques

ADMSCs can be obtained from different sources and by different techniques. The two major sources are abdominal fat and infrapatellar fat pad (IFP). Techniques and protocols for ADMSC harvest and isolation vary based on different laboratory groups. Abdominal fat can be harvested from subcutaneous tissue via abdominoplasty or arthroscopy.

The IFP (Figure 1(a)) is an emerging source of MSCs for cartilage tissue engineering [24, 25]. IFP can be opportunistically harvested (Figure 1(a)) during routine surgical procedures such as knee arthroplasty (Figures 1(b) and 1(c)) or arthroscopy (Figures 1(d) and 1(e)) and is known to have high chondrogenic potential [26]. Although there is less fat volume in the IFP compared to abdominal fat, chondrogenic potential has been shown to higher in ADMSCs sourced from the IFP [27, 28]. The proximity of the IFP to the knee joint may account for this higher potential.

These results could pave the way for future novel advances in minimally invasive arthroscopy or techniques for pure fat pad harvesting as opposed to opportunistic harvest and, better yet, the possible establishment of a single-step surgical repair technique using stem cell technology.

4. Cell Isolation Procedure

Obtaining a stem cell population requires several sequential steps, including harvest, mechanical breakdown, chemical breakdown, purification, and plastic adherence. After these steps, it is important to count and characterise cells and their stemness potential with appropriate investigations.

Cell expansion plays a crucial role to allow adequate cell numbers required for in vitro studies. However, when considering an in situ one-step regenerative procedure for chondral defects, initial cell harvest numbers will need to be adequate for repairing variably sized lesions. Approximately one million cells are needed for a 1 cm^3 lesion [29]. Therefore, studies into cell numbers per tissue unit harvested will be crucial. Recently, cell aggregates have demonstrated increased proliferative ability. This may be due to direct cell-cell contact, allowing better intracellular communication [30–32]. It will be important to now study the number of aggregated cells needed to repair variably sized lesions; if less than one million cells are needed per 1 cm^3 lesion, this could prove to be a major breakthrough.

The steps involved and respective timeframes when using standard protocols are shown below (Figure 2). With both sources, current techniques take >1 hour for cell isolation and subsequently require incubation for up to 24–48 hours to allow for plastic adherence [33]. This was proven to be a lengthy procedure which is not a major concern if only applied to in vitro studies.

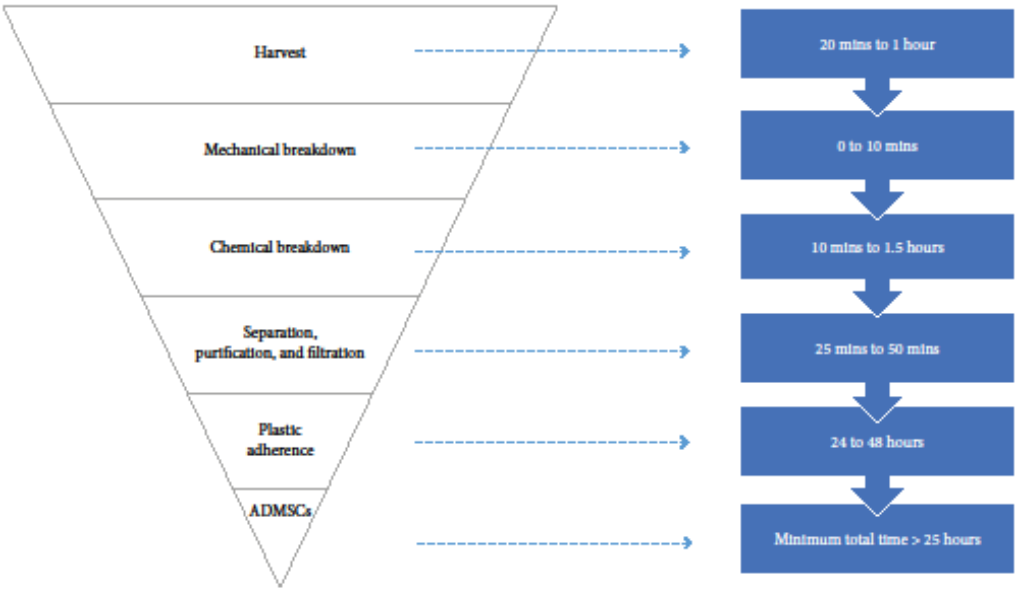


Figure 2: Adipose-derived mesenchymal stem cell (ADMSC) isolation protocol including timeframes.

4.1. Harvest. Abdominal fat can be harvested endoscopically or via abdominoplasty with no significant difference in cell structure and the number of cells yielded per unit of volume [34]. Both take minimal procedural time of <20 minutes; however, the intended abdominoplasty procedure may take much longer. Minimal comparisons are present in the literature. Two studies showed the comparable morphology of cells harvested from endoscopic (liposuction) and abdominoplasty (resection) techniques; however, inadequate phenotyping and characterisation of isolated cells were undertaken in both studies [35–37].

Infrapatellar fat pad (IFP) can be harvested via arthroscopy and opportunistically from arthroplasty. While both tissue harvesting techniques only require the minimal procedural time of <20 minutes, the overall arthroplasty procedure may take up to 2 hours. Additionally, isolated ADMSCs from IFP have been shown to have higher chondrogenic potential compared to cells isolated from bone marrow [26] and abdominal adipose tissue [27], making them a superior source.

4.2. Mechanical Breakdown. Abdominal fat harvested via liposuction is obtained in lipoaspirate form and does not require any further mechanical breakdown. IFP tissue requires separation of fat from the fibrous pad via a scalpel which takes roughly 10 minutes [38].

4.3. Chemical Breakdown. Once fat particles have been isolated from both sources, collagenase is added to the samples to allow chemical breakdown of the tissue. While a number of collagenases are available for ADMSC isolation (Table 1), type 1 collagenase is the preferred agent for isolation prior to chondrogenic lineage induction. Research shown using collagenase type 1 at 0.2% for 10 minutes of chemical/enzymatic breakdown can obtain a stromal vascular fraction [39]. Increased time > 30 minutes using collagenase digestion has been shown to reduce the number of viable adipocytes [40]. Adding trypsin to pure collagenase allows for maximal digestion [41]. Further study is warranted to find the optimal type and concentration of collagenase to enable rapid, effective, and efficient disaggregation of AMDSCs.

After the addition of collagenase, the samples are incubated and agitated with a rotating platform (≥100 revolutions per minute). During incubation on the platform, both chemical and mild mechanical agitations occur synergistically.

4.4. Purification. Purification refers to the separation of material, the removal of unrequired product, and filtration. Following mechanical and chemical breakdowns, the sample undergoes a universal step of centrifugation for 10 minutes [34, 38]. Next, the supernatant is removed, and the pellet is washed with phosphate buffer solution before being filtered through a sterile 100 μm filter. After another round of centrifugation for 5 minutes, the supernatant is discarded and the remaining pellet is then resuspended in 5 millilitres of red cell lysis buffer [28] for 10 minutes before being filtered through a sterile 40 μm filter [38]. After a final 5-minute round of centrifugation, the resulting supernatant is removed, leaving a cell pellet. This total purification procedure is reported to take anywhere between 25 and 50 minutes. Postpurification

Table 1: Comparison of human studies using enzymatic breakdown with collagenase for ADMSC isolation from subcutaneous tissue. Phosphate buffer solution (PBS), Hank's balanced salt solution (HBSS), bovine serum albumin (BSA), and Dulbecco's modified eagle's medium (DMEM).

Author	Collagenase	Concentration	Dilution media	Enzymatic duration
Cheng et al. [42]	Type 1	0.1%	PBS	60 minutes
Choudhery et al. [43]	Type 4	0.2%	PBS	20 minutes
Satish et al. [44]	Type 2	0.1%	HBSS/BSA	40 minutes
Kinoshita et al. [45]	Type 1	0.075%	PBS	30 minutes
Al-Saqi et al. [46]	Type 2	0.1%	Unspecified	45 minutes
Koellensperger et al. [47]	Type 1	0.15%	BSA	45 minutes
Najar et al. [48]	Type 1	0.1%	BSA	45 minutes
Cervelli et al. [49]	Type 1	0.1%	Unspecified	60 minutes
Wu et al. [50]	Type 1	0.1%	DMEM	90 minutes
Yang et al. [51]	Type 1	0.1%	PBS	60 minutes
Yu et al. [52]	Type 1	0.1%	DMEM	60minutes
Tan et al. [53]	Type 2	1.0%	HBSS/BSA	50 minutes
Kilroy et al. [54]	Type 1	0.1%	PBS/BSA	60 minutes
Jeon et al. [55]	Type 1	0.1%	HBSS/BSA	60 minutes
Rodriguez et al. [39]	Unspecified	0.2%	DMEM/BSA	10 minutes
Devireddy et al. [56]	Type 1	0.1%	PBS/BSA	60 minutes

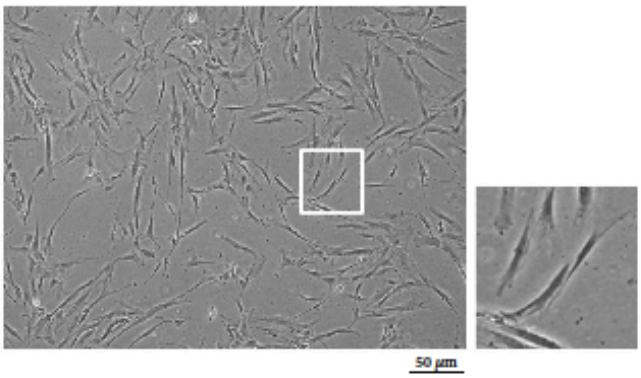


Figure 3: Plastic adherence and morphology of mesenchymal stem cells isolated from the infrapatellar fat pad, representative view using bright field microscopy.

cells are resuspended in culture media and then counted prior to being plated in flasks.

4.5. *Plastic Adherence.* Once cells are plated in appropriate flasks based on cell counts, they are incubated usually for 24–48 hours. Cell attachment to plastic is a key step for identifying and isolating cells with stem cell characteristics. Unattached cells are discarded. At this stage, the attached cells can be expanded and passaged or frozen in liquid nitrogen for later use. This plastic adherence step requires a minimum of 24 hours of incubation. Cell sorting using marker selection (flow sorting) is an alternative to plastic adherence with respect to isolating a pure ADMSC population [57]. The drawback to this technique is the time requirement and lack of exact phenotypic characterisation of ADMSCs.

4.6. *Phenotype.* As per the International Society for Cellular Therapy [58, 59], three criteria must be fulfilled for the MSC phenotype: adherence to plastic, appropriate surface antigens, and expression of multipotent differentiation potential.

Plastic adherence is a hallmark property of all MSC groups [60, 61]. Furthermore, typical morphology and colony formation can be observed under a microscope as seen in Figure 3.

To confirm the phenotype of cells isolated as MSCs, specific surface antigens are tested through immunophenotyping and can be done via flow cytometry [46]. MSCs generally express (≥95%) CD73, CD90, and CD105, while lacking expression (≤2%) of CD 11b, CD14, CD34, CD45, and CD79a [47].

Table 2: Mesenchymal stem cell differentiation testing. COL: collagen; OCN: osteocalcin; ALP: alkaline phosphatase; PPARG: peroxisome proliferator-activated receptor gamma; C/EBP: CCAAT/enhancer-binding protein; ACAN: aggrecan.

Lineage	Histological staining	qPCR gene expression
Osteoblasts	Alizarin Red, Von Kossa	COL 1A1, OCN, runx 2, ALP
Adipocytes	Oil Red O	PPARG 1 and 2, C/EBP a and d
Chondroblasts	Alcian blue	COL 2A1, SOX-9, ACAN

However, exact characterisation is still in development [57, 62], and surface phenotyping should be used in conjunction with other criteria to help best identify MSC.

Biologically, MSCs should display three lines of differentiation potential: osteoblasts, adipocytes, and chondroblasts [58]. Multipotent potential can be evidenced by differentiation into various lineages using different induction paths [16] and can be tested with staining and qPCR (Table 2).

5. Rapid Isolation Procedures in Literature

Over the past decade, several commercially available enzymatic and nonenzymatic adipose tissue cell isolation systems [63, 64] have achieved sterile processing and high yields of cells. However, these systems only isolate a stromal vascular fraction (SVF), implying that a plastic adherence step is still required for pure ADMSC isolation.

One published attempt at a rapid protocol using abdominal lipoaspirates achieved an SVF isolation within 30 minutes [12]. 2.5×10^5 ADMSCs were isolated using the 30-minute approach compared to 2.0×10^6 from the standard approach. The final step of plastic adherence to isolate a pure ADMSC population still required 24–48 hours of further incubation. Furthermore, the number of ADMSCs yielded was nearly 10 times less when compared to the standard procedure.

A purely nonenzymatic breakdown approach with blender mixing and sonication has been used to obtain an SVF within 25 minutes [65]. On average, 2.6×10^5 cells were isolated in the SVF, resulting in a very low average of 2.4×10^4 ADMSCs. Although SVF isolation is rapid, overnight (>24 hours) plastic adherence is once again still required to obtain a pure ADMSC population.

It is evident from these two approaches that a low number of cells are obtained, possibly due to toxicity from the methodology. Moreover, only an SVF was rapidly isolated as opposed to a pure ADMSC population, which still takes >24 hours.

The use of SVF alone, without the use of a pure ADMSC population, may be another therapeutic option. As mentioned earlier, given the superior chondrogenic potential of ADMSCs isolated from the IFP [27, 28], SVF populations from abdominal fat should be compared to IFP before trialling SVF as a direct one-step therapeutic option. However, the lack of cell-cell contact within an SVF due to scattered ADMSCs will lead to inferior cartilage repair as a result of reduced paracrine stimulation [30].

6. Where Can We Save Time?

There are three procedural steps where time could be saved. These are discussed below and also represented in Figure 4.

6.1. Mechanical Breakdown. The initial mechanical breakdown could be further enhanced by adding mechanical agitation through shaking, vortexing, and possibly adding sterile solid materials during chemical breakdown to synergistically assist the breakdown of tissue. Sterile beads have been used commercially in liposuction kits to help emulsify tissue [66]. If such materials were to be used, they need to be sterilisable and nontoxic and show a consistent and predictable effect on tissue breakdown based on morphology and weight. These factors will need proper investigation prior incorporation into isolation techniques. The risk of these more vigorous approaches is cell damage and death; therefore, it will be important to assess cell viability in such intended studies.

Although it currently only takes 0–10 minutes to break tissue down depending on the source, the more vigorous breakdown of tissue earlier, particularly of IFP tissue, may help reduce the total time needed for the subsequent step of chemical breakdown.

6.2. Chemical Breakdown. The chemical breakdown shows varying timeframes with reports of 10 minutes for the breakdown of tissue into an SVF [39]. Higher concentrations of collagenase with the addition of trypsin may allow for the maximal breakdown, while higher rpm use on rotating platforms may enable synergistic breakdown. Once again, the possibility of cell toxicity will need to be investigated [40].

6.3. Plastic Adherence. Plastic adherence forms the major time barrier (minimum of 24 hours). A new rapid technique needs to be established in this step as this timeframe is not clinically feasible.

Recent literature has reported the high affinity of articular progenitor cells (APCs) to fibronectin, with research showing APC adherence to fibronectin-coated wells in 20 minutes [67]. Although lacking clearly defined markers, these APCs, also known as chondrogenic progenitor cells, have shown stem cell potential and are similar to and possibly more differentiated forms of ADMSCs [68].

This is a major finding supporting the use of fibronectin-coated wells or plates to isolate ADMSCs if it can be demonstrated through immunophenotyping that stem cells are attaching selectively to the coating.

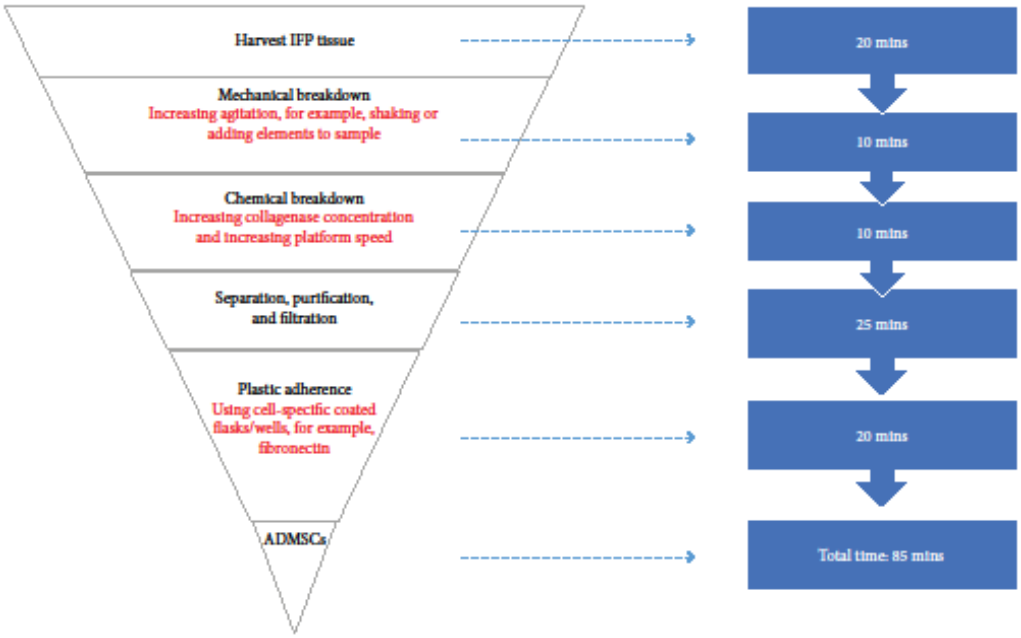


Figure 4: Proposed rapid adipose-derived mesenchymal stem cell (ADMSC) isolation procedure from the infrapatellar fat pad (IFP). The three major changes proposed are highlighted in red.

7. Conclusion and Future Clinical Applicability

A rapid ADMSC isolation technique is necessary for a single-step, tissue engineering-based surgical repair of cartilage tissue. Literature to date suggests IFP-harvested ADMSCs to be the most promising in chondrogenic potential. If a procedure can isolate ADMSCs using an approach such as that described in Figure 4, then incorporating the cells into a matrix and implanting them into a defect using handheld bioprinters [69–71] may pave the way for a single-step intraoperative cartilage repair technique. When leveraging the advantages of a day-only minimal incision surgery, such as arthroscopy, there may be significant clinical outcome and health care cost gains.

The future of cartilage repair is promising. By speeding up cell isolation techniques, a major time barrier can be overcome, translating a clinically to a nonlaboratory-based procedure, shorter surgical time, quicker recovery for the patient, and a smaller burden on the health care system. Younger patients can now hope for a simple, low-risk treatment option that aids in preventing the onset of osteoarthritis.

Abbreviations

MSCs: Mesenchymal stem cells
ADMSCs: Adipose-derived mesenchymal stem cells
IFP: Infrapatellar fat pad
BM: Bone marrow
SVF: Stromal vascular fraction
APC: Articular progenitor cells.

Conflicts of Interest

The authors declare that there is no conflict of interest regarding the publication of this paper.

References

[1] J. E. Jeon, K. Schrobback, D. W. Hutmacher, and T. J. Klein, "Dynamic compression improves biosynthesis of human zonal chondrocytes from osteoarthritis patients," *Osteoarthritis and Cartilage*, vol. 20, no. 8, pp. 906–915, 2012.

[2] A. P. Hollander, S. C. Dickinson, and W. Kafienah, "Stem cells and cartilage development: complexities of a simple tissue," *Stem Cells*, vol. 28, no. 11, pp. 1992–1996, 2010.

[3] O. Robertsson, A. Stefánsdóttir, L. Lidgren, and J. Ranstam, "Increased long-term mortality in patients less than 55 years old who have undergone knee replacement for osteoarthritis," *The Journal of Bone and Joint Surgery*, vol. 89-B, no. 5, pp. 599–603, 2007.

[4] J. Julin, E. Jämsen, T. Puolakka, Y. T. Konttinen, and T. Moilanen, "Younger age increases the risk of early prosthesis failure following primary total knee replacement for osteoarthritis," *Acta Orthopaedica*, vol. 81, no. 4, pp. 413–419, 2010.

[5] CITER (Cardiff Institute of Tissue Engineering and Repair), Cardiff School of Biosciences, Museum Avenue, Cardiff, CF10 3US, Wales, UK, S. N. Redman, S. F. Oldfield, and

C. W. Archer, "Current strategies for articular cartilage repair," *European Cells & Materials*, vol. 9, pp. 23–32, 2005.

[6] B. Bunnell, M. Flaat, C. Gagliardi, B. Patel, and C. Ripoll, "Adipose-derived stem cells: isolation, expansion and differentiation," *Methods*, vol. 45, no. 2, pp. 115–120, 2008.

[7] P. V. Giannoudis, T. A. Einhorn, and D. Marsh, "Fracture healing: the diamond concept," *Injury*, vol. 38, pp. S3–S6, 2007.

[8] M. L. Torre, E. Lucarelli, S. Guidi et al., "Ex vivo expanded mesenchymal stromal cell minimal quality requirements for clinical application," *Stem Cells and Development*, vol. 24, no. 6, pp. 677–685, 2015.

[9] K. Beitzel, M. B. McCarthy, M. P. Cote et al., "Rapid isolation of human stem cells (connective progenitor cells) from the distal femur during arthroscopic knee surgery," *Arthroscopy*, vol. 28, no. 1, pp. 74–84, 2012.

[10] A. D. Mazzocca, M. B. R. McCarthy, D. M. Chowaniec, M. P. Cote, R. A. Arciero, and H. Drissi, "Rapid isolation of human stem cells (connective tissue progenitor cells) from the proximal humerus during arthroscopic rotator cuff surgery," *The American Journal of Sports Medicine*, vol. 38, no. 7, pp. 1438–1447, 2010.

[11] B. Dozza, G. Gobbi, E. Lucarelli et al., "A rapid method for obtaining mesenchymal stem cells and platelets from bone marrow aspirate," *Journal of Tissue Engineering and Regenerative Medicine*, vol. 8, no. 6, pp. 483–492, 2014.

[12] M. P. Francis, P. C. Sachs, L. W. Elmore, and S. E. Holt, "Isolating adipose-derived mesenchymal stem cells from lipoaspirate blood and saline fraction," *Organogenesis*, vol. 6, no. 1, pp. 11–14, 2014.

[13] P. A. Zuk, M. Zhu, H. Mizuno et al., "Multilineage cells from human adipose tissue: implications for cell-based therapies," *Tissue Engineering*, vol. 7, no. 2, pp. 211–228, 2001.

[14] A. J. Becker, E. A. Mcculloch, and J. E. Till, "Cytological demonstration of the clonal nature of spleen colonies derived from transplanted mouse marrow cells," *Nature*, vol. 197, no. 4866, pp. 452–454, 1963.

[15] A. J. Friedenstein, U. F. Deriglasova, N. N. Kulagina et al., "Precursors for fibroblasts in different populations of hematopoietic cells as detected by the in vitro colony assay method," *Experimental Hematology*, vol. 2, no. 2, pp. 83–92, 1974.

[16] M. F. Pittenger, A. M. Mackay, S. C. Beck et al., "Multilineage potential of adult human mesenchymal stem cells," *Science*, vol. 284, no. 5411, pp. 143–147, 1999.

[17] T. Rada, R. L. Reis, and M. E. Gomes, "Adipose tissue-derived stem cells and their application in bone and cartilage tissue engineering," *Tissue Engineering Part B: Reviews*, vol. 15, no. 2, pp. 113–125, 2009.

[18] F. Veronesi, M. Maglio, M. Tschon, N. N. Aldini, and M. Fini, "Adipose-derived mesenchymal stem cells for cartilage tissue engineering: state-of-the-art in in vivo studies," *Journal of Biomedical Materials Research Part A*, vol. 102, no. 7, pp. 2448–2466, 2014.

[19] G. Sheng, "The developmental basis of mesenchymal stem/stromal cells (MSCs)," *BMC Developmental Biology*, vol. 15, no. 1, p. 44, 2015.

[20] M.-C. Kastrinaki, I. Andreakou, P. Charbord, and H. A. Papadaki, "Isolation of human bone marrow mesenchymal stem cells using different membrane markers: comparison of colony/cloning efficiency, differentiation potential, and molecular profile," *Tissue Engineering Part C: Methods*, vol. 14, no. 4, pp. 333–339, 2008.

[21] M. C. Ronzière, E. Perrier, F. Mallein-Gerin, and A. M. Freyria, "Chondrogenic potential of bone marrow- and adipose tissue-derived adult human mesenchymal stem cells," *Biomedical Materials and Engineering*, vol. 20, no. 3, pp. 145–158, 2010.

[22] M. Strioga, S. Viswanathan, A. Darinskas, O. Slaby, and J. Michalek, "Same or not the same? Comparison of adipose tissue-derived versus bone marrow-derived mesenchymal stem and stromal cells," *Stem Cells and Development*, vol. 21, no. 14, pp. 2724–2752, 2012.

[23] Y. Jang, Y. G. Koh, Y. J. Choi et al., "Characterization of adipose tissue-derived stromal vascular fraction for clinical application to cartilage regeneration," *In Vitro Cellular & Developmental Biology. Animal*, vol. 51, no. 2, pp. 142–150, 2015.

[24] J. L. Dragoo, B. Samimi, M. Zhu et al., "Tissue-engineered cartilage and bone using stem cells from human infrapatellar fat pads," *The Journal of Bone and Joint Surgery, British Volume*, vol. 85-B, no. 5, pp. 740–747, 2003.

[25] C. T. Buckley, T. Vinardell, S. D. Thorpe et al., "Functional properties of cartilaginous tissues engineered from infrapatellar fat pad-derived mesenchymal stem cells," *Journal of Biomechanics*, vol. 43, no. 5, pp. 920–926, 2010.

[26] P. Hindle, N. Khan, L. Biant, and B. Péault, "The Infrapatellar fat pad as a source of perivascular stem cells with increased chondrogenic potential for regenerative medicine," *Stem Cells Translational Medicine*, vol. 6, no. 1, pp. 77–87, 2017.

[27] S. Lopa, A. Colombini, D. Stanco, L. de Girolamo, V. Sansone, and M. Moretti, "Donor-matched mesenchymal stem cells from knee infrapatellar and subcutaneous adipose tissue of osteoarthritic donors display differential chondrogenic and osteogenic commitment," *European Cells & Materials*, vol. 27, pp. 298–311, 2014.

[28] R. Felimban, K. Ye, K. Traianedes et al., "Differentiation of stem cells from human infrapatellar fat pad: characterization of cells undergoing chondrogenesis," *Tissue Engineering Part A*, vol. 20, no. 15-16, pp. 2213–2223, 2014.

[29] A. Singh, S. C. Goel, K. K. Gupta et al., "The role of stem cells in osteoarthritis: an experimental study in rabbits," *Bone & Joint Research*, vol. 3, no. 2, pp. 32–37, 2014.

[30] B. Sridharan, S. M. Lin, A. T. Hwu, A. D. Laflin, and M. S. Detamore, "Stem cells in aggregate form to enhance chondrogenesis in hydrogels," *PLoS One*, vol. 10, no. 12, article e0141479, 2015.

[31] G. M. van Buul, E. Villafuertes, P. K. Bos et al., "Mesenchymal stem cells secrete factors that inhibit inflammatory processes in short-term osteoarthritic synovium and cartilage explant culture," *Osteoarthritis and Cartilage*, vol. 20, no. 10, pp. 1186–1196, 2012.

[32] I. Linero and O. Chaparro, "Paracrine effect of mesenchymal stem cells derived from human adipose tissue in bone regeneration," *PLoS One*, vol. 9, no. 9, article e107001, 2014.

[33] S. Nae, I. Bordeianu, A. T. Stăncioiu, and N. Antohi, "Human adipose-derived stem cells: definition, isolation, tissue-engineering applications," *Romanian Journal of Morphology and Embryology*, vol. 54, no. 4, pp. 919–924, 2013.

[34] S. Schneider, M. Unger, M. van Griensven, and E. R. Balmayor, "Adipose-derived mesenchymal stem cells from liposuction and resected fat are feasible sources for regenerative medicine," *European Journal of Medical Research*, vol. 22, no. 1, p. 17, 2017.

[35] H. Busser, M. Najar, G. Raicevic et al., "Isolation and characterization of human mesenchymal stromal cell subpopulations: comparison of bone marrow and adipose tissue," *Stem Cells and Development*, vol. 24, no. 18, pp. 2142–2157, 2015.

[36] H. Eto, H. Suga, D. Matsumoto et al., "Characterization of structure and cellular components of aspirated and excised adipose tissue," *Plastic and Reconstructive Surgery*, vol. 124, no. 4, pp. 1087–1097, 2009.

[37] M. Faustini, M. Bucco, T. Chlapanidas et al., "Nonexpanded mesenchymal stem cells for regenerative medicine: yield in stromal vascular fraction from adipose tissues," *Tissue Engineering Part C: Methods*, vol. 16, no. 6, pp. 1515–1521, 2010.

[38] P. Tangchitphisut, N. Srikaew, S. Numhom et al., "Infrapatellar fat pad: an alternative source of adipose-derived mesenchymal stem cells," *Arthritis*, vol. 2016, Article ID 4019873, 10 pages, 2016.

[39] A. M. Rodriguez, D. Pisani, C. A. Dechesne et al., "Transplantation of a multipotent cell population from human adipose tissue induces dystrophin expression in the immunocompetent mdx mouse," *The Journal of Experimental Medicine*, vol. 201, no. 9, pp. 1397–1405, 2005.

[40] S. A. Seaman, S. C. Tannan, Y. Cao, S. M. Peirce, and K. Y. Lin, "Differential effects of processing time and duration of collagenase digestion on human and murine fat grafts," *Plastic and Reconstructive Surgery*, vol. 136, no. 2, pp. 189e–199e, 2015.

[41] S. K. Williams, S. Mckenney, and B. E. Jarrell, "Collagenase lot selection and purification for adipose tissue digestion," *Cell Transplantation*, vol. 4, no. 3, pp. 281–289, 2017.

[42] N. C. Cheng, T. Y. Hsieh, H. S. Lai, and T. H. Young, "High glucose-induced reactive oxygen species generation promotes stemness in human adipose-derived stem cells," *Cytotherapy*, vol. 18, no. 3, pp. 371–383, 2016.

[43] M. S. Choudhery, M. Badowski, A. Muise, and D. T. Harris, "Effect of mild heat stress on the proliferative and differentiative ability of human mesenchymal stromal cells," *Cytotherapy*, vol. 17, no. 4, pp. 359–368, 2015.

[44] L. Satish, J. M. Krill-Burger, P. H. Gallo et al., "Expression analysis of human adipose-derived stem cells during in vitro differentiation to an adipocyte lineage," *BMC Medical Genomics*, vol. 8, no. 1, p. 41, 2015.

[45] K. Kinoshita, S. Kuno, H. Ishimine et al., "Therapeutic potential of adipose-derived SSEA-3-positive muse cells for treating diabetic skin ulcers," *Stem Cells Translational Medicine*, vol. 4, no. 2, pp. 146–155, 2015.

[46] S. H. Al-Saqi, M. Saliem, S. Asikainen et al., "Defined serum-free media for in vitro expansion of adipose-derived mesenchymal stem cells," *Cytotherapy*, vol. 16, no. 7, pp. 915–926, 2014.

[47] E. Koellensperger, N. Bollinger, V. Dexheimer, F. Gramley, G. Germann, and U. Leimer, "Choosing the right type of serum for different applications of human adipose tissue-derived stem cells: influence on proliferation and differentiation abilities," *Cytotherapy*, vol. 16, no. 6, pp. 789–799, 2014.

[48] M. Najar, R. M. Rodrigues, K. Buyl et al., "Proliferative and phenotypical characteristics of human adipose tissue-derived stem cells: comparison of Ficoll gradient centrifugation and red blood cell lysis buffer treatment purification methods," *Cytotherapy*, vol. 16, no. 9, pp. 1220–1228, 2014.

[49] V. Cervelli, M. G. Scioli, P. Gentile et al., "Platelet-rich plasma greatly potentiates insulin-induced adipogenic differentiation of human adipose-derived stem cells through a serine/threonine kinase Akt-dependent mechanism and promotes clinical fat graft maintenance," *Stem Cells Translational Medicine*, vol. 1, no. 3, pp. 206–220, 2012.

[50] I. Wu, Z. Nahas, K. A. Kimmerling, G. D. Rosson, and J. H. Elisseeff, "An injectable adipose matrix for soft-tissue reconstruction," *Plastic and Reconstructive Surgery*, vol. 129, no. 6, pp. 1247–1257, 2012.

[51] X. F. Yang, X. He, J. He et al., "High efficient isolation and systematic identification of human adipose-derived mesenchymal stem cells," *Journal of Biomedical Science*, vol. 18, no. 1, p. 59, 2011.

[52] G. Yu, Z. E. Floyd, X. Wu, Y.-D. C. Halvorsen, and J. M. Gimble, "Isolation of human adipose-derived stem cells from lipoaspirates," *Methods in Molecular Biology*, vol. 702, pp. 17–27, 2011.

[53] H. Tan, A. J. DeFail, J. P. Rubin, C. R. Chu, and K. G. Marra, "Novel multiarm PEG-based hydrogels for tissue engineering," *Journal of Biomedical Materials Research Part A*, vol. 92A, no. 3, pp. 979–987, 2009.

[54] G. E. Kilroy, S. J. Foster, X. Wu et al., "Cytokine profile of human adipose-derived stem cells: expression of angiogenic, hematopoietic, and pro-inflammatory factors," *Journal of Cellular Physiology*, vol. 212, no. 3, pp. 702–709, 2007.

[55] E. S. Jeon, H. Y. Song, M. R. Kim et al., "Sphingosylphosphorylcholine induces proliferation of human adipose tissue-derived mesenchymal stem cells via activation of JNK," *Journal of Lipid Research*, vol. 47, no. 3, pp. 653–664, 2006.

[56] R. Devireddy, S. Thirumala, and J. Gimble, "Cellular response of adipose derived passage-4 adult stem cells to freezing stress," *Journal of Biomechanical Engineering*, vol. 127, no. 7, pp. 1081–1086, 2005.

[57] U. D. Wankhade, M. Shen, R. Kolhe, and S. Fulzele, "Advances in adipose-derived stem cells isolation, characterization, and application in regenerative tissue engineering," *Stem Cells International*, vol. 2016, Article ID 3206807, 9 pages, 2016.

[58] M. Dominici, K. le Blanc, I. Mueller et al., "Minimal criteria for defining multipotent mesenchymal stromal cells. The International Society for Cellular Therapy position statement," *Cytotherapy*, vol. 8, no. 4, pp. 315–317, 2006.

[59] M. Krampera, J. Galipeau, Y. Shi, K. Tarte, L. Sensebe, and MSC Committee of the International Society for Cellular Therapy (ISCT), "Immunological characterization of multipotent mesenchymal stromal cells—The International Society for Cellular Therapy (ISCT) working proposal," *Cytotherapy*, vol. 15, no. 9, pp. 1054–1061, 2013.

[60] D. C. Colter, R. Class, C. M. DiGirolamo, and D. J. Prockop, "Rapid expansion of recycling stem cells in cultures of plastic-adherent cells from human bone marrow," *Proceedings of the National Academy of Sciences of the United States of America*, vol. 97, no. 7, pp. 3213–3218, 2000.

[61] Y. Jiang, B. N. Jahagirdar, R. L. Reinhardt et al., "Pluripotency of mesenchymal stem cells derived from adult marrow," *Nature*, vol. 418, no. 6893, pp. 41–49, 2002.

[62] F. Sabatini, L. Petecchia, M. Tavian, V. J. de Villeroché, G. A. Rossi, and D. Brouty-Boyé, "Human bronchial fibroblasts exhibit a mesenchymal stem cell phenotype and multilineage differentiating potentialities," *Laboratory Investigation*, vol. 85, no. 8, pp. 962–971, 2005.

[63] E. Oberbauer, C. Steffenhagen, C. Wurzer, C. Gabriel, H. Redl, and S. Wolbank, "Enzymatic and non-enzymatic isolation

systems for adipose tissue-derived cells: current state of the art," *Cell Regeneration*, vol. 4, no. 1, p. 4:7, 2015.

[64] E. Raposio, F. Simonacci, and R. E. Perrotta, "Adipose-derived stem cells: comparison between two methods of isolation for clinical applications," *Annals of Medicine and Surgery*, vol. 20, pp. 87–91, 2017.

[65] M. A. Amirkhani, R. Mohseni, M. Soleimani, A. Shoae-Hassani, and M. A. Nilforoushzadeh, "A rapid sonication based method for preparation of stromal vascular fraction and mesenchymal stem cells from fat tissue," *Bioimpacts*, vol. 6, no. 2, pp. 99–104, 2016.

[66] February 2018, http://www.lipogems.eu/lipoaspiration-procedure.html.

[67] G. P. Dowthwaite, J. C. Bishop, S. N. Redman et al., "The surface of articular cartilage contains a progenitor cell population," *Journal of Cell Science*, vol. 117, no. 6, pp. 889–897, 2004.

[68] Y. Jiang and R. S. Tuan, "Origin and function of cartilage stem/progenitor cells in osteoarthritis," *Nature Reviews Rheumatology*, vol. 11, no. 4, pp. 206–212, 2015.

[69] C. Di Bella, A. Fosang, D. M. Donati, G. G. Wallace, and P. F. M. Choong, "3D bioprinting of cartilage for orthopedic surgeons: reading between the lines," *Frontiers in Surgery*, vol. 2, 2015.

[70] C. D. O'Connell, C. Di Bella, F. Thompson et al., "Development of the Biopen: a handheld device for surgical printing of adipose stem cells at a chondral wound site," *Biofabrication*, vol. 8, no. 1, 2016.

[71] S. Duchi, C. Onofrillo, C. D. O'Connell et al., "Handheld co-axial bioprinting: application to in situ surgical cartilage repair," *Scientific Reports*, vol. 7, no. 1, p. 5837, 2017.

APPENDIX 3: FLOW CYTOMETRY FROM THREE DIFFERENT CELL TYPES

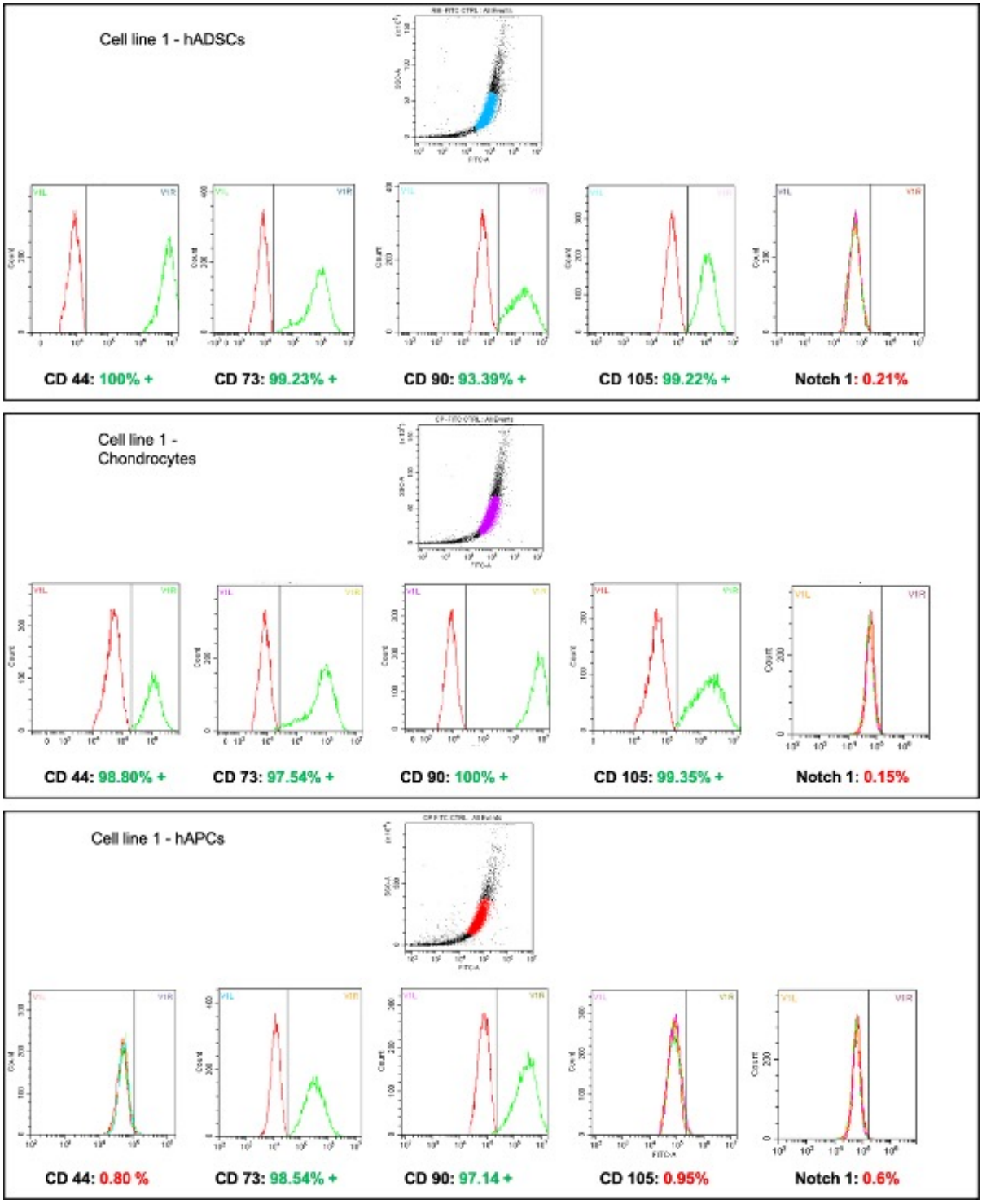


Figure A1. Flow cytometry profiles of hADSCs, Chondrocytes and hAPCs from one patient tested. Graphs represent the cytofluorimetric analyses of the stemness markers used to characterise the cells in both control and rapid isolation groups. Red lines represent the control staining with only the secondary antibody, while the green lines show the profile of fluorophore-conjugated target antibody

APPENDIX 4: FLOW CYTOMETRY FROM THREE DIFFERENT PATIENT LINES

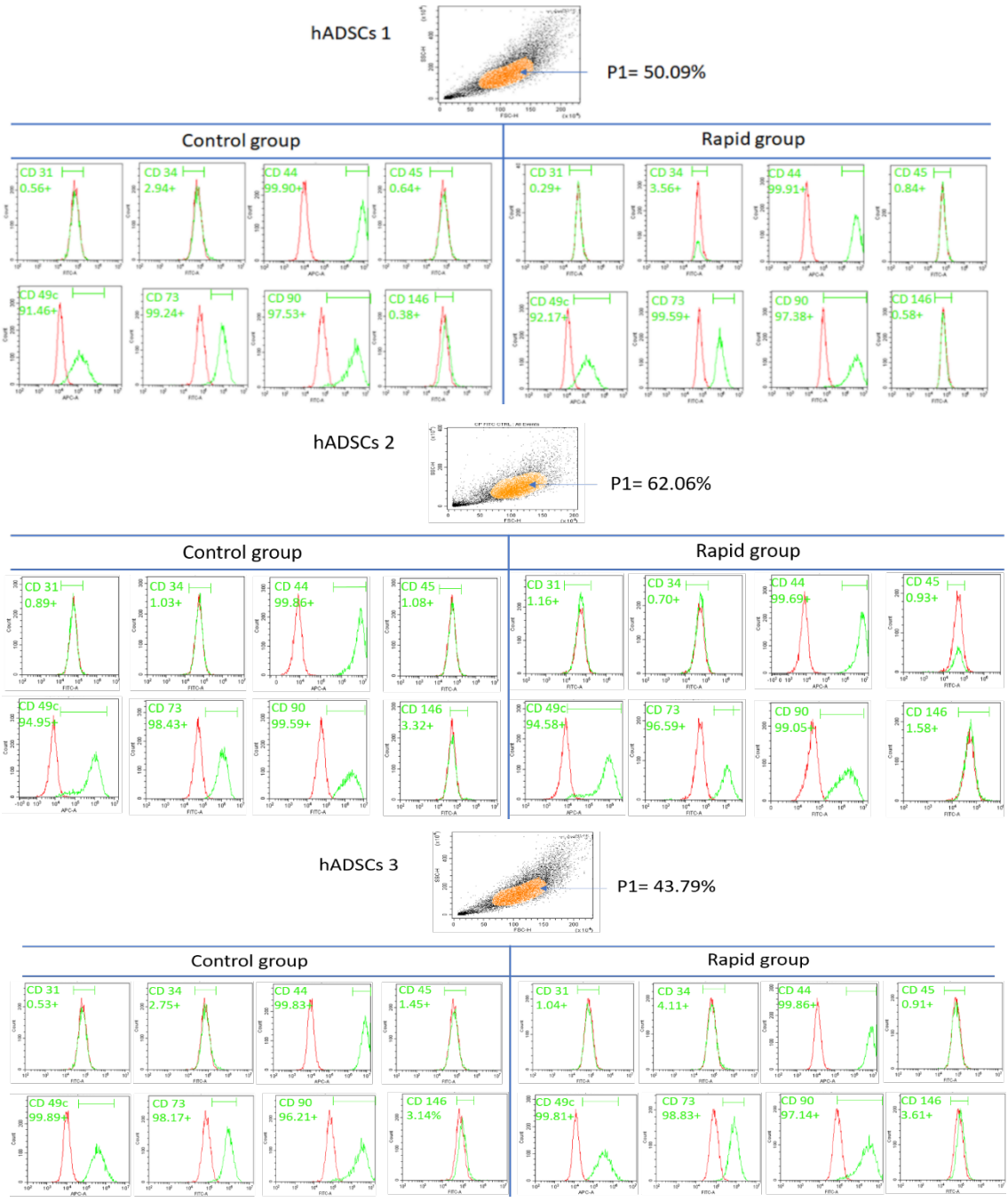


Figure A2. Flow cytometry profiles of hADSCs from three different patient lines tested. Graphs represent the cytofluorimetric analyses of the stemness markers used to characterise the cells in both control and rapid isolation groups. Red lines represent the control staining with only the secondary antibody, while the green lines show the profile of fluorophore-conjugated target antibody. P represents the gated cell population of interest. Positive expression (>90%) is seen with markers CD44, CD49c, CD73 and CD90 (as expected), negative expression (<3%) is evident with markers of CD31, CD34, CD45 and CD146 (as expected).

APPENDIX 5: EFFECT OF DIFFERENT SOURCES OF COATED TCPS ON CELLULAR ATTACHMENT

Autologous and synthetic TCPS (Tissue culture polystyrene) coatings were evaluated. Platelet-rich plasma (PRP) can be autologously harvested from human serum and contains ECM proteins which can facilitate cellular attachment. Poly -L- lysine is a well-studied synthetic polymer that can facilitate cellular attachment. In this developing body of work, cellular attachment to these sources was evaluated over timeframes of 15 and 30 minutes and compared to Matrigel-coated TCPS adherence.

TCPS-coated surfaces used:

1) Matrigel (Animal-derived), *[Sigma Aldrich].* Control
2) Poly -L- Lysine (Synthetic Polymer), *[Sigma Aldrich]*
3) PRP at 5% in PBS (Autologously derived- Human) *[Allocuro system*]*
4) PRP at 10% in PBS (Autologously derived- Human) *[Allocuro system*]*

**PRP was prepared according to the manufacture's protocol (http://www.alocuro.com.au) before being used as a coating.*

CELLULAR ADHERENCE

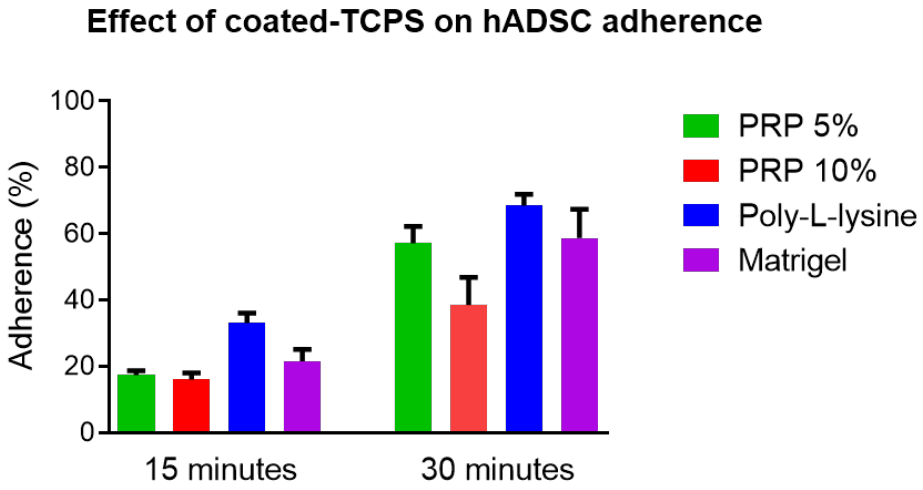


Figure A3. Effect of different Tissue culture polystyrene (TCPS) coatings on cellular attachment. PRP - Platelet-rich plasma and hADSC – human adipose derived mesenchymal stem cell. Data are presented as mean +/- SEM, (n=2), significant activity was calculated with unpaired t-test.

After 15 minutes, the poly-L-lysine coated TCPS group showed the highest level of cellular adherence compared to the other groups, however, overall, there was still <40% attached in all four coated TCPS groups at this time point, (Supplementary Figure 1). After 30 minutes, both the PRP 5% (67%) and Poly -L-Lysine (72%) coated TCPS groups were comparable to the Matrigel-coated TCPS group (70%) for cellular adherence. The PRP 10%-coated TCPSs group after 30 minutes only achieved a 47% level of adherence. No significant statistical difference between any of the groups is observed given only an n=2 sample has been tested at this preliminary stage.

IMMUNOPHENOTYPE

**For phenotypical assessment the PRP 10% group was abandoned given the PRP 5% concentration had a higher level of cellular adherence.*

During cellular expansion, cells appeared morphologically similar in all three groups and were typical of a mesenchymal stem cell population (Data not shown). Cells were expanded until passage three and underwent immunophenotyping with flow cytometry. All positive markers of the expected hADSCs phenotype were expressed as >90% in all three groups as shown in Supplementary Table 1, and all negative markers of the hADSCs phenotype were expressed as <3% in all three groups.

Marker	**Expected hADSCs phenotype**	**PRP 5% TCPS group (%)**	**Poly -L-lysine TCPS group (%)**	**Matrigel-coated TCPS group (%)**
CD 44	+	99.98	99.94	100
CD 49c	+	92.5	94.59	96.74
CD 73	+	99.65	99.36	99.11
CD 90	+	98.33	98.10	99.33
CD 31, 34, 45 and 146	-	< 3%	< 3%	< 3%

Table A1. Flow cytometry results summary of key markers tested for with the hADSCs phenotype. PRP - Platelet-rich plasma and hADSCs– human adipose derived mesenchymal stem cells. *Data are presented as a mean of two different patients (n=2).*

Early results from this body of work suggest that PRP 5% and Poly-L-lysine coated TCPS are both comparable to Matrigel-coated TCPS for hADSCs attachment. Furthermore, the phenotype of selectively attached cells is consistent with that of a hADSCs. These results are promising and suggest that autologous or synthetically derived coatings can be substituted for the Matrigel-coated TCPS utilised in the newly devised rapid IFP-derived hADSCs isolation procedure. Further validation and optimisation of such TCPS coatings and their role/contribution to the overall biofabrication technique are being explored and refined.